UNIVERSIDAD COMPLUTENSE DE MADRID
FACULTAD DE CIENCIAS QUÍMICAS

TESIS DOCTORAL

Estudio estructural y funcional de proteínas formadoras de poros de venenos
Structural and functional characterization of venom pore forming proteins

MEMORIA PARA OPTAR AL GRADO DE DOCTOR

PRESENTADA POR

Esperanza Rivera de Torre

Directores

José Gregorio Gavilanes Franco
Álvaro Martínez del Poz

Madrid

UNIVERSIDAD COMPLUTENSE DE MADRID

FACULTAD DE CIENCIAS QUÍMICAS

DEPARTAMENTO DE BIOQUÍMICA Y BIOLOGÍA MOLECULAR

TESIS DOCTORAL

ESTUDIO ESTRUCTURAL Y FUNCIONAL DE PROTEÍNAS FORMADORAS DE POROS DE VENENOS

STRUCTURAL AND FUNCTIONAL CHARACTERIZATION OF VENOM PORE-FORMING PROTEINS

MEMORIA PARA OPTAR AL GRADO DE DOCTOR

PRESENTADA POR:

Esperanza Rivera de Torre

DIRECTORES:

Dr. José Gregorio Gavilanes Franco

Dr. Álvaro Martínez del Pozo

MADRID, 2020

A mi madre y Vicente
A mi hermana
A Álvaro

A mi director de Tesis Álvaro le tengo que agradecer mucho más que la excelente formación que he recibido estos años. Gracias por hacer de psicólogo, ayudarme a relativizar y ser el mejor padre científico que podría haber tenido. Gracias por el ímpetu y por recordarnos que en esta profesión podemos hacer nuestra vida relevante para la sociedad. A mi director de tesis Pepe le agradezco su dedicación y sus acertados consejos. Sois ambos el espejo en el que me miro personal y profesionalmente.

Thank you Jessica and her team (Lindsay, Winny, Evelyn, Erin, Robert, Fitz) for making my stay in Lowell so profitable from both personal and professional points of view. You made me feel home.

I want to thank Peter and his group (Thomas, Anna, Sazzad, Oskar, Kay Lin). It was a pleasure to be part of your team. I will always remember my stay in Turku as one of the most peaceful periods of my life.

Queremos agradecer a nuestros colaboradores María Ángeles Jiménez, Belén Patiño, Pilar Medina y sus respectivos equipos de trabajo sin los que no habría sido posible sacar adelante el proyecto de las latrodectinas. Hacéis que la colaboración y el trabajo en equipo cobren sentido con vuestras aportaciones.

Gracias a todos los habitantes del L3, que han contribuido al buen ambiente de trabajo que ha hecho que apeteciera venir a trabajar cada día. Javier, que me confirmaba o desmentía bandas fantasmas en los geles e imponía sus manos a todo aparato que decidía dejar de funcionar; Mercedes, por su cariño y por recordarme cada día lo fuertes que somos; Julián siempre tan madrugador y eficiente en la organización; Lucía, esa voz de la experiencia cercana que ayudaba a mantener los pies en la tierra. Y al resto de profesores que han hecho de mi paso por el departamento un momento de aprendizaje y crecimiento personal: Belén, Mayte, Rosalía, Eva, Nacho, Inma.

Hago mención especial al L13 y su “club del café”, Javier Turnay y Nieves que siempre han estado dispuestos a ayudar, aunque estuvieran hasta arriba de trabajo. Y M. Antonia, que te fuiste de pronto de manera injusta. Gracias por ofrecerme siempre un sitio en tu despacho para huir del ruido de mi poyata.

No me puedo olvidar de mis compañeros. Sara, gracias por ser la mejor mentora y tener paciencia infinita para enseñarme y ser una experta buscando dobles espacios. Juan, que tanto en sus periodos en España como en Finlandia siempre ha tenido algo nuevo que enseñarme y alguna que otra figura que mejorarme. Mi compañero de poyata, Javi Narbona que tantas risas me ha provocado en los días buenos, pero también en los muy malos. Gracias a todos los estudiantes que han pasado por el L3 y han dejado su huella en esta tesis, como Moisés y ese programa que me ha ahorrado horas de análisis. Y toda mi gratitud a los compañeros que han hecho de los cafés y las comidas un oasis de paz y risas en el ritmo frenético del día a día: Sara Abián y su infinito apoyo y alegría, Cris y las Lauras por propiciar algunas de las carcajadas más sonoras de la tesis, Pablo por acompañarme desde que pisamos el aula magna en la presentación del curso y recordarme que podemos leer papers por gusto además de por trabajo, Juan Carlos que además de ser la disciplina en persona tiene un corazón que no le cabe en el pecho, Carmen por ser el reflejo de que la perseverancia tiene recompensa.

AGRADECIMIENTOS/ACKNOWLEDGEMENTS

Los nuevos “minions” que han llegado al laboratorio durante los últimos meses de mi tesis, gracias por traer frescura y buen ambiente al laboratorio, por vuestra energía inagotable.

A todos los becarios del departamento que me han seguido la corriente en mis convocatorias sociales para hacer de nuestro lugar de trabajo un lugar al que querer venir cada mañana a dar lo mejor de nosotros.

El L3 ha sido mi casa durante los últimos años y no creo que pudiera haber caído en mejor lugar para formarme como investigadora y como persona.

A mi familia, que es pequeña pero más que suficiente, mi madre, Vicente y mi hermana. Me han dado siempre todo lo que he necesitado, y mi hermana me ha proporcionado de las mejores risas de estos años. Por eso esta tesis es también vuestra. También gracias a familia política, Manolo, Violeta y Manuel. Y la familia que se elige Pablo, Elena, Jose, Adri y Aitana, Sonia y CD por haber comprendido en todo momento el trabajo que conllevaba realizar una tesis doctoral y haberme regalado momentos de desconexión que no tienen precio.

A mi Álvaro. Que ha estado siempre ahí, hayamos estado cerca o lejos siempre hemos estado juntos. Tienes ganado el cielo, ya lo sabes. Tenemos toda la vida y aun así me van a faltar días para que pueda seguir agradeciéndote el infinito apoyo que has significado para mí.

INDEX

ABBREVIATIONS 1

SUMMARY/RESUMEN 5

INTRODUCTION 15

OBJECTIVES 31

MATERIALS AND METHODS 35

RESULTS 59

BLOCK I: Actinoporins: membrane pore-forming toxins produced by sea anemones 61

Article I: One single salt bridge explains the different cytolytic activities shown by actinoporins sticholysin I and II from the venom of *Stichodactyla helianthus* 63

Article II: Synergistic action of actinoporin isoforms from the same sea anemone species assembled into functionally active heteropores 77

Article III: *Stichodactyla helianthus*' de novo transcriptome assembly: Discovery of a new actinoporin isoform 91

Article IV: Structural and functional characterization of StnIII: A newly discovered actinoporin within the venom of the sea anemone *Stichodactyla helianthus*. 103

BLOCK II: The membrane pore-forming *latrotoxin macromolecular complex*: latrodectins and latroinsectotoxins produced by black widow spiders. 125

Article V: Structural and functional characterization of Latrodectins I and II, low molecular weight components from black widow spider venom. 127

Article VI: Heterologous production and characterization of δ-latroinsectotoxin, a huge insecticidal protein from black widow spider venom. 145

Summary and future perspectives 159

Article VIII: Pore-Forming Proteins from Cnidarians and Arachnids as Potential Biotechnological Tools 161

DISCUSSION 185

CONCLUSIONS 195

BIBLIOGRAPHY 199

ANNEX 209

ABBREVIATIONS

Amp	ampicilin
A_{nm}	absorbance at the indicated wavelength
BAK	Bcl-2 homologous antagonist/killer
BAX	Bcl-2 associated X protein
Bcl-2	B cell lymphoma 2
BMD	buffered minimal medium containing dextrose
BMGY	buffered glycerol-complex medium
BMM	buffered minimal medium containing methanol
BMMY	buffered methanol-complex medium
BSA	bovine serum albumin
BUSCO	benchmarking universal single-copy orthologs
CD	circular dichroism
cDNA	complementary DNA
CfTX1	*Chinorex fleckeri* toxin 1
CfTX2	*Chinorex* fleckeri toxin 2
Chol	cholesterol
CM-52	carboxymethylcellulose chromatographic support
Cryo-EM	cryo-electron microscopy
DAB	3,3'-diaminobenzidine
DEAE-cellulose	diethylaminoethyl-cellulose chromatographic support
di-18	1-PC: 1,2-dioleoyl-sn-glycero-3-phosphocholine
di-20	1-PC: 1,2-dieicosenoyl-sn-glycero-3-phosphocholine
DOPC	dioleyl- phosphatidylcholine
dsDNA	double strand DNA
$E^{0.1\%}$	extinction coefficient ($mL \cdot mg^{-1} \cdot cm^{-1}$)
EDTA	ethylenediaminetetraacetic acid
FgAFP	*Fusarium graminearum* antifungal protein
FraC	fragaceatoxin C
GRAS	generally regarded as safe
HC50	protein concentration necessary to reach 50% of total hemolysis in 10 min.
IPTG	isopropyl-β-D-thiogalactoside
ITC	isothermal titration calorimetry
LB media	Luria Bertani culture media
LCT	latrocrustaceatoxin
LIT	latroinsectotoxin
Ltds	Latrodectins
LTX	latrotoxin
LTXs	latrotoxin family
LUVs	large unilamellar vesicles
MACPF	membrane attack complex/perforin family
MALDI-TOF	matrix-assisted laser desorption ionization time-of-flight
MOPS	3-(N-morpholino)propanesulfonic acid
NMR	nuclear magnetic resonance
OD_{nm}	optical density at indicated wavelength
ORF	open reading frame
PBS	phosphate-buffered saline

PCR	polymerase chain reaction
PFP	pore-forming protein
PFT	pore-porming toxin
PLA2s	phospholipase A2
PMSF	phenylmethylsulfonyl fluoride
POC	phosphorylcholine
POPC	palmitoyl-oleyl-phosphatidylcholine
qPCR	quantitative PCR
RHA	relative hemolytic activity
RMB	relative membrane binding
S.O.C media	super optimal broth culture media
SDS-PAGE	polyacrylamide gel electrophoresis in the presence of sodium dodecylsulfate
SM	sphingomyelin
StnI	sticholysin I
StnII	sticholysin II
TAE	0.045 mM Tris-HCl, 0.001% (v/v) glacial acetic acid, 1 mM EDTA pH 8.0
TfB1	transformation buffer 1
TfB2	transformation buffer 2
T_m	protein denaturation temperature
wt	wild-type
YNB	yeast nitrogen base
YPD media	yeast, peptone, dextrose media
YPDS media	yeast, peptone, dextrose sorbitol media
Zeo	zeocin

SUMMARY/RESUMEN

Summary

1. Introduction

Pore forming proteins (PFPs) are a family of toxins that form pores in cell membranes leading to cell death by osmotic shock. These proteins remain stably folded and soluble in aqueous solution. Upon interaction with a specific receptor in the membrane (protein, lipid or sugar), they bind, oligomerize and form a pore through the membrane hydrophobic core.

Actinoporins are α-PFPs produced by sea anemones as part of their venomous cocktail. They are small (≈ 20 kDa) and usually have a basic isoelectric point (≈ 9). They share a common fold characterized by a β-sandwich flanked by two α-helices. Their specific membrane receptor is sphingomyelin. When actinoporins bind to a membrane containing this sphingolipid, they extend their N-terminal α-helical segment, oligomerize and form a cation selective pore by inserting the α-helices through the membrane core. However, the specific step order leading to a final pore, the necessity of a pre-pore and the final stoichiometry are still debated. Actinoporins constitute multigene families: A single species produces a variety of similar toxins which not necessarily display identical lytic activity or specificity. Because of their simplicity, they are an appropriate model to study the biophysical challenging transition from a water-soluble protein to a membrane bound state.

The sea anemone *Stichodactyla helianthus* produces two actinoporin isoforms: Sticholysins I and II (StnI and StnII) which are 93 % identical at the protein level but show different activity, being StnII four-fold more active than StnI when assayed against sheep erythrocytes. The reason why a single species of sea anemone usually produces a variety of toxins is still unknown. Maybe the expansion of genes coding toxin proteins increases venom effectivity by widening the range of accessible prey. Therefore, actinoporins also represent an excellent example to study this complex relationship network.

Nevertheless, PFPs are widespread toxins that in many cases appear as part of heterogeneous mixtures in which other venom components could have critical effect in PFPs toxicity. Within this framework, black widow spiders (*Latrodectus* spp.) produce latrotoxins (LTXs) which are huge (≈ 100 kDa) proteins, with acidic isoelectric point (≈ 5), that form pores in the presynaptic neurons of the neuromuscular junctions. Once made the pore, they provoke massive neurotransmitter release that leads to intense pain and paralysis. They are classified according to their prey specificity. Latroinsectotoxins (LITs), specifically affecting insects, are an interesting subfamily because of their potential biotechnological applications as bioinsecticides. LTXs assemble into a macromolecular complex whose structural and functional details have been barely studied. They appear in association with latrodectins (Ltds), which are small (≈ 6-8 kDa) and acid (pI ≈ 5) peptides which seem to be components of this *latrotoxin macromolecular complex*.

2. Objectives

Actinoporins

i. Study of the structural differences between StnI and II leading to their different hemolytic activity

ii. Analysis of their potential interaction as a modulation mechanism of their activity.
iii. Assembly of the *de novo* transcriptome of *S. helianthus* in order to search for sticholysins heterogeneity.
iv. Heterologous production and characterization of StnIII, a newly discovered actinoporin isoform.

<u>*Latrotoxin macromolecular complex*</u>

v. Heterologous production and characterization of the most highly expressed Ltds in *L. hesperus*'s venom.
vi. Heterologous production and characterization of the insect specific δ-LIT from *L. hesperus*'s venom.

3. Results and discussion

Site-directed mutagenesis experiments comprising residues within the N-terminal region of StnI and StnII revealed the presence of a key salt bridge in StnI. This bond with the β-sandwich core impairs the indispensable α-helix detachment for pore formation. Such a salt bridge is absent in StnII what justifies its higher lytic activity against erythrocytes and model lipid vesicles.

StnI and StnII were assayed in controlled proportions mixtures and characterized through cross-linking experiments, hemolysis and calcein leakage assays, as well as ITC measurements. These results show the existence of synergy between both proteins and their capacity to assemble together into functionally active heteropores. Synergy takes place at the membrane binding step. This discovery opens the door to a new and more complex regulatory dimension of the sea anemone venom toxicity.

The transcriptome of *S. helianthus* was *de novo* assembled using Illumina RNA-sequencing method. It allowed the analysis of the composition of the venom, highlighting that, although cytolysins are not the largest group in terms of variability, quantitatively speaking they do represent the majority of the transcripts analyzed. StnIII, a new actinoporin isoform, was discovered by this transcriptomic analysis. StnIII expression was significantly lower when compared with StnI and II mRNA levels.

StnIII was cloned, produced in *E. coli*, and purified to homogeneity. Its spectroscopic characterization was compatible with a folded protein resembling the archetypical actinoporin fold. It is, however, less thermostable than StnI and II. Its functional characterization showed that the minimal concentration needed to form effective pores was higher in comparison with the other two well-known actinoporins. Finally, StnIII also displayed synergy with StnII.

Regarding the characterization of the *latrotoxin macromolecular complex*, LtdI and II were cloned, produced in *Pichia pastoris* and purified to homogeneity. They are α-helical rich peptides, highly thermostable, with 6 Cys residues assembled into disulfide bonds, as confirmed by mass spectrometry experiments. Preliminary NMR data of ^{13}C-^{15}N-labelled LtdII allowed atomic assignation of two α-helical regions. LtdII did not show insecticidal or antifungal activities.

δ-LIT from *L. hesperus* was also cloned, produced in *P. pastoris* and purified to homogeneity. The spectroscopic characterization by far-UV circular dichroism was compatible with an unstructured polypeptide. Therefore, optimization of the protocols used is needed.

4. Conclusions

StnI establishes a salt bridge which suggests a mechanism that could be of general application to actinoporins and reinforces the key importance of this bond factor in their functionality.

Synergy among actinoporins represents a new dimension in venom activity regulation, increasing the versatility of defense/attack responses. The existence of StnIII reinforces the complex network stablished among actinoporins, rising the biological significance of its discovery.

Both Ltds and δ-LITs can be produced in *P. pastoris* with high yield. Their study in combination will elucidate the latrotoxin macromolecular complex mechanism from structural and functional points of view, facilitating its application as bioinsecticides.

Resumen

1. Introducción

Las proteínas formadoras de poros (PFP) son una familia de toxinas capaces de matar células por choque osmótico, precisamente porque forman poros en sus membranas. En disolución acuosa, estas proteínas permanecen plegadas y estables. Al interactuar con un receptor específico de la membrana (proteína, lípido o azúcar), se unen a ella, oligomerizan y forman un poro a través del núcleo hidrófobo de la membrana.

Las actinoporinas son α-PFPs producidas por anémonas marinas como parte de su cóctel venenoso. Son pequeñas (≈ 20 kDa) y suelen tener un punto isoeléctrico básico (≈ 9). Comparten un motivo conformacional común, caracterizado por un sándwich β flanqueado por dos hélices α. Su receptor de membrana específico es la esfingomielina. Cuando las actinoporinas se unen a una membrana que contiene este esfingolípido, extienden su segmento helicoidal N-terminal, oligomerizan y forman un poro selectivo de cationes, insertando sus hélices α del extremo N-terminal a través del núcleo de la membrana. Sin embargo, el orden específico de las etapas que conducen a la formación del poro, así como la naturaleza de posibles estados intermedios, o su estequiometría final, todavía son objeto de debate. Estas actinoporinas constituyen además familias multigénicas: una sola especie produce una variedad de toxinas similares que no necesariamente muestran una actividad lítica o una especificidad idénticas. Debido a su simplicidad, son un modelo apropiado para estudiar la todavía no bien comprendida transición de una proteína soluble en agua a un estado en el que se integra en membrana.

La anémona de mar *Stichodactyla helianthus* produce dos isoformas de actinoporina: las sticholisinas I y II (StnI y StnII), que son un 93 % idénticas pero muestran una actividad diferente, siendo StnII cuatro veces más activa que StnI cuando se ensayan contra los eritrocitos ovinos. Todavía se desconoce la razón por la que una sola especie produce diferentes toxinas. Tal vez la expansión de los genes que codifican para proteínas tóxicas aumenta la eficacia del veneno al ampliar la gama de presas accesibles. Por lo tanto, las actinoporinas también representan un excelente ejemplo para estudiar esta compleja red de relaciones.

No obstante, las PFPs son toxinas muy abundantes que, en muchos casos, aparecen como parte de mezclas heterogéneas en las que otros componentes del veneno podrían tener un efecto crítico en su toxicidad. En ese marco, la araña viuda negra (*Latrodectus* spp.) produce latrotoxinas (LTXs), que son proteínas enormes (≈ 100 kDa) con punto isoeléctrico ácido (≈ 5), que forman poros en las presinapsis neuronales de las uniones neuromusculares. Una vez formados los poros, provocan una liberación masiva de neurotransmisores que produce dolor intenso y parálisis. Se clasifican según la especificidad de su presa. Las latroinsectotoxinas (LITs), que afectan específicamente a los insectos, son una subfamilia interesante por sus potenciales aplicaciones biotecnológicas como bioinsecticidas. Las LTXs se ensamblan en un complejo macromolecular cuyos detalles estructurales y funcionales apenas han sido estudiados, y en el que aparecen asociadas a las latrodectinas (Ltds), que son péptidos pequeños (≈ 6-8 kDa), también ácidos (pI ≈ 5), que parecen ser componentes del *complejo macromolecular latrotoxina*.

2. Objetivos

Actinoporinas

i. Estudio de las diferencias estructurales entre StnI y II que conducen a su diferente actividad hemolítica.
ii. Análisis de su posible interacción, como mecanismo de modulación de su actividad.
iii. Ensamblaje *de novo* del transcriptoma de *S. helianthus* con el fin de estudiar la heterogeneidad de las sticholisinas.
iv. Producción y caracterización heteróloga de StnIII, una isoforma de actinoporina recientemente descubierta.

El complejo macromolecular latrotoxina

v. Producción y caracterización heteróloga de las Ltds más expresadas en el veneno de *L. hesperus*.
vi. Producción y caracterización heteróloga de δ-LIT, una latrotoxina del veneno de *L. hesperus* que es específica de insectos.

3. Resultados y discusión

Experimentos de mutagénesis dirigida sobre residuos comprendidos dentro de la región N-terminal de StnI y II revelaron la presencia de un puente salino clave en la funcionalidad de StnI. Al establecerse con el sándwich β, perjudica el indispensable desprendimiento de la hélice α para que se formen los poros. Tal puente salino está ausente en StnII, lo que explica su mayor actividad lítica contra los eritrocitos y vesículas modelo.

StnI y StnII fueron ensayadas en mezclas de diferentes proporciones usando experimentos de entrecruzamiento, ensayos de hemólisis y de liberación de calceína, así como mediante medidas de ITC. Estos resultados muestran la existencia de sinergia entre ambas proteínas y su capacidad de ensamblarse en heteroporos funcionalmente activos. La sinergia tiene lugar en el paso de unión a la membrana. Este descubrimiento abre la puerta a una nueva y más compleja dimensión reguladora de la toxicidad del veneno de la anémona de mar.

El transcriptoma de *S. helianthus* fue ensamblado *de novo* usando el método de secuenciación de RNA de Illumina. El análisis de la composición del veneno reveló que, si bien las citolisinas no son el grupo más numeroso en términos de variabilidad, cuantitativamente sí representan la mayoría de los tránscritos analizados. StnIII, una nueva isoforma de actinoporina, fue descubierta gracias a este análisis transcriptómico. La expresión de StnIII fue significativamente menor cuando se comparó con los niveles de mRNA de StnI y II.

StnIII fue clonada, producida en *E. coli* y purificada a homogeneidad. Sus características espectroscópicas son compatibles con una proteína correctamente plegada con la conformación arquetípica de las actinoporinas. Sin embargo, es menos termoestable que StnI y II. Su caracterización funcional demostró que la concentración mínima necesaria para formar poros efectivos era mayor que en el caso de las otras dos actinoporinas conocidas. Por último, StnIII también mostró sinergia con StnII.

En cuanto a la caracterización del *complejo macromolecular latrotoxina*, LtdI y II fueron clonadas, producidas en *Pichia pastoris* y purificadas a homogeneidad. Son péptidos ricos en estructura helicoidal, altamente termoestables y con sus 6 Cys ensambladas en enlaces disulfuro, como se ha confirmado mediante experimentos de espectrometría de masas. Los

datos preliminares de RMN usando LtdII etiquetada con ^{13}C-^{15}N permitieron la asignación a nivel atómico de dos regiones helicoidales α. LtdII no mostró actividades insecticidas o antimicóticas.

δ-LIT de *L. hesperus* también fue clonada, producida en *P. pastoris* y purificada a homogeneidad. La caracterización espectroscópica mediante dicroísmo circular en el ultravioleta lejano fue compatible con un polipéptido no estructurado. Es necesario por tanto optimizar los protocolos utilizados.

4. Conclusiones

StnI establece un puente salino que sugiere un mecanismo que podría ser de aplicación general a las actinoporinas y refuerza la importancia clave de este tipo de unión en su funcionalidad.

La sinergia entre las actinoporinas representa una nueva dimensión en la regulación de la actividad del veneno, aumentando la versatilidad de las respuestas de defensa o ataque. La existencia de StnIII refuerza la existencia de una compleja red de relaciones establecida entre las actinoporinas, aumentando la importancia biológica de su descubrimiento.

Tanto las Ltds como la δ-LIT pueden ser producidas en *P. pastoris* con alto rendimiento. Su estudio en combinación permitirá dilucidar el mecanismo del *complejo macromolecular latrotoxina* tanto desde el punto de vista estructural como funcional, facilitando su aplicación como bioinsecticidas.

INTRODUCTION

1. Venoms through history

Venoms and toxic compounds have developed an important role in human history. These compounds remain hidden in plain sight, causing fatal outcomes by contact or ingestion. The very first example is the Biblical story starred by Adam and Eve within the Book of Genesis (Genesis 3:1). There were two venomous elements that triggered the expulsion of Adam and Eve from the Garden of Eden: a wise snake and a poisonous apple tree. Snakes are common venomous animals that provoke an inherent fear in the humankind. God warned about the poisonous apple tree "*If you take of it or put your hands on it, death will come to you*" (Genesis 3:3). This allegoric story about obedience and temptation reflects the fear of the consequences caused by venom and poison. But this is only one of the many examples we can found through history. The Greek philosopher Socrates was condemned to death by drinking poison hemlock, according to Plato's *Phaedo*. The Egyptian governor Cleopatra VII committed suicide by poisoning herself although the definite method is still unknown and varies from using a toxic unguent to allowing an asp to bite her.

These, among other events, described in ancient history increased the inherent apprehension to venom and poison. Most venomous animals are small size compared to their predators and, in many cases, they do not seem dangerous at first sight. This is the case of sea anemones, corals and jellyfishes for example. On the other hand, and at least from the point of view of humans, arachnids (in general) and spiders (in particular) usually produce fear, probably because, as terrestrial animals that we are, we have a greater baggage of coexistence with them. Nevertheless, it is possible to find venomous animals from a wide variety of far related phylogenetic origins from vertebrates like reptiles, amphibians, and even mammals, to invertebrates like insects, arachnids and elder phylum like cnidaria. All these animals use venom for predatory, defensive or competitive purposes.

However, ancient civilizations have also taken advantage of venom effects on the organism to use them as drugs to treat diseases, obviously only based on experience and without any mechanistic or molecular knowledge (King 2011, Machkour-M'Rabet 2011)

2. Venom evolution

It is usual to confuse the terms 'poisonous' and 'venomous', which are sometimes wrongly used indistinctly. However, poisonous refers to a passive delivery by contact, either through the skin or by ingestion, whereas venomous refers to an active delivery of toxic compounds from predator to prey, usually through specialized stinging structures like fangs (snakes), spines (fishes), nematocysts (sea anemones), or chelicerae (spiders). Maybe due to this active behavior, venoms are then the product of an evolutionary adaptation that balances predator-prey relationships forcing them both to co-evolve for survival. Thus, we are talking of a "molecular dance" where preys develop venom resistance through different mechanisms to escape from predators which, simultaneously are continuously adapting their toxic cocktail to the new evolutive landscape in order to keep being able of damaging their preys (Arbuckle 2017, Calvete 2017, Casewell 2013).

An extended hypothesis about how venom appears into species is that a proto-toxin gene is duplicated, and its new copy of the gene is then expressed in the venom gland. Once in

its new location, this new venom gland-expressed gene suffers multiplication events and produces different protein isoforms that gain a new function related to toxicity. Due to this duplication-neofunctionalization mechanism, it is usual to find venom toxins genetically structured as multigene families (Calvete 2017, Rivera-de-Torre 2018, Valle 2015). This theory is sustained because most protein products present in venom develop physiological functions when expressed in other locations. For example, phospholipases A2 (PLA2s), which are enzymes that catalyze the hydrolysis of glycerophospholipids at the sn-2 position to release free fatty acids and lysophospholipids and are involved in cell signaling, are also frequent venom toxins with the aim of damaging the cell membrane of their targets because the resulting enzymatic products modify membrane curvature and trigger stress and inflammation signals (Trento 2019).

Venom is an example of convergent evolution, since venomous system can be found in far related species but is not present in their last common ancestor, as happens with other structures like echolocation system in bats and cetaceans, wings in insects and birds, or the most well-known example, the eyes, that can be found in cephalopods (octopus), vertebrates and even cnidaria (jellyfishes) (Schendel 2019).

Venoms are complex biochemical cocktails containing salts, peptides, proteins and small metabolites acting as bioactive compounds (Schendel 2019). Upon delivery, these toxins interact with prey cellular structures to cause damage, altering physiological and signaling processes. A mechanism which implicates an interaction, at the molecular level, between the toxic components of the venom and cellular structures of the target (King 2011). Delivery systems like chelicerae in spiders and nematocysts in cnidarians run through the first barrier encountered in the prey, the epithelium. These piercing structures inflict a first harmful injury and deliver toxins closer to the final molecular target. A process which is eased specialized toxins, like metalloproteases for example, that digest extracellular matrix components and scaffold proteins present in the cell interstitial space. Coagulation cascade is a common target of small non-proteinaceous metabolites like histamine or serotonin, which interfere by altering coagulation time or provoking vasodilatation, and thus unleashing fatal consequences for the attacked organism. The most obvious second line of cell-defense is the boundary defined by the plasma membrane. A boundary composed of lipid and proteins, which defines the cell as a compartment separated from the extracellular environment, establishing a well-defined frontier between the intra and extracellular compartments which display very different physicochemical properties and composition (Goñi 2014). Thus, the most widespread structures encountered by venomous cocktails on any type of prey are the transmembrane and peripherical proteins integrated within the lipidic bilayer, as well as the lipid membrane itself. Within this idea, ion channels are commonly targeted by toxins that block or prevent closing the gate defined by the channels. Consequences of this molecular action are derived from the ion imbalance between inside and outside the cell, usually producing intense pain, paralysis, massive release of neurotransmitters or cell death by depolarization of the membrane. Another type of membrane-targeting toxic proteins frequently appearing in venoms are targeted not to its protein constituents but directly to its structural integrity, such as the aforementioned phospholipases or the widespread pore-forming toxins (PFTs). Since the plasma membrane has critical importance for cell viability, its disruption has important consequences that, in many cases, imply cell death by osmotic shock.

Finally, some venom toxins are also aimed to intracellular structures, disabling key processes like protein production or oxidative phosphorylation in mitochondria (Figure 1).

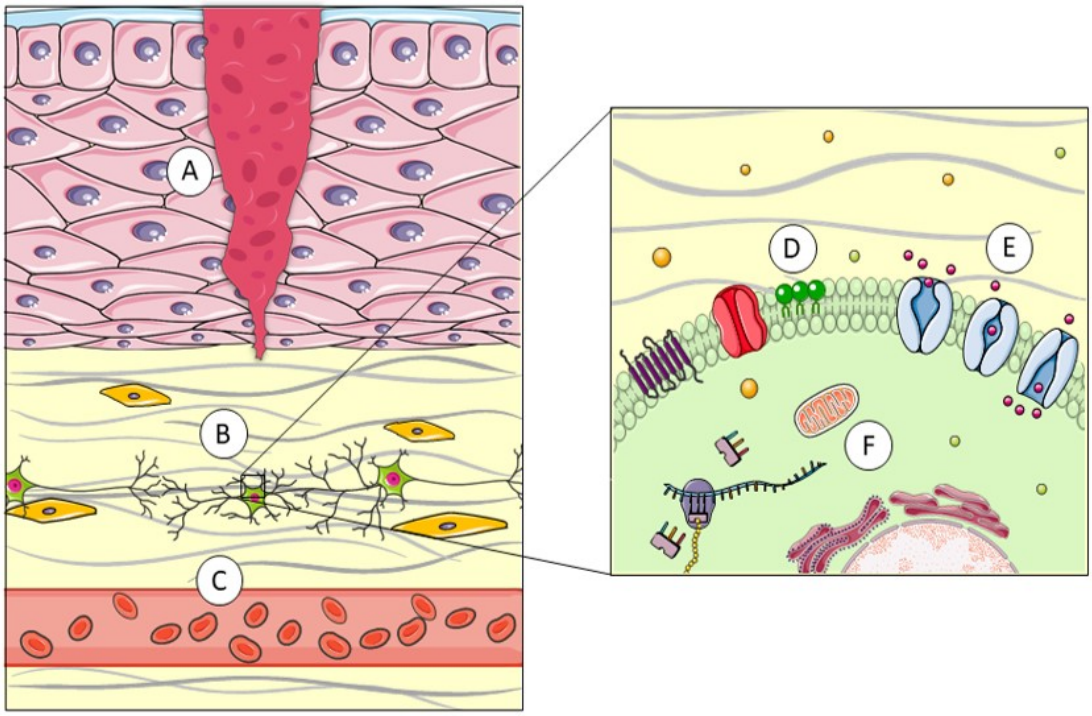

Figure 1. Venomous animals inflict damage in target individuals because they are able to interact with their molecular structures dysregularing the metabolic pathways and processes they are involved in. Piercing delivery systems disruptes epithelium, cause physical damage and approximate venom to final targets (A). Proteases diggest the extracellular matrix (B) easing other venom components reaching cells. Some toxins affect circulatory system increasing or decreasing arterial pressure or inducing vasodilatation (C). Plasma membrane, probably the most frequent toxins' target in nature, is attacked by phospholipases and pore-forming toxins which modify its curvature or compromise its integrity (D). Neurotoxins binds to ion channels disrupting the balance stablished across the membrane (E). Other toxins act intracellularly, affecting mitochondrial oxidative phosphorylation or inhibiting ribosomal protein production, for example (F) (Rivera-de-Torre 2019).

As stated before, ancient civilizations used venoms as empirical treatments for a wide variety of diseases. Within the context of the pathologically affected metabolic pathways, we now know that some toxins have the ability stablish high affinity interaction with specific molecules, balancing or modulating disease effects. Nowadays, it is possible to study venom components in detail and reveal the molecular features of these interactions, allowing to synthetize and test native or modified molecules that serve as therapeutic treatments (King 2011).

3. Pore forming proteins (PFPs)

PFPs are a family of toxins whose toxic activity relies in the disruption of the lipidic membrane by forming pores within. This kind of toxins escape to the archetypal biochemical classification that sorts proteins into water-soluble or membrane macromolecules (García-Linares 2017, Lella and Mahalakshmi 2017, Tanaka 2015b). They remain stably folded and soluble but, upon interaction with a membrane receptor in the target cell, that can be a membrane bound or transmembrane protein, a sugar, or a specific lipid, undergo a metamorphosis from a monomeric water-soluble protein to an oligomeric transmembrane

assemble, that forms a pore within the membrane core. The specific pore-formation mechanism driving this transformation largely depends on the toxin, but all of them take advantage of the local concentration increase, once the protein is bound to the membrane, to trigger oligomerization. Given that, in those conditions, diffusion is restricted to a bidimensional plane, oligomerization and final pore formation appears to be favored. Depending on the size and the physicochemical properties of the resulting channel, the resulting pore can be permeable to different ions, or even small proteins or peptides. In most cases, the outcome is cell death by osmotic shock.

There are many ways to categorize PFPs. The most extended one classifies them regarding the secondary structure of the protein fragment that builds the pore wall. Hence if pore walls are formed by α-helices, they are classified as α-PFPs; on the other hand; if they are defined by β-sheets, the protein is considered a β-PFP (García-Ortega 2011, Parker and Feil 2005).

PFPs are implicated in both physiological and pathological functions. They are produced by many pathogenic bacteria, playing a major role as virulence factors (Anderluh and Lakey 2008, Dorca-Arevalo 2018, Gonzalez-Bullon 2019, Kondos 2010, Law 2010). They can also be found in more complex organisms such as mammals, where they usually develop non-pathological but physiological functions. Most probably, the best mammals' examples would be the complement system (MACPF), involved in the action of both the innate and adaptive immune systems of vertebrates, and the BAX/BAK protein families, responsible for the apoptosis regulation at the mitochondrial level (Pena-Blanco and Garcia-Saez 2018).

This large and widespread family of proteins are considered highly damaging molecules since, as stated before, they attack the primordial feature of any living cell: the plasma membrane. Among the existing mechanisms used by PFPs to target their objective the most common ones are the interaction with a specific lipid, like cholesterol (Chol) (Rossjohn 1997, Rossjohn 2007) or sphingomyelin (SM) (Anderluh and Lakey 2008, Bakrač 2008, Endapally 2019, García-Linares 2016b, Palacios-Ortega 2019), or the recognition of a specific membrane protein receptor. PFPs targeting certain abundant lipids may seem not highly specific, but as part of the venom complex mixture constitute key elements to pursue a wide range of enemies. Finally, it is also remarkable how PFPs usually show fast kinetics (García-Linares 2016b, García-Linares 2017), explaining why they can be used for both predatory and defensive purposes (Casewell 2013, Clark 2019)

3.1 Cnidarian's Pore Forming Proteins

Cnidaria is the oldest linage of venomous animals. Its study from the evolutionary and phylogenetic point of view is interesting to fill the gaps in most general genetic and phylogenetic studies focused not only on venom evolution (Calvete 2017), but also in the appearance of the nervous system or the generation of bilateralism (Technau and Steele 2011). The phylum cnidaria comprises around 9000-10000 aquatic species, most of them living in salt-water. The phylum is divided in two main groups. Anthozoa is a class that includes sea anemones and corals species living as sessile polyps and it is subsequently divided into the subclasses Hexacorallia and Octocorallia, according to their different fold radial body symmetries. The other group is the subphylum Medusozoa, which comprises four other classes: Hydrozoa (*Hydra* and colonial polyps), Scyphozoa (true jellyfishes), Cubozoa (box jellyfishes) and Staurozoa (Stalked

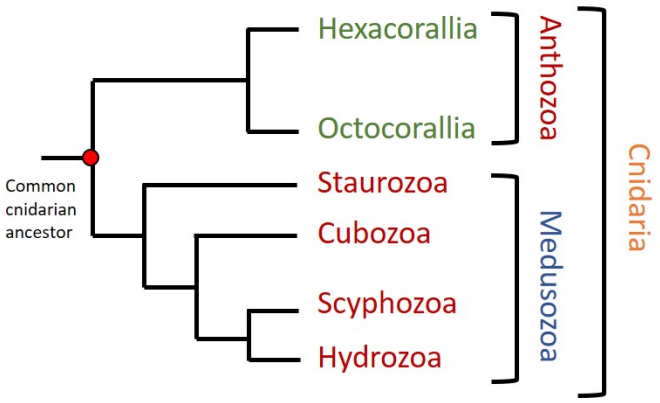

Figure 2. Phylogenetic tree of cnidaria phylum. Cnidaria are divided in two groups: The Anthozoa, containing Hexacorallia and Octocorallia subclasses and Medusozoa, including Staurozoa, Cubozoa, Scyphozoa an Hydrozoa classes. Classes are highlided in red, subclasses in green, subphylum in blue and phylum in orange. Modified from (Technau and Steele 2011)and (Koch and Grimmelikhuijzen 2019).

jellyfishes). Most species in this group have a life cycle including polyp and medusa stages (Kayal 2018, Koch and Grimmelikhuijzen 2019, Technau and Steele 2011) (Figure 2). These animals are clinically relevant because of their venomous effects. The consequences of their sting vary from non-hazardous symptoms like burning feeling, itching and redness typically caused by sea anemones and corals (Tezcan and Gozer 2015) to important grievances like severe pain, cardiovascular distress and loss of conscious caused by the most dangerous species like the Australian box jellyfish (*Chironex fleckeri*)(Andreosso 2018, Beadnell 1992, Lau 2019).

As stated before, animals have stinging venom administration systems. These specialized structures responsible to traverse the epidermal barrier and inject the venom in prey are called nematocysts in sea anemones. They discharge upon pressure activation of specialized cnidocytes cells (Arbuckle 2017, Casewell 2013). Cnidaria lineage lacks a centralized venomous system so cnidocytes are not only present in tentacles to entrap the prey, but also surrounding in the oral disk to paralyze the prey or even within the column base, as part of specialized structures used for inter- and intra-specific competition (Macrander 2015b, Rojko 2016).

Like most animal venoms, Cnidarian venom is composed by salts, small metabolites, peptides and proteins. Within the last group, PFPs constitute one of the most important toxin class in cnidarians (Macrander 2015a, Madio 2019, Madio 2017, Rivera-de-Torre 2018). These toxins play a major role in their toxicity. The aforementioned Cubozoan Australian Box Jellyfish (*Chironex fleckeri*), for example, owes its extreme venomous potency to two highly abundant PFPs, CfTX-1 and 2, displaying potent hemolytic activity (Andreosso 2018, Brinkman and Burnell 2007, Brinkman 2014). In fact, sea anemones host one of the most important and well-studied families of PFPs: actinoporins.

3.1.1 Actinoporins

Actinoporins are a well-studied group of α-PFPs produced by sea anemones as part of their venom. Regarding their physicochemical properties, actinoporins are relatively small proteins (around 20kDa) that usually exhibit a basic isoelectric point (around 9) and lack cysteines. They are produced as immature products comprising a pre-propeptide region and a mature toxin. The toxin matures by cleavage of the pre-propeptide upon secretion to the cnidocyte lumen (Rivera-de-Torre 2018, Valle 2015). They appear as multigene families, therefore, a single sea anemone species has several genes for similar but no-identical

actinoporins. As explained above, this is quite common in venoms and is probably generated by gene duplication, as an evolutionary advantage to fit into, or colonize, new landscapes, driven by the innate pressure of the predatory and defensive competition for survival (Macrander and Daly 2016, Valle 2015). Actinoporins do not need a protein receptor to bind the membrane, but a specific lipidic one, SM (Bakrač 2008, Bernheimer and Avigad 1976, Bjorkbom 2010, García-Ortega 2011). In addition, Chol is not strictly needed but its presence modulates pore-formation mechanism (Alm 2015, García-Linares 2015, García-Linares 2016b, Palacios-Ortega 2016), a very important observation given the high percentange of this steroid in vertebrate membranes. Indeed, actinoporins represent a simple, and therefore optimum, model to study the biophysical aspects of the transformation of a water-soluble protein into a membrane integrated structure.

Actinoporins have been found in at least 20 venomous sea anemone species (Macrander and Daly 2016). They are conserved inter and intraspecific among all them, reaching sequence identity values over 90% in many instances (García-Linares 2016b, Valle 2015). This high sequence conservation is consequently reflected by a characteristic conserved three-dimensional protein fold (Athanasiadis 2001, García-Linares 2013, Hinds 2002, Mancheño 2003, Mechaly 2011, Tanaka 2015a), consisting of a β-sandwich flanked by two short α-helices (Figure 3). Despite of their similarity in terms of sequences and global structure, they display different toxic properties, showing a high variability regarding membrane binding and pore formation. This variability is attributed to the trend to expand the range of prey that can attack the sea anemones that produce actinoporins.

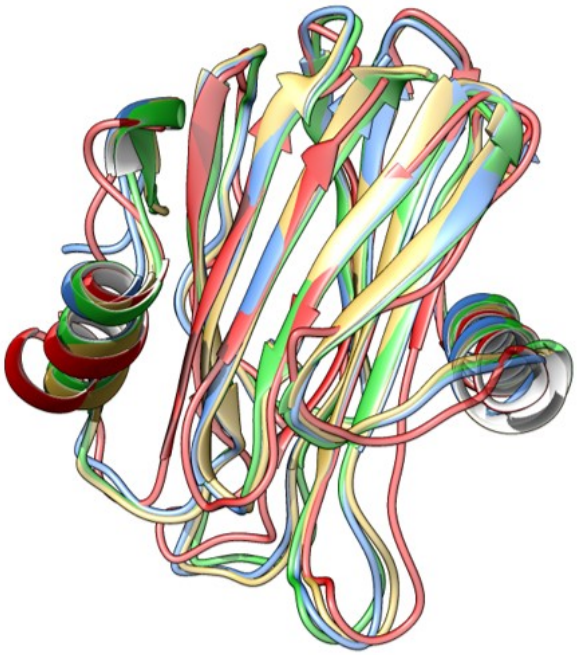

Figure 3. Overlapping actinoporin structures. StnI (2KS4, red) and StnII (1GWY, blue) from S. helianthus, FraC (3W9P, green) from A. fragacea, and EqtII (1IAZ, yellow) from A. equina. The four of them share a common characteristic fold, a β-sandwich flanked by two short α-helices.

Actinoporins remain stably folded and soluble in water solution but, upon interaction with lipid membranes containing SM, they bind to the bilayer and detach their N-terminal stretch from the β-sandwich core This segment then lies parallel to the membrane surface while actinoporin monomers begin to establish protein-protein interactions to oligomerize. Simultaneously, the amphipathic N-terminal α-helix extends and penetrates the membrane hydrophobic core, finally forming a cation-selective pore (Alegre-Cebollada 2007b, Alegre-Cebollada 2007c, Bakrač and Anderluh 2009, Cosentino 2016, García-Linares 2015, García-Linares 2017, García-Ortega 2011) (Figure 4). This is a mechanism draft which is subject of general consensus but, however, the specific step order leading to the final pore formation

(Cosentino 2016, Morante 2016, Subburaj 2015, Tanaka 2015a, Tanaka 2015b), the implication of 'pre-pore' structures during the process(Morante 2016, Rojko 2013), and, last but not least, the stoichiometry and detailed pore structure (Cosentino 2016, Mancheño 2003, Mechaly 2011,

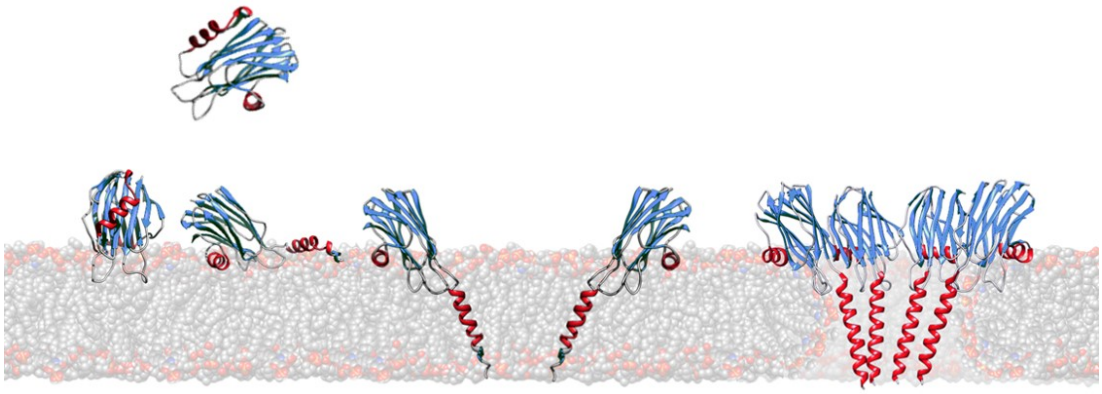

Figure 4. Actinoporin's pore formation mechanism overview. Actinoporins remain stably folded and soluble in water solution but upon interaction with lipid membrane containing SM, they detach N-terminal α-helix domain parallel to the membrane. Then, monomers oligomerize and insert N-terminal domain within the hydrophobic membrane pore, finally stablishing a cation selective

Subburaj 2015, Tanaka 2015a) are still controversial.

There are three different solved structures of actinoporins' transmembrane pore published, but only two of them are widely accepted as a significant biologically active and functional ensemble. Attending to the chronological order of publication, the first of them suggested a tetrameric toroidal protein-lipid structure (Martín-Benito 2000, Rojko 2014, Rojko 2013), where phospholipid heads would play a key role in lining the lumen of the pore channel (Figure 5). Nonetheless, some years later, a non-toroidal nonameric pore was also proposed based on a detergent containing crystalline structure for fragaceatoxin C (FraC), an actinoporin produced by *Actinia fragacea* (Mechaly 2011). This FraC model was later amended by the very last and most detailed model of actinoporins' pore, solved at atomic resolution from a crystalline lipid-containing octameric lipid-containing pore (Tanaka 2015a) (Figure 5). In this structure, lipids also play an important role in configuring the channel walls by accommodating through fenestrations (Figure 5). Considering these three structures solved so far, and the assembling kinetic studies performed by some other authors(García-Linares 2016a, García-Linares 2014, García-Linares 2017, Subburaj 2015), it seems feasible to speculate that the three of them just represent different frames of the same movie. The highly dynamic movie of actinoporins' pore formation where the different frames (intermediate oligomeric species) would be better represented depending on the protocols followed to freeze them in order to be study a "static" thermodynamically stable structure.

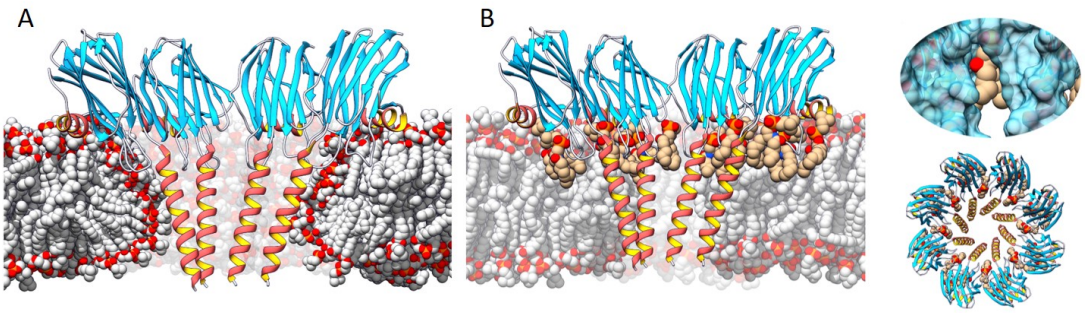

Figure 5. Two main models have been proposed for actinoporins' pore structure. A tetrameric structure in which membrane adopts a toroidal shape around the pore walls (A), and an octameric lipid-protein structure in which lipids (in tan color) are accommodated through pore walls fenestrations (see inserts on the right) (B). Adapted from (Rivera-de-Torre 2019).

Regarding the water-soluble monomeric structures, in combination with the now solved pore structures (Castrillo 2009, Mancheño 2003, Tanaka 2015a), it is possible to differentiate at least four well defined functionally relevant domains: a cluster of aromatic amino acid residues, an array of basic amino acids, a phosphorylcholine (POC) binding site, and the N-terminal, α-helix containing, fragment of the first 30 residues (Figure 6). The exposed cluster of aromatic residues has an important role in the very first membrane binding steps, indeed, mutations in this region result in less hemolytic variants with reduced membrane affinity (Alegre-Cebollada 2008, Alegre-Cebollada 2004, García-Linares 2015, García-Linares 2016a). The array of basic amino acids has also been proposed to be critical in the initial steps of membrane recognition via interaction with negatively charged regions of the lipid head groups (García-Ortega 2011, Hinds 2002). The POC binding site is responsible of SM head recognition. It is partly hydrophobic and partly hydrophilic with the interesting feature that some of the participating residues are also members of the aromatic cluster. During the interaction, the positively charged head of the POC is stabilized by π-cation interactions with the aromatic ring of two tyrosine residues,

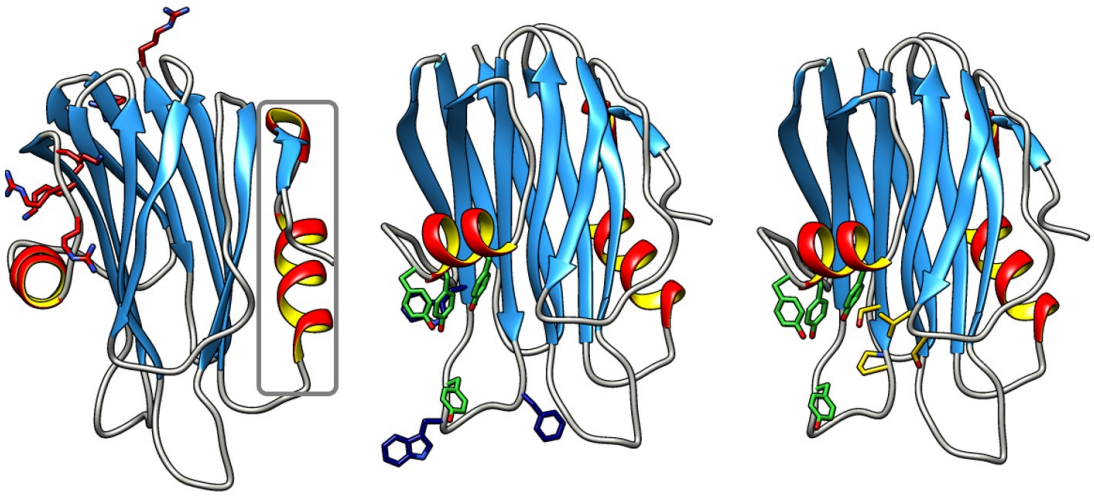

Figure 6. Four different functionally relevant domains can be distinguished in StnII water-soluble three-dimensional structure (PDB: 1GWY). The N-terminal α-helix containing domain squared in grey), an array of exposed and basic amino acids (in red), a cluster of aromatic residues (in navy blue), and the POC binding site (in yellow). Residues taking part in both the cluster of aromatic residues and the POC binding site are highlighted in green.

whereas the phosphate group interacts with the phenolic hydroxyl groups of these residues and is also probably stabilized by cationic side chain of basic amino acids (García-Ortega 2011, Mancheño 2003). The latest octameric pore structure of FraC proposes the existence of additional lipid-binding sites, mostly SM, but their existence has not been proved in enough detail yet, though is considered as highly probable. Finally, the N-terminal 30 residues long stretch, comprising one of the two α-helices, is the domain detaching from the β-sheet core to form the pore walls (Figures 3, 4 and 5). It is crucial segment for pore formation, but it does not

appear to be involved in membrane attachment (Hong 2002, Kristan 2007). This region is precisely the most variable region within actinoporin sequences. Slightly differences in this region seem have dramatic consequences regarding conductivity properties of the pore, accounting for the differences in toxicity (Casallanovo 2006, Ros 2012) (Figure 6).

3.1.1.1 Sticholysins

Stichodactyla helianthus, commonly known as sun anemone, is a carpet-like anemone from the Caribbean Sea. It belongs Stichodactylidae family and as other members of this family it is a venomous individual. *S. helianthus* produces two well-known actinoporin isoforms: Sticholysin I (StnI) and sticholysin II (StnII) that can be easily detected in the crude venom (Lanio 2001). They share 93% of their sequence but show quite different membrane binding affinities and subsequently pore forming and hemolytic activities (Alegre-Cebollada 2007a, Álvarez 2009, García-Linares 2013, García-Linares 2016b, Martínez 2002, Ros 2012, Valcarcel 2001). In agreement with their high identity, they also show almost identical three-dimensional structures (Castrillo 2009, Mancheño 2003) (Figure 7), what is reflected by the indistinguishable far-UV circular dichroism spectra (Figure 8).

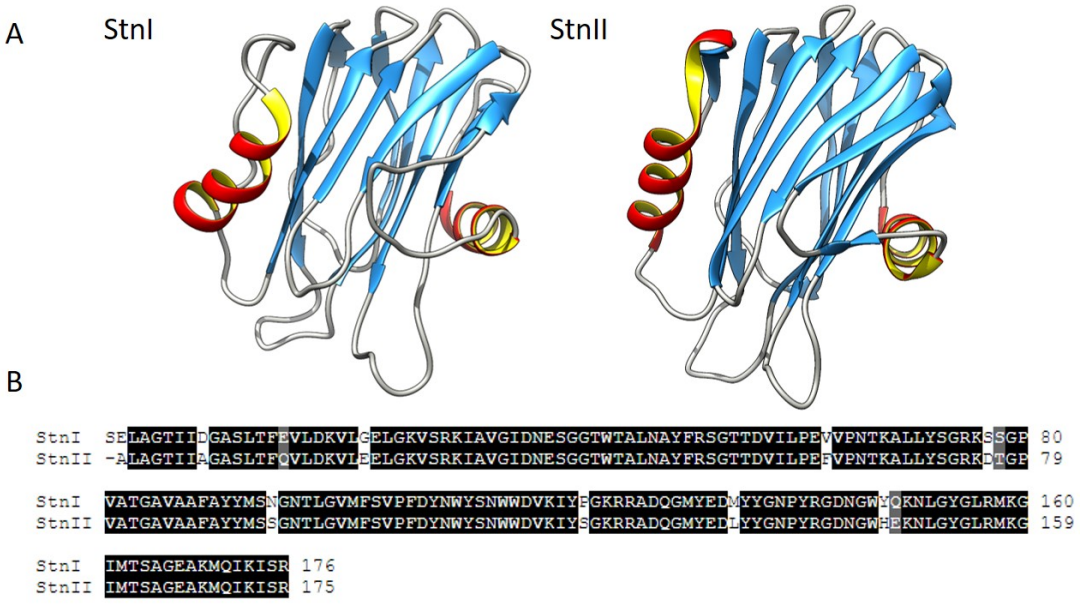

Figure 7. Three-dimensional structures of StnI (2KS4) and StnII (1GWY) (A). StnI and StnII protein sequence alignment (B). Identical residues are highlighted in black, chemically conserved residues are highlighted in grey and non-conserved residues remain backgrounded in white.

StnI and II can be independently produced in *E. coli* on their mature active form, avoiding the risk of cross-contamination (Alegre-Cebollada 2007a). This has allowed the study of both isoforms independently. At the beginning of this thesis it was yet unknown whether they could interact with each other in order to modulate both their toxic individual effects. StnII is around seven-fold more active than StnI, at least in terms of hemolytic potency when assayed against sheep erythrocytes. It also displays five-fold better binding ability to model membranes containing SM and Chol than StnI. Both have similar aromatic residues content, so they share similar spectroscopic characteristics such as molar extinction coefficients or relative emission Trp yield (Table 1). Small differences in their near-UV circular dichroism spectra are just due to the extra Tyr present in StnI (StnI Tyr 148) (Figure 8).

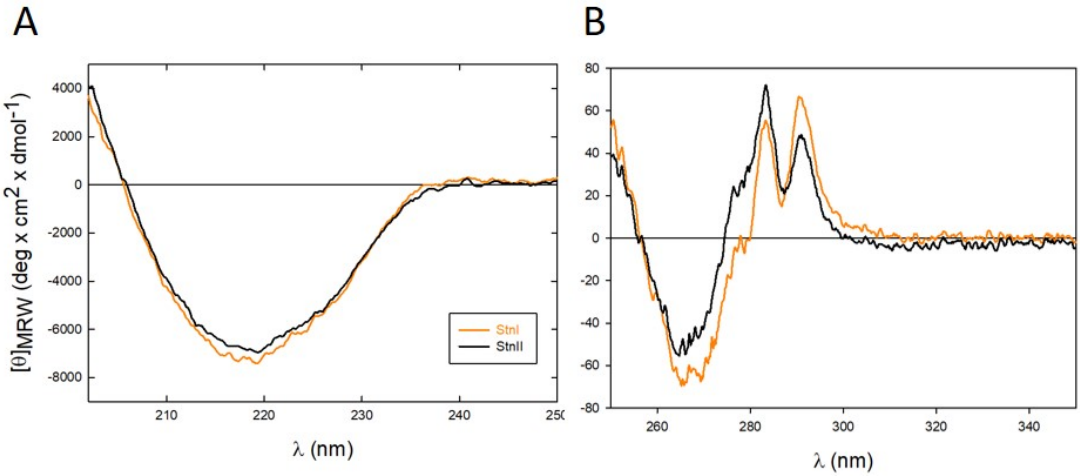

Figure 8. (A) Far-UV circular dichroism spectra for StnI and StnII show identical shape since they share a common secondary structure core. (B) Near-UV circular dichroism spectra for StnI and StnII shows slight differences due to the different content in Tyr residues. StnI is showed in orange and StnII in black.

As with many other actinoporins, most differences between StnI and II are concentrated in the N-terminal segment and involves changes from hydrophobic to charged residues, shifting the net hydrophobicity of the sequence, a feature which might accomplish for their toxicity differences.

Table 1. Calculated extinction coefficients, content of Trp and Tyr residues, predicted pI, HC50 and relative hemolytic activity (RHA) Values. ITC binding data to DOPC:SM:Chol (1:1:1) LUVs are also shown. (García-Linares 2016a).

	$E^{0.1\%}$	Number of Tyr residues	Number of Trp residues	Predicted pI value	HC_{50} (nM)	RHA[a]	ITC binding to (DOPC:SM:Chol) 1:1:1		
							n	K_b ($x10^{-8}$ M^{-1})	RMB[b]
StnI	2.55	13	5	8.96	3.0	0.133	47±4	0.49±0.15	0.23
StnII	2.54	12	5	8.99	0.4	1.000	39±4	1.70±0.90	1.00

[a]Relative hemoliytic activity calculated as HC_{50}(StnII)/HC_{50}(StnI)
[b]Relative membrane binding values calculated according to [n(StnII) × K(StnI)]/[n(StnI) × K(StnII)] where n is the number of lipid molecules affected by each protein molecule bound.

3.2 Arachnid's Pore Forming Toxins

Aranae is the largest order of arachnids with around 40000 member species. This group includes air-breathing animals that have eight legs, like spiders, mites or harvestmen. Spiders

have some other mobile appendixes, like pedipalps, which are adapted to a wide variety of functions from feeding to reproduction, and chelicerae, which in most venomous species are connected to venom glands and are involved in predatory feeding function. Venomous spiders comprise around 100 families. In contrast to cnidarians, they have a localized venom system, in which paired venom glands are connected through a canal with fangs located at the edge of the chelicerae appendixes. Venom production is mediated by holocrine secretion: venom components are produced intracellularly and stored in the cytosol of the cell. Then, productive cells disintegrate emptying their content within venom gland lumen. Considering the high diversity of spider species, it can be said that they represent the largest clade of venomous animals. However, biochemical study of spider venom has been mostly focused on species related with human envenomation events because they have an obvious and direct effect on human health.

Spiders are professional insect hunters, whose venomous arsenal has been adapted to specifically attack, immobilize and kill their specific preys. Nevertheless, some spiders have developed the ability to damage mammals, or crustaceans, presumably as an adaptative defensive feature against predation. Within this idea, individuals from *Latrodectus* genus, also known as black widow spiders, constitute a group within Theridiidae family that includes 32 different species ("World Spider Catalog: Species List for Latrodectus" 2019). They are among the most hazardous spiders due to their highly neurotoxic venom. Their bite causes immediate severe symptoms like intense pain, although the worst symptomatology in humans is developed in the medium-long term as a syndrome called "latrodectism". Latrodectism symptoms include body rigidity, widespread intense pain, profuse sweating, hypertension and difficulty breathing (Camp 2014, Vetter and Isbister 2008). Due to frequency of black widow biting events and the envenomation severity in humans, this spider family is classified as medically important (Ikonomopoulou 2018).

3.2.1 Latrotoxins

Latrotoxins (LTXs) are protein components of black widow spiders' venom which stand out as a class of huge understudied PFPs. specific from *Latrodectus* genus. They are high molecular weight (110-140 kDa) and acidic proteins (isoelectric point around 5.0) that also form cation (mostly Ca^{2+}) selective pores through biological membranes (Ushkaryov 2002, Ushkaryov 2004, Wang 2018, Yan and Wang 2015). This latrotoxin family is divided in three subfamilies regarding prey specificity. α-Latrotoxin (α-LTX) is the only member of a subfamily affecting vertebrates, as there is also one only member of a second subfamily capable to attack crustaceans, α-latrocrustaceatoxin (α-LCT). Notwithstanding, the third subfamily, grouping LTXs attacking insects, has five different members: α, β, γ, δ and ε-latroinsectotoxins (LITs) (Duan 2008, Rohou 2007). The LIT expansion is interesting from the evolutive point of view since it highlights the selective pressure for hunting, while crustaceans or mammals would be occasional predators, so the specific toxins directed to these animals is reduced in comparison to insects.

Neuron latrophilins and neurexins have been proposed as α-LTX receptors (Ushkaryov 2004). Although LITs receptors has not been already defined, there are orthologs of both membrane receptors in insects, suggesting that these related proteins could be involved in LIT recognition too. In fact, LITs and α-LTX have the ability to form pores on either cells expressing the aforementioned receptors or model lipid bilayers (Dulubova 1996, Orlova 2000). The biological disposition of these proteins to bind neuronal receptors, provokes massive neurotransmitter release upon pore formation followed by Ca^{2+} fluctuations, causing intense pain and paralysis of the prey (Sudhof 2001).

LTX family members are homologous to each other and share a common defined genetic structure. They are synthetized as huge inactive precursors around 140-160kDa that after cleavage on their N and C-termini become fully active (Dulubova 1996, McCowan and Garb 2014, Rohou 2007, Ushkaryov 2004). Genomic data confirm that these large precursors are intronless

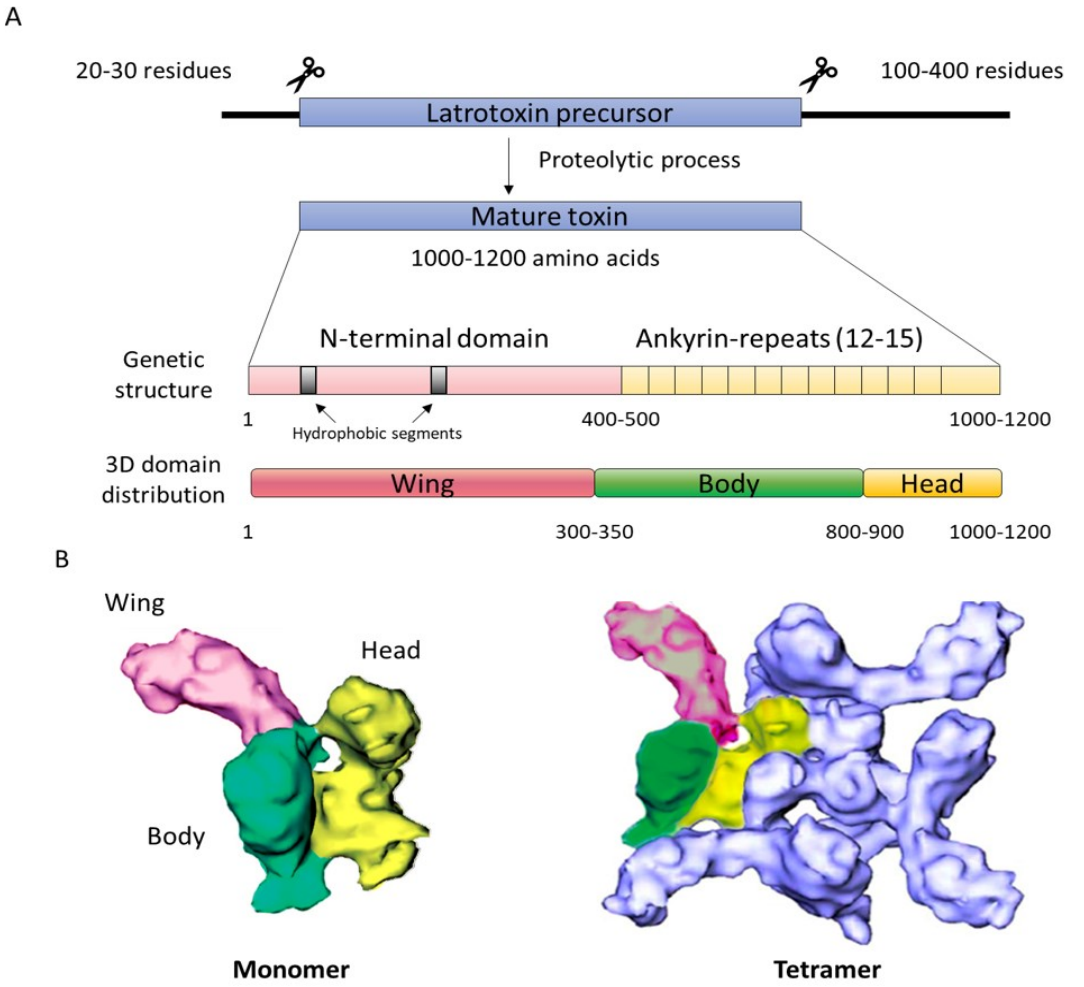

Figure 9. LTXs are produced as large inactive precursors which need proteolytic process in both N and C-termini. The codifying gene region is organized into two well-differentiated main regions: The characteristic N-terminal region, comprising two conserved hydrophobic regions, and the C-terminal region, rich in ankyrin-like repeats. Low- resolution three-dimensional structure of α-LTX obtained by cryo-EM shows three domains: the wing (pink), the body (green), and the head (yellow) (A). Final pore structure is a tetramer in which wing region is involved in receptor/membrane recognition and the head and the body play the main role in pore-formation and protein-protein interactions (B). Modified from (Rivera-de-Torre 2019).

(Garb and Hayashi 2013, Gendreau 2017). Regarding gene organization, two different domains can be described (Figure 9). The N-terminal one involves the first 400-500 amino acids and it is characteristic of the family. It contains three conserved cysteines residues and two hydrophobic sequences around 20-30 amino acids long. The second region, including the last 500-700 amino acids, is highly similar among all LTXs. This a domain is composed by imperfect ankyrin-like repeats, the number of repetitions varying among LTXs from 15 modules on δ-LIT to 22 on α-LTX. Regarding their three-dimensional structures, only there is information about one of very low resolution, solved for α-LTX by cryo-electron microscopy (cryo-EM) (Orlova 2000, Ushkaryov 2004) (Figure 8), almost 20 years ago. In this low-resolution structure, three significant domains can be still clearly distinguished (Figure 9): The *wing*, that contains most part of the characteristic N-terminal domain and is presumably involved in receptor recognition, the *body*, and the *head* including the ankyrin-like repeats, probably involved in protein-protein interactions and channel formation. The water-soluble version of the protein has a dimer arrangement in the absence of divalent cations like Ca^{2+} and Mg^{2+}, but adopts a tetrameric arrangement in their presence, with a well-defined central channel (Figure 9). In the very low-resolution reconstruction of the membrane bound structure (Orlova 2000), it is however still possible to differentiate fenestrations in the pore lumen, as in the actinoporins example, suggesting the implication of lipids in the final pore structure. This structure was not only of very low resolution and obtained in the absence of any protein membrane receptor, but the bilayer used just composed of palmitoyl-oleyl-phosphatidylcholine (POPC). This model membrane is way far from mimicking a real biological membrane, which includes essential lipids like Chol (30-50%), SM (4%), phosphatidylserine (7%) and phosphatidylinositols (1%) and was certainly not at all representative of a neuron membrane, the natural target of LTXs. Furthermore, considering that the toxin used in this study was purified from crude venom, it was not possible to assure that traces of some other venom components were not present in the protein preparation used. Maybe some of these components constitute too essential elements of the final pore (see below). In conclusion, the structure-function relationships of these proteins are still far from being solved. In addition, there is not any structural information about LITs either. They certainly share genetic structure with α-LTX and show 50% identity. Therefore, it is safe to assume that they will fold into a very similar structure. However, an again, this problem is not only far from being solved but has not even been approached, according to the available scientific literature. Interestingly, LITs isoforms have been tested as insecticides against *Galleria mellonella* larvae (Krasnoperov 1990), showing very different toxicity activities. Within this idea, LITs stand out as highly promising candidates to be engineered in order to produce sustainable and highly specific bioinsecticides after the needed detailed characterization of their structures and specific functionalities to better understand the molecular details underlining their toxicity.

3.2.2 Latrodectins

When α-LTX is purified from venom glands, it usually appears associated with low-molecular-weight peptides originally abbreviated as black widow LMW but nowadays known as latrodectins (Ltds) (Kiyatkin 1992). These peptides are about 70 amino acids long (6-8kDa), have an acidic isoelectric point (around 4.0) and show a conserved 6 cysteines arrangement pattern, forming three disulfide bonds. Ltds show distant homology with crustacean hyperglycemic hormones, suggesting that they have derived from an invertebrate neuropeptide (Gasparini 1994). The association between LTXs and Ltds seems to be crucial since it does not seem possible

to purify α-LTX to homogeneity when purified from the crude venom by conventional methods (Kiyatkin 1992, Kiyatkin 1990, Volkova 1995). So, purified α-LTX is actually a *high-molecular-weight complex* in solution that implies high affinity-bound Ltds, as judged by sucrose gradient centrifugation(Petrenko 1993, Sudhof 2001). Apart from presumably being part of this macromolecular latrotoxin complex, Ltds natural function remains unknown. The few studies available suggest that these peptides are crucial to increase membrane affinity of LTXs, given that they have not been found to be toxic neither against vertebrates or insects (Grishin 1993, Kiyatkin 1995, Pescatori 1995, Volkova 1995) when eassayed in the absence of LTXs. Despite their small size, their only structural information available is a circular dichroism spectrum suggesting high α-helical content (Gasparini 1994). Although they are not PFTs by themselves, they are extremely interesting in the context of the project herein describe given that they appear to be critical for the formation of the toxic LTXs macromolecular complexes.

OBJECTIVES

Block I. Actinoporins: membrane pore-forming toxins produced by sea anemones

- Analysis of the sequence differences between StnI and StnII leading to functional distinct behavior in terms of membrane binding affinity, pore formation and hemolytic activity.
- Analysis of the potential StnI-StnII interaction as a resource for modulation of *S. helianthus*' venomous activity.
- *De novo* transcriptomic analysis of *S. helianthus*' venom and discovery of potentially new actinoporin variants.
- Cloning, production, and characterization of sticholysin III (StnIII), a new actinoporin from *S. helianthus*.

Block II. The membrane pore-forming *latrotoxin macromolecular complex*: latrodectins and latroinsectotoxins produced by black widow spiders

- Cloning, production, and characterization of the most highly expressed latrodectins (Ltds) from the black widow (*L. hesperus*) spider's venom.
- Cloning, production, and characterization of the insects specific δ-latroinsectotoxin (δ-LIT) from the black widow (*L. hesperus*) spider's venom.

MATERIALS AND METHODS

1. Nucleic acids manipulation procedures

1.1 Agarose electrophoresis

- TAE running buffer: 0.045 mM Tris-HCl, 0.001% (v/v) glacial acetic acid, 1 mM EDTA pH 8.0.
- Loading buffer (6X): 0.25% (w/v) bromophenol blue, 0.25% (w/v) xylene cianol, 30% (v/v) glycerol.
- Agarose or Low melt agarose (Conda).
- Molecular weight pattern: SmartLadder Eurogentec (200bp – 10.000bp).
- Staining solution: 1 µg/mL Ethidium bromide.
- Image digitalization: BioRad Molecular Imager Gel Doc XR System.
- Power Supply: BioRad Power Pac 300.

Agarose gels were prepared by adding adequate amount of agarose in TAE running buffer depending on the molecular size intended to separate from 0.7% to 1% (w/v). After boiling to complete dissolution of the agarose, the mixture was then cooled and poured in a mold that shapes the gel with wells. Samples prepared by diluting them with the corresponding volume of 6X loading buffer. Electrophoresis were developed applying constant 100 V at room temperature for regular agarose and 4°C for low-melt agarose gels. Samples were always run in parallel with a molecular weight pattern. For detection, the gel was immersed in ethidium bromide 1µg/mL solution for 15 min. Electrophoresis result was revealed by exposing the gel to UV light, and the image was digitalized.

1.2 Polymerase chain reaction (PCR)

- Pfu DNA polymerase (2u/µL) (Promega).
- Pfu polymerase buffer 10x (Promega): 200 mM Tris-HCl-HCl, 100mM KCl, 100mM $(NH_4)_2SO_4$, 20mM $MgSO_4$, 1mg/mL nuclease-free BSA, 1% (v/v) Triton X-100.
- 10 mM (2.5 mM dATP, 2.5 mM dTTP, 2.5 mM dCTP, 2.5 mM dGTP) dNTP mix.
- Custom Oligonucleotides (Conda, Metabion).
- Nuclease-free water.
- Thermocycler: Perkin Elmer GeneAmp PCR System 2400 or Eppendorf Mastercycler.

PCR is a molecular biology technique used to amplify DNA, plasmids, or to introduce site-directed mutations within already cloned sequences.

1.2.1 PCR for amplification

In general terms, PCR mix was prepared to reach the following final concentrations: 1.25 u/50µL Pfu DNA pol, 0.5 µM upstream/downstream primers, <0.5µg/50µL template DNA, 50-200 µM dNTP mix, and Pfu polymerase buffer 10-fold diluted with nuclease-free water. Final volume preparation ranges between 20 and 50 µL. Reactions were performed following manufacturer guidelines. Briefly, initial denaturation at 95°C for 1-2 min is followed by 25-30 cycles alternating denaturation (95°C for 1-2min), annealing (5°C below oligonucleotide's Tm for

30s) and extension (72°C for 2-4 min). Final extension step was programmed for 5 min at 72°C. Samples were stored at -20°C until results visualization through agarose electrophoresis.

1.2.2 Site-directed mutagenesis by overlap extension using PCR (Ho 1989)

PCR was used to introduce single amino acid mutations within a sequence cloned in a bacterial expression vector. The protocol is summarized in figure 1. Complementary oligonucleotides and PCR reaction were used to generate two DNA fragments with overlapping ends containing the desired mutation. These fragments were combined in a subsequent reaction in which the overlapping fragments anneal, allowing 3' overlap of each strand to serve as primer for the extension of the complementary strand.

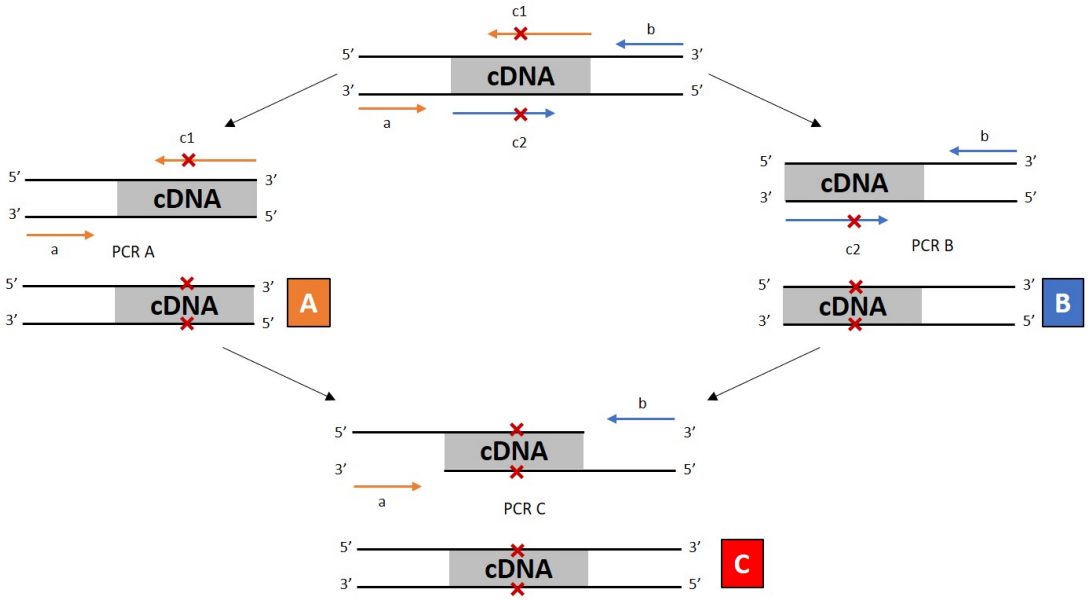

Figure 1. Site-directed mutagenesis by overlap extension using PCR. Oligonucleotides a and b are external to cloned cDNA. They are conveniently mixed in PCR reactions A and B with overlapping primers (c1 and c2) containing the desired mutation. DNA products A and B are mixed in a third PCR reaction were 3' overlap of each strands serve al primer for the extension of the complementary strands, obtaining a PCR product (C) containing the designed mutation in both strands.

1.3 Digestion with restriction enzymes

- Restriction enzymes: EcoRI, BglII, HindIII, NcoI, XhoI, XbaI, NotI (Roche), PmeI (New England Biolabs) 10 u/µL.
- Digestion Buffers (10x): H and B (Roche), CutSmart buffer (New England Biolabs)
- BSA (10x): 1 mg/mL.
- Nuclease-free water.

Digestion mixture was performed following manufacturer instructions. Briefly, up to 1 µg of dsDNA is digested by adding, BSA at 0.1 mg/mL, the corresponding volume of 10X digestion buffer and the corresponding restriction enzymes at a final concentration of 1u/50µL. These digestion reactions were used with at least three different purposes: Preparative digestions are performed overnight at 37 °C to a) obtain DNA fragments with compatible ends to subsequently ligate them to the expression vector or b) to linearize pPICZα plasmids in order to electroporate

electrocompetent *P. pastoris*. Finally, c) analytical digestions were also made to control correct plasmid insertions (37 °C, 1 hour). Prior to analyze the result in an agarose electrophoresis, enzymes were inactivated at 65 °C for 10 min.

1.4 Purification of DNA fragments

Two different DNA purification methods were used. Purified DNA was always tested by agarose gel electrophoresis.

1.4.1 DNA gel extraction kit (Millipore)

The sample was regularly prepared with the corresponding loading buffer and run onto a gel prepared with a TAE buffer version containing a reduced concentration of EDTA (0.1 mM). After development of the electrophoresis and regular staining with ethidium bromide, the gel was illuminated with UV light in an open system protected by a methacrylate screen and the desired band can be detected, cut with a scalpel and transferred to a special tube provided in the kit. Then, it was centrifugated at 10.000xg. The tube has a nebulizer piece that retains agarose and let DNA dissolved in TAE go through and be collected into an Eppendorf tube.

1.4.2 Wizard PCR Preps DNA purification System (Promega)

For this method, samples were loaded in a low-melt agarose gel, that runs at 80 V for 75 min at 4 °C. After regular staining, the band was cut as in the previous method and melt after 10 min at 70 °C. Following the manufacturer instructions, a DNA binding resin was added to the mixture and built into a column. After washing this 80% isopropanol the DNA fragment was eluted with pre-heated nuclease-free water at 80 °C.

1.5 DNA ligation

- T4 DNA ligase 1-3 U/µL (Promega).
- Ligation Buffer 10x (Promega).
- DNA fragments with overlapping 5'-3'termini.
- Thermo block.
- Expression vectors:
    - pQE-60 (Qiagen) for heterologous expression in *E. coli*.
    - pPICZαA (Thermofisher) for heterologous expression in *P. pastoris*.

Following digestion of vector and DNA insert with the same or compatible restriction enzymes leaving overlapping 5' and 3' overhands, fragments were mixed in a vector:insert ratio 1:5. The corresponding buffer containing 1 mM ATP is added and nuclease-free water is used to adjust final concentration in 20 µL volume. Reactions was incubated at 20°C overnight and then stopped by inactivation at 65°C for 10 min.

1.6 Subcloning TOPO TA Cloning kit (Invitrogen)

PCR product amplified with specific primers from total cDNA mixture, is incubated with 1 u of Taq polymerase (rTaq, Takara) for 10 min at 72°C to obtain adenine overhangs on both 5' and 3' edges. Ligation reaction between resulting fragment and TOPO vector (pCR™2.1 TOPO®) is performed at room temperature for 5 min in the presence of a mixture of salts supplied by

the manufacturer. Then, TOP10 *E.coli* competent cells are transformed by 30 s thermal shock at 42°C, followed by addition of S.O.C medium. Transformant white colonies are selected in LB-Amp (50 µg/mL) plates supplemented with 40 µL of 2% (w/v) X-Gal and 40 µL of 100 mM IPTG.

1.7 Plasmids isolation

- TE buffer: 10 mM Tris-HCl-HCl, 0.1 mM EDTA, pH 8.0.

Plasmid DNA was isolated following using a commercial kit and following the method suggested by the manufacturer. Depending on the desired amount of product, two kits were used: Minipreps (Sigma-Aldrich) or Maxipreps (Qiagen). The basis of both procedures is the same; only the volume of the starting culture varies from 5 mL for Minipreps to 250 mL for Maxipreps. Briefly, culture is harvested by centrifugation, cells are lysated and after pH neutralization, the cellular soluble fraction is loaded in a commercial column that retains plasmid DNA. Bound DNA was washed with ethanol containing solutions and it was finally eluted from the column in sterile water or TE buffer by centrifugation. Resulting product was analyzed by electrophoresis.

1.8 RNA extraction and single-strand cDNA production

- TRIZol (Sigma-Aldrich).
- Chloroform (Merck).
- Isopropanol (Merck).
- 75% (v/v) ethanol.
- DNase TURBO DNA-free kit (Ambion, Life technologies).
- RNA quantification: Qubit 3.0 (Thermo Scientific).
- Capilar electrophoresis: 2100 BioAnalyzer (Agilent Technologies).
- Retrotranscriptase SuperScript III First-Strand Synthesis SuperMix kit (Thermo Fisher).

Total RNA was extracted through the standard protocol recommended for TRIZol (Chomczynski 1993). Briefly, homogenized tissue was incubated at room temperature for 5 min and then chloroform was added to the samples. After vigorous shaking, the mixtures were centrifugated at 12000×g for 15 min at 4 °C. The aqueous phase was then recovered in a new tube. RNA was precipitated with isopropanol, recovered by centrifugation and followed by several washing steps with 75 % (v/v) ethanol. Dried RNA samples were dissolved in RNase-free water. Samples were then DNase treated with the TURBO DNA-free kit. Finally, RNA is stored at −80 °C until use. The RNA concentration was quantified with a Qubit 3.0 and its integrity was confirmed though 2100 BioAnalyzer analysis. cDNA was then synthesized with the SuperScript III First-Strand Synthesis SuperMix kit using the extracted RNA.

2. General bacterial procedures with the bacteria *E. coli*

2.1 Strains

- RB791: used for the amplification and isolation of plasmids as well as for protein expression of genes under *Lac* promoter.
- DH5α: used for amplification and isolation of plasmids.

- TOP10: used for subcloning with TOPO TA Cloning kit.

2.2 Culture media

- ψ-Broth: rich media for competent cells preparation and transformation by thermal shock. 2% (w/v) tryptone, 0.5% (w/v) yeast extract, 0.4% (w/v) $MgSO_4$, 10mM KCl, pH 7.6.
- LB-media: rich media for general culture of bacteria. 5 g/L yeast extract, 10g/L tryptone, 10 g/L NaCl.
- Low salt LB media: used for selection of transformed bacteria resistant to Zeocin. Same composition as LB media but only 5 g/L of NaCl.
- S.O.C: commercial rich media for TOP10 *E. coli* competent cells transformation by thermal shock. 2% (w/v) tryptone, 10 mM NaCl, 2.5 mM KCl, 10 mM $MgCl_2$, 10 mM $MgSO_4$, and 20 mM dextrose.

All media are sterilized by autoclaving for 20 min at 120 °C. For solid media 15 g/L of agar is added to the broth.

2.3 Antibiotics used for strains selection

- Ampicilin (Amp) (Sigma-Aldrich): for selection of transformed bacteria with pQE-60 plasmid.
- Zeocin (Zeo) (Invitrogen): for selection of transformed bacteria with pPICZαA plasmid.

Both are dissolved in miliQ water to 100 mg/mL and sterilized by filtration.

2.4 Preparation of chemically competent cells

- Transformation buffer 1 (TfB1): 100 mM RbCl, 50mM $MnCl_2$, 30 mM Potassium acetate, 10 mM $CaCl_2 \cdot H_2O$, 15% (v/v) Glycerol, pH 5.8 . It is sterilized by filtration (Whatman FP 30/0.2 CA-5 0.2µM) and stored at 4°C.
- Transformation buffer 2 (TfB2): 10 mM Mops, 10mM RbCl, $CaCl_2 \cdot 75$ mM H_2O, 15 % (v/v) Glycerol, pH 7.0. It is sterilized by autoclave and stored at 4 °C.

Bacteria which had been stored frozen at -80 °C are seeded on LB plates by streaking to be able to isolate a single colony after overnight incubation at 37 °C. Single colonies were plated in a new LB plate to obtain larger number of cells. First, there was a pre-inoculation culture in 5 mL of ψ-Broth. This culture was maintained at 37 °C with vigorous shaking until optical density at 600 nm (OD_{600}) is 0.3. Then 100 mL of ψ-Broth were inoculated with these cells and the new mixture is again incubated in the same conditions until OD_{600} reached a value of 0.48. Cells were then harvested by centrifugation at 2500 rpm for 20 min at 4°C. From this moment on, the cells were always kept refrigerated at 4°C or in ice. The resulting cellular pellet was dried with a sterile swap and resuspended in 30 mL of cold TfB1 buffer. After 90 min of incubation at 4 °C, it was centrifuged in the same aforementioned conditions. The new pellet was then suspended in 4 mL of TfB2 buffer and divided into 200 µL aliquots. These aliquots of competent cells were stored frozen at -80 °C until use.

2.5 Transformation by thermal shock

Competent cells were thawed on ice. 10-100 µg of DNA (Plasmid or Ligation reaction) were added in a volume no larger than 50 µL. After 15 min on ice, cells were subjected to a thermal shock at 37 °C for 4 min, then they were immediately transferred to ice and four volumes of ψ-Broth (≈800 µL) were added to the cells which were subsequently incubated for 1 h at 37 °C with shaking. Variable volumes of transformed cells were plated in appropriated media with the selection antibiotic for the plasmid resistance. Plates were incubated overnight at 37 °C and single colonies are plated in new selective agar plates.

3. Heterologous production of Stns in the bacterial system *E. coli* and their purification

3.1 Stn production

Sticholysins are small, highly soluble and cysteineless proteins whose heterologous production was successfully developed in the bacterial system *E. coli*.

- Plasmids:
  - pQE60-StnI (cloned in EcoRI-BglII).
  - pQE60-StnII (cloned in NcoI-BglII).
  - pQE60-StnIII (cloned in EcoRI-HindIII).

These plasmids contain wild-type proteins cDNA and they were used as templates for site-directed mutagenesis.

Competent *E.coli* RB791 bacteria were transformed with the desired plasmid for protein production. Transformed bacteria were selected in LB-Amp (100 µg/mL) plates.

The liquid cultures were started by inoculating 120mL of LB-Amp (100µg/mL) with a fresh individual colony and then incubated overnight at 37 °C with vigorous shaking. This culture was then used to inoculate 2L of LB-Amp (100µg/mL) (25 mL of pre-inoculation for every 500 mL). Inoculated broth was incubated in the same conditions until OD_{600} reaches a value of 1.0. Hereafter, protein production was induced by adding IPTG to a final concentration of 1 mM and the culture was incubated for 4 hours. Protein was produced intracellularly so to harvest cells the culture is centrifugated for 30 min at 6000xg at room temperature. Pellet was frozen with liquid nitrogen and stored at -80 °C until protein purification is begun.

3.2 Stns purification

Purification protocol was set up considering the physicochemical properties of Stns, particularly, their molecular weight and isoelectric point values.

- Ion-exchange chromatography: CM-52 (Whatman).
  - Ion exchange chromatography buffer: 50mM Tris-HCl-HCl at pH values of 6.8 (StnI), 7.8 (StnII), or 8.8 (StnIII).
  - Continuous elution linear gradient: starting and ending solutions are prepared with the same buffer. Starting buffer does not contain NaCl but ending solutions contain 0.3 M (StnI), 0.5 (StnII) or 0.6M (StnIII) NaCl.

- Size exclusion chromatography: Biogel-P2 (BioRad).
    - Size exclusion chromatography buffer: 50 mM NH_4HCO_3 pH 7.0.
- Dialysis membrane cut-off 6-8000 Da (Spectra Pore).

Frozen cells were thawed on ice and resuspended in 50 mL of Ion exchange buffer (with the adequate pH for every specific protein) containing 1% (v/v)Tween 20. Cells were lysed on ice, via tip sonication, applying 40 % amplitude for 7 cycles alternating 1 min sonication followed by one more minute of waiting to avoid overheat. The soluble fraction was recovered by 30 min of centrifugation at 40.000xg at 4 °C. The resulting supernatant was then loaded with the CM-52 chromatographic support, equilibrated in the corresponding buffer. The non-retained fraction was discarded and the chromatographic beads were thoroughly washed with the same buffer. Then, protein was eluted using 300 mL of continuous NaCl gradient adapted to each protein (see above). Fractions of 3 mL were collected and the column elution profile is plotted by representing A_{280} of each fraction. Since Stns are not enzymes their identification was made through spectroscopic analysis and SDS-PAGE analysis of selected fractions. The fractions containing the protein were pooled in a unique fraction which is then loaded onto a Biogel-P2 size exclusion chromatography (4 cm x 18 cm) equilibrated in 50mM NH_4HCO_3 pH 7.0 buffer. This chromatography was intended to change the buffer to another one made of volatile components. Fractions eluting at the void volume of the column, containing the purified proteins, were pooled, extensively dialyzed for 2 hours against water, lyophilized and stored at -20°C until use.

4. General procedures with the yeast *P. pastoris*

4.1 Strains

- KM71H: used for production of proteins.
- SMD11198: deficient in proteases. Used for production of proteins.

4.2 Culture media

- Stock solutions
    - 10X YNB: 13.4% yeast nitrogen base with ammonium sulfate and without amino acids. YNB without ammonium sulfate and without amino acids is supplemented with 10% (w/v) of ammonium sulfate. Sterilized by filtration.
    - 500X Biotin: 0.02% (w/v) biotin. Sterilized by filtration.
    - 10X Dextrose: 20% (w/v) dextrose. Sterilized by filtration.
    - 10X Methanol: 5% (v/v) methanol. Sterilized by filtration.
    - 10X Glycerol: 10% (v/v) glycerol. Sterilized by autoclaving.
    - 10X Potassium phosphate buffer. pH 6.0: 1M potassium phosphate buffer pH 6.0. Sterilized by autoclaving.
    - 1M Sorbitol.
- Media recipes
    - YPD: Yeast extract Peptone Dextrose medium. Rich and complex broth used for general growth and storage. 1% (w/v) yeast extract, 2% (w/v) peptone, 2% (w/v) dextrose.

- YPDS: YPD medium with 1M Sorbitol. For preparation of electrocompetent yeast and in the presence of the adequate antibiotic, selection of transformed *P. pastoris* by electroporation.
- BMGY: Buffered Glycerol-Complex Medium, used to control the pH of the medium, decrease protease activity, and generate biomass. 1% (w/v) yeast extract, 2% (w/v) peptone, 100 mM potassium phosphate, pH 6.0 1.34% YNB, $4 \cdot 10^{-5}$% (w/v) biotin, 1% (v/v) glycerol.
- BMMY: Buffered Methanol-complex Medium, used to control the pH of the medium, decrease protease activity and induce expression. 1% (w/v) yeast extract, 2% (w/v) peptone, 100 mM potassium phosphate, pH 6.0 1.34% YNB, $4 \cdot 10^{-5}$% (w/v) biotin, 0.5% (v/v) methanol.
- BMD: Buffered minimal medium containing dextrose, used to control the pH of the medium, decrease protease activity, and generate biomass. 100 mM potassium phosphate, pH 6.0 1.34% YNB, $4 \cdot 10^{-5}$ % (w/v) biotin, 0.5% dextrose. Suitable for uniformly labelled protein production with stable isotopes for NMR three-dimensional structure determination (by substituting dextrose by ^{13}C-Dextrose).
- BMM: Buffered minimal medium containing methanol used to control the pH of the medium, decrease protease activity, and induce production of the desired protein. 100 mM potassium phosphate, pH 6.0 1.34% YNB without amino acids and with 1% (w/v) ammonium sulfate, $4 \cdot 10^{-5}$ % (w/v) biotin, 0.5% (v/v) methanol. Suitable for uniformly labelled protein production with stable isotopes for NMR three-dimensional structure determination (by substituting methanol by ^{13}C-methanol and ^{15}N ammonium sulfate).

4.3 Selection antibiotic

- Zeocin (Zeo) (Invitrogen): for selection of transformed yeast with pPICZαA expression vector.

4.4 Preparation of electrocompetent cells

5 mL of freshly plated *P. pastoris* strain were grown at 30°C with vigorous shaking overnight to induce 50 mL of YPD an grown them again overnight in the same conditions. Cells were harvested by 5 min centrifugation at 4 °C at 1.500xg. Pellet was resuspended in 50mL of cold sterile water. Then it was centrifuged twice again, first resuspending the cellular pellet in 25 mL and finally in 10 mL of cold sterile water. Two consecutive centrifugations were performed by resuspending the cells in 4 mL of cold 1 M Sorbitol. Electrocompetent cells were kept on ice and used the same day for electroporation.

4.5 Transformation by electroporation

80 µL of freshly prepared electrocompetent *P. pastoris* cells were mixed with 10 µg of linearized pPICZαA vector containing cDNA insert dissolved in no more than 10 µL of sterile water. The mixture was transferred to an ice-cold 0.2 cm electroporation cuvette which was incubated for 5 min on ice. Cells were pulsed using a pre-set *P. pastoris* protocol (2000 V, 25 µF,

200 Ω) and immediately 1 mL of ice-cold 1M sorbitol was added to the cuvette. Cells were incubated on ice for 2 hours. Then, 1 mL of YPD was added and it was incubated for four more hours at 30°C and vigorous shaking. Cells were spread in YPDS plates containing increasing concentrations of Zeo (100, 500, 750, and 1500 µg/mL) for transformants selection. Plates were incubated for 3-4 days at 30°C until colonies are formed. These were picked and seeded again on fresh YPD or YPDS plates containing 100 µg/mL Zeo.

5. Heterologous production of Ltds in the yeast system *P. pastoris* and their purification

5.1 Ltds production

Latrodectins are small, highly soluble peptides with an acidic isoelectric point which heterologous production was developed in the yeast system *P. pastoris*.

- Plasmids
  - pPICZαA-LtdI (Cloned in EcoRI-XhoI).
  - pPICZαA. LtdII (Cloned in EcoRI-XhoI).

Electrocompetent *P. pastoris* KM71H were electroporated with 10 µg of linearized plasmid. Transformed yeast were selected in YPDS agar plates containing increasing concentration of Zeo ranging 100-1500 µg/mL.

The liquid cultures were started by inoculating 1L of BMG with a fresh individual colony and then incubated overnight at 30°C with vigorous shaking in baffled Erlenmeyer flasks. This culture was then centrifuged at 5000 rpm for 15 min to discard the media and resuspend the cellular pellet in 200 mL of BMM The culture is then incubated at 30 °C with vigorous shaking for 4 days. 1mL of pure methanol was added every 12 hours. After production extracellular media was harvested by centrifugation at 40.000xg at 4 °C for further purification of the produced proteins.

5.2 Ltds purification

Purification protocol was set up considering the physicochemical properties of Ltds, particularly, their molecular weight and isoelectric point values.

- Ion-exchange chromatography: DEAE-cellulose (Whatman).
  - Ion exchange chromatography buffer: 50mM Tris-HCl-HCl pH 7.5.
  - Continuous elution linear gradient: starting and ending solutions are prepared with the same buffer. Starting buffer does not contain NaCl but ending solutions contain 2 M NaCl.
- Size exclusion chromatography: Biogel-P2 (BioRad).
  - Size exclusion chromatography buffer: 50 mM NH_4HCO_3 pH 7.0.
- Äkta Purifier FPLC System. Superdex G75 10/300GL size exclusion column (GE Healthcare Life Sciences).
  - Size exclusion chromatography buffer: 50 mM NH_4HCO_3 pH 7.0.
- Uniformly ^{13}C and ^{15}N labeled compounds (^{13}C-glucose, ^{15}N-$(NH_4)_3SO_4$, ^{13}C-methanol) from Cambridge Isotope Laboratories (Cambridge, MA).

Harvested media is combined with 800 mL of ion exchange chromatography buffer and mixed with the DEAE chromatographic support, equilibrated in the corresponding buffer, and gently stirred overnight at 4 °C. The non-retained fraction is discarded and the chromatographic DEAE beads are mounted onto a glass column (2 cm x 18 cm) which is thoroughly washed. Then, protein is eluted using 300 mL of continuous NaCl gradient. Fractions of 3 mL are collected and the column elution profile is plotted by representing A_{280} of each fraction. Their identification was made through spectroscopic analysis and SDS-PAGE analysis of selected fractions. The fractions containing the protein were pooled in a unique fraction which is then loaded onto a Biogel-P2 size-exclusion chromatography (4 cm x 18 cm) equilibrated in the corresponding buffer. This chromatography is intended to change the buffer to another one made of volatile components and eliminate the high salt concentration derived from the previous chromatographic step. Fractions eluting in the void volume of the column, containing the purified proteins were pooled and analyzed again through SDS-PAGE and absorbance spectroscopy. Then, the proteins were lyophilized. Finally, these proteins were dissolved in 50 mM NH_4HCO_3 pH 7.0 buffer at 4 mg/mL and further purified by size-exclusion FPLC system. Fractions collected were analyzed through aforementioned methods and samples containing protein of interest were aliquoted and lyophilized until used.

To produce uniformly labelled $^{13}C/^{15}N$ proteins, the procedure was as described above, but carbon and nitrogen sources were substituted by uniformly ^{13}C and ^{15}N labeled compounds. *P. pastoris* growth step was carried out in BMG containing 2% (w/v) of ^{13}C-glucose instead of glycerol as carbon source. For induction phase, BMM was prepared with yeast nitrogen base (YNB) variant without amino acids and supplemented with 1% (w/v) of ^{15}N-$(NH_4)_3SO_4$, as nitrogen source, and 0.5% (v/v) ^{13}C-methanol as carbon source. ^{13}C-methanol was also added every 24h of culture. Purification was carried out as previously described.

6. Heterologous production of δ-LIT in the yeast system *P. pastoris* and their purification

6.1 δ-LIT production

Latrodectins are big, proteins with an acidic isoelectric point which heterologous production was developed in the yeast system *P. pastoris*.

- Plasmids
    - pPICZαA-δ-LIT (Cloned in XhoI-NotI).

Electrocompetent *P. pastoris* KM71H and SMD1168 were electroporated with 10 µg of linearized plasmid. Transformed yeast were selected in YPDS agar plates containing increasing concentration of Zeo ranging 100-1500 µg/mL.

The liquid cultures were started by inoculating 1L of BMGY with a fresh individual colony and then incubated overnight at 30°C with vigorous shaking in baffled Erlenmeyer flasks. This culture was then centrifuged at 5000 rpm for 15 min to discard the media and resuspend the cellular pellet in 200 mL of BMMY The culture is then incubated at 20 °C with vigorous shaking for 48 h. 1mL of pure methanol was added every 12 hours. After production extracellular media

was harvested by centrifugation at 40.000xg at 4 °C for further purification of the produced proteins.

6.2 δ-LIT purification

Purification protocol was set up considering the physicochemical properties of δ-LIT, particularly, its high molecular weight and acid isoelectric point value.

- Dialysis in 6-8000 Da cut off membranes (SpectraPore).
  - Buffer A: 50mM Tris-HCl-HCl pH 7.4 EDTA 10 mM).
  - Buffer B: 50mM Tris-HCl-HCl pH 7.4.
- Ion-exchange chromatography: DEAE-cellulose (Whatman).
  - Ion exchange chromatography buffer: 50mM Tris-HCl-HCl pH 7.4.
  - Continuous elution linear gradient: starting and ending solutions are prepared with the same buffer. Starting buffer does not contain NaCl but ending solutions contain 2 M NaCl.
  - PMSF: phenylmethylsulfonyl fluoride.
- Size exclusion chromatography: Biogel-P2 (BioRad).
  - Size exclusion chromatography buffer: 50 mM NH_4HCO_3 pH 7.0.
- Äkta Purifier FPLC System. Superdex G75 10/300GL size exclusion column (GE Healthcare Life Sciences).
  - Size exclusion chromatography buffer: 50 mM NH_4HCO_3 pH 7.0.

Harvested media is dialyzed for 6 h against dialysis buffer A followed by overnight dialysis against buffer B. Dialyzed media was mixed with the DEAE chromatographic support, equilibrated in the corresponding buffer, and gently stirred overnight at 4 °C. The non-retained fraction is discarded and the chromatographic DEAE beads are mounted onto a glass column (20 cm x 3 cm) which is thoroughly washed. Then, protein is eluted using 300 mL of continuous NaCl gradient. Fractions of 3 mL are collected and the column elution profile is plotted by representing A_{280} of each fraction. Their identification was made through spectroscopic analysis and SDS-PAGE analysis of selected fractions. The fractions containing the protein were pooled in a unique fraction which is then loaded onto a Biogel-P2 size-exclusion chromatography (4 cm x 18 cm) equilibrated in the corresponding buffer. This chromatography was intended to change the buffer to another one made of volatile components and eliminate the high salt concentration derived from the previous chromatographic step. Fractions eluting in the void volume of the column, containing the purified proteins were pooled and analyzed again through SDS-PAGE and absorbance spectroscopy. Then, the proteins were lyophilized. Finally, these proteins were dissolved in 50 mM NH_4HCO_3 pH 7.0 buffer and further purified by size-exclusion FPLC system. Collected fractions were analyzed through aforementioned methods and samples containing protein of interest were aliquoted and lyophilized until used.

7. Protein electrophoretic techniques

7.1 SDS-PAGE

- Running buffer: 25 mM Tris-HCl, 0.2 M glycine, 0.1% (w/v) Sodium dodecylsulfate (SDS) pH 8.5.

- Loading buffer (3x): 50 mM Tris-HCl-HCl, 2 mM EDTA, 1% (w/v) SDS, 10% (v/v) glycerol, 0.02 % (w/v) 0.02% (w/v) and 15 % (v/v) β-mercaptoethanol pH 7.6.
- Discontinuous polyacrilamide gels. Top concentrating gel at pH 6.8 and non-restrictive acrylamide-bisacrylamide concentration. Bottom separating gel at pH 8.8 ranging 10-17% acrylamide-bisacrylamide. Both parts containing 0.1% SDS.
- Molecular weight pattern: SDS-PAGE Molecular weight standard Low range BioRad.
- Staining solution: 5 % (v/v) acetic acid, 20% (v/v) methanol, 2.5 g/L Coomasie Blue R (Sigma).
- De-staining solution: same as staining solution but without Coomasie Blue.
- Image digitalization: BioRad Molecular Imager Gel Doc XR System.
- Power Supply: BioRad Power Pac 300.

Samples were prepared by mixing samples with the appropriate volume of concentrated loading buffer and they are boiled at 90 °C for 20 min to ensure complete denaturation. 5-20 µL of the sample were loaded in the 0.1 % (w/v) SDS- 10-15 % (w/v) PAGE wells. Electrophoresis was developed at constant 25 mA/gel until bromophenol blue escapes at the bottom of the gel. SDS-PAGE result was revealed by staining/de-staining with the corresponding solutions.

7.2 Western blotting

- Transference buffer: 48 mM Tris-HCl, 39 mM glycine, 0.0375 % (w/v) SDS, 20% (v/v) methanol, pH 9.0.
- Membrane: Inmobilon-P (Millipore).
- Whatman Grade 3 Filter paper.
- EZ-Run™ Prestained Rec Protein Ladder, Fisher BioReagents (Fisher Scientific).
- PBS: phosphate-buffered saline. 137 mM NaCl, 2.7 mM KCl, 10 mM Na_2HPO_4, 1.8 mM KH_2PO4.
- Blocking solution: PBS supplemented with 0.1% (w/v) milk.
- Washing solution: PBS supplemented with 0.1% (v/v) Tween 20.
- Mouse monoclonal anti-polyhistidine-peroxidase antibody (Sigma). 1/3000 dilution in PBS 0.1% (v/v) Tween 20, 1% (w/v) BSA.
- Rabbit polyclonal anti-StnI and anti-StnII antibody. $1/1{\cdot}10^5$ dilution in PBS 0.1% (w/v) milk.
- Goat monoclonal anti-rabbit-peroxidase antibody (Sigma). 1/3000 dilution in PBS 0.1% (w/v) milk.
- Peroxidase substrate DAB: 3,3'-diaminobenzidine (Sigma).
- H_2O_2 30 vol. (Panreac).
- Power Supply: BioRad Power Pac 300.

Proteins were separated in regular SDS-PAGE as previously described but using pre-stained patterns to ensure proper transference. Membrane was activated with methanol and both gel and membrane were embedded in transfer buffer. Sandwich was set between soaked filter paper and then proteins were transferred from SDS-PAGE to binding membrane applying

a constant current of 48 mA/gel. Membrane was blocked overnight at 4°C. After successive wash steps, it is incubated with the corresponding antibodies.

Recombinant proteins with a His6 tag can be directly detected by incubation with a commercial monoclonal antibody conjugated with peroxidase. Final wash is performed before detection

Polyclonal antibodies against StnI and StnII were produced by injecting the recombinant toxins to rabbits. After incubation with this primary antibody, a wash step was performed followed by incubation with a secondary commercial goat-anti-rabbit monoclonal antibody conjugated with peroxidase.

Wester-blot was revealed by submerging the membrane in on PBS containing 1 g/L of DAB as peroxidase substrate. Upon addition of H_2O_2, peroxidase catalyzed DAB transformation in an insoluble colored product.

8. Structural Characterization of Proteins

8.1 Amino acid analysis for molar extinction coefficient determination

- Hydrolysis solution: HCl 5.7N containing 11.9 mM N-Leu as internal standard.

Approximately 25 µg of proteins were mix with 100 µL of hydrolysis solution in glass tubes with are closed in vacuum conditions. Proteins are completely hydrolyzed by 24 h incubation at 110°C. Samples are dried and washed with miliQ water 3 times.

Amino acid analysis was performed on a Biochrom 20 automatic analyzer (Pharmacia). The results were used to estimate extinction coefficients for each protein, using a previous absorbance spectra and applying Lambert-Beer law.

Experimental molar extinction coefficients were then used to calculate protein concentrations

8.2 Absorbance spectra

- Spectrophotometer Shimadzu UV1800.
- Quartz cuvette: optical length 0.1 and 1.0 cm.

Absorbance spectra were used to calculate concentration of pure proteins. Protein solutions were centrifuged for 5 min at 10.000xg to sediment any insoluble particles. Clear supernatant was transferred to 0.1-1 cm quartz cuvette.

Absorbance spectra were performed between 240 – 350 nm, using 1 nm step, at 0.5 nm/s scan speed. If A_{280} was above 1, spectra was repeated reducing optical path or samples were diluted. Concentration was calculated according to Lambert-Beer law:

$$A_{280} = E^{0.1\%} \cdot c \cdot l$$

A_{280}= absorbance at 280 nm, $E^{0.1\%}$=extinction coefficient ($mL \cdot mg^{-1} \cdot cm^{-1}$), c=concentration (mg/mL), l: optical length (cm).

8.3 Circular dichroism (CD)

- Spectropolarimeter JASCO 715.
- Preferred buffer: 15 mM Mops, 0.1 M NaCl, pH 7.5.
- Parameters: data pitch 0.2 nm, scanning speed 50 nm/min, response 1 s, band width 2 nm.
- Thermostat Water Bath/Circulator: Neslab RTE-111.

Circular dichroism is an spectroscopic technique based on the differential absorption of right and left circular polarized light. Proteins are chiral active molecules that preferentially absorb one direction of the circularly polarized light. Such absorbance difference is related to structural features of the protein. During the measure, sample cabin was purged with N_2 to reduce O_2 absorbance contribution.

Final spectra were always plotted as molar ellipticity per residue (Θ – deg·cm^2·dmol^{-1}) against wavelength (λ - nm). Θ was represented by using as concentration unit the residue concentration. To obtain, the residue concentration of the samples the protein concentration alue was divided into the average molecular weight of the residues that are part of the protein.

$$Protein\ concentration : Average\ \ molecular\ weight\ of\ amino\ acids = Residue\ concentration$$

$$\frac{mg}{mL} : \frac{g}{mol} = \frac{mol}{L}$$

8.3.1 Far-UV CD

To measure far-UV CD, protein at 0.2 mg/mL is introduced in 0.1 cm cuvette. Far-UV CD is measured in the 190-250 nm range.

8.3.2 Near-UV CD

To measure near-UV CD protein at 1 mg/mL is introduced in 0.5 cm cuvette. Near-UV CD is measured in the 250-350 nm range.

8.3.3 Thermostability analysis

Thermostability of the proteins is determined by following CD variation at a characteristic minimum in the far-UV range while temperature is increased constantly. For this purpose, 0.2 mg/mL protein solution is introduced in a thermostat 0.1 cm cuvette. Temperature is increased by connecting a water-bath to the cuvette that heats from 25°C to 85°C at 0.5°C/min rate. Complete Far-UV CD spectra were made at 25°C and 85°C.

8.4 Intrinsic Fluorescence Emission Spectra

- Spectrofluorimeter SLM Aminco (Urbana, IL) model 8000.
- Preferred buffer: 15 mM Mops, 0.1 M NaCl, pH 7.5.
- Quartz cuvette. Optical paths 1.0 cm excitation/0.4 cm emission.
- Thermostat water bath Julabo F30-C.

Intrinsic fluorescence emission spectra of 0.1 mg/mL protein solutions was recorded at 25 °C using a slit width of 4 nm for both excitation and emission beams. The spectra were

recorded for excitation at 275 and 295 nm and both were normalized by considering that Tyr emission above 380 nm is negligible. The Tyr contribution was calculated as the difference between the two normalized spectra. The temperature was controlled using a circulating water bath. Relative Trp and Tyr emission yield for mutants was calculated as the area corresponding to the Trp and Tyr emission spectra of each protein referred to the emission of wild-type protein.

8.5 Mass spectrometry

- Mass Spectrometer: Voyager-DE PRO (Applied Biosystems).

Molecular weights of proteins were determined in purified samples dissolved in the same conditions as NMR samples (see below) by matrix-assisted laser desorption ionization time-of-flight (MALDI-TOF) mass spectrometry.

8.6 Three dimensional structure determination by NMR

NMR samples of LtdII and $^{13}C,^{15}N$-LtdII were prepared at 0.5-1.0 mM protein concentration in H_2O/D_2O 9:1 v/v at pH ~4.0. The pH was measured with a glass microelectrode and was not corrected for isotope effects. Spectra were recorded at 25 °C on a Bruker AV800 spectrometer equipped with a TCI cryoprobe and operating at 800.1 MHz for the proton. Using $^{13}C,^{15}N$-LtdII samples, the following experiments were acquired: 2D ^{1}H-^{15}N HSQC and 3D HNCO, HNcaCO, HNCA, HNcoCA, CBCANH, CBCAcoNH, HcccoNH and CccoNH experiments. Using LtdII samples, 2D homonuclear 2D ^{1}H-^{1}H TOCSY, ^{1}H-^{1}H NOESY and ^{1}H-^{13}CHSQC were recorded. Spectra were processed using either TOPSPIN v2.1 pl6 (Bruker, Inc) or NMRpipe (Delaglio 1995) and the istHMS reconstruction method was used to process the 3D spectra acquired using NUS (Hyberts 2009) The spectra were analyzed with the help of the SPARKY software (Goddard and Kneller 2005).

9. Functional characterization of actinoporins

9.1 Lipid vesicle preparation

- Lipids from Avanti Polar Lipids. 1,2-dioleoyl-sn-glycero-3-phosphocholine (DOPC), brain Sphingomyelin (SM), Cholesterol (Chol).
- Mini-extruder (Avanti Polar Lipids).
- Polycarbonate filters (100 nm pore size) (Nucleopore, Whatman).

DOPC:SM:Chol (1:1:1) phospholipid vesicles represent one of the standard models most widely used to characterize StnI and StnII pore formation behavior. A phospholipid (0.1–1.0 mg) solution in 2:1 (v:v) chloroform/methanol was dried under a flow of nitrogen, and the dry film obtained was used to prepare a lipid dispersion by adding 0.5–2.0 mL of Tris-NaCl buffer (the specific composition depends on the assay developed and is detailed below), briefly vortex mixing, and incubating for 1 h at 37 °C. This suspension of multilamellar vesicles was further subjected to five cycles of extrusion at 37 °C through polycarbonate filters to obtain a homogeneous population of unilamellar vesicles.

9.1.1 Isothermal Titration Calorimetry (ITC)

- VP-ITC (Malvern MicroCal)

- ITC buffer: 10 mM Tris pH 7.4, 100 mM NaCl, 1 mM EDTA.

The interaction between the actinoporins and LUVs prepared from DOPC, SM, and Chol (1:1:1 M ratio, 100 nm diameter) was measured by isothermal titration calorimetry (ITC) as previously described. Briefly, 0.5–10.0 µM protein solutions were titrated by injection of 10-20 µL aliquots of lipid suspensions (phospholipid concentration of 0.25–1.0 mM) at a constant temperature of 25 °C. Binding isotherms were adjusted to a model in which the protein binds to the membrane involving "n" lipid molecules(Alegre-Cebollada 2008).

9.1.2 Calcein Leakage assay

- Calcein buffer: 10 mM Tris, 140 mM NaCl, 1 mM EDTA, pH 7.4, containing 100 mM calcein.
- Sephacryl S200HR column.
- 10% (v/v) Triton X-100.

Prior to extrusion, the dry lipid films were hydrated for 1 h at 37 °C in Calcein buffer. The total lipid concentration was 1.25 mM. LUVs were separated from non-entrapped calcein by gel filtration on Sephacryl S200HR. These LUVs were used for permeabilization studies within 24 h. To measure calcein release two methods were used: (a) Emission at 550 nm was followed at 23 °C as a function of time (excitation at 480 nm) in the spectrofluorimeter (b) Using 96-multiwell plates emission at 520 nm was followed at 25 °C as a function of time (excitation at 485 nm). Fluorescence emission was measured on a FLUOstar OPTIMA microplate reader (BMG-Labtech, Ortenberg, Germany). Two-fold serial dilutions of the proteins were displayed in 96-multiwell plates and after addition of the same volume of calcein-entrapped LUVs (final concentration on the assay was 7.5 µM). Calcein leakage was automatically recorded every 3 s for 250 cycles (total time 12.5 min). One second of shaking was programmed before first measure to ensure the homogeneity within every well. To ensure that no major spontaneous leakage occurred, the emission was measured for each sample during 5 min before addition of toxin. A steady signal level, indicating intact vesicles, was observed for all samples. Maximum calcein release was determined upon LUV disintegration induced by 10 % (v/v) Triton X-100.

9.1.3 Phosphorus concentration determination

- H_2SO_4 10 N.
- Fiske-Subbarow reactive: 2.5 mg/mL 4-aminonaphthol sulfonic acid (ANSA) 200 mg/mL sodium metabisulphite. Freshly prepared, filtered and stored protected from light until use.
- 5 % (w/v) ammonium molybdate.
- H_2O_2 30 vol. (Panreac).
- $K_2PO_4 \cdot H_2O$ solution for calibration curve between 5 and 1000 ng of P.

Aliquots of freshly prepared LUVs between 10 and 25 µL were stored to determine the real concentration of phospholipids present in the mixture by phosphorus quantitation according to Bartlett method (Bartlett 1959). Briefly, samples were incubated with H_2SO_4 10 N for 2 h at 190°C to release inorganic P from lipid structures. Then H_2O_2 was added and incubated again for 2 h at the same temperature for phosphorus oxidation. After cooling the samples, ammonium molybdate and Fiske Subbarow reagents were added to the sample and they were incubated at 80°C until blue color is developed. Absorbance at 830 nm of each sample and the

calibration curve was measured in a spectrophotometer. The concentration of phosphorus of each sample is obtained by interpolation in the calibration curve built with known phosphorus concentration samples.

9.2 Hemolysis assay

- Hemolysis buffer: 10 mM Tris-HCl pH 7.4, 145 mM NaCl.
- 0.1% (w/v) Na_2CO_3.
- Defibrinated Sheep blood (Dismalab).
- Microplate reader: iMark microplate absorbance reader (Biorad).

Hemolysis assays were performed in 96-multiwell plates as previously described (Alegre-Cebollada 2008, Alegre-Cebollada 2007c). Briefly erythrocytes from defibrinated blood were washed in the hemolysis buffer through consecutive centrifugations at 700xg. Then, washed erythrocytes are diluted to a final OD_{655} of 0.8 when mixing equal volumes of the cell suspension and the buffer. Hemolysis was followed by measuring the decrease OD_{655} after addition of the erythrocyte preparation to different concentration of protein with a microplate reader. There were always controls for 0% (buffer) and 100% hemolysis (Na_2CO_3).

10. Functional characterization of latrodectins

10.1 Insecticidal activity

- *Spodoptera exigua* (Hübner) fifth stage larvae (Lepidoptera: Noctuidae).
- Protein solutions: 25 µM and 50 µM LtdII on 0.9 % (w/v) NaCl containing ProGel® food-grade as loading control.
- Vehicle solution: 0.9 % (w/v) NaCl containing ProGel® food-grade as loading control.

Insecticidal activity of LtdII was evaluated by means of tests performed by injection into *Spodoptera exigua* (Hübner) larvae. Larva e were treated with 4µL of indicated concentrations of LtdII and controls were performed with vehicle solution. All experiments were made by duplicate. Blue food dye was used as application control, in order to check that the entire volume loaded into the syringe had completely penetrated the larvae. Upon injection, the mortality of the larvae, the number of days until they died, the time it took for the survivors to reach adulthood and, in this case, the number of days they were in pupation were all evaluated. Upon injection, the percentage of dead larvae, the number of days until they died, the time it took for the survivors to reach adulthood and, in this case, the number of days they were in pupation were all evaluated.

10.2 Antifungal activity

- Fungal strains
    - *Fusarium proliferatum* (F2, maize, F47, maize).
    - *F. verticillioides* (F1, maize; F48, oat).
    - *F. graminearum* (F61, maize).
    - *F. langsethiae* (F23, oats).
    - *Aspergillus niger* (N1, oats).

- *A. welwitschiae* (N6, maize).
- *A. flavus* (A10, oats).
- *A. parasiticus* (A19, maize).

- Czapek Dox Modified Agar (Pronadisa): 0.01 g/L $FeSO^4$, 30 g/L sucrose, 0.5 g/L Magneisum glycerophosphate, 0.5 g/L KCl, 3 g/L $NaNO_3$, 1 g/L K_2SO_4, 15 g/L agar.
- Protein solutions: 7 µg/µL, 3.5 µg/µL, 1.4 µg/µL and 0.7 µg/µL of LtdII.

The fungal strains used were deposited in the collection of the laboratory of fungi and mycotoxins of the Teaching Unit of Microbiology at the Faculty of Biology (Complutense University of Madrid). They were isolated from oat and corn samples, and their classification was confirmed by molecular techniques (Garcia-Diaz 2020). Aforementioned fungal strains were maintained by regular subculturing on Czapek Dox Modified Agar. Spore suspensions of 10^5 spores/mL in 0.9 % (w/v) NaCl were obtained from a sporulating culture (7 day-old) on Czapek-Dox Modified Agar, and filtered through Whatman #1 paper. Spore concentrations were measured by microscopy using a Thoma counting chamber and the suspension was diluted to the final concentration

The effect of LtdII at different concentrations on fungal growth were evaluated using the method previously described (Patiño 2018). Briefly, 200 µL of spore suspension of each fungal strain were inoculated in 90 mm diameter plates with Czapek Dox Modified Agar. Subsequently, 6 mm diameter cellulose discs containing 10 µL of LtdII at different protein concentrations were deposited on the plated and incubated for 3 days at 25 °C. The effect of the protein was evaluated by the appearance of clear growth inhibition halos around the protein disks. All assays were carried out in triplicate. As a positive control of antifungal activity, the very well-known antifungal protein from *Fusarium graminearum* (FgAFP) (Patiño 2018) was also employed.

After a preliminary screening, interesting species regarding results obtained were further analysed. They were inoculated on 55 mm diameter plates containing 30 µL of the proteins, at a concentration of 1.5 µg/µL, which had been spread over the surface of the Modified Czapek Dox Agar. In the centre of the plate 2 µL of spore suspensions were inoculated (10^5 spores/mL). For each species, a control without protein was performed. These plates were maintained at 25 °C and the diameter of the surface grown by each fungus was measured 8 times along 121 h. After the test, these values representing fungal growth were plotted against time. The slope of the resulting curve was considered as the specific growth rate. The lag phase of each fungus was also estimated. Measurements were then analysed with the Microsoft Excel® software version 15.32 (Microsoft Corporation, USA). All tests were carried out in triplicate.

Statistical analyses were performed with the StatGraphics Centurion XVII® software (Statpoint Technologies, Inc., USA).

11. *S. helianthus' de novo* transcriptome assembly and analysis

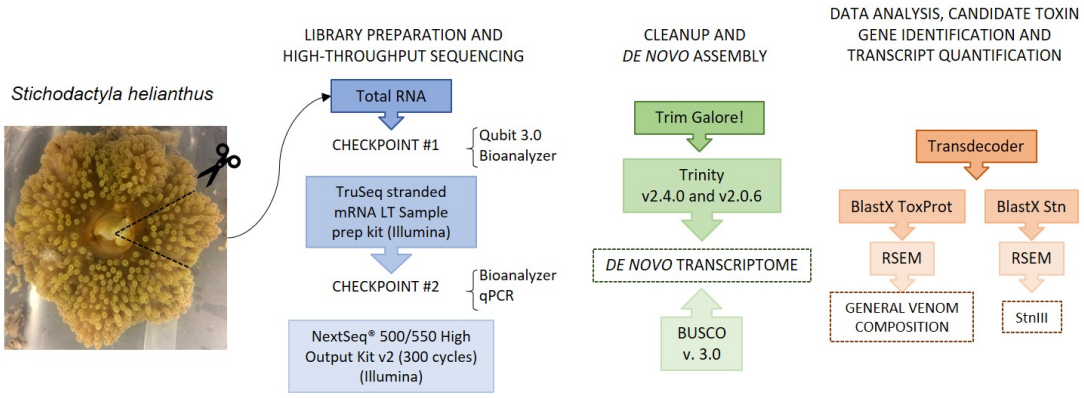

Figure 2. *S. helianthus*'s *de novo* transcriptome assembly and analysis workflow overview.

11.1 Library preparation and high-throughput sequencing

- Total RNA samples from two *S. helianthus* individuals extracted through TRIZol method.
- Library preparation kit: TruSeq stranded mRNA LT Sample prep kit (Illumina).
- Sequencing kit: NextSeq® 500/550 High Output Kit v2 (300 cycles) (Illumina).
- NextSeq 500 instrument.

Using the Library preparation kit, double-stranded cDNA libraries were obtained from total RNA samples. During this process, adaptors are attached to each cDNA molecule. This DNA fragments contain sequences intended to attach the molecules to the sequencing cell, amplify and sequence them and a bar-code so it was possible to identify the original RNA sample they were derived from. To test the quality of the libraries a BioAnalyzer chip was run. This is a high-resolution capillary automated electrophoresis intended to test the regular size of the cDNA fragments. The relative concentration of each bar-coded library was determined through qPCR and they were immediately pooled in a single sample considering that equivalent amounts of each library were present in the mixture. Libraries were sequenced on a single sequencing kit, on a NextSeq 500 instrument as a paired-end 150 base sequencing (Figure 2).

11.2 Cleanup and *de novo* assembly

- Cleanup raw reads: Trim Galore! tool.
- *De* novo transcriptome assembly: Trinity v2.4.0 and vTrinity 2.0.6.
- Completeness study: BUSCO v3 (Metazoa set).
- University of California Riverside Biocluster (Intel Broadwell 32 cores and 512 GB memory).

Raw Illumina reads from different libraries were de-multiplexed according to their barcoding label. Illumina adaptors were trimmed using the Trim Galore! tool (Krueger 2012). As a modification to the default setting, the unpaired reads were retained and 5 extra base pairs were cleaved at the 3' edge of the reverse reads to remove low-quality bases. The quality of these cleaned raw reads was verified with the FastQC reports in the Trim Galore! suite.

S. helianthus' RNA-seq cleaned data from the two libraries were put together in a de novo transcriptome assembly using Trinity v2.4.0 or Trinity v2.0.6 (Grabherr 2011) with default parameters. Two different versions of Trinity (v2.4.0 and v2.0.6) were compared to analyze potential differences in transcriptome fragmentation (Bryant 2017). Transcriptome completeness was determined using BUSCO v3 (Benchmarking Universal Single-Copy Orthologs) (Simao 2015)with the Metazoa data set. This program assayed the presence of 978 proteins conserved from 65 different species within this group (Figure 2).

11.3 Data analysis, candidate toxin gene identification and transcript quantification

- Phylogenetic analysis: MUSCLE implemented in Geneious 9.1.8 and MrBayes3.2.6.

The resulting transcriptome was annotated by identification of alignments through BLASTx with proteins in the National Center for Biotechnology Information (NCBI) with each transcript. The restrictions applied were an E-value <1x10-5 and allowing for a maximum of ten target sequences per query sequence.

Starting with the Trinity assembly file, we identified the open-reading frame (ORF) for each transcript with Transdecoder (Haas 2013). The default settings were modified to retain the longest ORF with the best BLASTx hit showing an E-value <10 or in absence of a BLASTx alignment, the longest ORF. In this way, we obtained a comprehensive protein prediction database if transcripts lacked a BLAST hit.

Relative expression levels for each transcript were calculated using the program RSEM (Li and Dewey 2011). This program mapped back the cleaned sequence reads to the assembly, estimating the number of transcripts as TPM (Transcripts Per Million).

A nucleotide database for BLAST searches was built with both Trinity assemblies from S. helianthus (obtained with Trinity v2.4.0 and v2.0.6 respectively). From the ToxProt data set (http://www.uniprot.org/program/Toxins last accession 2018/02/14), venom proteins and toxins sequences from different categories like KTX-I, KTX-III, NaTx, Metalloproteases, PLA2s and Cytolysins were pooled and extracted. These protein families are known to be present in sea anemone venoms (Macrander 2015a, Macrander 2015b, Macrander and Daly 2016, Madio 2017). A tBLASTn search of these toxin sets against the S. helianthus trinity assembly (E-value <10) was conducted to identify toxin sequence candidates. After eliminating the duplicated hits, the number of sequences per toxin category and the average expression within each category were analyzed.

StnI and StnII protein sequences were used as queries in a search against the *S. helianthus* transcriptome nucleotide sequences database using tBLASTn (E-value <1e-5, matching length >60%). We used tBLASTn because protein sequences are more conserved than nucleotides and the search was consequently less restrictive than the BLASTn query. The assembly and the subsequent analysis was performed on the University of California Riverside Biocluster (Figure 2).

A phylogenetic analysis of Stn transcripts was conducted along with other closely related actinoporin sequences. Closely related sequences were obtained by performing a BLASTx search of Uniprot using StnI and II as query sequences, taking the top 15 hits, and limiting analyses to hits with corresponding nucleotide sequences. Nucleotide sequences were trimmed to their coding sequence and aligned by their translated amino acids using MUSCLE implemented in Geneious 9.1.8, keeping translated codons in frame. MrModelTest2.3 (Nylander 2004) was used to determine an appropriate nucleotide substitution model (GTR+I+G), which was used in a Bayesian phylogenetic analysis with MrBayes3.2.6 (Ronquist 2012). The Bayesian analysis was run for $5x10^6$ generations, sampling trees every 1000 generations and discarding the first 25% of sampled trees as burn-in. A 50% majority-rule Bayesian consensus tree was computed from post burn-in trees to determine clade posterior probabilities and the consensus tree was mid-point rooted.

RESULTS

BLOCK I:

Actinoporins: membrane pore-forming toxins produced by sea anemones

Article I

One single salt bridge explains the different cytolytic activities shown by actinoporins sticholysin I and II from the venom of *Stichodactyla helianthus*

Esperanza Rivera-de-Torre, Juan Palacios-Ortega, Sara García-Linares, José G. Gavilanes, Álvaro Martínez-del-Pozo

Departamento de Bioquímica y Biología Molecular, Facultades de Química y Biología, Universidad Complutense, 28040 Madrid, Spain.

Archives of Biochemistry and Biophysics, 2017, 636, 79-89

DOI: https://doi.org/10.1016/j.abb.2017.11.005

Las sticholisinas I y II (StnI and StnII) son proteínas tóxicas formadoras de poros de tipo α, producidas por la anémona marina *Stichodactyla helianthus*. Se trata de macromoléculas solubles en agua que, al interaccionar con membranas lipídicas de una composición concreta, se unen a la bicapa, extienden e insertan su hélice α en la membrana, oligomerizan y se transforman en un poro que atraviesa la zona hidrófoba de la membrana. Un poro que provoca la muerte de la célula por choque osmótico. StnI y StnII presentan un 93% de identidad de secuencia, pero son diferentes con respecto a su actividad formadora de poros, siendo StnII hasta 4 veces más rápida que StnI cuando se ensaya su capacidad hemolítica frente a eritrocitos de carnero. El perfil de hidrofobicidad de los primeros 18 residuos revela diferencias que pueden ser anuladas sustituyendo los aminoácidos en las posiciones 2 y 9 de StnI por aquéllos que aparecen en posiciones equivalentes en StnII. En concordancia con lo expuesto, las proteínas mutadas StnID9A y StnIE2AD9A muestran una actividad hemolítica incrementada en comparación con su versión silvestre, asimilándose a la registrada para StnII. A partir del estudio de dichos mutantes se reveló el papel fundamental de un puente salino formado por el Asp9 y la Lys68 de StnI. Esta interacción no es posible en StnII, ya que en vez de una aspártico hay una alanina, pero aparece conservada en las otras dos actinoporinas bien caracterizadas hasta ahora, equinatoxina II y fragaceatoxina C. La caracterización funcional del mutante StnIIA8D muestra cómo basta con sustituir la mencionada alanina por el correspondiente aspártico para transformar StnII en una versión con menor actividad formadora de poros. En resumen, los resultados muestran la importancia de este puente salino, que une el fragmento N-terminal con el núcleo del sándwich β central. Una conclusión de aplicación general para la comprensión del papel de los puentes salinos en el diseño de proteínas, su plegamiento y estabilidad.

PhD candidate contributions

Esperanza Rivera de Torre contributed in conceiving, designing and conducting the experiments. She also took part in analyzing and discussing the results, writing and correcting the manuscript and suggesting modifications.

Archives of Biochemistry and Biophysics 636 (2017) 79–89

Contents lists available at ScienceDirect

Archives of Biochemistry and Biophysics

journal homepage: www.elsevier.com/locate/yabbi

One single salt bridge explains the different cytolytic activities shown by actinoporins sticholysin I and II from the venom of *Stichodactyla helianthus*

Esperanza Rivera-de-Torre, Juan Palacios-Ortega, Sara García-Linares, José G. Gavilanes*, Álvaro Martínez-del-Pozo**

Departamento de Bioquímica y Biología Molecular I, Facultades de Química y Biología, Universidad Complutense, 28040 Madrid, Spain

ARTICLE INFO

Keywords:
Pore-forming-toxin
Equinatoxin
Fragaceatoxin
Oligomerization
Ion-channel

ABSTRACT

Sticholysins I and II (StnI and StnII), α-pore forming toxins from the sea anemone *Stichodactyla helianthus*, are water-soluble toxic proteins which upon interaction with lipid membranes of specific composition bind to the bilayer, extend and insert their N-terminal α-helix, and become oligomeric integral membrane structures. The result is a pore that leads to cell death by osmotic shock. StnI and StnII show 93% of sequence identity, but also different membrane pore-forming activities. The hydrophobicity profile along the first 18 residues revealed differences which were canceled by substituting StnI amino acids 2 and 9. Accordingly, the StnID9A mutant, and the corresponding StnIE2AD9A variant, showed enhanced hemolytic activity. They also revealed a key role for an exposed salt bridge between Asp9 and Lys68. This interaction is not possible in StnII but appears conserved in the other two well-characterized actinoporins, equinatoxin II and fragaceatoxin C. The StnII mutant A8D showed that this single replacement was enough to transform StnII into a version with impaired pore-forming activity. Overall, the results show the key importance of this salt bridge linking the N-terminal stretch to the β-sandwich core. A conclusion of general application for the understanding of salt bridges role in protein design, folding and stability.

1. Introduction

Actinoporins are a family of cytolysins produced and secreted within the venom of sea anemones as single polypeptide chains of around 175 amino acids [1–4]. They are considered to belong to the α-pore-forming toxins (αPFTs) superfamily [5] because the pore forming domain that penetrates the membrane is an α-helix (Fig. 1). This group includes proteins with very different structures such as colicins and cytolysin A [6], both from *Escherichia coli*, and the apoptotic Bcl-2 protein Bax [7], for example. All four actinoporins whose water-soluble structure has been solved share a conserved fold composed of a β-sandwich core flanked by two short α-helices (Fig. 1a), one of them located at the N-terminal end of the protein which is involved in pore formation [8–13]. The toxicity of these proteins relies on the formation of pores within biological membranes. Challenging the archetypical classification of membrane-associated or soluble proteins, actinoporins remain stably folded and soluble in aqueous solution but, upon interaction with lipid membranes of specific composition, bind to the bilayer surface, extend their N-terminal α-helix and become oligomeric integral membrane structures by inserting this amphipathic helix within the membrane core [14–24]. The result is a pore that leads to cell death by osmotic shock (Fig. 1b).

There is not any known protein receptor for actinoporins, but it is well accepted that sphingomyelin (SM) would behave as specific lipidic receptor for this family of proteins [19,25,26]. Although the presence of SM is a requirement for actinoporins binding, the specific membrane composition and its physicochemical properties also play an important role in both binding and pore formation [25,27–34]. In fact, the effect of cholesterol (Chol) has been studied in great detail because it is one of the major promoters of phases coexistence in biological membranes and also because it eases actinoporins' biological action [29,31–39].

Actinoporins appear as multigene families within sea anemone genomes; i.e., a single anemone species has the potential to produce several different but highly similar isotoxins [40–45]. In addition, all known actinoporins display high sequence identity (between 60 and more than 90%, in some cases) and consequently very similar three-

Abbreviations: CD, circular dichroism; Chol, cholesterol; DOPC, 1,2-dioleoyl-sn-glycero-3-phosphocholine; EqtII, equinatoxin II; FraC, fragaceatoxin C; ITC, isothermal titration calorimetry; LUV, large unilamellar vesicle; PFT, pore forming toxin; RMB, relative membrane binding; SD, standard deviation; SM, porcine brain sphingomyelin; Stn, sticholysin

* Corresponding author.
** Corresponding author.
E-mail addresses: jggavila@ucm.es (J.G. Gavilanes), alvaromp@quim.ucm.es (Á. Martínez-del-Pozo).

https://doi.org/10.1016/j.abb.2017.11.005
Received 11 September 2017; Received in revised form 6 November 2017; Accepted 10 November 2017
Available online 11 November 2017
0003-9861/

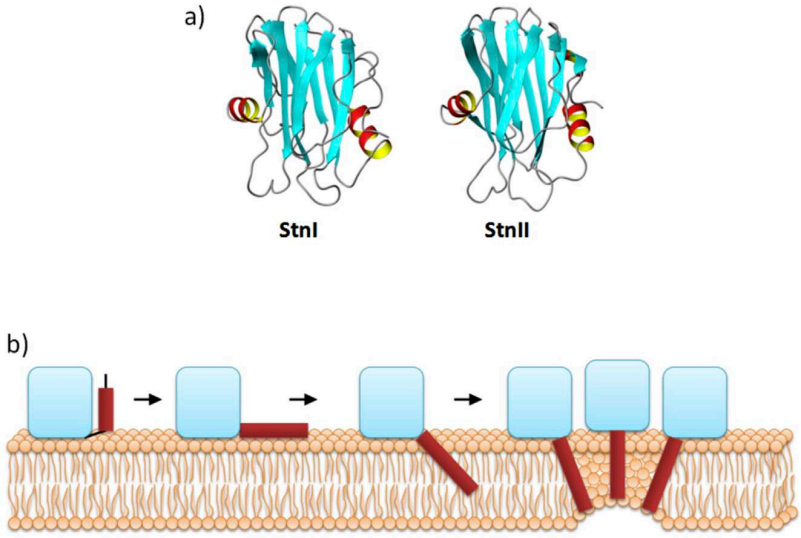

Fig. 1. Structural diagrams (a) **and general mechanism of action** (b) **of actinoporins StnI and StnII**. Diagrams show the three-dimensional soluble structures of sticholysins I (PDB 2KS4), and II (PDB 1GWY) and were made using MOLMOL program [83]. Regarding the mechanism, once the protein is attached to the membrane, the N-terminal α-helix extends, lies on the membrane surface and inserts into the bilayer. Finally, oligomerization leads to a pore. The order in which these events takes place, as well as the final structure and stoichiometry of the functional pore are still subject of intense studies [3,4,12,13,21,23,24]. The blue shape represents the β-sandwich core. The red dark bars represent the 30 first residues before and after the extension of the α helix. (For interpretation of the references to colour in this figure legend, the reader is referred to the web version of this article.)

dimensional structures [8–13] (Fig. 1a). Quite intriguingly, despite the small number of different amino acids existing among them, sometimes they suffice to promote significant differences in terms of solubility or pore-forming activity [33,43–46]. Sticholysin I and II (StnI and StnII) are the best example to analyze this observation, since they are not only produced by the same sea anemone (*Stichodactyla helianthus*) [44], but they are also two of the best characterized actinoporins [3,4,46–48] and can be independently produced in *E. coli* [47], completely ruling out the risk of cross-contamination. Furthermore, they share 93% of their sequence but, simultaneously, show high differences in their binding affinity to membranes and, consequently, hemolytic and pore-forming activities [33,44,47–52].

As explained above, the N-terminal stretch (around the first 30 amino acid residues) is the protein region which extends and inserts within the membrane, lining the walls of the pore (Fig. 1b), as well as the segment showing the highest rate of residue differences between both proteins. Interestingly, the variability in this region of the actinoporins sequence is quite evident in terms of hydrophobicity and charged residues distribution [10,12,53]. These changes include StnI Asp9, apparently involved in a salt bridge with Lys68, which equivalent position is an Ala residue in StnII. The work presented now shows how replacement of only one residue within this N-terminal stretch, which is involved in a salt bridge, suffices to transform StnI into StnII in terms of hemolytic and calcein-release activities but, on the other hand, has no influence on the synergistic relationship recently proved to exist between both actinoporin isoforms [54].

2. Materials and methods

2.1. Materials

Dioleylphosphatidylcholine (DOPC), porcine brain SM, and cholesterol (Chol) were obtained from Avanti Polar Lipids (Alabaster, AL). Calcein was obtained from Sigma-Aldrich.

2.2. Protein production and purification

The preparation of the cDNA encoding the actinoporins, as well as the independent production and purification of both proteins, has been previously described for StnI and StnII [42,47]. Protein production in RB791 *E. coli* cells was induced at OD_{600} of 1.0 with 1 mM IPTG for 4 h at 37 °C. Then, cells were harvested, and cellular pellet was subjected to seven pulses of sonication (20 kc, 1 min) in an ice bath. Tris buffer (50 mM) including 1% Tween 20 was employed; pH was set depending on the theoretical pI value of the corresponding mutant (pH 6.5 for StnI and StnIIA8D, pH 7.5 for StnII, StnIE2A, StnID9A and StnIE2AD9A). The soluble fraction was loaded onto a carboxymethylcellulose CM52 (Whatman, Brentford, England, UK) and eluted with a 0–0.5 M NaCl (0–0.3 M NaCl when purifying protein versions with lower pI values) gradient in 50 mM Tris buffer after appropriate washing steps.

2.3. Homogeneity of protein preparations and spectroscopic characterization

All protein samples were purified to homogeneity in mg amounts according to their electrophoretic behavior analyzed by 0.1% (w/v) SDS − 15% (w/v) PAGE performed under standard conditions [55]. Furthermore, acid hydrolysis of the proteins (5.7 M HCl for 24 h at 110 °C) followed by the corresponding amino acid analyses made on a Biochrom 20 automatic analyzer (Pharmacia, Pfizer, New York, NY) confirmed the homogeneity of all protein samples used. These results were also used to calculate extinction coefficients for each actinoporin variant (Table 1), which were then used to measure protein concentrations in all experiments described below. All the protein batches used were also characterized in terms of recording their far- and near-UV circular dichroism (CD) spectra on a Jasco (Easton, MD) 715 spectropolarimeter and their fluorescence emission spectra on an SLM Aminco (Urbana, IL) model 8000 spectrofluorimeter, also as previously described [22,33,48,56–58]. Near and far-UV CD spectra were recorded at 1.0 and 0.2 mg/mL, respectively, in 0.1 M NaCl and 15 mM Mops (pH 7.5). An identical buffer was used for the fluorescence emission spectra with the proteins at concentrations of 0.1 mg/mL. Thermal denaturation was also evaluated as described before [17,47]. At neutral pH, thermal denaturation of StnII occurs simultaneously with a fast aggregation, which can be monitored as optical path clarification (aggregates settling) by CD measurements at 220 nm. Temperature scans were carried out at a rate of 0.5 °C/min. Results are expressed as percentages of the total CD variation versus temperature. T_m corresponds to the temperature at the midpoint of the monophasic thermal transition.

2.4. Hemolysis assays

Hemolysis assays were performed in 96-multiwell plates as previously described [17,47]. Briefly, erythrocytes from heparinized sheep

Table 1
Calculated extinction coefficients ($E^{0.1\%}$), content of Trp and Tyr residues, relative Trp and Tyr emission yields, and melting temperature (T_m) of the different actinoporin variants used in this study.

Actinoporin	$E^{0.1\%}$ (280 nm, 1 cm)	Number of Trp	Number of Tyr	Relative Trp emission yield[a]	Relative Tyr emission yield[a]	T_m (°C)
StnI	2.55	5	13	1.00	1.00	65.0 ± 0.1[b]
StnII	2.54	5	12	1.12	2.27	67.0 ± 0.2[b]
StnIE2A	2.31	5	13	0.91	1.66	66.0 ± 0.1
StnID9A	2.39	5	13	1.02	1.98	59.0 ± 0.5
StnIE2AD9A	2.59	5	13	1.13	2.01	59.0 ± 0.4
StnIIA8D	2.63	5	12	1.25	1.80	72.0 ± 0.2

[a] Calculated as the area corresponding to the Trp emission spectra of each protein (Fig. 4) referred to the emission of wild-type StnI [33].
[b] [47].

blood were washed in 10 mM Tris buffer (pH 7.4) containing 0.145 M NaCl, to a final OD_{655} of 0.7 when mixing equal volumes of the cell suspension and buffer. Hemolysis was followed by recording the decrease in OD_{655} after addition of the erythrocyte suspension to different final concentrations of protein. An Expert 96 microplate reader (Asys Hitech, GmbH, Eugendorf, Austria) was employed to measure OD_{655}. The value obtained with 0.1% (w/v) Na_2CO_3 was considered as 100% hemolysis.

2.5. Lipid vesicles preparation

DOPC/SM/Chol (1:1:1) phospholipid vesicles represent one of the standard models most widely used to characterize StnI and StnII pore formation behavior [17,27,29,31,32,48,58–60]. They were prepared as described previously [31,48,61]. Briefly, a phospholipid (0.1–1.0 mg) solution in 2:1 (v/v) chloroform/methanol was dried under a flow of nitrogen, and the dry film obtained was used to prepare a lipid dispersion by adding 0.5–2.0 mL of Tris-NaCl buffer (the specific composition depends on the assay developed and is detailed below), briefly vortex mixing, and incubating for 1 h at 37 °C. This suspension of multilamellar vesicles was further subjected to five cycles of extrusion at 37 °C through polycarbonate filters (100-nm pore size) (Nucleopore, Whatman) to obtain a homogeneous population of unilamellar vesicles. Aliquots of freshly prepared LUVs between 10 and 25 μL were stored to determine the real concentration of phospholipids present in the mixture by phosphorus quantitation [62].

2.6. Calcein leakage assay

Calcein-entrapped large unilamellar vesicles (LUVs) were prepared from DOPC, SM, and Chol (1:1:1 M ratio) by extrusion through 100 nm filters (Nucleopore, Whatman) at 37 °C [60], essentially as described above but, prior to extrusion, the dry lipid films were hydrated for 1 h at 37 °C in Tris buffer (10 mM Tris, 140 mM NaCl, 1 mM EDTA, pH 7.4), containing 100 mM calcein. After hydration, and still before extrusion, the mixture was through 10 freeze/thaw cycles with liquid nitrogen in order to improve calcein encapsulation. LUVs were then extruded and separated from non-entrapped calcein by gel filtration on Sephacryl S200HR column. LUVs were used for permeabilization studies within 24 h using 96-multiwell plates and optimized standard protocols [31,32]. Emission at 520 nm was followed at 25 °C as a function of time (excitation at 485 nm). Fluorescence emission was measured on a FLUOstar OPTIMA microplate reader (BMG-Labtech, Ortenberg, Germany). Two-fold serial dilutions of the proteins were displayed in 96-multiwell plates and after addition of the same volume of calcein-entrapped LUVs (final concentration on the assay was 7.5 μM). Calcein leakage was automatically recorded every 3 s for 250 cycles (total time 12.5 min). One second of shaking was programmed before first measure to ensure the homogeneity within every well. The released fraction of calcein was determined based on the maximal calcein release, which was induced by LUV disintegration in 0.05% (v/v) Triton X-100 (100% leakage). To ensure that no spontaneous leakage occurred, a 0% leakage control containing buffer and calcein-loaded vesicles was measured through the complete time of the assay. A steady signal level, indicating intact vesicles, was observed for all samples.

2.7. Isothermal titration calorimetry

The interaction between the actinoporins and LUVs prepared from DOPC, SM, and Chol (1:1:1 M ratio, 100 nm diameter) was measured by isothermal titration calorimetry (ITC) as previously described [17,22,63], using a VP-ITC calorimeter (Malvern MicroCal Worcestershire, U.K.). Briefly, 0.5–10.0 μM protein solutions were titrated by injection of 20 μL aliquots of lipid suspensions (phospholipid concentration of 0.25–1.0 mM) at a constant temperature of 25 °C. The buffer employed consisted of 10 mM Tris pH 7.4, 100 mM NaCl, and 1 mM EDTA. Binding isotherms were adjusted to a model in which the protein binds to the membrane involving “n” lipid molecules [17].

3. Results

3.1. Hydrophobicity analysis identifies residues potentially responsible for StnI and StnII different hemolytic activity

Sequence alignment of the N-terminal stretches of StnI and StnII reveals only four major differences between both proteins along their first 30 amino acid residues (Fig. 2a). All four correspond to a net change of electric charge from neutral (StnII) to negative (StnI) or *vice versa*. As explained above, this segment of the protein extends to configure a longer amphipatic α-helix which then penetrates the membrane hydrophobic core to form the pore (Fig. 1b). Accordingly, the analysis of the hydrophobicity profile performed just along the first 18 amino acid residues revealed a dramatic difference between both proteins, not only in terms of hydrophobicity, but also of hydrophobic moment (Fig. 2b and c), as had been reported before [51,53]. The magnitude of this moment measures the amphiphilicity of the helix, and hence its tendency to seek a surface between hydrophobic and hydrophilic phases, whereas the hydrophobicity measures its affinity for the membrane core [64], therefore suggesting that the StnII α-helix resulting from the N-terminal extension would more easily interact with the membrane hydrophobic moiety.

This different hydrophobicity relies on the quite distinct chemical nature between the acidic residues occupying the second and ninth positions of StnI sequence and the equivalent Ala appearing in StnII (Fig. 2a). Interestingly, *in silico* analysis of the exchange of these two amino acids to produce a potential double mutant suggested the synthesis of a new Stn variant with N-terminal α-helix amphiphilic features which were practically indistinguishable from those observed for StnII (Fig. 2b–d). Consequently, the production, isolation and characterization of the StnI single E2A and D9A mutants and its corresponding double version (StnIE2AD9A) was performed, as described in the following sections.

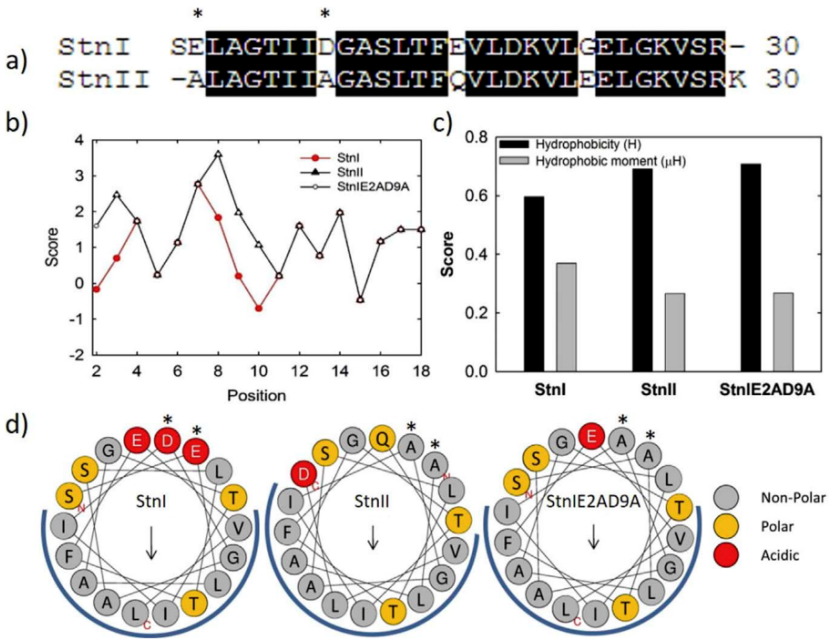

Fig. 2. Hydrophobicity of the N-terminal end. a) Sequence alignment of the first 30 residues of StnI and StnII. Conserved residues are highlighted in black. The residues mutated in this article are marked with an asterisk. b) Hydrophobicity profile of the first 18 residues according to [84]. The window size employed was 3 amino acids. Graph was made through simulation at Expasy ProScale web server tool (http://web.expasy.org/protscale/). c) Calculated hydrophobicity (H) and hydrophobic moment (μH) comparison among the first 18 N-terminal residues of wild-type StnI and II and the StnIE2AD9A variant. Data were calculated according to [64]. d) Helical wheel representation of the first 16 N-terminal amino acid residues of StnI, StnII and StnIE2AD9A, respectively. The arrow module indicates the hydrophobic moment and the direction marks the most hydrophobic face of the α-helix. The blue arc underlines the predicted hydrophobic surface of each amphipathic α-helix. N-termini and C-termini are indicated in red. Asterisks indicate the positions involved in the mutations made. Analysis performed using the web server HELIQUEST [85]. (For interpretation of the references to colour in this figure legend, the reader is referred to the web version of this article.)

3.2. The three StnI mutant variants retain the original water-soluble conformation of the wild-type protein

These three StnI mutants, as well as the wild-type protein, displayed identical far-UV CD spectra (Fig. 3A) showing that all proteins retained the characteristic water-soluble three-dimensional structure of actinoporins (Fig. 1). This observation was also confirmed by the practically indistinguishable near-UV CD (Fig. 3B) and fluorescence emission (Fig. 4) spectra, suggesting that not only the secondary structure content was identical but also that the arrangement of the aromatic amino acid side-chains was also preserved. Only Tyr emission was increased in the mutants (Table 1) suggesting a slight modification of the microenvironment of some Tyr side-chain in the vicinity of the residues mutated.

Wild-type StnII showed different spectroscopic features when compared to StnI or its mutants (Figs. 3 and 4), an observation which has been explained before [33,47,58] by its lower content of Tyr residues (Table 1).

StnI and StnII display similar T_m values [47]. However, whereas replacement of StnI Glu2 by Ala had a negligible effect on the thermostability of the protein, substitution of Asp9 rendered much less stable variants (Table 1), suggesting the participation of this Asp residue in establishing a stabilizing interaction within the core of the water-soluble monomeric structure (see below). Nevertheless, all

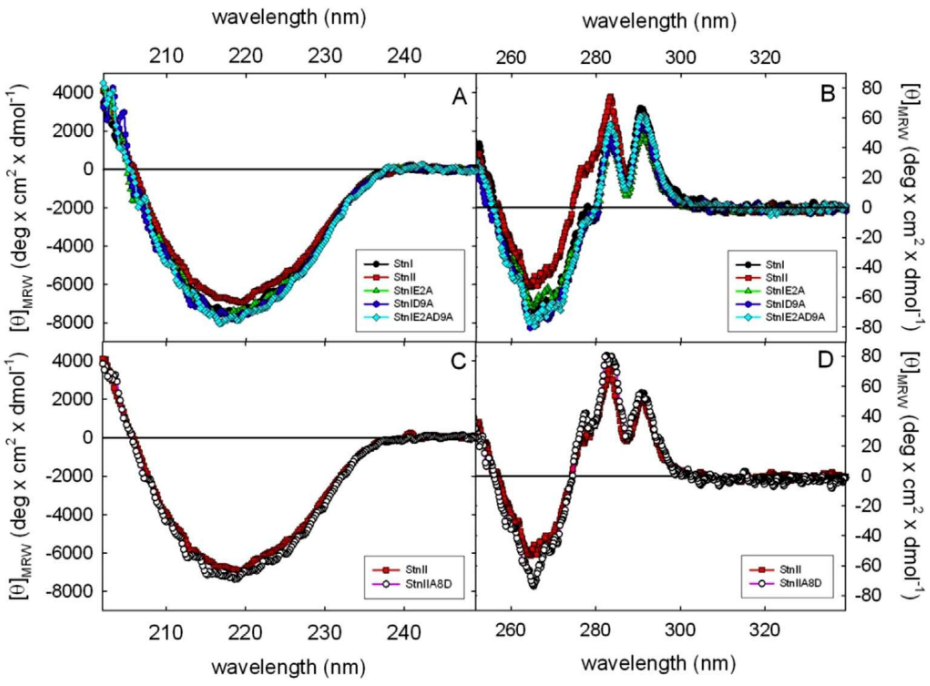

Fig. 3. Circular dichroism characterization. Far-UV (A and C) and near-UV (B and D) circular dichroism spectra of wild-type StnI and StnII and the four mutant variants studied.

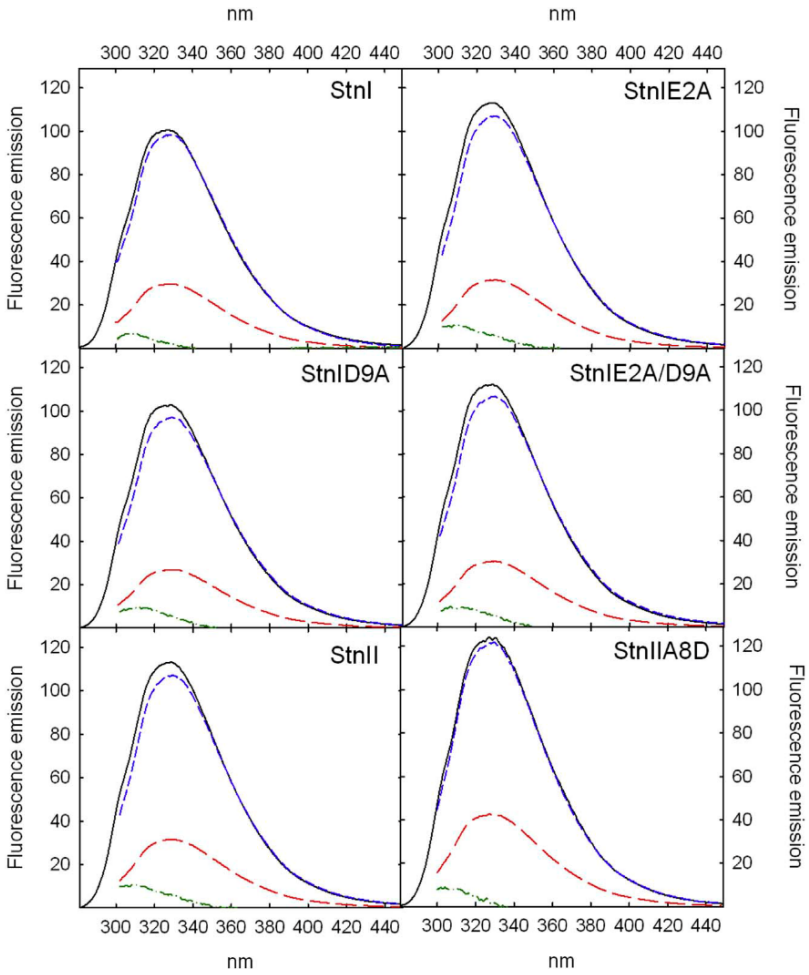

Fig. 4. Fluorescence emission spectra of wild-type StnI and StnII and the four mutant variants studied. All spectra were recorded at identical protein concentrations at excitation wavelengths of 275 nm (black solid lines) and 295 nm (red long dashed lines). These two spectra were normalized at wavelengths above 380 nm to obtain the Trp contribution (blue short dashed lines). Tyr contribution (green dashed-dot-dashed lines) was calculated by subtracting the Trp only contribution from the spectrum obtained after excitation at 275 nm. Fluorescence emission units were arbitrary, and referred to the maximum value of wild-type StnI upon excitation at 275 nm. (For interpretation of the references to colour in this figure legend, the reader is referred to the web version of this article.)

proteins studied still showed T_m values high above the temperatures used in all the other experiments performed, which allows to discard denaturation as a possible explanation of all the other results obtained and discussed in the following lines.

3.3. Substitution of StnI Asp9 by Ala produces a protein variant as hemolytic as wild-type StnII

Quantitation of the maximum hemolytic rates produced by the five (wild-type StnI and II and the three mutants described so far) revealed that substituting StnI Asp9 by Ala produced a protein variant as hemolytic as wild-type StnII, while replacement of Glu2 had an almost negligible effect (Fig. 5). This observation was further supported by leakage content experiments performed using DOPC/SM/Chol (1:1:1) calcein-containing LUVs where all proteins showed a behavior fully consistent with the hemolytic experiments (Fig. 6).

This functional behavior was further supported by the ITC characterization (Fig. 7). As described before [17,33,54], StnI and StnII display very different association constant values against DOPC/SM/Chol (1:1:1) LUVs which results in about 5-fold higher relative membrane binding (RMB) for StnII (Table 2). Interestingly, the number n of lipid molecules affected by StnII is consistently lower than those found for StnI (Table 2) maybe reflecting the observed higher oligomerization efficiency for the former one. This would also agree with the higher hemolytic activity of StnII. The three mutants studied, as well as both wild-type proteins, showed the enthalpy-driven process (Table 2) which is a distinct feature not only of actinoporins [17,33], but of several

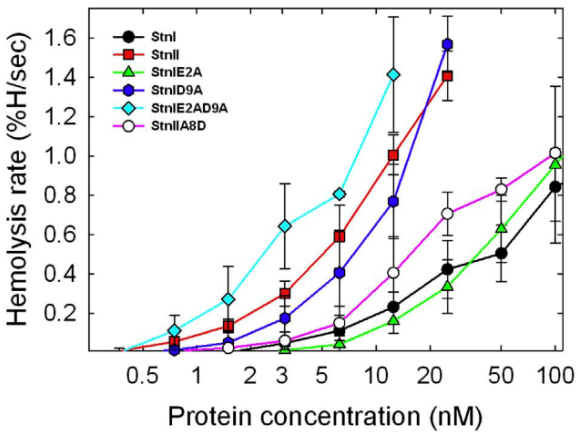

Fig. 5. Hemolysis. Maximum hemolytic activity rates of the wild-type and mutant actinoporins studied, expressed as a percentage of the hemolysis produced per second, is represented vs the logarithm of the protein concentration. The 100% value was calculated after addition of Na_2CO_3 to a final concentration of 0.1% (w/v). Results shown are the average of three independently performed experiments. Each of these experiments was made in duplicate. Error bars represent ± S.D.

other proteins whose behavior is dominated by an atypical hydrophobic interaction guided by favorable ΔH values [65,66]. Mutation of StnI Glu2 to Ala did already increase the K_a and RMB to values in the same order of magnitude as wild-type StnII (Table 2). As expected from the

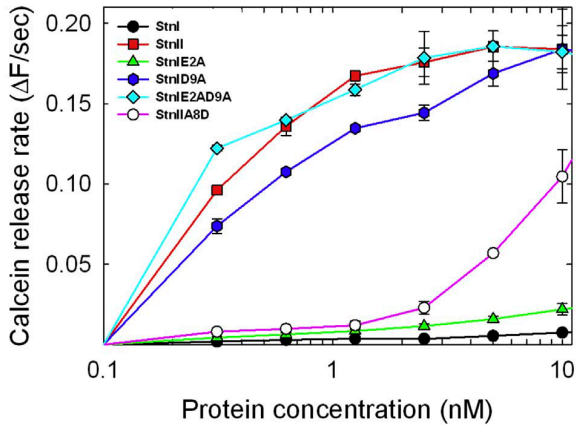

Fig. 6. Calcein release. Maximal rates of calcein release (expressed as normalized fluorescence intensity increment per second) vs the total protein concentration added to DOPC/SM/Chol (1:1:1) calcein-containing LUVs. Results shown are the average of three independently performed experiments. Each of these experiments was made in duplicate. Error bars represent ± S.D.

hemolytic and calcein-release results shown above, substitution of Asp9 had a much more dramatic effect on relative membrane binding (RMB) values, much higher than wild-type StnII, and a significant reduction in the number of lipid molecules (n) affected by the bound proteins (Table 2).

Overall, these results suggested that elimination of both negative electric charges of the residues mutated increases the affinity of StnI for the lipids but only removal of Asp9 did really influence oligomerization and pore formation efficiencies.

3.4. StnI Asp9 establishes a key ionic interaction with Lys68

Close inspection of the relative position of both acidic amino acids on the water-soluble three-dimensional structure of StnI revealed the existence of a salt bridge between the side-chains of Asp9 and Lys68 (Fig. 8). Lys68 is conserved among actinoporins but Ala is the amino acid occupying the equivalent residue of Asp9 in StnII (Fig. 2) [4]. This observation might be then interpreted as the mentioned salt bridge representing an impediment of the required N-terminal detachment for pore formation. This interaction could then be a major contributing factor to the minor pore-forming activity of StnI and the other two well-known actinoporins [33]. In fact, EqtII and FraC have an Asp residue at the corresponding position as well. It was therefore tempting to consider if replacement of this StnII Ala8 by Asp would yield a still more stable actinoporin version but with greatly diminished hemolytic activity.

When this StnIIA8D mutant was produced, isolated and characterized, it retained the structurally distinct spectroscopic features of wild-type StnII (Figs. 3 and 4) but was, in fact, much more thermostable (Table 1). Its T_m value was 7 °C higher than the wild-type protein. Consistent with the proposed hypothesis, it was also a mutant with diminished hemolytic and calcein-release activities (Figs. 5 and 6). ITC revealed a strong decrease in its binding affinity for the membranes employed (Fig. 7) with an RMB value of only 0.3, much lower than those ones obtained for StnI and StnII (1.0 and 5.2, respectively) (Table 2).

Altogether this set of results supported that the mentioned salt bridge is most probably a key element to explain the observed lower activity of StnI, EqtII, and FraC, when compared with wild-type StnII [33].

3.5. The mutations performed do not support the synergistic effect displayed by StnI and StnII

It has been recently shown how StnI and StnII can potentiate each other's activity because they can act in synergy to assemble into functional heteropores [54]. The effect is so dramatic that just traces of StnII in StnI/StnII mixtures have a major effect on binding affinity which is directly correlated with an enhancement of function [54]. Therefore, the hemolytic behavior of wild-type StnI and StnII in the absence or in the presence of only 1.0% of the four different mutants studied was also analyzed over a 1–10 nM concentration range (Fig. 9). As a positive control of this synergic effect, StnI:StnII (99:1) mixtures which behavior has been described before [54] were also included in the experiments. In this instance, however, none of the three mutant variants was able to reproduce the synergy previously attributed to the presence of wild-type StnII (Fig. 9). Only the wild-type StnI:StnIIA8D 99:1 mixture was able to support the synergy (Fig. 9B, green line) although to a much lesser extent, given the lower hemolytic activity of the StnII mutant employed. All these results together show that other protein regions apart from the N-terminal α–helix must be involved in this unique behavior. Finally, taking into account that it is widely accepted that the first N-terminal residues do not play a major role in actinoporins' binding to the membrane [17,59,67–69], these results would also support the previous observation that synergy appears at the membrane binding step rather than during the pore-formation phase [54].

4. Discussion

Actinoporins are multigene families which can potentially be produced as many different isoforms, not necessarily with the same specificity and/or toxic potency [40–43,45,46]. In fact, much is being speculated about the possible natural functional role for this molecular diversity within the same anemone species. Expanding the range of prey susceptible of being attacked, altogether with a much more modulated action of these proteins, including the existence of synergic effects, are among the preferred explanations. Furthermore, to add more complexity to an already complex scenario, in most of the examples known only one to three isoforms of the many more represented in their genomes seem to be produced in detectable amounts by these venomous animals [44,45,49,50,70].

Within this context, *S. helianthus* represents the optimal model of choice to study this network of relationships since not only two (StnI and StnII) of the several more actinoporin DNA sequences detected within its genome are produced by this anemone, but both isotoxins show different hemolytic and pore-forming activities [42,44,50]. This fairly distinguishable toxicity is indeed embedded within two very similar protein sequences showing 93% identity. The results shown now allow drawing key conclusions about the influence of a unique salt bridge, involving their N-terminal α-helix, on the actinoporins water-soluble structures and on their ability to oligomerize and produce a functional pore. Conclusions which are of general application given the amount of new results supporting the importance that salt bridges appear to have in protein design, folding and stability [71,72].

It was already well-known that N-terminal α-helices of StnI and StnII are the protein regions showing highest sequence variability and it had been even proposed, using 30 amino acids long peptide analogs, that their different activities were modulated by the hydrophobicity and electrostatic interactions of these N-terminal peptides [11,51]. However, this hypothesis had not been tested using the full-size proteins. Therefore, the work discussed now represents a highly significant step in understanding the pore-forming mechanism of α-PFTs at the molecular level.

The spectroscopic characterization performed was compatible with the four mutant proteins studied conserving the global water-soluble conformational fold of wild-type StnI and StnII. However, while replacement of StnI Glu2 by Ala had a negligible influence on the

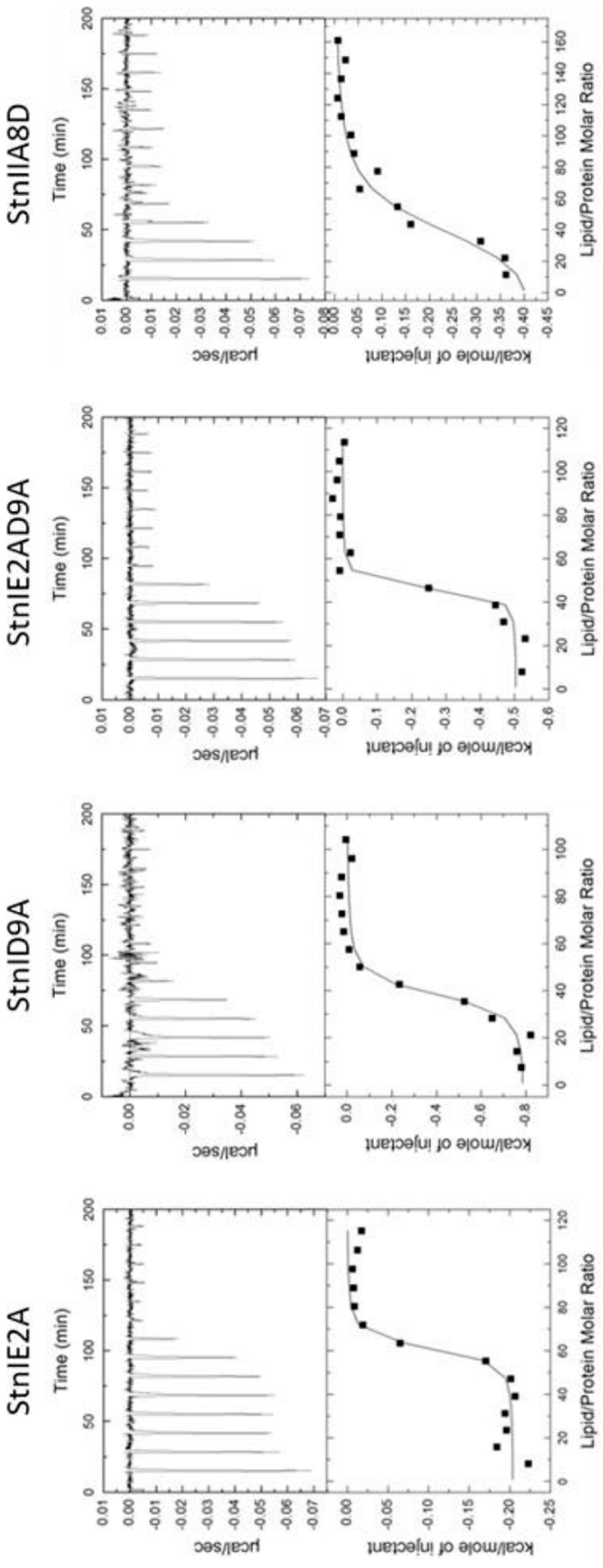

Fig. 7. ITC characterization. Lipid vesicles titration of the four different N-terminal mutants studied (molar ratios as indicated). DOPC/SM/Chol (1:1:1) vesicles were employed. Reactant concentrations for the examples shown were as indicated in Table 2, where P_0 refers to the initial total protein concentration within the calorimeter cell and L_0 is the lipid concentration within the dispensing auto-pipette. Binding isotherms were adjusted to a model in which protein membrane binding involves the participation of "n" lipid molecules [17,33,54]. The c values ($c = K_a \times P_0$) for the graphs shown were in the 1–1000 range.

Table 2
Binding of StnI, StnII, and the different N-terminal mutants studied to DOPC/SM/Chol (1:1:1) vesicles studied by ITC. P_0 refers to the initial total protein concentration within the calorimeter cell. Binding isotherms were adjusted to a previously described model in which protein membrane binding involves the participation of "n" lipid molecules [17,80,81]. The c values ($c = K_a \times P_0$) for all the graphs were in the range 1–1000, the needed requirement in order to produce thermograms with the curvature required for the simultaneous determination of K_a and ΔH [82]. K_a is the affinity constant calculated as described in Ref. [17]. Results shown are the average of at least three separate experiments. Parameters shown for wild-type StnI and StnII have been calculated before [17,33,54].

Protein	StnI	StnII	StnIE2A	StnID9A	StnIE2AD9A	StnIIA8D
K_a (M^{-1}) $\times 10^{-8}$	0.41 ± 0.03	1.7 ± 0.90	1.32 ± 1.00	2.85 ± 2.00	10 ± 1.67	0.10 ± 0.03
n	49 ± 1	39 ± 4	59 ± 3	34 ± 1	43 ± 1	41 ± 3
ΔH (kcal/mol)	−20.9 ± 2.1	−44.0 ± 3.0	−13.6 ± 2.0	−25.6 ± 2.0	−21.05 ± 0.6	−18.4 ± 1.4
ΔG (kcal/mol)	−8.21 ± 0.03	−9.1 ± 0.10	−7.98 ± 1.70	−9.47 ± 0.48	−10.15 ± 0.12	−7.50 ± 0.20
ΔS (cal/mol·K)	−42.84 ± 6.78	−115.00 ± 9.00	−18.90 ± 13.00	−54.30 ± 5.20	−36.56 ± 1.50	−36.70 ± 5.50
P_0 (μM)	10.0	1.5	1.5	0.5	0.5	0.75
$c = K_a \times P_0$	410	255	389	214	562	7
[a]RMB	1.0 ± 0.1	5.2 ± 1.8	2.7 ± 0.3	10.0 ± 1.0	27.8 ± 0.8	0.3 ± 0.1

[a] Relative membrane binding $[n_{(StnI)} \times K_{a(other)}]/[n_{(other)} \times K_{a(StnI)}]$ as explained in Ref. [17].

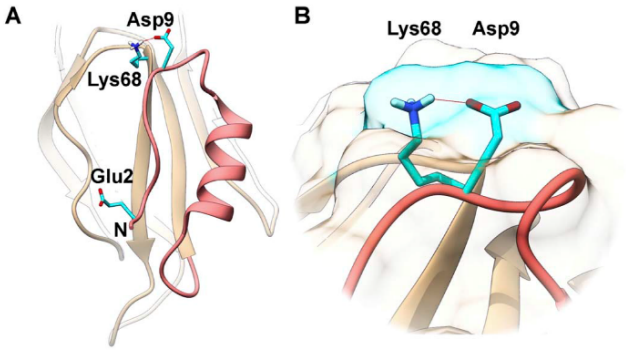

Fig. 8. Structural diagram showing the relative location of StnI mutated residues. (A) Partial representation of the three-dimensional soluble structure of sticholysin I (PDB 2KS4) showing the N-terminal stretch (in red color). The side-chains of Glu2, Asp9, and Lys68, as well as the position of the N-terminal end (N), are also indicated. (B) Close-up showing the solvent accessible surface surrounding the salt bridge between StnI Asp9 and Lys68. In wild-type StnII the equivalent residue to StnI Asp9 is Ala8 (StnII numbering). Diagram was made using UCSF-Chimera [86]. (For interpretation of the references to colour in this figure legend, the reader is referred to the web version of this article.)

thermostability of the protein, substitution of StnI Asp9 and StnII Ala8 had a dramatic effect on the T_m values of the mutants (Table 1). The results of these mutations were thus consistent with the existence of a salt bridge with StnI Lys68 (or StnII Lys 67 in the StnIIA8D mutant) which would not only greatly stabilize the protein but also impair the N-terminal extension and detachment required for pore formation. Conversely, decreased T_m for the StnID9A (unable to maintain the salt bridge) facilitated insertion while the substitution of Glu2 had a much less dramatic effect on the Tm value as well as on the hemolytic and calcein-release activities (Figs. 5 and 6). Another example supporting the general assumption that salt bridges can behave in much the same way as disulfide bonds in stabilizing and constraining protein structures [73]. It is in fact well-known how EqtII mutants artificially engineered to covalently attach their N-terminal stretch to the show highly impaired hemolytic activity [21].

This explanation is compatible with the former interpretation that the hydrophobicity and the amphiphilic properties of the extended N-terminal α-helices would also represent a key structural difference regarding the different hemolytic and pore-forming activities of the two actinoporins involved in this study. In fact, and as previously foreseen, replacement of the acidic amino acids by Ala residues, and most especially substitution of Asp9, produced mutants with RMB values greater than not only StnI but also StnII (Table 2). This increment in lipid-binding affinity was concomitant with a reduction in the number of lipid molecules affected by the protein (Table 2) suggesting an enhanced propensity to oligomerize and make a pore. All these determinations were also in perfect agreement with the observation that the StnI mutants where Asp9 had been substituted by Ala displayed hemolytic and calcein-release activities which were practically indistinguishable from those of StnII (Figs. 5 and 6). Within the same idea, replacement of StnII Ala8 by Asp rendered a protein with much less binding affinity. Therefore, it can be concluded that the lower hydrophobic moment and the increased amphiphilicity of StnII N-terminal extended α-helix are also major factors contributing to the increased membrane pore-formation activity of intact wild-type StnII. It would not be, however, the key structural element explaining the higher

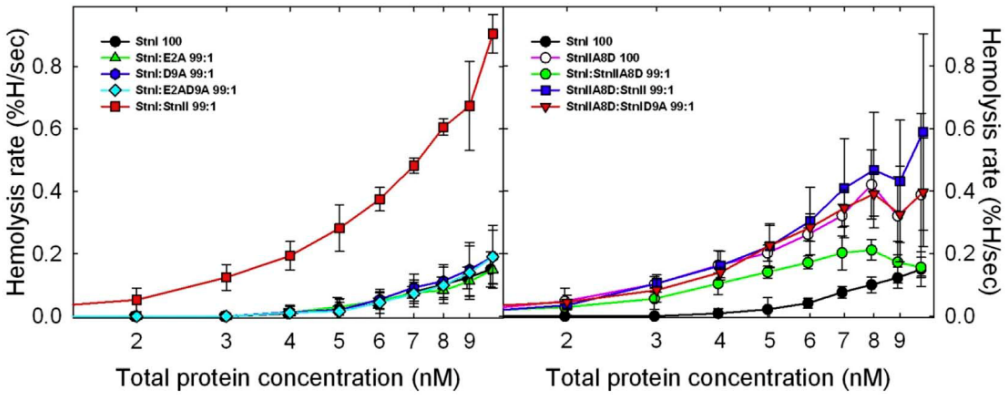

Fig. 9. Synergic effect on hemolysis. Maximum hemolytic rate values (expressed as percentage of hemolysis/sec) are represented vs the logarithm of total protein concentration of StnI, StnIIA8D or different 99:1 mixtures [54]. In these experiments the amount of wild-type StnII present in the corresponding mixture (red line, left panel) was so low that when assayed in the absence of StnI its hemolytic activity was undetectable in the time range measured. Results shown are the average of three independently performed experiments. Each of these experiments was made in duplicate. Error bars represent ± S.D. (For interpretation of the references to colour in this figure legend, the reader is referred to the web version of this article.)

hemolytic activity of StnII over the other three well-known actinoporins. These experiments do also suggest, as it was somehow expected, that membrane affinity, as measured by ITC, would not be only influenced by the actual fact of binding but also by the later events conducing to pore formation. Within this idea, the present results do also show that N-terminal α-helix extension and detachment would shift the binding equilibrium and therefore play an important role in actinoporins membrane recognition as well.

On the other hand, none of the substitutions performed was able to reproduce the observed synergic effect described for wild-type StnI and StnII [54] (Fig. 8), suggesting that some other residues apart from those appearing along the first 18 amino acids of both proteins must be responsible for establishing the required interactions needed to produce StnI-StnII heteropores [54], most probably affecting residues at the protomer-protomer interacting surfaces occurring upon oligomerization.

Interestingly, these results can be extrapolated to other pore-forming proteins such as the Bcl-2 family proteins, involved in the apoptosis process such as Bax and Bak, two of the most well studied pro-apoptotic proteins [5,74–77]. It is well known that they homodimerize to bind to the mitochondrial outer membrane forming a toroidal pore permeable to cytochrome C. This event precedes the apoptotic cascade whose final aim is the onset of programmed cell death. Binding of both proteins to the membrane is leaded by the insertion of α-helices as well, although in this instance they are located at their C-terminal ends. Hydrophobic analysis of these segments did also reveal that in both cases these helices have a high tendency to be immersed within the hydrophobic phase of the membrane. In fact, as it has been now shown for actinoporins, non-conservative mutations along these regions have profound effects in the function of these proteins, resulting in variants with less affinity for the membrane. Some of these non-conservative mutations have been even detected in some tumoral processes such as melanoma [78,79], for example. Therefore, the mechanism now reported for explaining the observed different actinoporins' activity might be of more general application to at least several other PFTs like the aforementioned pro-apoptotic proteins.

In conclusion, the results shown here demonstrate that replacement of a single StnI residue, Asp9 by Ala, is enough to transform this actinoporin into a mutated version with identical pore-forming activity as its much more hemolytic counterpart, the wild-type isotoxin StnII. Within this same idea, StnIIA8D was also much less active than the wild-type protein. These results can be safely interpreted as revealing the key importance of a salt bridge linking the N-terminal stretch of actinoporins to their β-sandwich core. These changes, however, do not fulfill the protomer-protomer interactions needed to explain the recently described synergy between both wild-type StnI and StnII. The mechanism described might be of general application to other well-known PFTs and sustains the more general conclusion that salt bridges can be key actors of protein design, folding and stability.

Author contributions

JPO, ERT, and SGL conducted the experiments. JPO, ERT, SGL, JGG, and AMP conceived and designed the experiments, analyzed and discussed the results, wrote and corrected the manuscript, and suggested modifications.

Acknowledgements

This work was supported in part by the following undergraduate fellowships: FPU from MCINN to SGL, UCM-Banco Santander to ERT, and UCM-collaboration to JPO. We want to thank Prof. J. Peter Slotte from Åbo Akademi University (Turku, Finland) for his continuous support and helpful discussions.

References

[1] P. Maček, Polypeptide cytolytic toxins from sea anemones (*Actiniaria*), FEMS Microbiol. Immunol. 5 (1992) 121–129.
[2] G. Anderluh, P. Maček, Cytolytic peptide and protein toxins from sea anemones (Anthozoa: Actiniaria), Toxicon 40 (2002) 111–124.
[3] J. Alegre-Cebollada, M. Oñaderra, J.G. Gavilanes, A. Martínez-del-Pozo, Sea anemone actinoporins: the transition from a folded soluble state to a functionally active membrane-bound oligomeric pore, Curr. Protein Pept. Sci. 8 (2007) 558–572.
[4] L. García-Ortega, J. Alegre-Cebollada, S. García-Linares, M. Bruix, A. Martínez-del-Pozo, J.G. Gavilanes, The behavior of sea anemone actinoporins at the water-membrane interface, Biochim. Biophys. Acta 1808 (2011) 2275–2288.
[5] K. Cosentino, U. Ros, A.J. García-Sáez, Assembling the puzzle: oligomerization of α-pore forming proteins in membranes, Biochim. Biophys. Acta 1858 (2016) 457–466.
[6] J.H. Lakey, S.L. Slatin, Pore-forming colicins and their relatives, Curr. Top. Microbiol. 257 (2001) 131–161.
[7] A.J. García-Sáez, G. Fuertes, J. Suckale, J. Salgado, Permeabilization of the outer mitochondrial membrane by Bcl-2 proteins, Adv. Exp. Med. Biol. 677 (2010) 91–105.
[8] A. Athanasiadis, G. Anderluh, P. Maček, D. Turk, Crystal structure of the soluble form of equinatoxin II, a pore-forming toxin from the sea anemone *Actinia equina*, Structure 9 (2001) 341–346.
[9] M.G. Hinds, W. Zhang, G. Anderluh, P.E. Hansen, R.S. Norton, Solution structure of the eukaryotic pore-forming cytolysin equinatoxin II: implications for pore formation, J. Mol. Biol. 315 (2002) 1219–1229.
[10] J.M. Mancheño, J. Martín-Benito, M. Martínez-Ripoll, J.G. Gavilanes, J.A. Hermoso, Crystal and electron microscopy structures of sticholysin II actinoporin reveal insights into the mechanism of membrane pore formation, Structure 11 (2003) 1319–1328.
[11] I. Castrillo, N.A. Araujo, J. Alegre-Cebollada, J.G. Gavilanes, A. Martínez-del-Pozo, M. Bruix, Specific interactions of sticholysin I with model membranes: an NMR study, Proteins 78 (2010) 1959–1970.
[12] A.E. Mechaly, A. Bellomio, D. Gil-Carton, K. Morante, M. Valle, J.M. González-Mañas, et al., Structural insights into the oligomerization and architecture of eukaryotic membrane pore-forming toxins, Structure 19 (2011) 181–191.
[13] K. Tanaka, J.M. Caaveiro, K. Morante, J.M. González-Mañas, K. Tsumoto, Structural basis for self-assembly of a cytolytic pore lined by protein and lipid, Nat. Commun. 6 (2015) 6337.
[14] G. Anderluh, M. Dalla Serra, G. Viero, G. Guella, P. Maček, G. Menestrina, Pore formation by equinatoxin II, a eukaryotic protein toxin, occurs by induction of nonlamellar lipid structures, J. Biol. Chem. 278 (2003) 45216–45223.
[15] P. Malovrh, G. Viero, M.D. Serra, Z. Podlesek, J.H. Lakey, P. Maček, et al., A novel mechanism of pore formation: membrane penetration by the N-terminal amphipathic region of equinatoxin, J. Biol. Chem. 278 (2003) 22678–22685.
[16] J. Alegre-Cebollada, A. Martínez-del-Pozo, J.G. Gavilanes, E. Goormaghtigh, Infrared spectroscopy study on the conformational changes leading to pore formation of the toxin sticholysin II, Biophys. J. 93 (2007) 3191–3201.
[17] J. Alegre-Cebollada, M. Cunietti, E. Herrero-Galán, J.G. Gavilanes, A. Martínez-del-Pozo, Calorimetric scrutiny of lipid binding by sticholysin II toxin mutants, J. Mol. Biol. 382 (2008) 920–930.
[18] B. Bakrač, I. Gutierrez-Aguirre, Z. Podlesek, A.F. Sonnen, R.J. Gilbert, P. Maček, et al., Molecular determinants of sphingomyelin specificity of a eukaryotic pore-forming toxin, J. Biol. Chem. 283 (2008) 18665–18677.
[19] B. Bakrač, G. Anderluh, Molecular mechanism of sphingomyelin-specific membrane binding and pore formation by actinoporins, Adv. Exp. Med. Biol. 677 (2010) 106–115.
[20] K.C. Kristan, G. Viero, M. Dalla Serra, P. Maček, G. Anderluh, Molecular mechanism of pore formation by actinoporins, Toxicon 54 (2009) 1125–1134.
[21] N. Rojko, K.C. Kristan, G. Viero, E. Zerovnik, P. Maček, M. Dalla Serra, et al., Membrane damage by an α-helical pore-forming protein, Equinatoxin II, proceeds through a succession of ordered steps, J. Biol. Chem. 288 (2013) 23704–23715.
[22] S. García-Linares, R. Richmond, M.F. García-Mayoral, N. Bustamante, M. Bruix, J.G. Gavilanes, et al., The sea anemone actinoporin (Arg-Gly-Asp) conserved motif is involved in maintaining the competent oligomerization state of these pore-forming toxins, FEBS J. 281 (2014) 1465–1478.
[23] K. Tanaka, J.M. Caaveiro, K. Tsumoto, Bidirectional transformation of a metamorphic protein between the water-soluble and transmembrane native states, Biochemistry-Us 54 (2015) 6863–6866.
[24] K. Morante, A. Bellomio, D. Gil-Carton, L. Redondo-Morata, J. Sot, S. Scheuring, et al., Identification of a membrane-bound prepore species clarifies the lytic mechanism of actinoporins, J. Biol. Chem. 291 (2016) 19210–19219.
[25] G. Belmonte, C. Pederzolli, P. Maček, G. Menestrina, Pore formation by the sea anemone cytolysin equinatoxin-II in red blood cells and model lipid membranes, J. Membr. Biol. 131 (1993) 11–22.
[26] M. Tejuca, M.D. Serra, M. Ferreras, M.E. Lanio, G. Menestrina, Mechanism of membrane permeabilization by sticholysin I, a cytolysin isolated from the venom of the sea anemone *Stichodactyla helianthus*, Biochemistry-Us 35 (1996) 14947–14957.
[27] J. Alegre-Cebollada, I. Rodríguez-Crespo, J.G. Gavilanes, A. Martínez-del-Pozo, Detergent-resistant membranes are platforms for actinoporin pore-forming activity on intact cells, FEBS J. 273 (2006) 863–871.
[28] M.L. Shin, D.W. Michaels, M.M. Mayer, Membrane damage by a toxin from the sea anemone *Stoichactis helianthus*. II. Effect of membrane lipid composition in a liposome system, Biochim. Biophys. Acta 555 (1979) 79–88.
[29] V. De los Ríos, J.M. Mancheño, M.E. Lanio, M. Oñaderra, J.G. Gavilanes,

Mechanism of the leakage induced on lipid model membranes by the hemolytic protein sticholysin II from the sea anemone *Stichodactyla helianthus*, Eur. J. Biochem. 252 (1998) 284–289.
[30] D. Martínez, A. Otero, C. Álvarez, F. Pazos, M. Tejuca, M.E. Lanio, et al., Effect of sphingomyelin and cholesterol on the interaction of St II with lipidic interfaces, Toxicon 49 (2007) 68–81.
[31] I. Alm, S. García-Linares, J.G. Gavilanes, A. Martínez-del-Pozo, J.P. Slotte, Cholesterol stimulates and ceramide inhibits sticholysin II-induced pore formation in complex bilayer membranes, Biochim. Biophys. Acta - Biomembr. 1848 (2015) 925–931.
[32] S. García-Linares, I. Alm, T. Maula, J.G. Gavilanes, J.P. Slotte, A. Martínez-Del-Pozo, The effect of cholesterol on the long-range network of interactions established among sea anemone Sticholysin II residues at the water-membrane interface, Mar. Drugs 13 (2015) 1647–1665.
[33] S. García-Linares, E. Rivera-de-Torre, K. Morante, K. Tsumoto, J.M. Caaveiro, J.G. Gavilanes, et al., Differential effect of membrane composition on the pore-forming ability of four different sea anemone actinoporins, Biochemistry-Us 55 (2016) 6630–6641.
[34] J. Palacios-Ortega, S. García-Linares, M. Astrand, M.A. Al Sazzad, J.G. Gavilanes, A. Martínez-del-Pozo, et al., Regulation of sticholysin II-induced pore formation by lipid bilayer composition, phase state, and interfacial properties, Langmuir 32 (2016) 3476–3484.
[35] J.M. Caaveiro, I. Echabe, I. Gutiérrez-Aguirre, J.L. Nieva, J.L. Arrondo, J.M. González-Mañas, Differential interaction of equinatoxin II with model membranes in response to lipid composition, Biophys. J. 80 (2001) 1343–1353.
[36] B. Bakrač, A. Kladnik, P. Maček, G. McHaffie, A. Werner, J.H. Lakey, et al., A toxin-based probe reveals cytoplasmic exposure of golgi sphingomyelin, J. Biol. Chem. 285 (2010) 22186–22195.
[37] K. Morante, J.M. Caaveiro, K. Tanaka, J.M. González-Mañas, K. Tsumoto, A pore-forming toxin requires a specific residue for its activity in membranes with particular physicochemical properties, J. Biol. Chem. 290 (2015) 10850–10861.
[38] L. Pedrera, A.B. Gomide, R.E. Sánchez, U. Ros, N. Wilke, F. Pazos, et al., The presence of sterols favors sticholysin I-membrane association and pore formation regardless of their ability to form laterally segregated domains, Langmuir 31 (2015) 9911–9923.
[39] H.P. Wacklin, B.B. Bremec, M. Moulin, N. Rojko, M. Haertlein, T. Forsyth, et al., Neutron reflection study of the interaction of the eukaryotic pore-forming actinoporin equinatoxin II with lipid membranes reveals intermediate states in pore formation, Biochim. Biophys. Acta 1858 (2016) 640–652.
[40] T. Turk, Cytolytic toxins from sea anemones, Toxin Rev. 10 (1991) 223–262.
[41] G. Anderluh, I. Krizaj, B. Strukelj, F. Gubensek, P. Maček, J. Pungercar, Equinatoxins, pore-forming proteins from the sea anemone *Actinia equina*, belong to a multigene family, Toxicon 37 (1999) 1391–1401.
[42] V. De los Ríos, M. Oñaderra, A. Martínez-Ruiz, J. Lacadena, J.M. Mancheño, A. Martínez-del-Pozo, et al., Overproduction in *Escherichia coli* and purification of the hemolytic protein sticholysin II from the sea anemone *Stichodactyla helianthus*, Protein Expr. Purif. 18 (2000) 71–76.
[43] Y. Wang, L.L. Yap, K.L. Chua, H.E. Khoo, A multigene family of *Heteractis* magnificalysins (HMgs), Toxicon 51 (2008) 1374–1382.
[44] C. Álvarez, J.M. Mancheño, D. Martínez, M. Tejuca, F. Pazos, M.E. Lanio, Sticholysins, two pore-forming toxins produced by the Caribbean sea anemone *Stichodactyla helianthus*: their interaction with membranes, Toxicon 54 (2009) 1135–1147.
[45] M. Monastyrnaya, E. Leychenko, M. Isaeva, G. Likhatskaya, E. Zelepuga, E. Kostina, et al., Actinoporins from the sea anemones, tropical *Radianthus macrodactylus* and northern *Oulactis orientalis*: comparative analysis of structure-function relationships, Toxicon 56 (2010) 1299–1314.
[46] G.I. Uechi, H. Toma, T. Arakawa, Y. Sato, Molecular characterization on the genome structure of hemolysin toxin isoforms isolated from sea anemone *Actineria villosa* and *Phyllodiscus semoni*, Toxicon 56 (2010) 1470–1476.
[47] J. Alegre-Cebollada, G. Clementi, M. Cunietti, C. Porres, M. Oñaderra, J.G. Gavilanes, et al., Silent mutations at the 5'-end of the cDNA of actinoporins from the sea anemone *Stichodactyla helianthus* allow their heterologous overproduction in *Escherichia coli*, J. Biotechnol. 127 (2007) 211–221.
[48] S. García-Linares, I. Castrillo, M. Bruix, M. Menéndez, J. Alegre-Cebollada, A. Martínez-del-Pozo, et al., Three-dimensional structure of the actinoporin sticholysin I. Influence of long-distance effects on protein function, Arch. Biochem. Biophys. 532 (2013) 39–45.
[49] C.A. Valcarcel, M. Dalla Serra, C. Potrich, I. Bernhart, M. Tejuca, D. Martínez, et al., Effects of lipid composition on membrane permeabilization by sticholysin I and II, two cytolysins of the sea anemone *Stichodactyla helianthus*, Biophys. J. 80 (2001) 2761–2774.
[50] D. Martínez, V. Morera, C. Álvarez, M. Tejuca, F. Pazos, Y. García, et al., Identity between cytolysins purified from two morphos of the Caribbean sea anemone *Stichodactyla helianthus*, Toxicon 40 (2002) 1219.
[51] U. Ros, L. Pedrera, D. Diaz, J.C. Karam, T.P. Sudbrack, P.A. Valiente, et al., The membranotropic activity of N-terminal peptides from the pore-forming proteins sticholysin I and II is modulated by hydrophobic and electrostatic interactions as well as lipid composition, J. Biosci. 36 (2011) 781–791.
[52] A. del Monte-Martínez, J. González-Bacerio, L. Romero, C. Aragon, D. Martínez, M.D.L.A. Chávez, et al., Improved purification and enzymatic properties of a mixture of Sticholysin I and II: isotoxins with hemolytic and phospholipase A(2) activities from the sea anemone *Stichodactyla helianthus*, Protein Expres Purif. 95 (2014) 57–66.
[53] U. Ros, W. Rodríguez-Vera, L. Pedrera, P.A. Valiente, S. Cabezas, M.E. Lanio, et al., Differences in activity of actinoporins are related with the hydrophobicity of their N-terminus, Biochimie 116 (2015) 70–78.
[54] E. Rivera-de-Torre, S. García-Linares, J. Alegre-Cebollada, J. Lacadena, J.G. Gavilanes, A. Martínez-Del-Pozo, Synergistic action of actinoporin isoforms from the same sea anemone species assembled into functionally active heteropores, J. Biol. Chem. 291 (2016) 14109–14119.
[55] U.K. Laemli, Cleavage of structural proteins during the assembly of the head of bacteriophage T4, Nature 227 (1970) 680–685.
[56] C. De Antonio, A. Martínez-del-Pozo, J.M. Mancheño, M. Oñaderra, J. Lacadena, A. Martínez-Ruiz, et al., Assignment of the contribution of the tryptophan residues to the spectroscopic and functional properties of the ribotoxin α-sarcin, Proteins 41 (2000) 350–361.
[57] M.A. Pardo-Cea, I. Castrillo, J. Alegre-Cebollada, A. Martínez-del-Pozo, J.G. Gavilanes, M. Bruix, Intrinsic local disorder and a network of charge-charge interactions are key to actinoporin membrane disruption and cytotoxicity, FEBS J. 278 (2011) 2080–2089.
[58] S. García-Linares, T. Maula, E. Rivera-de-Torre, J.G. Gavilanes, J.P. Slotte, A. Martínez-del-Pozo, Role of the tryptophan residues in the specific interaction of the sea anemone *Stichodactyla helianthus*'s actinoporin sticholysin II with biological membranes, Biochemistry-Us 55 (2016) 6406–6420.
[59] J. Alegre-Cebollada, V. Lacadena, M. Oñaderra, J.M. Mancheño, J.G. Gavilanes, A. Martínez-del-Pozo, Phenotypic selection and characterization of randomly produced non-haemolytic mutants of the toxic sea anemone protein sticholysin II, FEBS Lett. 575 (2004) 14–18.
[60] S. García-Linares, J. Palacios-Ortega, T. Yasuda, M. Astrand, J.G. Gavilanes, A. Martínez-del-Pozo, et al., Toxin-induced pore formation is hindered by intermolecular hydrogen bonding in sphingomyelin bilayers, Biochim. Biophys. Acta 1858 (2016) 1189–1195.
[61] A. Martínez-Ruiz, L. García-Ortega, R. Kao, J. Lacadena, M. Oñaderra, J.M. Mancheño, et al., RNase U2 and α-sarcin: a study of relationships, Methods Enzymol. 341 (2001) 335–351.
[62] G.R. Bartlett, Colorimetric assay methods for free and phosphorylated glyceric acids, J. Biol. Chem. 234 (1959) 469–471.
[63] T. Maula, Y.J. Isaksson, S. García-Linares, S. Niinivehmas, O.T. Pentikainen, M. Kurita, et al., 2NH and 3OH are crucial structural requirements in sphingomyelin for sticholysin II binding and pore formation in bilayer membranes, Biochim. Biophys. Acta 1828 (2013) 1390–1395.
[64] D. Eisenberg, E. Schwarz, M. Komaromy, R. Wall, Analysis of membrane and surface protein sequences with the hydrophobic moment plot, J. Mol. Biol. 179 (1984) 125–142.
[65] J. Seelig, Titration calorimetry of lipid-peptide interactions, Biochimica Biophysica Acta - Rev. Biomembr. 1331 (1997) 103–116.
[66] R. Malham, S. Johnstone, R.J. Bingham, E. Barratt, S.E. Phillips, C.A. Laughton, et al., Strong solute-solute dispersive interactions in a protein-ligand complex, J. Am. Chem. Soc. 127 (2005) 17061–17067.
[67] G. Anderluh, J. Pungercar, I. Krizaj, B. Strukelj, F. Gubensek, P. Maček, N-terminal truncation mutagenesis of equinatoxin II, a pore-forming protein from the sea anemone *Actinia equina*, Protein Eng. 10 (1997) 751–755.
[68] Q. Hong, I. Gutiérrez-Aguirre, A. Barlič, P. Malovrh, K. Kristan, Z. Podlesek, et al., Two-step membrane binding by equinatoxin II, a pore-forming toxin from the sea anemone, involves an exposed aromatic cluster and a flexible helix, J. Biol. Chem. 277 (2002) 41916–41924.
[69] K. Kristan, Z. Podlesek, V. Hojnik, I. Gutiérrez-Aguirre, G. Guncar, D. Turk, et al., pore formation by equinatoxin, a eukaryotic pore-forming toxin, requires a flexible N-terminal region and a stable β-sandwich, J. Biol. Chem. 279 (2004) 46509–46517.
[70] P. Maček, D. Lebez, Isolation and characterization of three lethal and hemolytic toxins from the sea anemone Actinia equina L, Toxicon 26 (1988) 441–451.
[71] J.E. Donald, D.W. Kulp, W.F. DeGrado, Salt bridges: geometrically specific, designable interactions, Proteins 79 (2011) 898–915.
[72] S. Basu, D. Mukharjee, Salt-bridge networks within globular and disordered proteins: characterizing trends for designable interactions, J. Mol. Model (2017) 23.
[73] U. Bastolla, L. Demetrius, Stability constraints and protein evolution: the role of chain length, composition and disulfide bonds, Protein Eng. Des. Sel. 18 (2005) 405–415.
[74] M. Suzuki, R.J. Youle, N. Tjandra, Structure of Bax: coregulation of dimer formation and intracellular localization, Cell 103 (2000) 645–654.
[75] R. Salvador-Gallego, M. Mund, K. Cosentino, J. Schneider, J. Unsay, U. Schraermeyer, et al., Bax assembly into rings and arcs in apoptotic mitochondria is linked to membrane pores, EMBO J. 35 (2016) 389–401.
[76] J.D. Unsay, K. Cosentino, K. Sporbeck, A.J. García-Sáez, Pro-apoptotic cBid and Bax exhibit distinct membrane remodeling activities: an AFM study, Biochim. Biophys. Acta 1859 (2016) 17–27.
[77] K. Cosentino, AJ. Bax García-Sáez, Bak Pores, Are we closing the circle? Trends Cell Biol. 27 (2017) 266–275.
[78] M.S. Kim, S.S. Kim, N.J. Yoo, S.H. Lee, Rare somatic mutation of pro-apoptotic BAX and BAK genes in common human cancers, Tumori 98 (2012) 149e-51e.
[79] S.I. Nikolaev, D. Rimoldi, C. Iseli, A. Valsesia, D. Robyr, C. Gehrig, et al., Exome sequencing identifies recurrent somatic MAP2K1 and MAP2K2 mutations in melanoma, Nat. Genet. 44 (2011) 133–139.
[80] M. Gasset, A. Martínez-del-Pozo, M. Oñaderra, J.G. Gavilanes, Study of the interaction between the antitumour protein α-sarcin and phospholipid vesicles, Biochem. J. 258 (1989) 569–575.
[81] J.B. Heymann, S.D. Zakharov, Y.L. Zhang, W.A. Cramer, Characterization of electrostatic and nonelectrostatic components of protein membrane binding interactions, Biochemistry-Us 35 (1996) 2717–2725.
[82] T. Wiseman, S. Williston, J.F. Brandts, L.N. Lin, Rapid measurement of binding

constants and heats of binding using a new titration calorimeter, Anal. Biochem. 179 (1989) 131–137.
[83] R. Koradi, M. Billeter, K. Wüthrich, MOLMOL: a program for display and analysis of macromolecular structures, J. Mol. Graph 14 (51–55) (1996) 29–32.
[84] J. Kyte, R.F. Doolittle, A simple method for displaying the hydropathic character of a protein, J. Mol. Biol. 157 (1982) 105–132.
[85] R. Gautier, D. Douguet, B. Antonny, G. Drin, Heliquest: a web server to screen sequences with specific α-helical properties, Bioinformatics 24 (2008) 2101–2102.
[86] E.F. Pettersen, T.D. Goddard, C.C. Huang, G.S. Couch, D.M. Greenblatt, E.C. Meng, et al., UCSF chimera - a visualization system for exploratory research and analysis, J. Comput. Chem. 25 (2004) 1605–1612.

Article II

Synergistic action of actinoporin isoforms from the same sea anemone species assembled into functionally active heteropores

Esperanza Rivera-de-Torre[1], Sara García-Linares[1], Jorge Alegre-Cebollada[2], Javier Lacadena[1], José G. Gavilanes[1], and Álvaro Martínez-del-Pozo[1]

[1] Departamento de Bioquímica y Biología Molecular, Facultades de Química y Biología, Universidad Complutense, 28040 Madrid
[2] Centro Nacional de Investigaciones Cardiovasculares Carlos III, 28029 Madrid, Spain

Journal of Biological Chemistry, 2016, 291 (27), 14109-14119

DOI: http://doi.org/10.1074/jbc.M115.710491

Entre las proteínas tóxicas secretadas en el veneno de las anémonas marinas, las actinoporinas son proteínas formadoras de poros cuya actividad tóxica reside en la formación de poros oligoméricos en el seno de membranas biológicas. Las actinoporinas aparecen como familias multigénicas que dan lugar a muchas isoformas proteicas en un mismo individuo, mostrando una elevada identidad de secuencia, pero también importantes diferencias a nivel funcional, especialmente con respecto a su actividad hemolítica, reflejo directo de su capacidad para formar poros ¿cuál es, entonces, la ventaja evolutiva de producir isotoxinas tan similares y, a la vez, tan distintas? Con el fin de contribuir a aportar pistas para contestar a esta pregunta, en este trabajo se estudian las actinoporinas sticholisina I y II (StnI y StnII), producidas por la anémona marina *Stichodactyla helianthus*, y se demuestra que estas dos isoformas cooperan de forma sinérgica para potenciar su actividad. A través de ensayos de hemolisis y de liberación de calceina encapsulada en vesículas modelo, se demuestra cómo mezclas de StnI y StnII son más líticas que preparaciones equivalentes que contienen dichas isoformas aisladas. Se propone también que esta sinergia se debe al ensamblaje de heteroporos formados por ambas proteínas porque (i) StnI y StnII se pueden entrecruzar entre ellas mediante un enlace covalente, usando un reactivo químico de entrecruzamiento de corto alcance, y sólo en presencia de membranas; y (ii) la afinidad de las mezclas de sticholisina se incrementa con respecto a cualquiera de ellas por separado, como se demuestra por experimentos de calorimetría de titulación isotérmica. Estos resultados ayudan a entender la naturaleza multigénica de las actinoporinas y pueden aplicarse también a otras familias de toxinas que requieren oligomerización para ejercer su actividad tóxica.

PhD candidate contributions

Esperanza Rivera de Torre contributed in conceiving, designing and conducting the experiments. She also took part in analyzing and discussing the results, writing and correcting the manuscript and suggesting modifications.

THE JOURNAL OF BIOLOGICAL CHEMISTRY VOL. 291, NO. 27, pp. 14109–14119, July 1, 2016

Synergistic Action of Actinoporin Isoforms from the Same Sea Anemone Species Assembled into Functionally Active Heteropores*

Received for publication, December 14, 2015, and in revised form, April 26, 2016 Published, JBC Papers in Press, April 27, 2016, DOI 10.1074/jbc.M115.710491

Esperanza Rivera-de-Torre[‡], Sara García-Linares[‡], Jorge Alegre-Cebollada[§], Javier Lacadena[‡], José G. Gavilanes[‡1], and Álvaro Martínez-del-Pozo[‡2]

From the [‡]Departamento de Bioquímica y Biología Molecular I, Facultades de Química y Biología, Universidad Complutense, 28040 Madrid and [§]Centro Nacional de Investigaciones Cardiovasculares Carlos III, 28029 Madrid, Spain

Among the toxic polypeptides secreted in the venom of sea anemones, actinoporins are the pore-forming toxins whose toxic activity relies on the formation of oligomeric pores within biological membranes. Intriguingly, actinoporins appear as multigene families that give rise to many protein isoforms in the same individual displaying high sequence identities but large functional differences. However, the evolutionary advantage of producing such similar isotoxins is not fully understood. Here, using sticholysins I and II (StnI and StnII) from the sea anemone *Stichodactyla helianthus*, it is shown that actinoporin isoforms can potentiate each other's activity. Through hemolysis and calcein releasing assays, it is revealed that mixtures of StnI and StnII are more lytic than equivalent preparations of the corresponding isolated isoforms. It is then proposed that this synergy is due to the assembly of heteropores because (i) StnI and StnII can be chemically cross-linked at the membrane and (ii) the affinity of sticholysin mixtures for the membrane is increased with respect to any of them acting in isolation, as revealed by isothermal titration calorimetry experiments. These results help us understand the multigene nature of actinoporins and may be extended to other families of toxins that require oligomerization to exert toxicity.

Actinoporins, single polypeptide chains of around 175 amino acids, constitute a family of toxic proteins produced by different sea anemone species. They show basic isoelectric point values and are usually cysteineless (1–4). Actinoporins belong to a much larger group of widely distributed proteins, known as pore-forming toxins, whose toxic activity relies on the formation of pores within biological membranes (5–9). All pore-forming toxins show a very similar dual behavior by which they remain mostly monomeric and stably folded in aqueous solution but become oligomeric integral proteins when encountering membranes (2–4, 10–23).

The incorporation of actinoporins into the membrane largely depends on lipid bilayer composition and membrane physicochemical state (18, 24–29). Both factors influence the conformational changes occurring during the transition from the water media to the inserted states of the protein (30, 31). Thus, high affinity recognition of sphingomyelin (SM)[3] is crucial for specific attachment to a membrane, but the subsequent effects observed also depend on the physical properties derived from its particular composition and not only from its SM content (23, 32). In fact, although still controversial, the presence of cholesterol and the coexistence of different phases in the membrane seem to be important factors, if not for binding then at least for the final formation of the pore (23, 28, 29, 32–36).

Actinoporins have been isolated from more than 20 different sea anemone species (1, 3, 37–41) in agreement with their rather ubiquitous distribution within the Actinaria order (1). They display high sequence identities (between 60 and 80%) and appear as multigene families, giving rise to many protein isoforms within the same individual (42–46). Despite the small number of amino acid changes between them, actinoporin isoforms usually result in substantial functional differences in terms of solubility and lytic activity (38, 45, 47–51), as exemplified by StnI and StnII, produced by *Stichodactyla helianthus*, and also two of the best characterized actinoporins (3, 4, 20, 22, 24, 47–50, 52).

The reason why a single anemone produces several isoforms of actinoporins in its venom is still not fully understood. One possible explanation would be to expand the range of prey susceptible of being attacked (53). Such a strategy would extend and modulate the range of action of sea anemones. It has even been proposed an analogy with immunoglobulins, which suggests that sea anemone tentacles could produce many actinoporin isoforms because they would represent the embryo of a rudimentary defense system (45). However, so far the possibility that these different isoforms show synergistic activity has not been explored. This possibility is interesting because it would lead to more efficient venoms. The results presented here not only prove that StnI and StnII potentiate their lytic activity when they act together but also indicate that they can

* This work was supported by Grant BFU2012-32404 from the Spanish Ministerio de Ciencia e Innovación (to A. M. P.), a Formación de Personal Universitario fellowship (to S. G. L.), a Universidad Complutense de Madrid collaboration fellowship (to E. R. T.), and Ramón y Cajal Award RYC-2014-16604) (to J. A. C.). The authors declare that they have no conflicts of interest with the contents of this article.

[1] To whom correspondence may be addressed. Tel.: 34-913944158; Fax: 34-913944159; E-mail: ppgf@bbm1.ucm.es.

[2] To whom correspondence may be addressed. Tel.: 34-913944158; Fax: 34-913944159; E-mail: alvaromp@quim.ucm.es.

[3] The abbreviations used are: SM, sphingomyelin; 6HStnII, sticholysin II tagged with six histidine residues at the N terminus; DOPC, 1,2-dioleoyl-*sn*-glycero-3-phosphocholine; DSS, disuccinimidyl suberate; ITC, isothermal titration calorimetry; LUV, large unilamellar vesicle; Stn, sticholysin; Chol, cholesterol.

establish functional heteropores, suggesting that actinoporins have a more deeply regulated physiological mode of action than previously believed.

Experimental Procedures

Materials—1,2-Dioleoyl-*sn*-glycero-3-phosphocholine (DOPC), cholesterol (Chol), and porcine brain SM were obtained from Avanti Polar Lipids. Disuccinimidyl suberate (DSS) was purchased from Pierce (Thermo Scientific). The preparation of the cDNA coding for StnI, StnII, and the six His-tagged version of StnII (6HStnII), as well as the production and purification of the three different proteins, has been described before (30, 50, 54). Homogeneity of all protein samples used was analyzed by 0.1% (w/v) SDS-12–15% PAGE (w/v) performed under standard conditions (55) and amino acid analysis after acid hydrolysis of the proteins (5.7 M HCl, 24 h, 110 °C). These amino acid analyses were performed on a Biochrom 20 automatic analyzer (GE Healthcare). All protein batches used were also previously characterized in terms of recording their far-UV circular dichroism (CD) spectra on a Jasco 715 spectropolarimeter, also as described (20, 21, 56, 57).

Hemolysis—Hemolysis assays were performed in 96-multiwell plates as described previously (30, 50). Briefly, erythrocytes from heparinized sheep blood were washed in 10 mM Tris buffer, pH 7.4, containing 145 mM NaCl, to a final A_{655} of 0.5 when mixing equal volumes of the cell suspension and buffer. The hemolysis was followed as a decrease in A_{655} after addition of the erythrocyte suspension to different final concentrations of protein. An Expert 96 microplate reader (Asys Hitech, GmbH, Eugendorf, Austria) was employed to measure A_{655}. The value obtained with 0.1% (w/v) Na_2CO_3 was considered as 100% hemolysis.

Lipid Vesicle Preparation—DOPC/SM/Chol (1:1:1) phospholipid vesicles were prepared as described previously (20, 23, 58). A phospholipid (0.1–1.0 mg) solution in 2:1 (v/v) chloroform/methanol was dried under a flow of nitrogen, and the dry film obtained was used to prepare a lipid dispersion by adding 0.5–2.0 ml of Tris-NaCl (10 mM Tris-HCl, pH 7.4, 140 mM NaCl), briefly vortex mixing, and incubating for 1 h at 37 °C. This suspension of multilamellar vesicles was further subjected to five cycles of extrusion at 37 °C through polycarbonate filters (100-nm pore size) to obtain a homogeneous population of unilamellar vesicles.

Calcein Leakage Assays—Calcein-entrapped DOPC/SM/Chol (1:1:1) large unilamellar vesicles (LUVs) were prepared as described (23) by extrusion through 100-nm filters (Nucleopore, Whatman) at 37 °C. Briefly, the desired lipids were mixed and dried under a stream of nitrogen. The lipids were re-dissolved in chloroform and dried again before removal of any traces of remaining solvent in vacuum for 60 min. Prior to extrusion, the dry lipid films were hydrated for 1 h at 37 °C in Tris buffer (10 mM Tris, 140 mM NaCl, 0.5 mM EDTA, pH 7.4), containing 100 mM calcein. The total lipid concentration was 1.25 mM. LUVs were separated from non-entrapped calcein by gel filtration on Sephacryl S200HR. These LUVs were used for permeabilization studies within 24 h. Phospholipid concentration was determined from measurement of phosphorus (59) after elution of vesicles during isolation. The concentrations of LUV phospholipids and protein during calcein leakage experiments were about 7.5 μM and 1–80 nM, respectively. Emission at 550 nm was followed at 23 °C as a function of time (excitation at 480 nm). Fluorescence emission was measured with an SLM Aminco 8000 spectrofluorimeter. To ensure that no major spontaneous leakage occurred, the emission was measured for each sample during 5 min before addition of toxin. A steady signal level, indicating intact vesicles, was observed for all samples. Maximum calcein release was determined upon LUV disintegration induced by 10% Triton X-100.

Cross-linking Experiments—Cross-linking was performed essentially as described before (60). DSS was used as the cross-linking reagent in a reaction that was performed by adding a small aliquot of a concentrated freshly prepared cross-linker solution to the protein sample at the required concentrations. Protein (wild-type StnI and a His_6-tagged version of StnII (6HStnII)) (50) and vesicle mixtures were prepared in 15 mM MOPS, pH 7.4, containing 50 mM NaCl, at the following final molar concentrations: 2.0 μM StnI, 0.5 μM 6HStnII, 0.1 μM (lipid concentration) DOPC/SM/Chol (1:1:1) phospholipid vesicles, and 0.04 μM DSS. The final concentration of each protein employed in this case was independent of the presence or not of the other actinoporin. A second set of cross-linking experiments was made with mixtures containing a constant concentration of 6HStnII and increasing amounts of StnI up to a StnI/6HStnII molar ratio of 95:5. The cross-linker was dissolved in dimethyl sulfoxide (DMSO). The protein/lipid reaction mixtures were incubated at 37 °C for 1 h, then the cross-linker was added and kept for 30 min at room temperature, and finally the mixtures were quenched for 15 min by adding an aliquot of the same buffer but containing 50 mM Lys. After addition of the corresponding electrophoresis loading buffer to each aliquot, they were boiled for 20 min in the presence of 0.5% (v/v) β-mercaptoethanol, and the cross-linked products were analyzed by SDS-PAGE following standard procedures (55). Western immunoblotting was used to detect 6HStnII using a mouse monoclonal anti-polyhistidine-peroxidase antibody from Sigma.

Protein Binding to Lipid Vesicles—Binding was measured using isothermal titration calorimetry (ITC) as described before (21, 30, 61), using a VP-ITC calorimeter (MicroCal). Briefly, protein solutions at 1.5–10.0 μM concentration were titrated by injection of 10- or 20-μl aliquots of lipid suspensions (phospholipid concentration, 0.85–5.00 mM). Binding isotherms were adjusted to a model where the protein binds to the membrane involving "*n*" lipid molecules (30).

Results

StnI and StnII Show Synergistic Hemolytic Activity—A hemolysis experiment was designed to study the potential formation of StnI/StnII heteropores and its functional consequences. With this idea, sheep erythrocyte hemolysis was assayed in the presence of isolated StnI or StnII at different concentrations or for a mixture of StnI/StnII at 80:20 constant molar ratio (Fig. 1). This experiment was so designed given the lower hemolytic activity of StnI. Inspection of results shown in Fig. 1 reveal how the mixture produced higher hemolysis rates

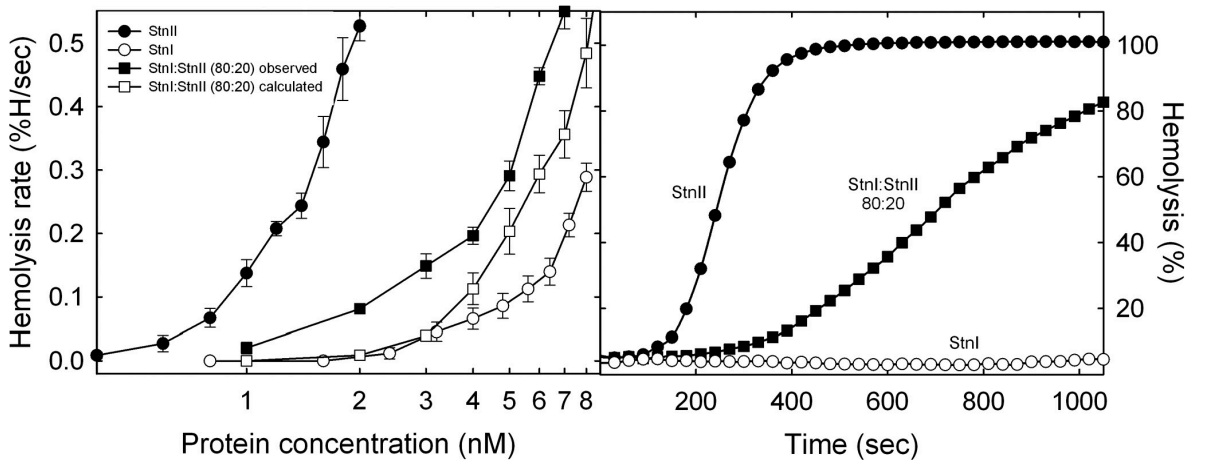

FIGURE 1. *Left panel,* maximum hemolytic rate values (expressed as percentage of hemolysis/s) are represented *versus* the logarithm of total protein concentration: StnI (*white dots*), StnII (*black dots*), and the StnI/StnII (80:20) mixture (*black squares*). The *white squares line* was obtained as the arithmetical addition of the rates obtained with the individual proteins for the real concentration of each one in the different mixtures employed. Results shown are the average of four independently performed experiments. Each of these experiments was made in duplicate. *Error bars* represent ±S.D. *Right panel,* as a representative example, the hemolytic activity curves of StnI (*white dots*), StnII (*black dots*), or a StnI/StnII (80:20) mixture (*black squares*), at a total protein concentration of 2 nM, are also shown.

than that one resulting from the arithmetical combination of the corresponding values obtained with the individual proteins.

To evaluate the specificity of this observation, two different StnII mutants were employed as controls. First, the same experiment as that described in Fig. 1 was made using StnII A10PS28P instead of the wild-type protein. This mutant has been previously described as retaining its full membrane binding activity but showing a highly diminished pore-forming ability due to its inability to extend the needed α-helical stretch (30). As shown in Fig. 2*A*, even though the mutant was completely unable to lyse the erythrocytes within the full concentration range assayed, the mixture still produced higher hemolysis rates than those resulting from the arithmetical combination of the corresponding values obtained with the individual proteins (wild-type StnI and A10PS28P StnII at a 80:20 ratio).

In the second control experiment performed, the StnII mutant used was Y111N. In this StnII variant a key residue of the so-called phosphocholine-binding site has been replaced rendering a protein that cannot bind to the membrane and therefore shows a dramatically reduced hemolytic activity (30, 54). It can be seen how in this case (Fig. 2*B*) the synergistic effect of StnII is not observed. Overall, the three sets of experiments suggest not only the existence of synergistic action between both actinoporin isoforms, StnI and StnII, but also that this synergy seems to occur at the membrane binding step of the pore formation mechanism.

StnI and StnII Show Synergistic Lytic Activity toward Lipid Model Vesicles—Erythrocytes are a rather complex model system to study protein-lipid interactions and assembly of pores at the membrane. Therefore, an experiment was designed to study leakage of calcein-containing DOPC/SM/Chol (1:1:1) phospholipid vesicles upon addition of different actinoporin concentrations. This type of vesicle represents one of the standard models most widely used to characterize StnI and StnII pore formation behavior (18, 20, 23, 28, 30, 54, 62). As can be observed in Fig. 3, the results obtained were similar to those corresponding to the hemolysis assays. The mixture of StnI and StnII produced higher calcein release rates than that resulting from the arithmetical combination of the corresponding values obtained with the individual proteins.

StnI and StnII Can Be Cross-linked in the Presence of Lipid Membranes—The results obtained from both sets of activity experiments, hemolysis and calcein release assays, show that StnI and StnII display synergistic activity. One explanation for this synergy would be the formation of active StnI/StnII heteropores. If this were the case, molecules from both proteins studied should be in close enough proximity as to be cross-linked using a short bifunctional reagent such as DSS (spacer arm, 1.1 nm), which reacts against exposed primary amines. Consequently, mixtures of StnI and StnII were incubated in the presence or absence of DOPC/SM/Chol (1:1:1) phospholipid vesicles and then DSS was added, following a standard protocol (63). The resulting mixture of proteins was analyzed by means of SDS-PAGE followed by Western blotting and immunodetection. For this purpose, instead of the wild-type protein, a His_6-tagged version of StnII (6HStnII) was employed. This protein has been described to retain the general features and molecular mechanism of wild-type StnII (50, 64). This 6HStnII variant shows two advantages for cross-linking experiments. First, the presence of the N-terminal poly(His) tag shifts its electrophoretic mobility to the point where it can be unequivocally distinguished from wild-type StnI (50). Second, it can be identified by an anti-poly-His antibody without cross-reactivity from StnI (18). Therefore, the results presented in blots of Figs. 4 and 5 reveal only the presence of 6HStnII, independently of the amount of StnI present.

In the absence of vesicles, only 6HStnII is detected in Fig. 4, *lanes 1* and *2*, despite the presence of a 4-fold higher concentration of StnI or the previous addition, or not, of the cross-linking agent. Fig. 4, *lanes 3* and *4*, shows the same set of results, cross-linked or not, but this time after incubation of both pro-

Functionally Active Actinoporin Heteropores

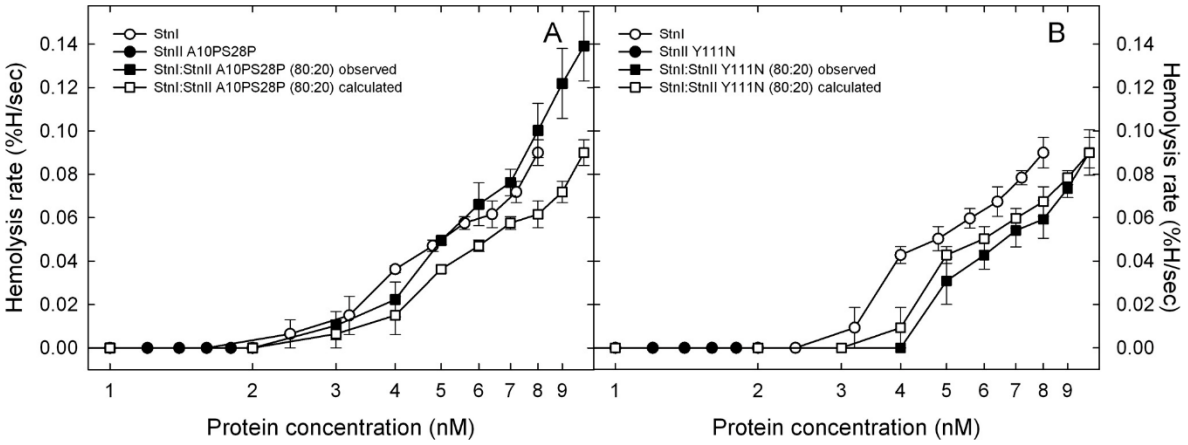

FIGURE 2. **Maximum hemolytic rate values (expressed as percentage of hemolysis/s) are represented *versus* the logarithm of total protein concentration of individual and two different actinoporin mixtures: wild-type StnI and A10PS28P (*A*) or Y111N (*B*) StnII mutants.** Both panels show the behavior of StnI (*white dots*), the StnII mutant (*black dots*), and the StnI/StnII mutant (80:20) mixture (*black squares*). The *white squares* line was obtained as the arithmetical addition of the rates obtained with the individual proteins for the real concentration of each one in the different mixtures employed. Results shown are the average of four independently performed experiments. Each of these experiments was made in duplicate. *Error bars* represent ±S.D.

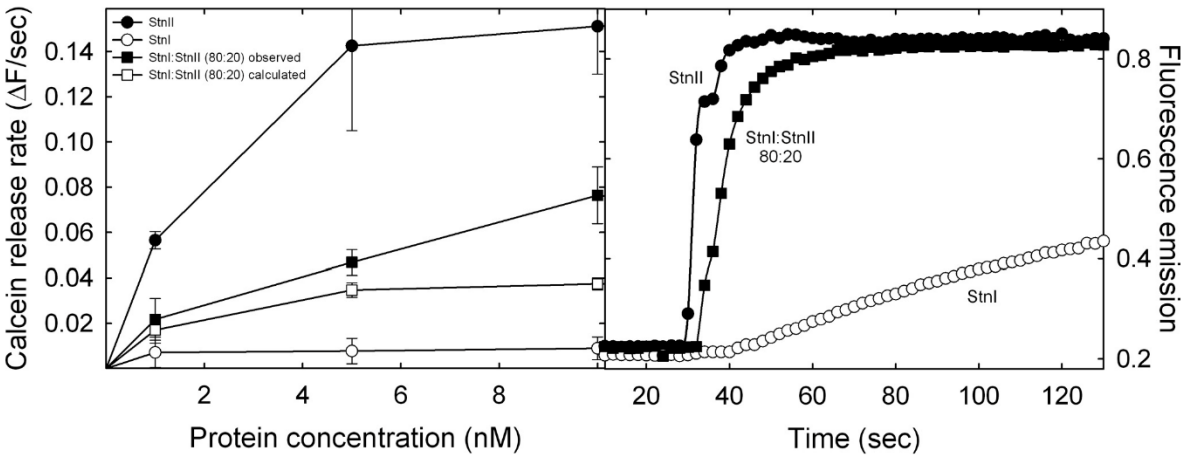

FIGURE 3. *Left panel,* calcein release of maximal rates (expressed as normalized fluorescence intensity increment/s) are represented *versus* the total protein concentration: StnI (*white dots*), StnII (*black dots*), and the StnI/StnII (80:20) mixture (*black squares*). The *white squares line* was obtained as the arithmetical addition of the rates obtained with the individual proteins taking into account the real concentration of each one of them in the different mixtures employed. Results shown are the average of three independently performed experiments. Each of these experiments was made in duplicate. *Error bars* represent ± S.D. *Right panel,* as a representative example, the calcein leakage traces of StnI (*white dots*), StnII (*black dots*), or an StnI/StnII (80:20) mixture (*black squares*), at a total protein concentration of 5 nM, are also shown.

teins with DOPC/SM/Chol (1:1:1) vesicles. Thus, again, in the absence of DSS, no other band but that one corresponding to monomeric 6HStnII was observed (Fig. 4, *lane 3*). However, when the cross-linker was present, new bands of different electrophoretic mobility were evident (Fig. 4, *lane 4*). At least two of these bands were not observed if 6HStnII (Fig. 4, *lane 5*) or StnI (*lane 6*) were the only proteins present. Therefore, they can only correspond to hetero-oligomers made of 6HStnII and wild-type StnI, the only situation that would explain their immunodetection by the anti-poly(His) antibody together with their singular electrophoretic mobility. It has been well determined that the presence of the six His tags at the N-terminal end of sticholysins has a deep impact on their electrophoretic mobility (50).

To show further evidence of the assembly of StnI and 6HStnII into cross-linkable heteropores, the titration experiment shown in Fig. 5 was performed. Again, under these conditions and in the absence of vesicles, only 6HStnII was detected in Fig. 5, *lane 1*. However, when cross-linker and vesicles were present, 6HStnII cross-linked oligomers could be detected (Fig. 5, *lane 2*). In fact, the observed distribution pattern is very similar to the one reported previously for equinatoxin II under almost identical conditions (25, 65). As shown in Fig. 5, *lanes 2–5*, upon increasing the StnI/6HStnII ratio, the appearance of the bands corresponding to cross-linked proteins is increasingly evident altogether with a decrease of the monomeric 6HStnII species. This second set of results not only confirms the presence of cross-linkable

	1	2	3	4	5	6
StnI (80)	+	+	+	+	-	+
6HStnII (20)	+	+	+	+	+	-
Vesicles	-	-	+	+	+	+
Cross-linker	-	+	-	+	+	+

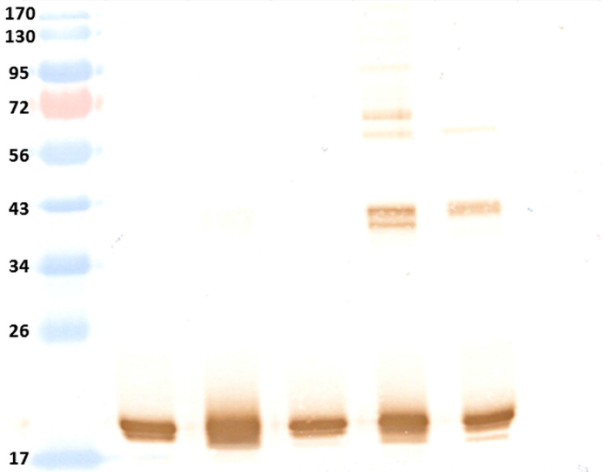

FIGURE 4. **Immunoblotting detection of 6HStnII previously incubated in the presence, or not, of wild-type StnI, DOPC/SM/Chol (1:1:1) phospholipid vesicles, and/or DSS, as indicated.** Proteins were detected using a mouse monoclonal anti-polyhistidine-peroxidase antibody. The amount of 6HStnII loaded was 2.5 pmol. The StnI:6HStnII molar ratio employed was 80:20 in all instances shown. Molecular weight standards (EZ-RUN™ pre-stained Rec Protein Ladder) were also loaded, and the corresponding molecular masses are indicated in kDa at the *left margin*.

	1	2	3	4	5	6
StnI (pmol)	0.0	0.0	10.0	22.5	47.5	47.5
6HStnII (pmol)	2.5	2.5	2.5	2.5	2.5	0.0
StnI:6HStnII	0.0	0.0	80:20	90:10	95:5	-
Vesicles	-	+	+	+	+	-
Cross-linker	-	+	+	+	+	-

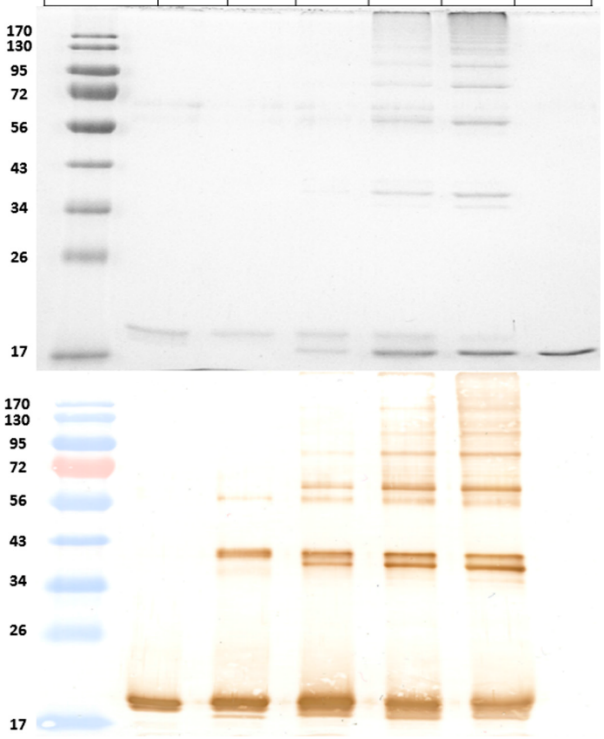

FIGURE 5. **Coomassie Blue-stained gel (*upper panel*) and the corresponding immunoblotting detection (*lower panel*) of 6HStnII titrated with increasing amounts of StnI are shown.** The proteins, and also the mixtures assayed, were incubated in the presence, or not, of wild-type StnI, DOPC/SM/Chol (1:1:1) phospholipid vesicles, and/or DSS, as indicated. Proteins were detected using a mouse monoclonal anti-polyhistidine-peroxidase antibody. The amount of 6HStnII loaded was 2.5 pmol in all instances shown. The StnI/6HStnII molar ratio employed is also indicated. Molecular weight standards (EZ-RUN™ pre-stained Rec Protein Ladder) were also loaded, and the corresponding molecular masses are indicated in kDa at the *left margin*.

heteropores on the bilayer but also its marked protein concentration and StnI/6HStnII ratio dependence. The presence of other hetero-oligomers of lower electrophoretic mobility is also detected but, given the inherent influence of the DSS reaction on band electrophoretic mobility and sharpness (60), it is not possible to assign specific stoichiometries. We also used Coomassie staining to analyze the results of cross-linking. Compared with the Western blotting results, we found that the lower mobility heterooligomer bands at around 40 kDa that become apparent at higher StnI/6HStnII ratios have a lower reactivity against the anti-His antibody, in agreement with the lower content of His tags in the heterooligomers. In summary, this set of experiments allowed us to conclude that, in the presence of membranes, actinoporins StnI and StnII are close enough as to be cross-linked by a short cross-linking agent, suggesting that heteropores of StnI and StnII are formed.

Mixtures of StnI and StnII Show Increased Membrane Affinity—The actinoporins pore formation mechanism has been thoroughly studied although some of its details are still the subject of dispute (17, 32, 66–70). In a simplified version of this mechanism, two different steps can be distinguished. First, the protein binds to the membrane, and second, it assembles into a functional oligomeric pore (18, 30). Within the context of this simplified picture, it can be assumed that binding assays by ITC measure the affinity of the proteins to the membrane (30). As observed in Fig. 6, the affinity of StnI for DOPC/SM/Chol (1:1:1) phospholipid vesicles is lower than that corresponding to StnII (Table 1). In terms of relative membrane binding affinity, StnII binding to the vesicles is 4-fold higher, a result that is good enough by itself to explain the long known differences in terms of hemolytic and calcein leakage activities between StnI and StnII (26, 71).

To explore whether improved binding could contribute to the synergistic lytic activity shown by sticholysins, we performed ITC binding experiments in which a total actinoporin concentration was fixed, but different StnI/StnII molar ratios were assayed (Fig. 7). Quite surprisingly, the binding affinity of

Functionally Active Actinoporin Heteropores

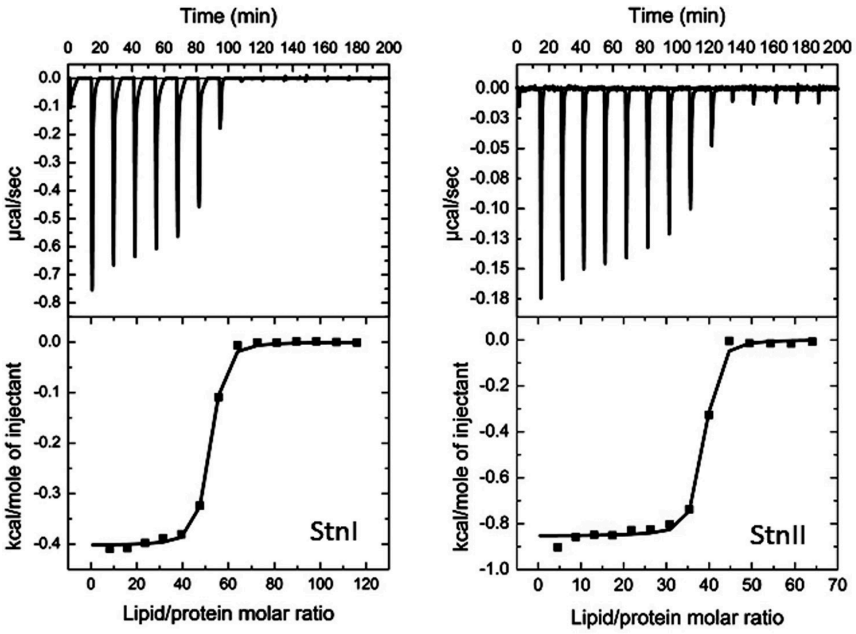

FIGURE 6. **Binding of StnI and StnII to DOPC/SM/Chol (1:1:1) vesicles studied by ITC.** Reactant concentrations were those ones shown in Table 1. Binding isotherms were adjusted to a model in which protein membrane binding involves the participation of "*n*" lipid molecules (30). The *c* values ($c = K_a \times P_0$) for the graphs shown are within the range 1–1000.

TABLE 1

Binding of StnI, StnII, or different StnI/StnII mixtures to DOPC/SM/Chol (1:1:1) vesicles studied by ITC

Thermodynamic parameters for protein mixtures StnI/StnII (95:5), StnI/StnII (90:10), and StnI/StnII (80:20) (Fig. 7) should be considered only as estimations and are shown only for trend consistency purposes because binding affinities were so high that keeping the *c* values within range involved dilutions below the recommended detection limits of the instrument. Therefore, the corresponding *c* values of the three mixtures containing the higher proportion of StnII are higher than the recommended ones. Results shown are the average of at least three separate experiments.

	StnI/StnII (100:0)	StnI/StnII (0:100)[a]	StnI/StnII (99:1)	StnI/StnII (95:5)	StnI/StnII (90:10)	StnI/StnII (80:20)
n	49 ± 1	39 ± 4	38 ± 1	42 ± 1	38 ± 1	47 ± 9
K_a (M^{-1}) × 10^{-8}	0.41 ± 0.03	1.70 ± 0.90	2.84 ± 0.91	33.90 ± 41.90	23.20 ± 19.90	237.00 ± 29.30
ΔG (kcal/mol)	−8.21 ± 0.03	−9.10 ± 0.50	−10.90 ± 0.48	−10.89 ± 0.48	−10.73 ± 0.37	−11.54 ± 1.29
ΔH (kcal/mol)	−20.9 ± 2.1	−44.0 ± 3.0	−9.1 ± 0.1	−11.1 ± 0.1	−14.0 ± 0.1	−27.3 ± 3.2
ΔS (cal/mol·K)	−42.84 ± 6.78	−115 ± 9.00	−1.2 ± 0.73	−0.8 ± 2.0	−14.0 ± 1.7	−52.9 ± 6.4
[Protein]	10.0 µM	1.5 µM	1.5 µM	1.5 µM	1.5 µM	1.0 µM
$c = K_a \times$ [Protein]	410	255	426	5090	3480	23700
RBM[b]	0.19	1.00	1.71	5.50	4.20	115.7

[a] See Ref. 30.
[b] Relative membrane binding $(n_{(StnII)} \times K_{(other)})/(n_{(other)} \times K_{(StnII)})$ as explained in Ref. 30.

mixtures of StnI and StnII was always higher than for any of the two actinoporins acting in isolation. This effect was already detected in the presence of trace amounts (1.0%) of StnII and correlated with increased relative membrane binding (Fig. 7 and Table 1). It is difficult to conceive how the binding affinity could increase without direct interaction between StnI and StnII. Hence, the ITC experiments lend additional support to the hypothesis that StnI and StnII can assemble into functional heteropores, leading to synergistic lytic activity.

Finally, given the large effect on affinity of only traces of StnII in the mixtures, we studied whether this increase in binding affinity was directly correlated with an enhancement of function. As can be seen in Fig. 8, just 1.0% of StnII in the mixtures was enough to dramatically improve their hemolytic activity, as revealed by the hemolysis assays performed with different StnI/StnII (99:1) mixtures over a 1–10 nM concentration range (Fig. 8).

Discussion

Sea anemones produce a wide variety of toxic compounds that are mainly stored in their nematocysts (72). Among them, actinoporins constitute a well studied family of toxic pore-forming proteins (3, 4, 70). It has long been known that individual sea anemone species produce many different actinoporin isoforms that, indeed, are very differently represented in terms of the amount present in their venomous secretions. In this regard, actinoporins represent a well established example of a multigenic protein family (38, 39, 43, 45, 46, 51, 73). They are not, however, the only example of toxic pore-forming multigene protein families (74), suggesting that the results shown now could be of larger significance and not only restricted to the actinoporin family. In fact, it has been very recently suggested that the pore responsible for damaging mitochondria during apoptosis could be made of hetero-oligomers of the Bax and Bak proteins (75). The natural biological function of this

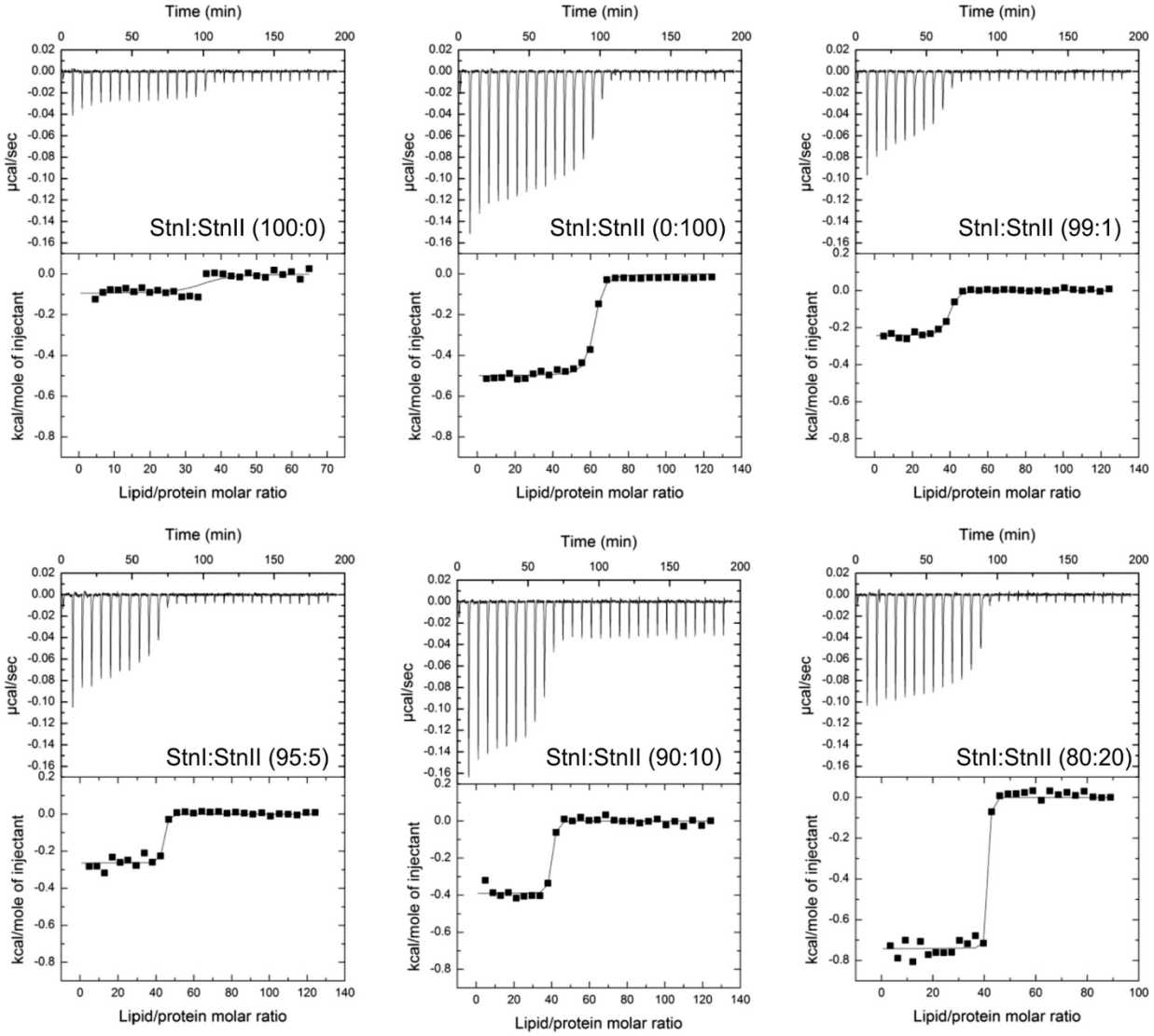

FIGURE 7. **Binding of StnI, StnII, and different StnI/StnII mixtures (molar ratios as indicated) to DOPC/SM/Chol (1:1:1) vesicles studied by ITC.** Reactant concentrations for the examples shown are P_0 = 1.5 μM and L_0 = 0.85 mM for all experiments, where P_0 refers to the initial total protein concentration within the calorimeter cell and L_0 is the lipid concentration within the dispensing auto-pipette. Binding isotherms were adjusted to a model in which protein membrane binding involves the participation of "*n*" lipid molecules (30). The *c* values ($c = K_a \times P_0$) for the graphs shown were in the 1–1000 range only for the StnI/StnII (0:100), StnI/StnII (99:1), and StnI/StnII (100:0). In the other three thermograms shown the binding affinities were so high that keeping the *c* values within range involved dilutions below the recommended detection limits of the instrument.

genetic multiplicity is indeed far from being understood. Regarding the actinoporin family, it has been proposed that the existence of multiple isoforms would broaden the range of possible prey for a given species (38, 39, 43, 45, 46, 51, 73). In this regard, actinoporins might be similar to immunoglobulins, which require a plethora of highly diverse genes to counteract foreign antigens (45).

Here, we propose a complementary hypothesis to explain the evolutionary advantage of multigenic actinoporins, formation of mixed functional pores. This mechanism would enable a much wider and finely tuned modulation of their toxicity and specificity. These results support the feasibility of this novel hypothesis.

StnI and StnII are two of the best well studied actinoporins and also constitute an optimum example of two almost identical isoforms (they share 91.0% of amino acid sequence identity) produced by the same sea anemone species but showing very different hemolytic activities (24, 47, 50, 76). Consequently, they were the model proteins chosen to study the possibility of molecularly different actinoporins assembling into the same functional pore structure. Indeed, the employment of independently produced and isolated recombinant protein species excludes artifacts produced by traces of cross-contamination in the experiments shown that were made with only one single protein component.

Actinoporin pore structure and stoichiometry are still highly controversial and far from being solved (22, 36, 66, 69,

Functionally Active Actinoporin Heteropores

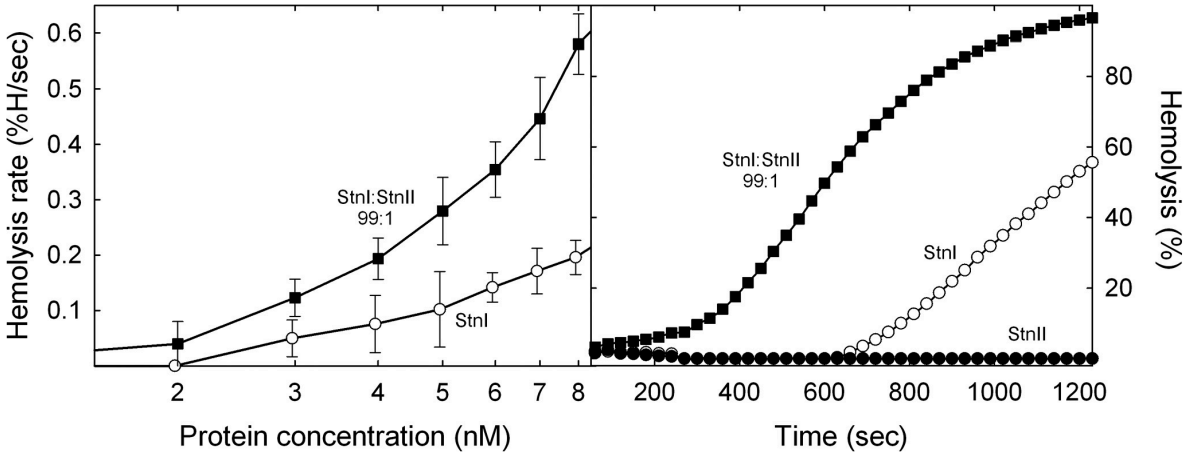

FIGURE 8. *Left panel,* maximum hemolytic rate values (expressed as percentage of hemolysis/s) are represented *versus* the logarithm of total protein concentration of StnI (*white dots*) and an StnI/StnII (99:1) mixture (*black squares*). In these experiments the amount of StnII present in all the mixtures was so low that, when assayed in the absence of StnI, its hemolytic activity was undetectable in the time range measured. Results shown are the average of four independently performed experiments. Each of these experiments was made in duplicate. *Error bars* represent ±S.D. *Right panel,* as a representative example, the hemolytic activity curves of StnI at 3.96 nM (*white dots*), StnII at 0.04 nM (*black dots*), and the corresponding StnI/StnII (99:1) 4 nM mixture (*black squares*) are also shown.

70, 77–79). The latest actinoporin pore-like oligomeric structure published is a crystalline octameric ensemble of FraC (66). According to those results, the two side-chain residues showing more buried surface upon oligomerization would be FraC Val-60 and Trp-149 (66, 80). These residues have their corresponding counterparts in StnI (Ile-59 and Trp-149) and StnII (Ile-58 and Trp-146). Both amino acids could nicely perform an identical function in the StnI-StnII mixed oligomers. Therefore, from a molecular point of view there would not be impediments for the formation of StnI-StnII heteropores.

Synergistic activity of StnI and StnII in both hemolysis and calcein-release experiments suggested that both proteins are in fact able to interact within the same pore structure (Figs. 1–3). Cross-linking experiments further support this observation because, and only in the presence of lipid vesicles, both StnI and StnII could be cross-linked with a short cross-linking agent (Figs. 4 and 5). Finally, we have also shown that mixtures of StnI and StnII show increased affinity for lipid vesicles, in agreement with the fact that both isoforms interact in the process of membrane binding and pore formation (Fig. 7). ITC and hemolytic experiments also show that 1.0% of StnII dramatically enhances StnI binding to lipid model vesicles driving a dramatic improvement of hemolytic activity. Taking into account the only moderate effects observed in calcein-leakage experiments, and the hemolysis results obtained with the two different StnII mutants used as control (Fig. 2), it can be also suggested that synergy between StnI and StnII could mostly be due to a better interaction with the membrane, although the final step of pore formation would not be strongly affected.

As stated above, actinoporins represent multigene families. However, only two or three different isoforms are usually produced by the same sea anemone species in amounts large enough to be detected and purified. For example, up to 19 different cDNA sequences have been detected for *S. helianthus*, the sea anemone producing StnI and StnII (43). Thus, taking into account this discrepancy between the number of actinoporin encoding genes found in sea anemones and the amount and diversity of isotoxins made, it is tempting to speculate that the less represented isoforms might play a role in regulating and/or potentiating the activity and specificity of those ones produced in larger amounts. Maybe this is just a strategy to fulfill a much more modulated and specific cytotoxic action against potential prey and/or predators.

Conclusions

Overall, the results presented here show that two different actinoporins produced by the same sea anemone species act in synergy, most probably interacting to form functional pores made of distinct protein isoforms. As far as we know, this observation has not been reported before. This interaction has sound consequences in terms of the biological functionality of actinoporins and suggests that it could represent a more general strategy employed by other pore-forming proteins. According to the results reported now, it can be speculated that one of the reasons for actinoporins being multigene families is the possibility of interaction among different isotoxins to exert a much more modulated and/or potentiated action against their prey and/or predators. This possibility would translate into more versatile defense and/or attack responses in their natural environment.

Author Contributions—E. R. T., S. G. L., and J. A. C. conducted the experiments. E. R. T., S. G. L., J. A. C., J. L., J. G. G., and A. M. P. conceived and designed the experiments, analyzed and discussed the results, wrote and corrected the manuscript, and suggested modifications.

References

1. Macek, P. (1992) Polypeptide cytolytic toxins from sea anemones (*Actiniaria*). *FEMS Microbiol. Immunol.* **5,** 121–129
2. Anderluh, G., and Macek, P. (2002) Cytolytic peptide and protein toxins from sea anemones (Anthozoa: *Actiniaria*). *Toxicon* **40,** 111–124
3. Alegre-Cebollada, J., Oñaderra, M., Gavilanes, J. G., and del Pozo, A.

(2007) Sea anemone actinoporins: the transition from a folded soluble state to a functionally active membrane-bound oligomeric pore. *Curr. Protein Pept. Sci.* **8,** 558–572
4. García-Ortega, L., Alegre-Cebollada, J., García-Linares, S., Bruix, M., Martínez-Del-Pozo, A., and Gavilanes, J. G. (2011) The behavior of sea anemone actinoporins at the water-membrane interface. *Biochim. Biophys. Acta* **1808,** 2275–2288
5. Parker, M. W., and Feil, S. C. (2005) Pore-forming protein toxins: from structure to function. *Prog. Biophys. Mol. Biol.* **88,** 91–142
6. Gonzalez, M. R., Bischofberger, M., Pernot, L., van der Goot, F. G., and Frêche, B. (2008) Bacterial pore-forming toxins: the (w)hole story? *Cell. Mol. Life Sci.* **65,** 493–507
7. Bischofberger, M., Iacovache, I., and van der Goot, F. G. (2012) Pathogenic pore-forming proteins: function and host response. *Cell Host Microbe* **12,** 266–275
8. Iacovache, I., van der Goot, F. G., and Pernot, L. (2008) Pore formation: an ancient yet complex form of attack. *Biochim. Biophys. Acta* **1778,** 1611–1623
9. Gouaux, E. (1997) Channel-forming toxins: tales of transformation. *Curr. Opin. Struct. Biol.* **7,** 566–573
10. Anderluh, G., Dalla Serra, M., Viero, G., Guella, G., Macek, P., and Menestrina, G. (2003) Pore formation by equinatoxin II, a eukaryotic protein toxin, occurs by induction of nonlamellar lipid structures. *J. Biol. Chem.* **278,** 45216–45223
11. Athanasiadis, A., Anderluh, G., Macek, P., and Turk, D. (2001) Crystal structure of the soluble form of equinatoxin II, a pore-forming toxin from the sea anemone *Actinia equina*. *Structure* **9,** 341–346
12. Kristan, K. C., Viero, G., Dalla Serra, M., Macek, P., and Anderluh, G. (2009) Molecular mechanism of pore formation by actinoporins. *Toxicon* **54,** 1125–1134
13. Gilbert, R. J., Dalla Serra, M., Froelich, C. J., Wallace, M. I., and Anderluh, G. (2014) Membrane pore formation at protein-lipid interfaces. *Trends Biochem. Sci.* **39,** 510–516
14. Hinds, M. G., Zhang, W., Anderluh, G., Hansen, P. E., and Norton, R. S. (2002) Solution structure of the eukaryotic pore-forming cytolysin equinatoxin II: implications for pore formation. *J. Mol. Biol.* **315,** 1219–1229
15. Marchioretto, M., Podobnik, M., Dalla Serra, M., and Anderluh, G. (2013) What planar lipid membranes tell us about the pore-forming activity of cholesterol-dependent cytolysins. *Biophys. Chem.* **182,** 64–70
16. Rojko, N., Cronin, B., Danial, J. S., Baker, M. A., Anderluh, G., and Wallace, M. I. (2014) Imaging the lipid-phase-dependent pore formation of equinatoxin II in droplet interface bilayers. *Biophys. J.* **106,** 1630–1637
17. Rojko, N., Kristan, K. Č., Viero, G., Žerovnik, E., Maček, P., Dalla Serra, M., and Anderluh, G. (2013) Membrane damage by an α-helical pore-forming protein, Equinatoxin II, proceeds through a succession of ordered steps. *J. Biol. Chem.* **288,** 23704–23715
18. Alegre-Cebollada, J., Rodríguez-Crespo, I., Gavilanes, J. G., and del Pozo, A. (2006) Detergent-resistant membranes are platforms for actinoporin pore-forming activity on intact cells. *FEBS J.* **273,** 863–871
19. Castrillo, I., Araujo, N. A., Alegre-Cebollada, J., Gavilanes, J. G., Martínez-del-Pozo, A., and Bruix, M. (2010) Specific interactions of sticholysin I with model membranes: an NMR study. *Proteins* **78,** 1959–1970
20. García-Linares, S., Castrillo, I., Bruix, M., Menéndez, M., Alegre-Cebollada, J., Martínez-del-Pozo, Á., and Gavilanes, J. G. (2013) Three-dimensional structure of the actinoporin sticholysin I. Influence of long-distance effects on protein function. *Arch. Biochem. Biophys.* **532,** 39–45
21. García-Linares, S., Richmond, R., García-Mayoral, M. F., Bustamante, N., Bruix, M., Gavilanes, J. G., and Martínez-Del-Pozo, A. (2014) The sea anemone actinoporin (Arg-Gly-Asp) conserved motif is involved in maintaining the competent oligomerization state of these pore-forming toxins. *FEBS J.* **281,** 1465–1478
22. Mancheño, J. M., Martín-Benito, J., Martínez-Ripoll, M., Gavilanes, J. G., and Hermoso, J. A. (2003) Crystal and electron microscopy structures of sticholysin II actinoporin reveal insights into the mechanism of membrane pore formation. *Structure* **11,** 1319–1328
23. Alm, I., García-Linares, S., Gavilanes, J. G., Martínez-Del-Pozo, Á., and Slotte, J. P. (2015) Cholesterol stimulates and ceramide inhibits sticholysin II-induced pore formation in complex bilayer membranes. *Biochim. Biophys. Acta* **1848,** 925–931
24. Valcarcel, C. A., Dalla Serra, M., Potrich, C., Bernhart, I., Tejuca, M., Martinez, D., Pazos, F., Lanio, M. E., and Menestrina, G. (2001) Effects of lipid composition on membrane permeabilization by sticholysin I and II, two cytolysins of the sea anemone *Stichodactyla helianthus*. *Biophys. J.* **80,** 2761–2774
25. Belmonte, G., Pederzolli, C., Macek, P., and Menestrina, G. (1993) Pore formation by the sea anemone cytolysin equinatoxin-II in red blood cells and model lipid membranes. *J. Membr. Biol.* **131,** 11–22
26. Tejuca, M., Serra, M. D., Ferreras, M., Lanio, M. E., and Menestrina, G. (1996) Mechanism of membrane permeabilization by sticholysin I, a cytolysin isolated from the venom of the sea anemone *Stichodactyla helianthus*. *Biochemistry* **35,** 14947–14957
27. Shin, M. L., Michaels, D. W., and Mayer, M. M. (1979) Membrane damage by a toxin from the sea anemone *Stoichactis helianthus*. II. Effect of membrane lipid composition in a liposome system. *Biochim. Biophys. Acta* **555,** 79–88
28. de los Ríos, V., Mancheño, J. M., Lanio, M. E., Oñaderra, M., and Gavilanes, J. G. (1998) Mechanism of the leakage induced on lipid model membranes by the hemolytic protein sticholysin II from the sea anemone *Stichodactyla helianthus*. *Eur. J. Biochem.* **252,** 284–289
29. Martínez, D., Otero, A., Alvarez, C., Pazos, F., Tejuca, M., Lanio, M. E., Gutiérrez-Aguirre, I., Barlic, A., Iloro, I., Arrondo, J. L., González-Mañas, J. M., and Lissi, E. (2007) Effect of sphingomyelin and cholesterol on the interaction of St II with lipidic interfaces. *Toxicon* **49,** 68–81
30. Alegre-Cebollada, J., Cunietti, M., Herrero-Galán, E., Gavilanes, J. G., and Martínez-del-Pozo, A. (2008) Calorimetric scrutiny of lipid binding by sticholysin II toxin mutants. *J. Mol. Biol.* **382,** 920–930
31. Menestrina, G., Cabiaux, V., and Tejuca, M. (1999) Secondary structure of sea anemone cytolysins in soluble and membrane bound form by infrared spectroscopy. *Biochem. Biophys. Res. Commun.* **254,** 174–180
32. Pedrera, L., Gomide, A. B., Sánchez, R. E., Ros, U., Wilke, N., Pazos, F., Lanio, M. E., Itri, R., Fanani, M. L., and Alvarez, C. (2015) The presence of sterols favors sticholysin I-membrane association and pore formation regardless of their ability to form laterally segregated domains. *Langmuir* **31,** 9911–9923
33. Bakrac, B., and Anderluh, G. (2010) Molecular mechanism of sphingomyelin-specific membrane binding and pore formation by actinoporins. *Adv. Exp. Med. Biol.* **677,** 106–115
34. Barlic, A., Gutiérrez-Aguirre, I., Caaveiro, J. M., Cruz, A., Ruiz-Argüello, M. B., Pérez-Gil, J., and González-Mañas, J. M. (2004) Lipid phase coexistence favors membrane insertion of equinatoxin-II, a pore-forming toxin from *Actinia equina*. *J. Biol. Chem.* **279,** 34209–34216
35. Caaveiro, J. M., Echabe, I., Gutiérrez-Aguirre, I., Nieva, J. L., Arrondo, J. L., and González-Mañas, J. M. (2001) Differential interaction of equinatoxin II with model membranes in response to lipid composition. *Biophys. J.* **80,** 1343–1353
36. Wacklin, H. P., Bremec, B. B., Moulin, M., Rojko, N., Haertlein, M., Forsyth, T., Anderluh, G., and Norton, R. S. (2016) Neutron reflection study of the interaction of the eukaryotic pore-forming actinoporin equinatoxin II with lipid membranes reveals intermediate states in pore formation. *Biochim. Biophys. Acta* **1858,** 640–652
37. Bellomío, A., Morante, K., Barlic, A., Gutiérrez-Aguirre, I., Viguera, A. R., and González-Mañas, J. M. (2009) Purification, cloning and characterization of fragaceatoxin C, a novel actinoporin from the sea anemone *Actinia fragacea*. *Toxicon* **54,** 869–880
38. Monastyrnaya, M., Leychenko, E., Isaeva, M., Likhatskaya, G., Zelepuga, E., Kostina, E., Trifonov, E., Nurminski, E., and Kozlovskaya, E. (2010) Actinoporins from the sea anemones, tropical *Radianthus macrodactylus* and northern *Oulactis orientalis*: comparative analysis of structure-function relationships. *Toxicon* **56,** 1299–1314
39. Monastyrnaya, M. M., Zykova, T. A., Apalikova, O. V., Shwets, T. V., and Kozlovskaya, E. P. (2002) Biologically active polypeptides from the tropical sea anemone *Radianthus macrodactylus*. *Toxicon* **40,** 1197–1217
40. Leichenko, E. V., Monastirnaya, M. M., Zelepuga, E. A., Tkacheva, E. S., Isaeva, M. P., Likhatskaya, G. N., Anastyuk, S. D., and Kozlovskaya, E. P. (2014) Hct-A is a new actinoporin family from the *Heteractis crispa* sea anemone. *Acta Naturae* **6,** 89–98

Functionally Active Actinoporin Heteropores

41. Hu, B., Guo, W., Wang, L. H., Wang, J. G., Liu, X. Y., and Jiao, B. H. (2011) Purification and characterization of gigantoxin-4, a new actinoporin from the sea anemone *Stichodactyla gigantea*. *Int. J. Biol. Sci.* **7,** 729–739
42. Anderluh, G., Barlic, A., Podlesek, Z., Macek, P., Pungercar, J., Gubensek, F., Zecchini, M. L., Serra, M. D., and Menestrina, G. (1999) Cysteine-scanning mutagenesis of an eukaryotic pore-forming toxin from sea anemone: topology in lipid membranes. *Eur. J. Biochem.* **263,** 128–136
43. de los Ríos, V., Oñaderra, M., Martínez-Ruiz, A., Lacadena, J., Mancheño, J. M., Martínez del Pozo, A., and Gavilanes, J. G. (2000) Overproduction in *Escherichia coli* and purification of the hemolytic protein sticholysin II from the sea anemone *Stichodactyla helianthus*. *Protein Expr. Purif.* **18,** 71–76
44. Turk, T. (1991) Cytolytic toxins from sea anemones. *J. Toxicol. Toxin Rev.* **10,** 223–262
45. Wang, Y., Yap, L. L., Chua, K. L., and Khoo, H. E. (2008) A multigene family of *Heteractis* magnificalysins (HMgs). *Toxicon* **51,** 1374–1382
46. Anderluh, G., Krizaj, I., Strukelj, B., Gubensek, F., Macek, P., and Pungercar, J. (1999) Equinatoxins, pore-forming proteins from the sea anemone *Actinia equina*, belong to a multigene family. *Toxicon* **37,** 1391–1401
47. Alvarez, C., Mancheño, J. M., Martínez, D., Tejuca, M., Pazos, F., and Lanio, M. E. (2009) Sticholysins, two pore-forming toxins produced by the Caribbean sea anemone *Stichodactyla helianthus*: their interaction with membranes. *Toxicon* **54,** 1135–1147
48. del Monte-Martínez, A., González-Bacerio, J., Romero, L., Aragón, C., Martínez, D., de Los Á Chávez, M., Álvarez, C., Lanio, M. E., Guisán, J. M., and Díaz, J. (2014) Improved purification and enzymatic properties of a mixture of sticholysin I and II: isotoxins with hemolytic and phospholipase A activities from the sea anemone *Stichodactyla helianthus*. *Protein Expr. Purif.* **95,** 57–66
49. Martínez, D., Morera, V., Alvarez, C., Tejuca, M., Pazos, F., García, Y., Raida, M., Padrón, G., and Eliana Lanio, M. (2002) Identity between cytolysins purified from two morphos of the Caribbean sea anemone *Stichodactyla helianthus*. *Toxicon* **40,** 1219–1221
50. Alegre-Cebollada, J., Clementi, G., Cunietti, M., Porres, C., Oñaderra, M., Gavilanes, J. G., and Pozo, A. M. (2007) Silent mutations at the 5′-end of the cDNA of actinoporins from the sea anemone *Stichodactyla helianthus* allow their heterologous overproduction in *Escherichia coli*. *J. Biotechnol.* **127,** 211–221
51. Uechi, G., Toma, H., Arakawa, T., and Sato, Y. (2010) Molecular characterization on the genome structure of hemolysin toxin isoforms isolated from sea anemone *Actineria villosa* and *Phyllodiscus semoni*. *Toxicon* **56,** 1470–1476
52. Ros, U., Pedrera, L., Díaz, D., Karam, J. C., Sudbrack, T. P., Valiente, P. A., Martínez, D., Cilli, E. M., Pazos, F., Itri, R., Lanio, M. E., Schreier, S., and Álvarez, C. (2011) The membranotropic activity of N-terminal peptides from the pore-forming proteins sticholysin I and II is modulated by hydrophobic and electrostatic interactions as well as lipid composition. *J. Biosci.* **36,** 781–791
53. Olivera, B. M., Rivier, J., Clark, C., Ramilo, C. A., Corpuz, G. P., Abogadie, F. C., Mena, E. E., Woodward, S. R., Hillyard, D. R., and Cruz, L. J. (1990) Diversity of *Conus* neuropeptides. *Science* **249,** 257–263
54. Alegre-Cebollada, J., Lacadena, V., Oñaderra, M., Mancheño, J. M., Gavilanes, J. G., and del Pozo, A. M. (2004) Phenotypic selection and characterization of randomly produced non-haemolytic mutants of the toxic sea anemone protein sticholysin II. *FEBS Lett.* **575,** 14–18
55. Laemmli, U. K. (1970) Cleavage of structural proteins during the assembly of the head of bacteriophage T4. *Nature* **227,** 680–685
56. Alegre-Cebollada, J., Martínez del Pozo, A., Gavilanes, J. G., and Goormaghtigh, E. (2007) Infrared spectroscopy study on the conformational changes leading to pore formation of the toxin sticholysin II. *Biophys. J.* **93,** 3191–3201
57. Pardo-Cea, M. A., Castrillo, I., Alegre-Cebollada, J., Martínez-del-Pozo, Á., Gavilanes, J. G., and Bruix, M. (2011) Intrinsic local disorder and a network of charge-charge interactions are key to actinoporin membrane disruption and cytotoxicity. *FEBS J.* **278,** 2080–2089
58. Martínez-Ruiz, A., García-Ortega, L., Kao, R., Lacadena, J., Oñaderra, M., Mancheño, J. M., Davies, J., Martínez del Pozo, A., and Gavilanes, J. G. (2001) RNase U2 and α-sarcin: A study of relationships. *Methods Enzymol.* **341,** 335–351
59. Bartlett, G. R. (1959) Colorimetric assay methods for free and phosphorylated glyceric acids. *J. Biol. Chem.* **234,** 469–471
60. Oñaderra, M., Mancheño, J. M., Lacadena, J., de los Rios, V., Martínez del Pozo, A., and Gavilanes, J. G. (1998) Oligomerization of the cytotoxin α-sarcin associated with phospholipid membranes. *Mol. Membr. Biol.* **15,** 141–144
61. Maula, T., Isaksson, Y. J., García-Linares, S., Niinivehmas, S., Pentikäinen, O. T., Kurita, M., Yamaguchi, S., Yamamoto, T., Katsumura, S., Gavilanes, J. G., Martínez-del-Pozo, A., and Slotte, J. P. (2013) 2NH and 3OH are crucial structural requirements in sphingomyelin for sticholysin II binding and pore formation in bilayer membranes. *Biochim. Biophys. Acta* **1828,** 1390–1395
62. García-Linares, S., Alm, I., Maula, T., Gavilanes, J. G., Slotte, J. P., and Martínez-Del-Pozo, Á. (2015) The effect of cholesterol on the long-range network of interactions established among sea anemone Sticholysin II residues at the water-membrane interface. *Mar. Drugs* **13,** 1647–1665
63. de los Ríos, V., Mancheño, J. M., Martínez del Pozo, A., Alfonso, C., Rivas, G., Oñaderra, M., and Gavilanes, J. G. (1999) Sticholysin II, a cytolysin from the sea anemone *Stichodactyla helianthus*, is a monomer-tetramer associating protein. *FEBS Lett.* **455,** 27–30
64. Pazos, I. F., Martínez, D., Tejuca, M., Valle, A., del Pozo, A., Alvarez, C., Lanio, M. E., and Lissi, E. A. (2003) Comparison of pore-forming ability in membranes of a native and a recombinant variant of Sticholysin II from *Stichodactyla helianthus*. *Toxicon* **42,** 571–578
65. Macek, P., Belmonte, G., Pederzolli, C., and Menestrina, G. (1994) Mechanism of action of equinatoxin II, a cytolysin from the sea anemone *Actinia equina* L. belonging to the family of actinoporins. *Toxicology* **87,** 205–227
66. Tanaka, K., Caaveiro, J. M., Morante, K., González-Mañas, J. M., and Tsumoto, K. (2015) Structural basis for self-assembly of a cytolytic pore lined by protein and lipid. *Nat. Commun.* **6,** 6337
67. Cosentino, K., Ros, U., and García-Sáez, A. J. (2016) Assembling the puzzle: oligomerization of α-pore forming proteins in membranes. *Biochim. Biophys. Acta* **1858,** 457–466
68. Ros, U., and García-Sáez, A. J. (2015) More than a pore: the interplay of pore-forming proteins and lipid membranes. *J. Membr. Biol.* **248,** 545–561
69. Subburaj, Y., Ros, U., Hermann, E., Tong, R., and García-Sáez, A. J. (2015) Toxicity of an α-pore-forming toxin depends on the assembly mechanism on the target membrane as revealed by single-molecule imaging. *J. Biol. Chem.* **290,** 4856–4865
70. Rojko, N., Dalla Serra, M., Maček, P., and Anderluh, G. (2016) Pore formation by actinoporins, cytolysins from sea anemones. *Biochim. Biophys. Acta* **1858,** 446–456
71. Martínez, D., Campos, A. M., Pazos, F., Alvarez, C., Lanio, M. E., Casallanovo, F., Schreier, S., Salinas, R. K., Vergara, C., and Lissi, E. (2001) Properties of St I and St II, two isotoxins isolated from *Stichodactyla helianthus*: a comparison. *Toxicon* **39,** 1547–1560
72. Wong, E. S., and Belov, K. (2012) Venom evolution through gene duplications. *Gene* **496,** 1–7
73. Valle, A., Alvarado-Mesén, J., Lanio, M. E., Álvarez, C., Barbosa, J. A., and Pazos, I. F. (2015) The multigene families of actinoporins (part I): isoforms and genetic structure. *Toxicon* **103,** 176–187
74. Brinkman, D. L., Konstantakopoulos, N., McInerney, B. V., Mulvenna, J., Seymour, J. E., Isbister, G. K., and Hodgson, W. C. (2014) *Chironex fleckeri* (box jellyfish) venom proteins: expansion of a cnidarian toxin family that elicits variable cytolytic and cardiovascular effects. *J. Biol. Chem.* **289,** 4798–4812
75. Dewson, G. (2016) Doughnuts, daisy chains and crescent moons: the quest for the elusive apoptotic pore. *EMBO J.* **35,** 371–373
76. Ros, U., Rodríguez-Vera, W., Pedrera, L., Valiente, P. A., Cabezas, S., Lanio, M. E., García-Sáez, A. J., and Alvarez, C. (2015) Differences in activity of actinoporins are related with the hydrophobicity of their N terminus. *Biochimie* **116,** 70–78
77. Martín-Benito, J., Gavilanes, F., de Los Ríos, V., Mancheño, J. M., Fernández, J. J., and Gavilanes, J. G. (2000) Two-dimensional crystal-

lization on lipid monolayers and three-dimensional structure of stícholysín II, a cytolysin from the sea anemone *Stichodactyla helianthus*. *Biophys. J.* **78,** 3186–3194

78. Mechaly, A. E., Bellomío, A., Gil-Cartón, D., Morante, K., Valle, M., González-Mañas, J. M., and Guérin, D. M. (2011) Structural insights into the oligomerization and architecture of eukaryotic membrane pore-forming toxins. *Structure* **19,** 181–191
79. Baker, M. A., Rojko, N., Cronín, B., Anderluh, G., and Wallace, M. I. (2014) Photobleaching reveals heterogeneous stoichiometry for equinatoxin II oligomers. *Chembiochem* **15,** 2139–2145
80. Morante, K., Caaveiro, J. M., Viguera, A. R., Tsumoto, K., and González-Mañas, J. M. (2015) Functional characterization of Val60, a key residue involved in the membrane-oligomerization of fragaceatoxin C, an actinoporin from *Actinia fragacea*. *FEBS Lett.* **589,** 1840–1846

Article III

Stichodactyla helianthus' de novo transcriptome assembly: Discovery of a new actinoporin isoform

Esperanza Rivera-de-Torre[1,2], Álvaro Martínez-del-Pozo[2], Jessica E. Garb[1]

[1]Department of Biological Sciences, University of Massachusetts Lowell, Lowell, MA, USA
[2]Departamento de Bioquímica y Biología Molecular, Facultad de CC. Químicas, Universidad Complutense de Madrid, 28040, Madrid, Spain

Toxicon, 2018, 150, 105-114

DOI: https://doi.org/10.1016/j.toxicon.2018.05.014

El análisis transcriptómico de los tejidos productores de veneno de diferentes animales es una aproximación efectiva para descubrir nuevas toxinas útiles desde el punto de vista biotecnológico y de las aplicaciones farmacéuticas, así como del estudio comparativo evolutivo de animales venenosos. *Stichodactyla helianthus* es una anémona marina del mar Caribe que produce actinoporinas como parte de su veneno. Esta familia de proteínas formadoras de poros son multigénicas y al menos dos isoformas diferentes, codificadas por genes independientes, son producidas por esta anémona. Estas isoformas, sticholisina I y II (StnI and StnII), comparten un 93% de identidad de secuencia pero difieren en su actividad formadora de poros y actúan de forma sinérgica. Esta observación sugiere que otras isoformas de actinoporinas, si estuvieran presentes en la mezcla del veneno, podrían contribuir al establecimiento de una ventajosa estrategia molecular de modulación de la actividad del conjunto del veneno. Utilizando técnicas de secuenciación de alto rendimiento, se ensambló el primer transcriptoma *de novo* de *S. helianthus* y se determinó la expresión relativa de los tránscritos, utilizando RNA-Seq para caracterizar los componentes del veneno de esta especie, centrando el foco en la diversidad de actinoporinas. Aplicando esta aproximación, se determinó la composición proteica general del veneno de la anémona y se descubrió la existencia de al menos unas nueva variante de actinoporina producida por *S. helianthus*, denominada sticholisina III (StnIII).

PhD candidate contributions

Esperanza Rivera de Torre conceived, designed and conducted the experiments. She also played a major and principal role in analyzing and discussing the results, writing and correcting the manuscript and suggesting modifications. Consequently, she also is the corresponding author of this publication.

Toxicon 150 (2018) 105–114

Contents lists available at ScienceDirect

Toxicon

journal homepage: www.elsevier.com/locate/toxicon

Stichodactyla helianthus' *de novo* transcriptome assembly: Discovery of a new actinoporin isoform

Esperanza Rivera-de-Torre[a,b,*], Álvaro Martínez-del-Pozo[b], Jessica E. Garb[a]

[a] Department of Biological Sciences, University of Massachusetts Lowell, Lowell, MA, USA
[b] Departamento de Bioquímica y Biología Molecular, Facultad de CC. Químicas, Universidad Complutense de Madrid, 28040, Madrid, Spain

ARTICLE INFO

Keywords:
Transcriptome
Anemone
Actinoporin
Toxin
Isoform

ABSTRACT

Transcriptomic profiling of venom producing tissues from different animals is an effective approach for discovering new toxins useful in biotechnological and pharmaceutical applications, as well in evolutionary comparative studies of venomous animals. *Stichodactyla helianthus* is a Caribbean sea anemone which produces actinoporins as part of its toxic venom. This family of pore forming toxins is multigenic and at least two different isoforms, encoded by separate genes, are produced by *S. helianthus*. These isoforms, sticholysins I and II, share 93% amino acid identity but differ in their pore forming activity and act synergistically. This observation suggests that other actinoporin isoforms, if present in the venomous mixture, could offer an advantageous strategy to modulate whole venom activity. Using high-throughput sequencing we generated a *de novo* transcriptome of *S. helianthus* and determined the relative expression of assembled transcripts using RNA-Seq to better characterize components of this species' venom, focusing on actinoporin diversity. Applying this approach, we have discovered at least one new actinoporin variant from *S. helianthus* in addition to several other putative venom components.

1. Introduction

Sea anemones belong to one of the oldest venomous lineages, the phylum *Cnidaria*. Since these animals usually live fixed to a substrate, their predatory and defensive abilities rely on the production of potent toxins. The predominant toxins in sea anemone venoms studied so far include phospholipases A2s (PLA2s), cytolysins and neurotoxins, like potassium and sodium gated channels inhibitors (KTxs and NaTxs) (Madio et al., 2017; Macrander et al., 2015a, 2016). Other minor components like metalloproteases and cysteine rich peptides are also found in anemone venoms (Macrander et al., 2015a). This toxic cocktail is usually stored in a specialized organelle called the nematocyst, a stinging capsule that injects the venom upon activation by contact. Anemone venom components work together in remodeling target membranes (e.g., PLA2s), producing prey cell death by osmotic shock (cytolysins) and provoking pain and paralysis by altering neurotransmission secretion (neurotoxins) (Suput, 2009). In combination, these toxins cause paralysis and death in small fishes and crustaceans (Salgado and Kem, 1992). Past work showed that nematocysts were only present in the tentacles, which surround the anemone oral disc, and this was expected given the role of tentacles in attracting and catching prey (Basulto et al., 2006). Recent studies question this observation, suggesting that the toxic secretion can be detected across most of the sea anemone tissues (Rojko et al., 2016).

Among the sea anemone cytolysins (cell-lysing toxins), actinoporins are pore-forming proteins. They constitute multigenic families (Wang et al., 2008), where a single individual expresses different genes coding for several isotoxins with distinct activities (Wang et al., 2008; Monastyrnaya et al., 2010). *Stichodactyla helianthus* is a Caribbean sea anemone which produces large amounts of two easily detectable actinoporin variants: sticholysin I (StnI) and sticholysin II (StnII) (Lanio et al., 2001). StnII is the most potent actinoporin of those that have been studied with molecular detail (Garcia-Linares et al., 2016a). StnI is approximately four times less active than StnII in terms of hemolytic activity (Monastyrnaya et al., 2010; Garcia-Linares et al., 2016a). Both isoforms interact with each other to produce a synergistic effect; just trace amount of StnII enhances StnI binding to lipid model vesicles driving a dramatic improvement of hemolytic activity (Rivera-de-Torre et al., 2016). These observations extend the complexity and regulatory capacity of toxin function, similar to a rudimentary immune system (Wang et al., 2008), potentially increasing the range of species *S. helianthus* can capture or defend itself from.

As mentioned above, only StnI and StnII have been detected in *S. helianthus* lysates thus far (Lanio et al., 2001; Valle et al., 2015). Both

* Corresponding author. Departamento de Bioquímica y Biología Molecular, Facultad de CC. Químicas, Universidad Complutense de Madrid, 28040, Madrid, Spain.
E-mail address: esperanza.rivera.detorre@gmail.com (E. Rivera-de-Torre).

https://doi.org/10.1016/j.toxicon.2018.05.014
Received 8 January 2018; Received in revised form 17 May 2018; Accepted 18 May 2018
Available online 19 May 2018

are produced in high concentration, although it remains unclear which one is more abundant (Lanio et al., 2001). However, considering their synergistic interaction (Rivera-de-Torre et al., 2016) and the multigene character of this protein family (Wang et al., 2008), it has been hypothesized (Rivera-de-Torre et al., 2016) that small amounts of other actinoporins, not yet detected in the lysate, might be produced to further modulate whole venom activity.

Next-generation RNA-sequencing is a powerful technology which is the emerging method of choice in the analysis of venoms because of the massive amounts of sequence data that can be rapidly obtained. Specifically, a single Illumina instrument run can capture enough data to fully characterize a venom transcriptome, including all its constituent transcripts and their encoded proteins, and enabling estimation of the relative abundance of assembled transcripts through read mapping (Macrander et al., 2015a, 2015b, 2016). Further analysis can be helpful in reconstructing the evolutionary relationships of toxins within and across different species, which can also illuminate how sea anemone species have diversified their venom composition (Haney et al., 2016; Garb et al., 2004; Garb and Hayashi, 2005; Kitchen et al., 2015; Macrander and Daly, 2016).

In this study we utilized Illumina RNA-seq methods to sequence and assemble a first draft of the *Stichodactyla helianthus* transcriptome. We used this new database to identify and quantify the relative expression of candidate venom toxins, focusing on characterizing novel putatively active actinoporins, in addition to other toxic proteins.

2. Materials and methods

2.1. Specimens

Two specimens of *Stichodactyla helianthus* were purchased from Dynasty Marine Associates, Inc (Marathon, Florida), which were collected from Big Pine Key, Florida (Biosample PRJNA464282). The specimens were cut into thin radial pieces comprising all the structures in the sea anemone, principally the tentacles and column. This tissue was dissolved in TRIzol (Ambion, Life Technologies) up to a final concentration of 100 μg/mL by homogenization with a rotar-stator homogenizer when it was still fresh, and they were frozen at −80 °C for less than a week before RNA extraction.

2.2. RNA extraction

Total RNA was extracted through the standard protocol recommended for TRIzol (Chomczynski, 1993). Briefly, homogenized tissue was incubated at room temperature for 5 min and then chloroform was added to the samples. After vigorous shaking, the mixtures were centrifugated at 12000 × g for 15 min at 4 °C. The aqueous phase was recovered in a new tube. RNA was precipitated with isopropanol recovered by centrifugation followed by several washing steps with 75% ethanol. Dried RNA samples were dissolved in RNase-free water. Samples were DNase treated with the TURBO DNA-free kit (Ambion, Life technologies). Finally, RNA was stored at −80 °C until utilization. The RNA concentration was quantified with a Qubit 3.0 (Thermo Scientific) and its integrity was confirmed though 2100 BioAnalyzer (Agilent Technologies) analysis.

2.3. Library preparation and high-throughput sequencing

Using the TruSeq stranded mRNA LT Sample prep kit (Illumina), double-stranded cDNA libraries were obtained from the two total RNA samples. To test the quality of the libraries a BioAnalyzer chip (Agilent Technologies) was run. The relative concentration of each bar-coded library was determined through qPCR and they were immediately pooled in a single sample considering that equivalent amounts of each library were present in the mixture. Libraries were sequenced on a single NextSeq® 500/550 High Output Kit v2 (300 cycles) (Illumina), on a NextSeq 500 instrument as a paired-end 150 base sequencing.

2.4. Cleanup and de novo assembly

Raw Illumina reads from different libraries were de-multiplexed according to their barcoding label. Illumina adaptors were trimmed using the Trim Galore! tool (Krueger, 2012). As a modification to the default setting, the unpaired reads were retained and 5 extra base pairs were cleaved at the 3′ edge of the reverse reads to remove low-quality bases. The quality of these cleaned raw reads was verified with the FastQC reports in the Trim Galore! suite. Cleaned reads were deposited in NCBI's SRA database (Accession: SRR7126073) within Bioproject PRJNA464282.

S. helianthus' RNA-seq cleaned data from the two libraries were put together in a *de novo* transcriptome assembly using Trinity v2.4.0 or Trinity v2.0.6 (Grabherr et al., 2011) with default parameters. Two different versions of Trinity (v2.4.0 and v2.0.6) were compared to analyze potential differences in transcriptome fragmentation (Bryant et al., 2017). Transcriptome completeness was determined using BUSCO v3 (Benchmarking Universal Single-Copy Orthologs (Simao et al., 2015)) with the Metazoa data set. This program assayed the presence of 978 proteins conserved from 65 different species within this group. Transcripts were deposited in the TSA database (GGNY00000000).

2.5. Data analysis, candidate toxin gene identification and transcript quantification

The resulting transcriptome was annotated by identification of alignments through BLASTx with proteins in the National Center for Biotechnology Information (NCBI) with each transcript. The restrictions applied were an E-value $< 1 \times 10^{-5}$ and allowing for a maximum of ten target sequences per query sequence.

Starting with the Trinity assembly file, we identified the open-reading frame (ORF) for each transcript with Transdecoder (Haas et al., 2013). The default settings were modified to retain the longest ORF with the best BLASTx hit showing an E-value < 10 or in absence of a BLASTx alignment, the longest ORF. In this way, we obtained a comprehensive protein prediction database if transcripts lacked a BLAST hit.

Relative expression levels for each transcript were calculated using the program RSEM (Li and Dewey, 2011). This program mapped back the cleaned sequence reads to the assembly, estimating the number of transcripts as TPM (Transcripts Per Million).

A nucleotide database for BLAST searches was built with both Trinity assemblies from *S. helianthus* (obtained with Trinity v2.4.0 and v2.0.6 respectively). From the ToxProt data set (http://www.uniprot.org/program/Toxins last accession 2018/02/14), venom proteins and toxins sequences from different categories like KTX-I, KTX-III, NaTx, Metalloproteases, PLA2s and Cytolysins were pooled and extracted. These protein families are known to be present in sea anemone venoms (Madio et al., 2017; Macrander et al., 2015a, 2015b, 2016; Macrander and Daly, 2016). A tBLASTn search of these toxin sets against the *S. helianthus* trinity assembly (E-value < 10) was conducted to identify toxin sequence candidates. After eliminating the duplicated hits, the number of sequences per toxin category and the average expression within each category were analyzed.

StnI and StnII protein sequences were used as queries in a search against the *S. helianthus* transcriptome nucleotide sequences database using tBLASTn (E-value < 1e-5, matching length > 60%). We used tBLASTn because protein sequences are more conserved than nucleotides and the search was consequently less restrictive than the BLASTn query. The assembly and the subsequent analysis was performed on the University of California Riverside Biocluster (Intel Broadwell 32 cores and 512 GB memory).

A phylogenetic analysis of Stn transcripts was conducted along with

other closely related actinoporin sequences. The purpose was to assess relationships of previously known and novel Stn toxins, rather than to reconstruct a comprehensive phylogenetic tree for all actinoporins as in Macrander and Daly (2016). Closely related sequences were obtained by performing a BLASTx search of Uniprot using StnI and II as query sequences, taking the top 15 hits, and limiting analyses to hits with corresponding nucleotide sequences. Nucleotide sequences were trimmed to their coding sequence and aligned by their translated amino acids using MUSCLE implemented in geneious 9.1.8, keeping translated codons in frame. MrModelTest2.3 (Nylander, 2004) was used to determine an appropriate nucleotide substitution model (GTR + I + G), which was used in a Bayesian phylogenetic analysis with MrBayes3.2.6 (Ronquist et al., 2012). The Bayesian analysis was run for 5×10^6 generations, sampling trees every 1000 generations and discarding the first 25% of sampled trees as burn-in. A 50% majority-rule Bayesian consensus tree was computed from post burn-in trees to determine clade posterior probabilities and the consensus tree was mid-point rooted.

2.6. Novel actinoporin complete sequence determination

Two potential new actinoporin sequences discovered through the BLAST search against *S. helianthus' de novo* transcriptome assembly database (termed StnIII and IV) were PCR-amplified. First cDNA was synthesized with the SuperScript III First-Strand Synthesis SuperMix kit (Thermo Fisher) using RNA extracted from the same anemone individual used for the high-throughput sequencing described above. In order to obtain the sequence of mature StnIII, a complementary primer was designed against its 5′ edge (5′-ATGAATCCTTTAGCAGTCGCTGG TGC-3′). Taking into account the lack of differences between StnI and II at their 3′ end and minor variation in putative StnIII and IV, a degenerate 3′ primer was designed to match these sequences: (C/T)TA(A/G) (C/T)G(A/T)GA(A/G)ATCT(C/T)AAATTTGCA(G/T)TTTTGCTTC GCC-3′). A PCR program was run in two phases: five initial cycles at a low annealing temperature (40 °C) followed by 30 cycles at 55 °C as the annealing temperature. The resulting amplified product was purified and Sanger sequenced.

3. Results and discussion

3.1. Sequencing and assembly

The obtained transcriptome was assembled from 42,678,357 paired-end reads. The assembly quality data is summarized in Table 1. The two assemblies generated with different versions of Trinity yielded a number of genes (177,655–v2.4.0– and 140,745–v2.0.6) and isoforms (226,240–v2.4.0– and 194,773–v2.0.6) comparable with other previously described sea anemone's transcriptomes (Macrander et al., 2015a, 2015b, 2016; Ayala-Sumuano et al., 2017; Tulin et al., 2013). N50 parameters were high enough to ensure a sufficiently good assembly with large contigs (N50 1544–v2.4.0– and 1590–v2.0.6) and again, comparable to other sea anemone's assemblies obtained with the same program (N50 392–1832) (Macrander et al., 2015a, 2015b, 2016; Ayala-Sumuano et al., 2017). Although both Trinity versions yielded similar results, the absolute isoform and gene numbers were higher when using Trinity v2.4.0, with a higher degree of fragmentation of the contigs. The N50 parameter and average contig length comparison between both methods suggested that Trinity v2.0.6 rendered a less fragmented assembly presenting larger contigs and a reduced number of total predicted genes and isoforms.

Table 1
Statistics of the *S. helianthus* assembly with two different Trinity versions.

Trinity version	2.4.0	2.0.6
No. of paired-end reads	42,678,357	
No. of total assembled bases	183,455,014	171,292,869
No. of assembled genes	171,655	140,745
No. of assembled transcripts	226,240	194,773
Assembly GC percent	39.74	39.72
Contig N50	1544	1590
Average contig	810.89	879.45

Table 2
BUSCO statistics for both assemblies with different Trinity versions.

Trinity version	2.4.0	2.0.6
Total BUSCO groups searched	978	
Complete BUSCOs	918/93.9%	921/94.2%
Fragmented BUSCOs	45/4.6%	43/4.4%
Missing BUSCOs	15/1.5%	14/1.4%

Completeness scores calculated with BUSCO software are shown in Table 2. BUSCO's completeness scores were high for both assembly's attempts, performed with v2.4.0 and v2.0.6 (93.9% and 94.2% expected conserved full-length proteins were found respectively), and the missing BUSCOs were low (1.5% and 1.4%), showing that both Trinity assemblies contained nearly all expected proteins in an unfragmented state.

3.2. Toxin protein venom profile

Sea anemone venoms are composed of a complex mixture of toxins. Some of the most common/abundant toxins are the neurotoxins KTxs-I, KTxs-III and NaTxs, the cytolysins, which include actinoporins and other pore forming toxins, and enzymes capable of modifying membranes and extracellular matrix like phospholipases and metalloproteases. All these toxins were considered for the profiling analysis performed. In addition, the main venomous components whose proteomic evidence has been recently described for *Stichodacthyla haddoni* (Madio et al., 2017), an anemone species belonging to the same genus as *S. helianthus,* were included, for example Ankyrin-repeat proteins, S1 peptidases and FBG-domain proteins. Considering the slightly improved, less fragmented assembly obtained with Trinity v2.0.6 all further analyses were continued with these transcripts.

All sequences present in the ToxProt data set, whose description contained the keyword for each kind of anemone toxin described above, were pooled in a single multiFASTA file. These sequences were used as a query against the database built with the *S. helianthus* assembly in tBLASn search. The results showed phospholipases A2 (PLA2s) represented the most numerous category regarding toxin isoforms number, while cytolysins corresponded to one of the smallest categories (Fig. 1A). However, in terms of relative expression, the highest average value was by far found for cytolysins, while the lowest one was represented by metalloproteases (M12A and M13 subgroups) (Fig. 1B). Overall, this distribution would be consistent with the fact that actinoporins are not enzymes and therefore they do not show catalytic effects as phospholipases and metalloproteases do. StnII is the most potent actinoporin known from cytolytic assays against red blood cells (Garcia-Linares et al., 2016a). Our present results show it is also the most highly expressed Stn (Table 3) in *S. helianthus*, potentially explaining the potency of its venom in causing cell lysis.

We found that the total number and abundance (in terms of TPM) of the toxin categories differed substantially between *S. helianthus* and that reported for *S. haddoni* (Madio et al., 2017). But this pattern of high variability of toxin cocktails among closely related species has been noted for other anemones (Macrander et al., 2016). Considering that the condition of the anemones in our study prior to dissection may have influenced expression levels, and that our transcriptome represents a whole-body transcriptome, rather than one specific to venom-secreting tissues as produced for *S. haddoni* (Madio et al., 2017), our estimates of sequence diversity and expression levels may not be directly

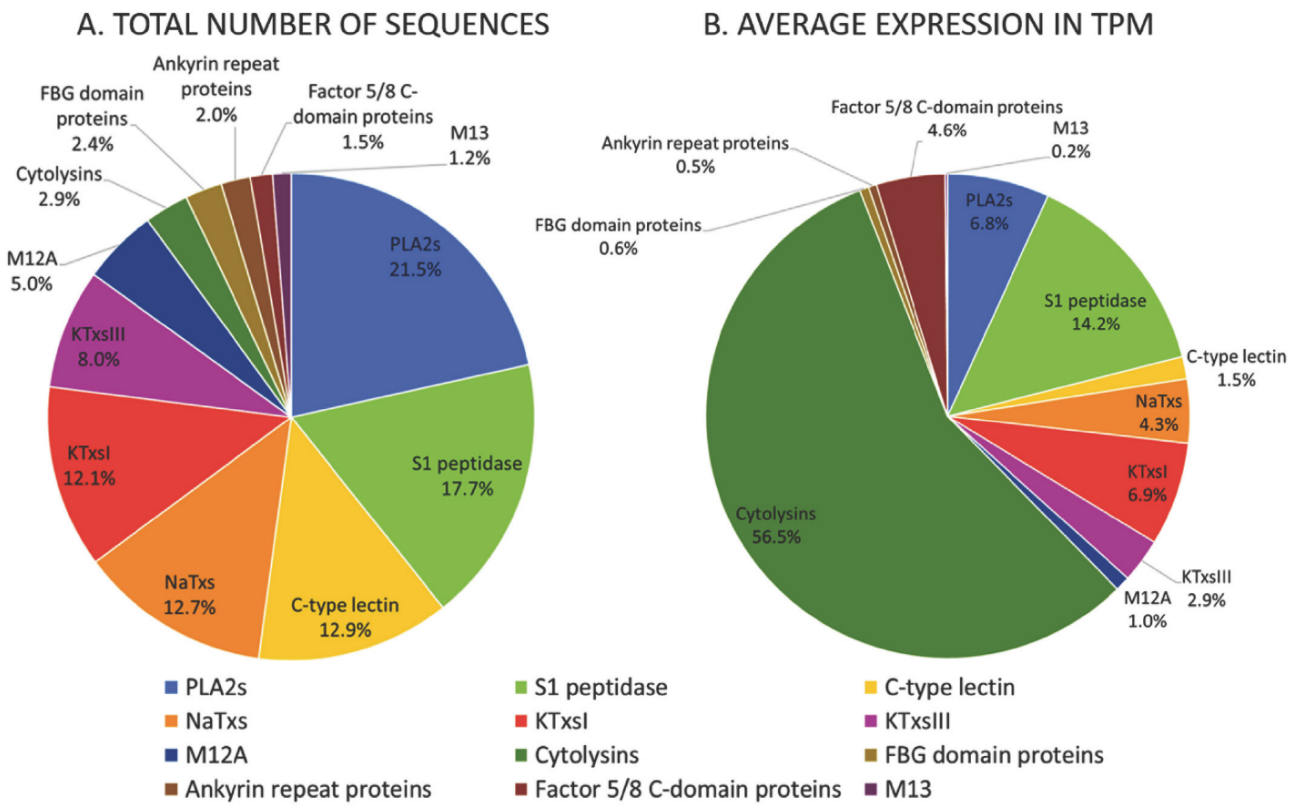

Fig. 1. Summary of the putative components of the *S. helianthus* venom secretion. (A) Total number of sequences found for each toxin type. (B) Average expression of the transcripts recovered in TPM for each toxin category. Selected toxins types in this study are indicated in the legend.

Table 3
Average RSEM calculated Transcripts per Million (TPM) for the Stn predicted transcripts.

Trinity version	2.4.0	2.0.6
StnI	389	455
StnII	704	733
StnIII	129	125
StnIV	113	62

comparable. Thus, our results should be considered a first approximation for *S. helianthus* in terms of relative expression values, given that the putative toxins identified in this study could also expressed in non-venomous tissues and have alternative functions. Further, it is unlikely that all the transcripts we identified as toxins are functionally venomous because the criteria for inclusion was based solely on BLAST search e-scores and the prediction of a function does not guarantee actual function.

A tBLASTn search was also performed with the complete ToxProt database against the *S. helianthus* transcriptome assembly to find putative toxin sequences corresponding to other proteins not necessarily specific to sea anemones venom. Highly similar hits (e-value $< 1e^{-5}$ and an overlapping length > 60%) were the subject of the search. After merging the list with the expression data obtained with RSEM, the ten most highly expressed sequences were examined for further analysis (Table 4). Some of the most highly expressed predicted toxic proteins did not have their top BLAST hit to sea anemone toxins. Instead, their top BLAST hits to ToxProt proteins were to toxins in families such as calmodulin, PLA2s and cysteine-rich proteins from snakes, scorpions and corals. However, PLA2s and cysteine-rich proteins are some of the most well studied toxin families in sea anemones, and these results may simply be due to the absence of these anemone toxin proteins in the ToxProt database. Nevertheless, the most highly expressed toxins were identified as known anemone venom compounds such as the most highly expressed hit U-actitoxin-Avd8b (P0DMZ4) from *Anemonia viridis*, the specific function of which is still unknown. In this analysis, StnI and StnII did not appear as hits because they are not included in the ToxProt database. The contigs corresponding to StnI and StnII found however a highly similar protein in actinoporins from *A. villosa* (Q5R231) and *A. equina* (P6191), which were the second and third most highly expressed transcripts, respectively (Table 4). Indeed, the expression values for these proteins match the data recorded in Table 3 regarding expression levels for StnI and StnII. The fourth sequence on the list is a voltage-gated sodium channel inhibitor and the fifth on the list includes the first PLA2 (Table 4).

3.3. New sticholysin sequence prediction and evolution

Though the older Trinity version (v2.0.6) resulted in lower fragmentation, having longer contigs and slightly better BUSCO scores, we kept both program assemblies when looking for new potential actinoporins because these toxins are extremely similar at the nucleotide level (StnI and StnII share 93% of their amino acid residues). Trinity can collapse fragment reads from different isoforms into the same transcript because some fragment reads from different isoforms may be nearly identical in certain regions. Thus, we compared the results from both assemblies since the one obtained with Trinity v2.4.0 is more fragmented so this version may have assembled fewer fragments into the same transcript. Trinity v2.4.0 offers a more conservative assembly approach, although it returns more incomplete transcripts. On the other hand, while the 2.0.6 version gives back less fragmented transcripts, it is combining reads to build a single transcript so it could return more complete sequences.

A tBLASTn search using Stn I and II against a database built with

Table 4
Most highly expressed transcripts among all the ToxProt data tBLASTn hits. Actinoporins are marked with an asterisk.

Transcript ID	TPM	UniProtKB	Animal group	Gene name	E-value
TR74943|c0_g1_i1	1291	P0DMZ4	Anemone	U-actitoxin-Avd8b	2.00E-25
*TR72237|c1_g3_i1	734	Q5R231	Anemone	DELTA-thalatoxin-Avl1a	2.00E-62
*TR72237|c1_g3_i2	455	P61914	Anemone	DELTA-actitoxin-Aeq1a	4.00E-93
TR22445|c1_g4_i1	421	E2S064	Anemone	Kappa-thalatoxin-Cad2a	7.00E-42
TR56102|c1_g1_i5	285	Q9PUG8	Snake	Acidic phospholipase A2 S16-19	3.00E-18
TR59776|c1_g1_i7	201	Q8AY75	Snake	Calglandulin	5.00E-35
TR51365|c5_g3_i1	190	P0CJ14	Scorpion	Venom protein 302	2.00E-09
TR62101|c0_g8_i4	136	P0DL54	Anemone	Delta-actitoxin-Avd1e 3	6.00E-06
TR52902|c1_g1_i4	80	C0H691	Coral	Small cysteine-rich protein 2	1.00E-07
TR2041|c1_g2_i2	74	P0DMZ6	Anemone	U-actitoxin-Avd8d	5.00E-41

both Trinity assemblies was performed which found the following result: 25 or 21 different actinoporin candidates using v2.4.0 or v2.0.6, respectively. After pulling out the nucleotide sequences and the Transdecoder predicted ORF for each candidate transcript, alignments with StnI and StnII were performed through Clustal Omega (Sievers et al., 2011). Most of these potential actinoporins showed a universally conserved motif present in all previously characterized actinoporins: "**Y/FDYNW**Y**SNWW**" (Garcia-Linares et al., 2016a). Residues in bold are part of a cluster of aromatic residues involved in membrane binding (Garcia-Linares et al., 2016b; Garcia-Ortega et al., 2011; Malovrh et al., 2000), while the underlined tyrosine belongs to the sphingomyelin-specific phosphorylcholine binding site (Mancheno et al., 2003). These are two of the most significant structural signatures regarding actinoporin activity. Closer inspection of each alignment revealed that not all the potentially new toxins shared this conserved domain. Thus, they were discarded as new actinoporins. In addition, considering that actinoporins are generally cysteine-less and their average size is around 175 amino acids, these two criteria were also used to identify potential new actinoporins. Small fragments with an overlapping identity score over 80% were kept. After this strict selection, only four transcripts for each version (v2.4.0 and v2.0.6) were finally retrieved. The resulting selected actinoporins were used as a query for a new search in the *S. helianthus* transcriptome but it did not render any new hits different from the ones obtained in the first search.

In both transcriptomes, two of the four retrieved actinoporin sequences were the already known StnI and StnII, having 100% identity with StnI and 100% identity with StnII reported by Huerta & col. in 2001 (Huerta et al., 2001). Only the older Trinity version (2.0.6) retrieved complete sequences, while the newest version showed StnI and II with a truncated C-termini. Both assemblies yielded a similar, though not identical sequence, here termed StnIII (Fig. 2). This sequence was almost complete in both cases and only lacked a small fragment at the C-terminal edge. However, this missing fragment occurs in a sequence stretch which is also conserved across all the most-well studied actinoporins (Garcia-Linares et al., 2016a).

A fourth transcriptomic sequence, we initially named StnIV, was also found in both assemblies, though containing only the C-terminal stretch (Fig. 2). This feature precluded its complete analysis given that major differences in these proteins primarily accumulate at the N-terminal end (Garcia-Linares et al., 2016a; Ros et al., 2015). However, the sequences recovered as StnIV in the two assemblies were not identical but differed at some positions as well as to StnI and II. One possible explanation for this observation was that StnIV represented the protein of a different paralog to those encoding StnI-III. However, PCR amplification and sequencing of Stn III (see below) shows it is nearly identical at its overlap with Stn IV, suggesting they may represent allelic variants of the same locus.

All actinoporin sequences starting from a methionine codon (StnI, II and III) present a signal peptide, reported before for other actinoporins such as equinatoxin (Anderluh et al, 1999, 2000; Pungercar et al., 1997) but never before described for sticholysins (Fig. 3). This signal peptide comprises the first 34 amino acids of the deduced protein sequence and it shows the typical arrangement of a eukaryotic signal peptide (Kapp et al., 2009). This region can be divided into two functionally well-defined domains: a signal peptide, followed by a pro-sequence region, both of them leading actinoporins to their presumed final localization in nematocysts. The signal peptide region is constituted by a standard distribution made of a hydrophilic positively charged N-terminal, followed by a hydrophobic stretch. Overall, this signal sequence constitutes a motif which is conserved in other known actinoporins (Fig. 3). The pro-part region comprises the last 15–16 amino acids. This region is mainly polar and charged, highly conserved among the actinoporins within the same species, but highly variable in terms of length and net change among different species. The predicted cleavage site is a conserved Lys/Arg pair (Kex2-like and subtilisin-like proteases).

As described above, the predicted transcripts for StnI and StnII showed the highest expression levels while the new potential variants had a much-reduced representation in comparison. For example, the StnII transcript was around seven times more abundant than presumed StnIII and StnIV isotoxins. Both assemblies gave similar expression data, again confirming that the assembly merged into a similar number of fragments.

The main difference between both assembly methods was also reflected in the relative expression values obtained for the sequence provisionally designated as StnIV. This sequence was lowly expressed which likely accounts for it being fragmented and incomplete. This ambiguity might be solved through more deeply sequencing the transcriptome. It is easier to assemble sequences when the transcripts are more abundant in the mixture and therefore, considering that actinoporins share high identity, the Trinity program might be collapsing similar but not identical sequences, reducing the potential to retrieve variant sequences. This would explain why StnI and StnII were obtained as full-length sequences while the less highly expressed sequences were fragmented and missing pieces (Table 3). The reduced expression of StnIII could be also an artifact if its expression was suppressed under laboratory conditions and would be more accurately assessed in transcriptomes derived from venom-producing tissues. Nevertheless, if indeed lowly expressed, StnIII could still induce dramatic effects in the activity of *S. helianthus* venom given that small amounts of StnII can enhance Stn I binding to lipid model vesicles and hemolysis.

Our phylogenetic analysis of *S. helianthus* sticholysins show StnI and II as most closely related to each other, but that StnIII is divergent and instead is placed as more closely related to other species' actinoporins (Fig. 5). As actinoporins appear to be encoded by a multi-genic family in other closely related anemone species (Macrander and Daly, 2016), this suggests that StnI and II potentially arose following a species-specific gene duplication event. In contrast, the phylogenetic position of StnIII suggests the duplication event giving rise to this toxin gene predates the origin of *S. helianthus* and the duplication event that generated Stn I and II. The greater divergence of StnIII relative to Stn I and II reinforces the need to functionally evaluate the role of StnIII in *S.*

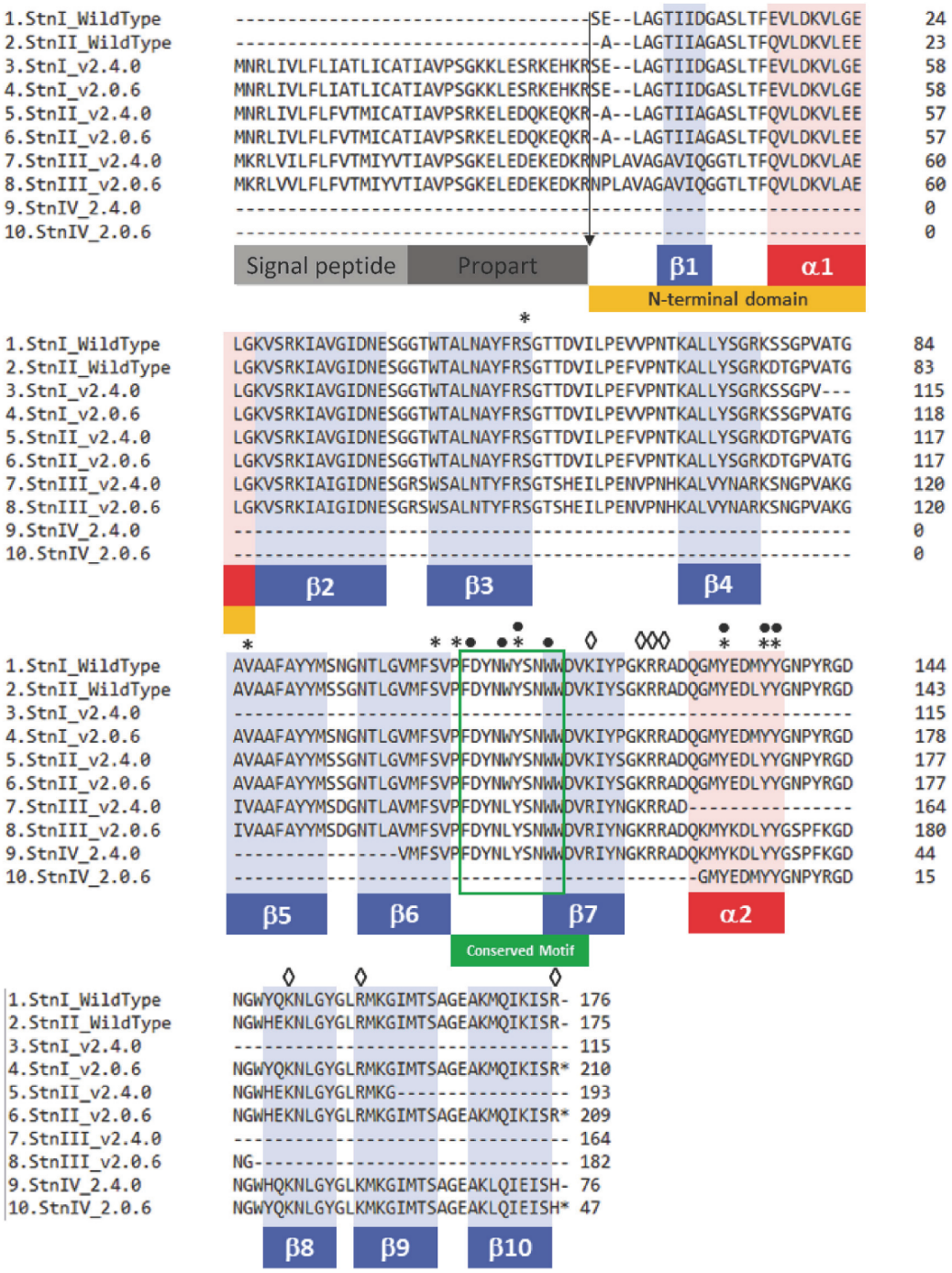

Fig. 2. Predicted protein sequence alignments for the tBLASTn selected hits for the wild type toxins StnI and StnII (sequences 1 and 2). Two Trinity versions were assayed for the *de novo* assembly: Trinity v2.4.0 and Trinity v2.0.6. The transcripts are sorted by decreasing identity percentage when compared with wild type StnI and StnII. Alignment performed with Clustal Omega. In light grey the signal peptide sequence followed by the propart in dark grey. A dashed arrow marks the excision position. Highlighted in blue the β-sheets and in red the α-helices experimentally determined for StnI and StnII wild type. In orange the N-terminal domain. Squared in green is the conserved motif cited in the text. Residues part of the phosphorylcholine binding site are marked with an asterisk. Black dots marks residues belonging to the cluster of aromatic residues. Diamonds point out the array of basic amino acids. (For interpretation of the references to colour in this figure legend, the reader is referred to the Web version of this article.)

helianthus venom, given its potential to modulate the toxicity of StnI and II in a synergistic fashion.

3.4. Novel actinoporin complete sequence and structrual prediction

Heterologous production and functional and structural characterization of newly discovered actinoporins will be extremely helpful in improving our understanding of the role of these proteins within sea

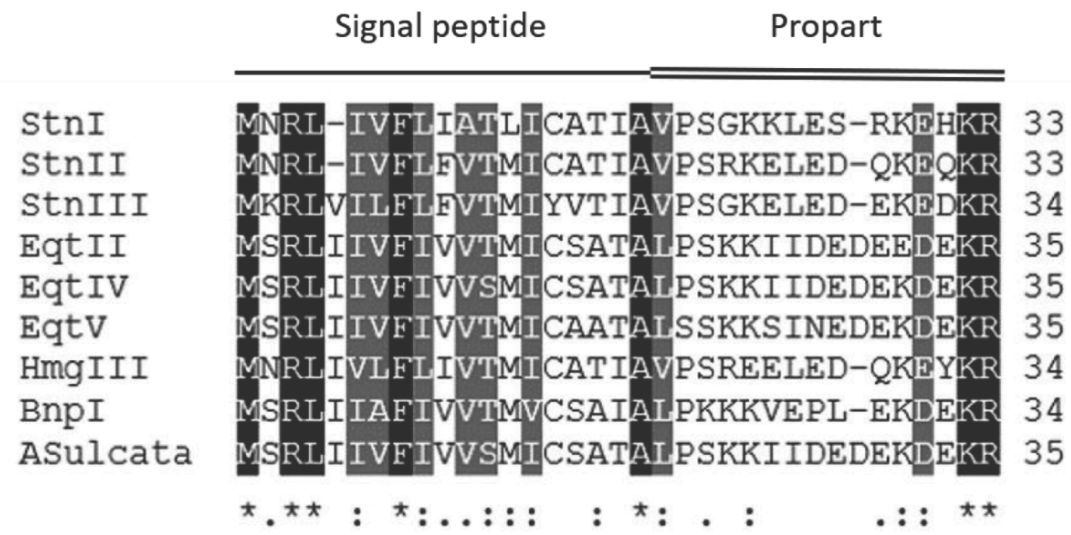

Fig. 3. Aligned signal peptides (single line) and propart (double-line) from different actinoporins. StnI, StnII and StnIII signal peptides were obtained in the Trinity assembly from this study. Other sequences were obtained from UniprotKB. Accession codes are the following: EqtII-P61914, EqtIV-Q9Y1U9, EqtV-Q93109, HmgIII-Q9U6X1, BnpI-C5NSL2, *A. sulcata*- A0A0S1M135. Black shade and asterisks mark identical residues, grey shade and colons (:) highlight conserved substitutions between groups of strongly similar properties, and dots (.) indicate conservation between groups of weakly similar properties.

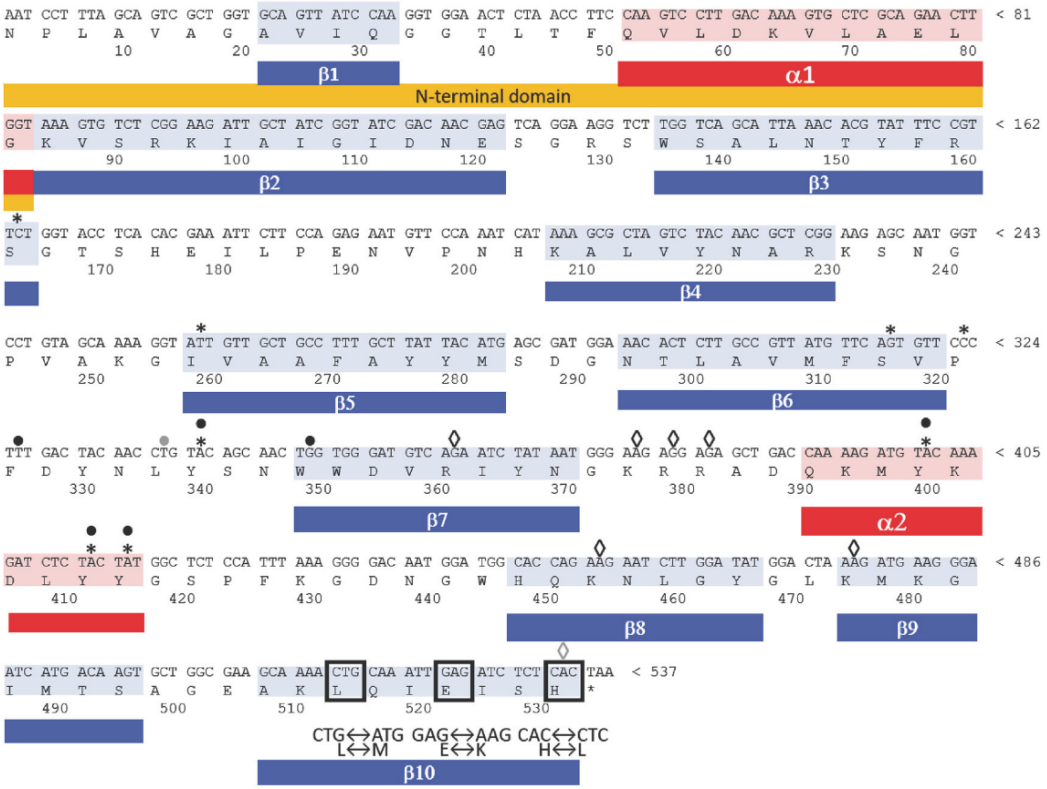

Fig. 4. StnIII mature sequence translated from sequenced PCR product (MH327769). Highlighted in blue the β-sheets and in red the α-helices experimentally determined for StnI and StnII wild type. In orange the N-terminal domain. Residues part of the phosphorylcholine binding site are marked with an asterisk. Black dots mark residues belonging to the cluster of aromatic residues. Diamonds indicate the array of basic amino acids. Grey dot (CTG-337) and grey diamond (CAC-533) indicate a residue part of the cluster of aromatic residues and the array of basic amino acids not conserved with respect to StnI and StnII. Squared in black are differences in the StnIII sequence relative to StnIV at their overlap (see Fig. 2). (For interpretation of the references to colour in this figure legend, the reader is referred to the Web version of this article.)

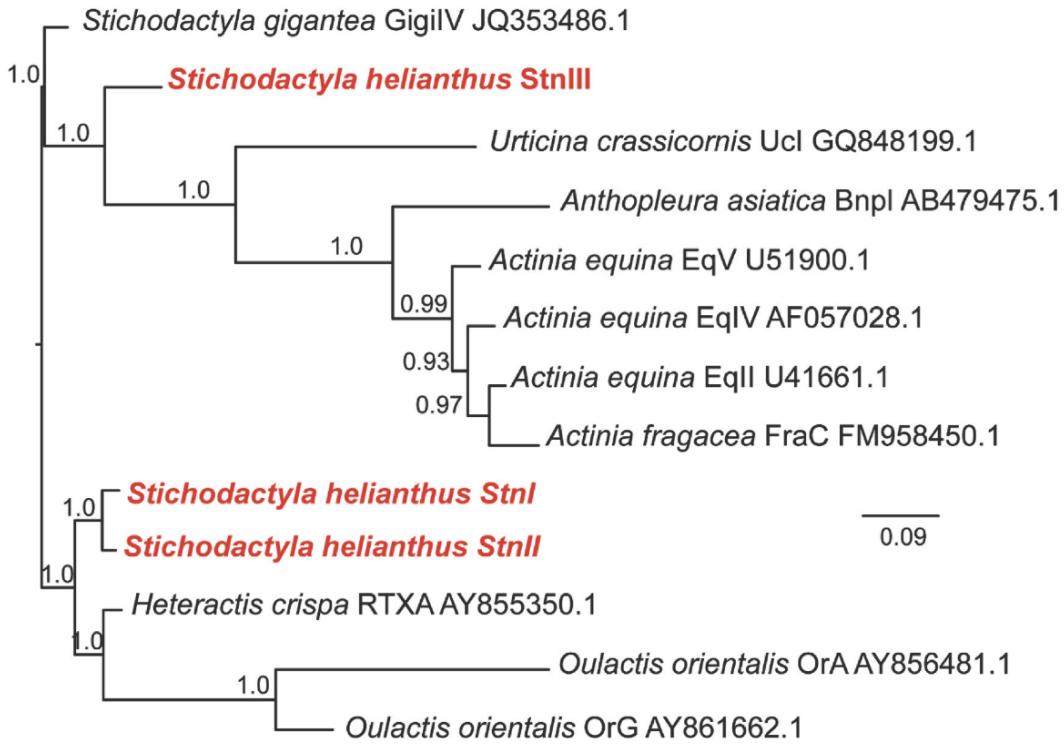

Fig. 5. Phylogenetic tree (Bayesian consensus) depicting relationships of *S. helianthus* sticholysins (StnI-III – in bold red text) in relation to closely related actinoporin sequences. Numbers at nodes indicate clade posterior probabilities computed from post burn-in trees. Tree is 50% majority rule of post burn-in trees, and is mid-point rooted. (For interpretation of the references to colour in this figure legend, the reader is referred to the Web version of this article.)

anemones venom. Thus, we fully sequenced the mature form of StnIII from a single band that was PCR-amplified from cDNA from one of the same individuals used for the transcriptome. The C-terminal domain of StnIII overlapped with the sequence obtained for StnIV and exhibited only three non-synonymous differences (Fig. 4). We therefore conclude that StnIII and IV may correspond to allelic variants of the same locus. However, given the C-terminal region is relatively invariant, we cannot unequivocally reject the possibility that the StnIV fragment is encoded by a different locus and may be connected to a more variable upstream region we were unable to obtain. The complete sequence determined for StnIII was deposited in NCBI's GenBank database (MH327769).

StnI and II share 93% amino acid identity, whereas StnIII is 76% identical to StnI and 77% to StnII at the protein level. This sequence conservation allowed the prediction of StnIII's three-dimensional structure by comparing with the already known 3D structures of StnI and StnII (Mancheno et al., 2003; Castrillo et al., 2009). This prediction was achieved using the Phyre2 web portal software (Kelley et al., 2015) which compares the primary sequence of the query with the amino acid sequence of already known structures. As expected, the model for StnIII's structural prediction displays the typical actinoporin folding assembly: an antiparallel β-sandwich flanked by two α-helices (Fig. 6).

Amino acid sequence comparison also shows that the N-terminal stretch of StnIII is 2 and 3 residues longer than the corresponding region in StnI and StnII. The hydrophobicity index of its 18 first residues (calculated according to (Eisenberg et al., 1984)), a critical feature for its cytolytic properties (Rivera-de-Torre et al., 2017), was very similar to StnI (Rivera-de-Torre et al., 2017). The hydrophobic moment, a magnitude that measures the affinity for the membrane core, is lower than StnI and StnII (0.209), suggesting a lower tendency to cross the membrane.

All the residues comprising important domains for the actinoporins function (Garcia-Ortega et al., 2011) are basically conserved or substituted by residues with similar physicochemical properties in StnIII. Within this context, Leu-113 in StnIII, corresponding to Trp-111 in StnI and Trp-110 in StnII stands out because this residue belongs to the so called cluster of aromatic residues, responsible for driving membrane binding and involved in maintaining the required hydrophobicity to achieve that goal. In agreement with this observation, StnII Trp-110 has been recently described as penetrating the hydrophobic membrane core (Garcia-Linares et al., 2016b). Accordingly, substitution by another highly hydrophobic amino acid, as is the case with Leu-113, is expected to have only minor influence on StnIII membrane interaction ability.

A more specific analysis of the different structural features and functionalities among the three sticholysins will still have to wait for the heterologous production of StnIII and its corresponding structural and functional analysis.

4. Conclusions

Sea anemone venom has been studied from different points of view and for different reasons, such as elucidating the molecular evolution of cnidarians (Macrander et al., 2016; Valle et al., 2015; Macrander and Daly, 2016) or obtaining biotechnological tools (Deng et al., 2016). Among the most well studied toxins in the sea anemone venom, PLA2s represent the largest family, with at least 50% more members than the next more representative group, NaTxs. Cytolysins are a much less diverse family but they show much higher average levels of expression. That is to say, they constitute a very important component of the toxic mixture in quantitative terms. This would also agree with the non-enzymatic character of their toxic effect. Interestingly, we found that actinoporins are some of the most highly expressed toxins considering all the possible venom and toxins hits gathered in the ToxProt data set. Therefore, actinoporins may be one of the main components in many sea anemone venoms. In the specific case of *S. helianthus* two actinoporin isoforms had been previously studied in deep detail (Garcia-Linares et al, 2013, 2016a, 2016b, 2016c; Maula et al., 2013). StnII is

Fig. 6. Three-dimensional soluble structures of sticholysins I (PDB 2KS4), and II (PDB 1GWY) in comparison to the StnIII 3D structural prediction. All figures were made using Pymol 1.3 modeling software (The PyMOL). β-sheets are shown in blue, α-helices in red-yellow and disordered loops are grey. (For interpretation of the references to colour in this figure legend, the reader is referred to the Web version of this article.)

the most potent actinoporin among the most well studied ones (Garcia-Linares et al., 2016a) and displays a synergistic effect in combination with StnI (Rivera-de-Torre et al., 2016). After our transcriptome analysis, we can conclude that there is at least one new actinoporin isoform which had not been described before even though there was evidence of the existence of other actinoporin variants in this anemone species (de los Rios et al., 2000). Transcriptomic approaches have become common to study the composition and diversity of venom, as well as the evolutionary genomics of venom production, with special emphasis on the evolution of multigene families. While transcriptome analysis is based on predictions around sequence similarity, it is necessary to perform functional studies of the main toxins to determine toxin activity, and to understand the ecological role of venom toxins. Thus, StnIII from *S. helianthus* venom must be the subject of further study given that it could be a key factor in modulating the toxic effect and range of prey targeted by sea anemones.

Acknowledgements

We thank Robert Haney, Erin Sullivan, Fitz Anthony Forsyth and Evelyn Schwager for their support in experimental design and data analysis. This work was supported by a Banco Santander-UCM fellow and an Erasmus + short fellowship to E.R.-d.-T, as well as a Major Research Instrumentation Grant from the US National Science Foundation (DBI-1429212) to UMass Lowell and Santander-UCM Project PR41_17_2012 to AMP. We also thank Jack Lepine and the UMass Lowell CRF for support in the Illumina sequencing.

References

Anderluh, G., et al., 1999. Equinatoxins, pore-forming proteins from the sea anemone Actinia equina, belong to a multigene family. Toxicon 37 (10), 1391–1401.
Anderluh, G., Podlesek, Z., Macek, P., 2000. *A common motif in proparts of Cnidarian toxins and nematocyst collagens and its putative role.* Biochim Biophys Acta. 1476 (2), 372–376.
Ayala-Sumuano, J.T., et al., 2017. Sequencing and de novo transcriptome assembly of Anthopleura dowii Verrill (1869), from Mexico. Genom Data. 11. pp. 92–94.
Basulto, A., et al., 2006. Immunohistochemical targeting of sea anemone cytolysins on tentacles, mesenteric filaments and isolated nematocysts of Stichodactyla helianthus. J. Exp. Zool. Comp. Exp. Biol. 305 (3), 253–258.
Bryant, D.M., et al., 2017. A tissue-mapped axolotl de novo transcriptome enables identification of limb regeneration factors. Cell Rep. 18 (3), 762–776.
Castrillo, I., et al., 2009. 1H, 13C, and 15N NMR assignments of the actinoporin Sticholysin I. Biomol NMR Assign 3 (1), 5–7.
Chomczynski, P., 1993. A reagent for the single-step simultaneous isolation of RNA, DNA and proteins from cell and tissue samples. Biotechniques 15 (3), 532–534 536-7.
de los Rios, V., et al., 2000. Overproduction in Escherichia coli and purification of the hemolytic protein sticholysin II from the sea anemone Stichodactyla helianthus. Protein Expr. Purif. 18 (1), 71–76.
Deng, Y., et al., 2016. Sphingomyelin is sorted at the trans Golgi network into a distinct class of secretory vesicle. Proc. Natl. Acad. Sci. U. S. A. 113 (24), 6677–6682.
Eisenberg, D., et al., 1984. Analysis of membrane and surface protein sequences with the hydrophobic moment plot. J. Mol. Biol. 179 (1), 125–142.
Garb, J.E., Hayashi, C.Y., 2005. Modular evolution of egg case silk genes across orb-weaving spider superfamilies. Proc. Natl. Acad. Sci. U. S. A. 102 (32), 11379–11384.
Garb, J.E., Gonzalez, A., Gillespie, R.G., 2004. The black widow spider genus Latrodectus (Araneae: theridiidae): phylogeny, biogeography, and invasion history. Mol. Phylogenet. Evol. 31 (3), 1127–1142.
Garcia-Linares, S., et al., 2013. Three-dimensional structure of the actinoporin sticholysin I. Influence of long-distance effects on protein function. Arch. Biochem. Biophys. 532 (1), 39–45.
Garcia-Linares, S., et al., 2016a. Differential effect of membrane composition on the pore-forming ability of four different sea anemone actinoporins. Biochemistry 55 (48), 6630–6641.
Garcia-Linares, S., et al., 2016b. Role of the tryptophan residues in the specific interaction of the sea anemone Stichodactyla helianthus's actinoporin sticholysin II with biological membranes. Biochemistry 55 (46), 6406–6420.
Garcia-Linares, S., et al., 2016c. Toxin-induced pore formation is hindered by intermolecular hydrogen bonding in sphingomyelin bilayers. Biochim. Biophys. Acta 1858 (6), 1189–1195.
Garcia-Ortega, L., et al., 2011. The behavior of sea anemone actinoporins at the water-membrane interface. Biochim. Biophys. Acta 1808 (9), 2275–2288.
Grabherr, M.G., et al., 2011. Full-length transcriptome assembly from RNA-Seq data without a reference genome. Nat. Biotechnol. 29 (7), 644–652.
Haas, B.J., et al., 2013. De novo transcript sequence reconstruction from RNA-seq using the Trinity platform for reference generation and analysis. Nat. Protoc. 8 (8), 1494–1512.
Haney, R.A., et al., 2016. Effects of gene duplication, positive selection, and shifts in gene expression on the evolution of the venom gland transcriptome in widow spiders. Genome Biol Evol 8 (1), 228–242.
Huerta, V., et al., 2001. Primary structure of two cytolysin isoforms from Stichodactyla helianthus differing in their hemolytic activity. Toxicon 39 (8), 1253–1256.
Kapp, K.S.S., Lemberg, M.K., Dobberstein, B., 2009. Post-targeting Functions of Signal Peptides., in Protein Transport into the Endoplasmic Reticulum. (Landes Bioscience).
Kelley, L.A., et al., 2015. The Phyre2 web portal for protein modeling, prediction and analysis. Nat. Protoc. 10 (6), 845–858.
Kitchen, S.A., et al., 2015. De novo assembly and characterization of four anthozoan (phylum Cnidaria) transcriptomes. G3 (Bethesda) 5 (11), 2441–2452.
Krueger, F., 2012. Trim Galore! Version 0.4.3. Available from: http://www.bioinformatics.babraham.ac.uk/projects/trim_galore/.
Lanio, M.E., et al., 2001. Purification and characterization of two hemolysins from Stichodactyla helianthus. Toxicon 39 (2–3), 187–194.
Li, B., Dewey, C.N., 2011. RSEM: accurate transcript quantification from RNA-Seq data with or without a reference genome. BMC Bioinf. 12, 323.
Macrander, J., Daly, M., 2016. Evolution of the cytolytic pore-forming proteins (actinoporins) in sea anemones. Toxins 8 (12).
Macrander, J., Brugler, M.R., Daly, M., 2015a. A RNA-seq approach to identify putative toxins from acrorhagi in aggressive and non-aggressive Anthopleura elegantissima polyps. BMC Genom. 16, 221.
Macrander, J., Broe, M., Daly, M., 2015b. Multi-copy venom genes hidden in de novo transcriptome assemblies, a cautionary tale with the snakelocks sea anemone Anemonia sulcata (Pennant, 1977). Toxicon 108, 184–188.
Macrander, J., Broe, M., Daly, M., 2016. Tissue-specific venom composition and differential gene expression in sea anemones. Genome Biol Evol 8 (8), 2358–2375.
Madio, B., Undheim, E.A.B., King, G.F., 2017. Revisiting venom of the sea anemone Stichodactyla haddoni: omics techniques reveal the complete toxin arsenal of a well-studied sea anemone genus. J Proteomics 166, 83–92.

Malovrh, P., et al., 2000. Structure-function studies of tryptophan mutants of equinatoxin II, a sea anemone pore-forming protein. Biochem. J. 223–232 346 Pt 1.
Mancheno, J.M., et al., 2003. Crystal and electron microscopy structures of sticholysin II actinoporin reveal insights into the mechanism of membrane pore formation. Structure 11 (11), 1319–1328.
Maula, T., et al., 2013. 2NH and 3OH are crucial structural requirements in sphingomyelin for sticholysin II binding and pore formation in bilayer membranes. Biochim. Biophys. Acta 1828 (5), 1390–1395.
Monastyrnaya, M., et al., 2010. Actinoporins from the sea anemones, tropical Radianthus macrodactylus and northern Oulactis orientalis: comparative analysis of structure-function relationships. Toxicon 56 (8), 1299–1314.
Nylander, J.A.A., 2004. MrModeltest V2. Program Distributed by the Author. Evolutionary Biology Centre, Uppsala University.
Pungercar, J., et al., 1997. Sequence analysis of the cDNA encoding the precursor of equinatoxin V, a newly discovered hemolysin from the sea anemone Actinia equina. Biochim. Biophys. Acta 1341 (2), 105–107.
Rivera-de-Torre, E., et al., 2016. Synergistic action of actinoporin isoforms from the same sea anemone species assembled into functionally active heteropores. J. Biol. Chem. 291 (27), 14109–14119.
Rivera-de-Torre, E., et al., 2017. One single salt bridge explains the different cytolytic activities shown by actinoporins sticholysin I and II from the venom of Stichodactyla helianthus. Arch. Biochem. Biophys. 636, 79–89.
Rojko, N., et al., 2016. Pore formation by actinoporins, cytolysins from sea anemones. Biochim. Biophys. Acta 1858 (3), 446–456.
Ronquist, F., et al., 2012. MrBayes 3.2: efficient Bayesian phylogenetic inference and model choice across a large model space. Syst. Biol. 61 (3), 539–542.
Ros, U., et al., 2015. Differences in activity of actinoporins are related with the hydrophobicity of their N-terminus. Biochimie 116, 70–78.
Salgado, V.L., Kem, W.R., 1992. Actions of three structurally distinct sea anemone toxins on crustacean and insect sodium channels. Toxicon 30 (11), 1365–1381.
Sievers, F., et al., 2011. Fast, scalable generation of high-quality protein multiple sequence alignments using Clustal Omega. Mol. Syst. Biol. 7, 539.
Simao, F.A., et al., 2015. BUSCO: assessing genome assembly and annotation completeness with single-copy orthologs. Bioinformatics 31 (19), 3210–3212.
Suput, D., 2009. In vivo effects of cnidarian toxins and venoms. Toxicon 54 (8), 1190–1200.
The PyMOL Molecular Graphics System, Version 2.0 Schrödinger, LLC.
Tulin, S., et al., 2013. A quantitative reference transcriptome for Nematostella vectensis early embryonic development: a pipeline for de novo assembly in emerging model systems. EvoDevo 4, 16.
Valle, A., et al., 2015. The multigene families of actinoporins (part I): isoforms and genetic structure. Toxicon 103, 176–187.
Wang, Y., et al., 2008. A multigene family of Heteractis magnificalysins (HMgs). Toxicon 51 (8), 1374–1382.

Article IV *Accepted for publication in Archives of Biochemistry and Biophysics 25th of May 2020*

Structural and functional characterization of StnIII: A newly discovered actinoporin within the venom of the sea anemone *Stichodactyla helianthus*

Esperanza Rivera-de-Torre[1,2,3], Juan Palacios-Ortega[1,2], Jessica E. Garb[3], J. Peter Slotte[2], José G. Gavilanes[1] and Álvaro Martínez-del-Pozo[1,*]

[1]Departamento de Bioquímica y Biología Molecular, Facultad de Ciencias Químicas, Universidad Complutense de Madrid, Madrid, Spain.
[2]Biochemistry, Faculty of Science and Engineering, Åbo Akademi University, Turku, Finland.
[3]Department of Biological Sciences, University of Massachusetts Lowell, Lowell, MA, USA.

**Corresponding autor*

Las actinoporinas son una familia de toxinas formadoras de poros producidas por anémonas marinas como parte de su cóctel venenoso. Estas proteínas permanecen solubles, y plegadas de manera estable en disolución acuosa pero, al interactuar con membranas lipídicas que contienen esfingomielina, se convierten en estructuras oligoméricas integrales de membrana, que forman un poro permeable a cationes. Dicho proceso conduce a la muerte celular por choque osmótico. Estas actinoporinas aparecen como familias multigénicas en el genoma de las anémonas: existen varios genes que codifican actinoporinas muy similares, pero no idénticas, dentro de una misma especie. Se sabe que la anémona del Mar Caribe *Stichodactyla helianthus* produce, al menos, tres actinoporinas muy parecidas (sticholisinas I, II y III; StnI, StnII y StnIII) que difieren en su potencia tóxica. StnI y StnII han sido caracterizadas en gran detalle. Entre sus principales características destaca que StnII es alrededor de cuatro veces más efectiva que StnI frente a eritrocitos de carnero y que pueden interactuar entre sí de forma sinérgica. StnIII, descubierta recientemente al ensamblar *de novo* el transcriptoma de *S. helianthus*, no había sido caracterizada hasta ahora. En este trabajo se detalla su caracterización estructural y funcional y su potencial para interaccionar con las otras dos actinoporinas ya conocidas. StnIII parece mantener el plegamiento común, bien conservado, de todas las actinoporinas, caracterizado por un alto contenido en lámina β, pero es sensiblemente menos termoestable. Su caracterización funcional demuestra que su concentración crítica necesaria para formar poros activos es mayor que en el caso de StnI y StnII, lo que sugiere diferencias en su oligomerización sobre la superficie de las membranas. Además, mezclas de StnII y StnIII revelan la existencia de un efecto sinérgico entre ellas, probablemente al facilitar la unión de StnIII a la membrana. Los resultados obtenidos permiten concluir que StnIII es una nueva pieza en el rompecabezas de la modulación de la actividad del veneno de esta especie de anémona caribeña.

PhD candidate contributions

Esperanza Rivera de Torre conceived, designed and conducted most of the experiments as well as significantly contributed to analyzing and discussing the results, writing and correcting the manuscript, and suggesting modifications.

Abstract

Actinoporins are a family of pore-forming toxins produced by sea anemones as part of their venomous cocktail. These proteins remain soluble and stably folded in aqueous solution, but when interacting with sphingomyelin-containing lipid membranes, they become integral oligomeric membrane structures that form a pore permeable to cations, which leads to cell death by osmotic shock. Actinoporins appear as multigenic families within the genome of sea anemones: several genes encoding very similar, but not identical, actinoporins are detected within the same species. The Caribbean Sea anemone *Stichodactyla helianthus* produces three actinoporins (sticholysins I, II and III; StnI, StnII and StnIII) that differ in their toxic potency. Among their main characteristics, StnII is about four-fold more effective than StnI against sheep erythrocytes in causing hemolysis, and they can interact with each other synergistically. However, StnIII, recently discovered in the *S. helianthus* transcriptome, has not been characterized so far. Here we describe StnIII's spectroscopic and functional properties and show its potential to interact with the other Stns. StnIII seems to maintain the well-preserved fold of all actinoporins, characterized by a high content of β-sheets, but it is significantly less thermostable. Its functional characterization shows that the critical concentration needed to form active pores is higher than for either StnI or StnII, suggesting differences in behavior when oligomerizing on membrane surfaces. Furthermore, mixtures of StnII and StnIII reveal a synergistic effect between them, probably by facilitating the binding of StnIII to the membrane. Our results demonstrate that StnIII is an interesting and unexpected piece in the puzzle of how this Caribbean Sea anemone species modulates its poisonous activity.

Introduction

Protein components of venoms often appear as multigene families: a single animal species usually expresses several isotoxins as products of different genes. Such isotoxins are usually highly similar but display distinct activities derived from sequence differences among them (García-Linares 2016c, Leychenko 2018, Monastyrnaya 2010, Rivera-de-Torre 2017, Wang 2008). This is also the case of actinoporins, highly representative protein toxins from the venom of sea anemones. Actinoporins are cytolysins which belong to the α-pore-forming-proteins (α-PFPs) family (Anderluh and Lakey 2008, Parker and Feil 2005). All actinoporins whose three-dimensional structure has been solved share a common fold pattern (Athanasiadis 2001, García-Linares 2013, Hinds 2002, Mancheño 2003, Mechaly 2011, Tanaka 2015). It consists of a compact hydrophobic β-sandwich core flanked by two α-helices (Figure 1A). Within this structural arrangement, it is also well-known that their N-terminal α-helix plays a key role in their pore-forming activity (Castrillo 2010, Palacios-Ortega 2017, Rivera-de-Torre 2017, Rojko 2013, Ros 2015), since this protein stretch detaches from the β-sandwich core and extends to become a rather long α-helix, which is responsible for penetrating the membrane and forming the pore walls (Alegre-Cebollada 2008, Alegre-Cebollada 2007b, Hong 2002, Kristan 2004, Malovrh 2003). These toxins remain stably folded, monomeric and perfectly soluble in water solution, but upon interaction with cell membranes of specific composition, they become oligomeric transmembrane structures (Anderluh and Maček 2002, García-Linares 2017, García-Ortega 2011), forming pores that lead to the death of the targeted cell by osmotic shock(Alegre-Cebollada 2007c, García-Linares 2017, García-Ortega 2011). In particular, the pore-formation

triggering condition for actinoporins is the presence of sphingomyelin (SM) within the target cell membrane.

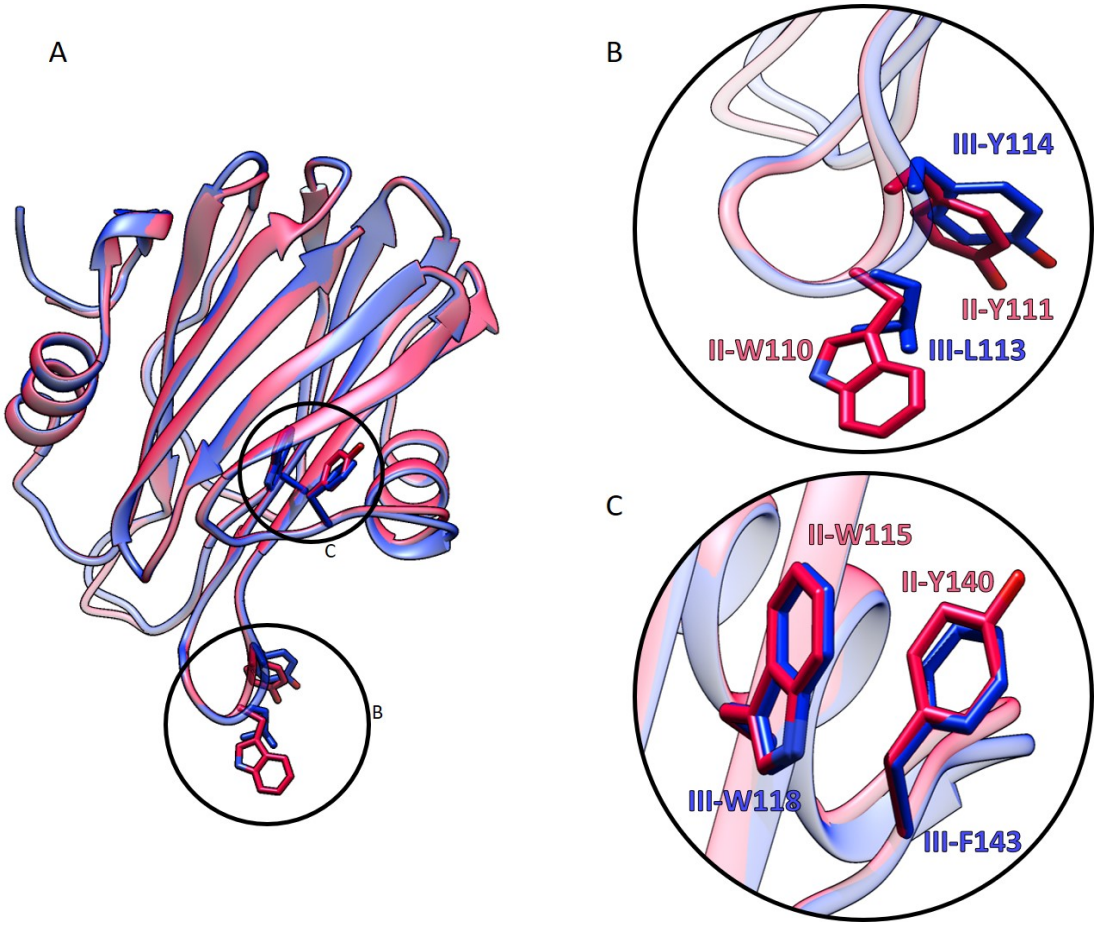

Figure 1. (A) StnII (pink, PDB: 1GWY) and StnIII (blue, predicted structure with Phyre2(Kelley 2015)) aligned three-dimensional structures. Circles indicate the close-up views. (B) Close-up showing the relative positions of StnII W110 and Y111 (pink), StnIII L113 and Y114 (blue). (C) Close-up of the three-dimensional structure showing the relative positions of StnII Y140 and W115 (pink), StnIII F143 and W118 (blue).

It is well known that the Caribbean sea anemone *Stichodactyla helianthus* produces two easily detectable actinoporin variants: sticholysin I (StnI) and sticholysin II (StnII) (García-Linares 2016c, Lanio 2001). Both have been very well characterized, and their three-dimensional structures are known with atomic resolution. They show an almost identical conformation, in good agreement with their 93% sequence identity at the amino acid level (Figure 2) (García-Linares 2013, Mancheño 2003) and the aforementioned actinoporins common fold (Athanasiadis 2001, García-Linares 2013, Hinds 2002, Mancheño 2003, Tanaka 2015). The StnI isotoxin is approximately four-fold less effective than StnII in terms of hemolytic activity (García-Linares 2016c, Rivera-de-Torre 2017). Interestingly, both actinoporins interact with each other to exert a synergistic effect. Trace amounts of StnII enhance StnI binding affinity to cell membranes, driving a dramatic improvement of hemolytic activity (Rivera-de-Torre 2016). This StnI-StnII interacting behavior seems to be the basis for expanding the complexity and regulatory capacity of these toxins' action, potentially increasing the range of species *S. helianthus* can capture or defend itself from.

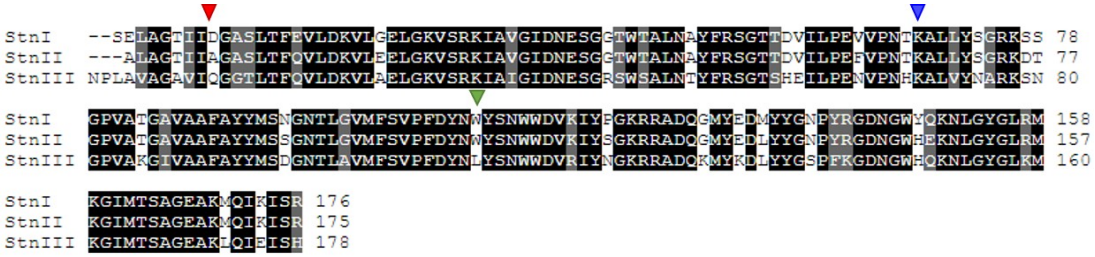

Figure 2. Sequence alignment of the three Stns produced by S. helianthus. Black background indicates conservation of the same amino acid while grey is for conservative substitutions. Red arrowhead indicates StnI D9 (A8 and Q11 in StnII and StnIII respectively). Blue arrowhead indicates conserved K in StnI, II and III occupying positions 68, 67 and 70 respectively. Green arrowhead indicated non-conserved substitution in StnIII (L113) in comparison with StnI (W111) and StnII (W110).

Transcriptomic profiling of *S. helianthus* was performed as an effective approach for discovering new toxins produced by this sea anemone (Rivera-de-Torre 2018). After this analysis was made, at least one more actinoporin isoform was discovered, which was designated as sticholysin III (StnIII). Phylogenetic analysis revealed that this StnIII is more closely related to other species' actinoporins rather than to the other Stn isotoxins produced by *S. helianthus* (Rivera-de-Torre 2018), an interesting feature from the evolutionary point of view. In fact, at the protein level, StnIII is only 76% identical to StnI and 77% to StnII (Figure 2), while StnI and StnII are 93% identical. This sequence conservation was still similar enough to allow the prediction of StnIII's three-dimensional structure, which resulted in a conformation perfectly compatible with the actinoporins' standard fold (García-Linares 2013, Mancheño 2003). However, even if StnII's three-dimensional structure resembles that of StnI and StnII, amino acid sequence comparison showed significant differences, which might also lead to functional differences, especially at their N-terminal stretches (Figure 2). This greater divergence of StnIII relative to both Stn I and II reinforces the need to functionally evaluate its role in *S. helianthus* venom, given its potential to modulate the toxicity of the other Stns known to cooperate in a synergistic fashion. To this end, we have produced StnIII in *Escherichia coli*, and then purified and characterized it at spectroscopic and functional levels. The results obtained reveal different characteristics when compared to previously known Stns, allowing to us to hypothesize a potential role for StnIII within the venomous arsenal of *S. helianthus*.

Materials and methods

StnIII cloning for production in *E. coli*

The complete cDNA sequence coding for StnIII, signal peptide included, had been previously determined and deposited in NCBI's GenBank database (MH327769) (Rivera-de-Torre 2018). Thus, in order to amplify and clone the mature form of StnIII (without its signal peptide) (Figure 2), two deoxyoligonucleotides were designed: 5'ACA*GAATTC*ATTAAAGAGGAGAAATTAACC**ATG**AATCCTTTAGC3' and 5'ATT*AAGCTT***TTA**GTGAGAGATCTCAATTTGCAG3'. Restriction sites for EcoRI (GAATTC) and HindIII (AAGCTT) (as italic letters in the sequences), and the corresponding initial (ATG) and stop (TAA) codons (bold letters) were included in these oligonucleotides. The amplified PCR product was digested with both restriction enzymes and cloned within a modified version of the pQE60

plasmid, which constitutes the gold standard approach used by our group to produce Stns in *E. coli* in milligram amounts (Alegre-Cebollada 2007a, De los Ríos 2000).

Protein production and purification

The procedure used for the production and purification of the three actinoporins used in this study (StnI, II, and III) has been previously described in detail (Alegre-Cebollada 2007a, De los Ríos 2000, Rivera-de-Torre 2018, Rivera-de-Torre 2017). Protein production in RB791 *E. coli* cells is induced at OD_{600} of 1.0 with 1 mM IPTG for 4 h at 37 °C. Then, cells are harvested, and the cellular pellet is subjected to seven pulses of sonication (20 kc, 1 min) in an ice bath. HCl-Tris buffer (50 mM) including 1 % (v/v) Tween 20 is employed; buffer pH values (6.5 for StnI, 7.5 for StnII, and 8.5 for StnIII) were set depending on the theoretical pI value of each actinoporin. The water-soluble fraction of this homogenate is loaded onto a column filled with carboxymethylcellulose CM52 (Whatman, Brentford, England, UK) and eluted with a NaCl gradient (0-0.3 M NaCl StnI, 0-0.5 M NaCl for StnII or 0-0.6M NaCl for StnIII) in 50 mM HCl-Tris buffer, after appropriate washing steps.

Homogeneity of protein preparations and structural spectroscopic characterization

All protein samples were purified to homogeneity in mg amounts according to their electrophoretic behavior analyzed by 0.1 % (w/v) SDS−15 % (w/v) PAGE performed under standard conditions (Laemli 1970). Western blots were performed according to standardized procedures described before(Martínez-Ruiz 2000, Rivera-de-Torre 2016), using a rabbit polyclonal antibody raised against purified StnI. Acid hydrolysis of the proteins (5.7 M HCl for 24 h at 110 °C) followed by the corresponding amino acid analyses made on a Biochrom 20 automatic analyzer (Pharmacia, Pfizer, New York, NY) confirmed the homogeneity of all protein samples used. These results were also used to calculate extinction coefficients for each actinoporin variant (Table 1), which were then used to measure protein concentrations in all

experiments described below. All the protein batches used were also characterized by recording their far- and near-UV circular dichroism (CD) spectra on a Jasco 715 spectropolarimeter (Easton, MD) and their fluorescence emission spectra on an SLM Aminco

Table 1. Calculated extinction coefficients ($E^{0.1\%}$), content of Trp and Tyr residues, relative Trp and Tyr emission yields, and melting temperature (T_m), HC_{50}, and Relative Hemolytic Activity (RHA) values of the three sticholysin natural variants used in this study.

	$E^{0.1\%}$ (280 nm, 1 cm)	Number of Trp	Number of Tyr	Relative Trp emission yield[a]	Relative Tyr emission yield[a]	T_m (°C)	HC_{50} (nM)	RHA[b]
StnI	2.55[c]	5	13	1.00	1.00	65.0 ± 0.1[c]	3.0[c]	1.00
StnII	2.54[c]	5	12	1.22	2.11	67.0 ± 0.1[c]	0.4[c]	7.50
StnIII	2.55	4	11	0.96	9.14	50.0 ± 0.2	12.0	0.25

[a]Calculated as the area corresponding to the Trp or Tyr emission spectra of each protein (Figure 6) referred to the StnI emission(García-Linares 2016a, García-Linares 2016c)
[b]Calculated as HC_{50}(StnI)/HC_{50}(StnII or StnIII) (Alegre-Cebollada 2008)
[c]Calculated in (Alegre-Cebollada 2008, García-Linares 2016c)

model 8000 spectrofluorometer (Urbana, IL), also as previously described (De Antonio 2000, García-Linares 2013, García-Linares 2016a, García-Linares 2014, García-Linares 2016c, Pardo-Cea 2011). Near and far-UV CD spectra were recorded at 1.0 and 0.2 mg/mL, respectively, in 0.1 M NaCl and 15 mM Mops (pH 7.5). An identical buffer was used for the fluorescence emission spectra with the proteins at concentrations of 0.1 mg/mL. Thermal denaturation was also evaluated as described before (Alegre-Cebollada 2007a, Alegre-Cebollada 2008, Alegre-Cebollada 2007c). At neutral pH, thermal denaturation of Stns occurs simultaneously with a fast aggregation, which can be monitored as optical path clarification (aggregates settling) by CD measurements at 220 nm. Temperature scans were carried out at a rate of 0.5 °C/min. Results are expressed as percentages of the total CD variation versus temperature. T_m corresponds to the temperature at the midpoint of the monophasic transition observed.

Storage stability study

StnIII storage stability was tested by dissolving lyophilized StnIII in 50 mM HCl-Tris pH 7.4, 145 mM NaCl and storing aliquots at 4 °C, -20 °C and -80 °C. Aliquots were analyzed at 24 h, 72 h and 1 week upon storage and analyzed through 0.1% (w/v) SDS−15% (w/v) PAGE.

Hemolysis assays

Hemolysis assays were performed in 96-multiwell plates as previously described (Alegre-Cebollada 2007a, Alegre-Cebollada 2008, García-Linares 2016a, García-Linares 2016c, Rivera-de-Torre 2016, Rivera-de-Torre 2017). Briefly, erythrocytes from heparinized sheep blood were washed in 10 mM HCl-Tris buffer (pH 7.4) containing 0.145 M NaCl, to a final OD_{655} of 0.7 when mixing equal volumes of the cell suspension and buffer. Hemolysis was followed by recording the decrease in OD_{655} after addition of the erythrocyte suspension to different final concentrations of protein. An iMark™ Microplate Absorbance Reader (Bio-Rad, California, USA) was employed to measure OD_{655}.The value obtained with 0.1% (w/v) Na_2CO_3 was considered as 100% hemolysis. HC_{50} values were calculated as the concentration needed to get 50% of hemolysis after 10 minutes of protein addition.

Lipid vesicles preparation

Large unilamelar vesicles (LUVs) of DOPC:SM:Chol (1:1:1) represent one of the standard membrane models most frequently used to characterize actinoporins pore formation behavior (Alegre-Cebollada 2008, Alegre-Cebollada 2004, Alegre-Cebollada 2006, Alm 2015b, De los Ríos 1998, García-Linares 2015, García-Linares 2013, García-Linares 2016a, García-Linares 2016b, García-Linares 2014, García-Linares 2016c, García-Linares 2017, Palacios-Ortega 2016, Palacios-Ortega 2017, 2019, Rivera-de-Torre 2016, Rivera-de-Torre 2017). They were also prepared as described previously (Alm 2015a, García-Linares 2013, Martínez-Ruiz 2001). Briefly, a phospholipid (0.1–1.0 mg) solution in 2:1 (v:v) chloroform:methanol was dried under a flow of nitrogen, and the dry film obtained was used to prepare a lipid dispersion by adding 0.5–2.0 mL of HCl-Tris-NaCl buffer (the specific composition depends on the assay developed and is detailed below), briefly vortex mixing, and incubating for 1 h at 37 °C. This suspension of multilamellar vesicles was further subjected to twelve cycles of extrusion at 37 °C through polycarbonate filters (100-nm pore size) (Nucleopore, Whatman) to obtain a homogeneous population of unilamelar vesicles. Aliquots (between 10 and 25 µL) of freshly prepared LUVs were stored to

determine the concentration of phospholipids present in the mixture by means of phosphorus quantitation(Bartlett 1959).

Calcein leakage assay

Calcein-containing LUVs were also prepared by extrusion through 100 nm filters (Nucleopore, Whatman) at 37 °C(García-Linares 2016b), essentially as described above but, prior to extrusion, the dry lipid films were hydrated for 1 h at 37 °C in HCl-Tris buffer (10 mM HCl-Tris, 140 mM NaCl, 1 mM EDTA, pH 7.4), containing 100 mM calcein. After hydration, and still before extrusion, the mixture was subjected to 10 freeze/thaw cycles in liquid nitrogen in order to improve calcein encapsulation. LUVs were then extruded, and subsequently separated from non-entrapped calcein by size exclusion chromatography on Sephacryl S200HR column. LUVs were always used for permeabilization studies within the first 24 h after preparation, using 96-multiwell plates and optimized standard protocols(Alegre-Cebollada 2007a, Alegre-Cebollada 2008, Alegre-Cebollada 2004, De los Ríos 1998, Rivera-de-Torre 2016). Emission at 520 nm was followed at 25 °C as a function of time (excitation at 485 nm). Fluorescence emission was measured on a FLUOstar OPTIMA microplate reader (BMG-Labtech, Ortenberg, Germany). Two-fold serial dilutions of the proteins were displayed in 96-multiwell plates and after addition of the same volume of calcein-entrapped LUVs (final concentration on the assay was 7.5 μM). Calcein leakage was automatically recorded every 3 s for 250 cycles (total time 12.5 min). One second of shaking was programmed before first measure to ensure the homogeneity within every well. The released fraction of calcein was determined based on the maximal calcein release, which was induced by LUV disintegration in 0.05 % (v/v) Triton X-100 (100% leakage). To ensure that no spontaneous leakage occurred, a 0% leakage control containing buffer and calcein-loaded vesicles was measured through the complete time of the assay. A steady signal level, indicating intact vesicles, was observed for all samples.

Isothermal titration calorimetry

The interaction between actinoporins and LUVs was also quantitated by isothermal titration calorimetry (ITC), as previously described (Alegre-Cebollada 2008, García-Linares 2014, Maula 2013, Rivera-de-Torre 2017), using a VP-ITC calorimeter (Malvern MicroCal Worcestershire, U.K.). Briefly, 0.5–10.0 μM protein solutions were titrated by injection of 20 μL aliquots of lipid suspensions (phospholipid concentration of 0.25–1.0 mM) at a constant temperature of 25 °C. The buffer employed consisted of 10 mM Tris pH 7.4, 100 mM NaCl, and 1 mM EDTA. Binding isotherms were adjusted to a model in which the protein binds to the membrane involving “n” lipid molecules (Alegre-Cebollada 2008).

Results

StnIII purification and sequence differences identification

StnIII was produced in *E. coli* RB791 and purified to homogeneity according to the 0.1% SDS - 15% PAGE analysis of the samples (Figure 3A). Yield of the different purifications was always around 5.0 mg/per liter of original culture broth employed. The amino acid analysis revealed a composition which was consistent with the values expected from the cDNA sequence

cloned. This analysis, altogether with the corresponding UV absorption spectrum was also used to calculate an $E^{01\%}$ (280 nm, 1 cm) value of 2.55 (Table 1).

Western blot detection of the purified three *S. helianthus* actinoporins (StnI, II, and III) revealed low immune cross-reactivity of StnIII when assayed against a rabbit polyclonal antibody preparation raised against purified StnI (Figure 3B). On the other hand, and as it was already known (Rivera-de-Torre 2016), StnI and StnII were almost indistinguishable by this analysis, in good agreement with their much higher degree of amino acid sequence identity. As stated above, StnI and StnII are 93% identical while they only share 76% and 77% sequence identity with StnIII, respectively.

Inspection of Stn I-III's amino acid sequences confirmed that their sequence differences are concentrated along their N-terminal stretches. Also, the N-terminal end of StnIII is 2 and 3 residues longer than the corresponding region in StnI and StnII, respectively (Figure 2) (Rivera-de-Torre 2018). Another remarkable difference is the presence of a Pro residue at the second position of the StnIII sequence (Figure 2), an amino acid rather incompatible with the formation of an α-helix. These observations should be considered given that previous work shows the N-terminal region of StnII is optimized for spanning a membrane whose bilayer thickness would correspond to vesicles mostly made of di-18:1-PC (DOPC) (Palacios-Ortega 2017). StnIII's longer N-terminal stretch suggests the possibility of different membrane thickness preference for pore formation, thicker in comparison with the optimum value required for StnI and StnII(Palacios-Ortega 2017).

It has been also shown that an exposed salt bridge between StnI Asp9 and Lys68 explains StnII's higher activity (Rivera-de-Torre 2017). This difference was attributed to the presence of Ala at the corresponding StnII position, a residue with a non-charged and rather hydrophobic sidechain. Interestingly, the corresponding StnIII amino acid is Gln (Figure 2). Gln is also a non-charged residue but still displaying enough negative charge density to be able to interact with the corresponding conserved Lys (Figure 2).

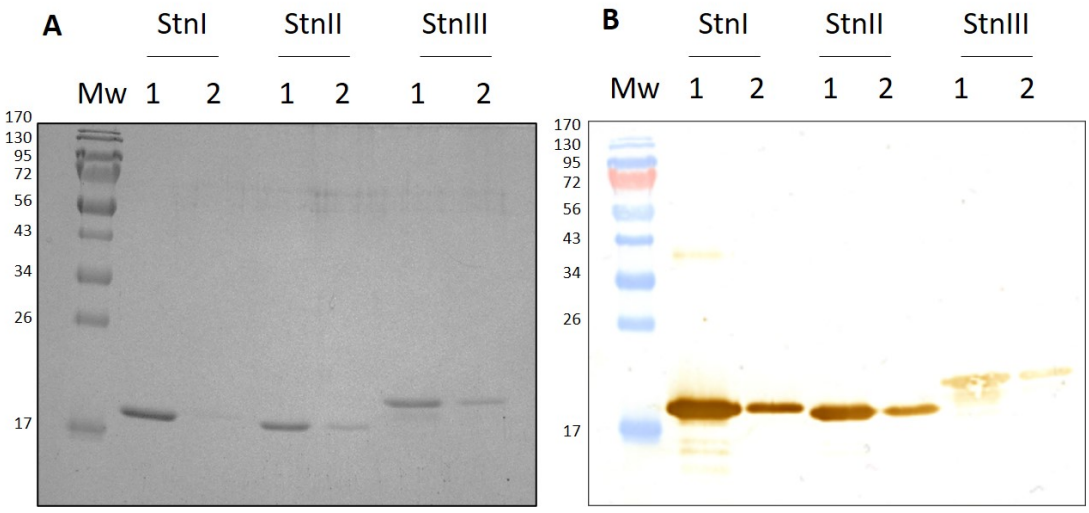

Figure 3. Electrophoretic and western blot analysis of the purified proteins. (Mw) Molecular weight standard (EZ-RUNTM pre-stained Rec Protein Ladder – Fisher Scientific) were also loaded, and the corresponding molecular masses are indicated in kDa at the left margin. (1) 0.5 µg and (2) 0.1 µg of StnI, StnII or StnIII, as indicated. (A) 0.1% SDS - 15% PAGE analysis of the three purified sticholysin natural variants. (B) Western Blot using a rabbit polyclonal serum raised against StnI.

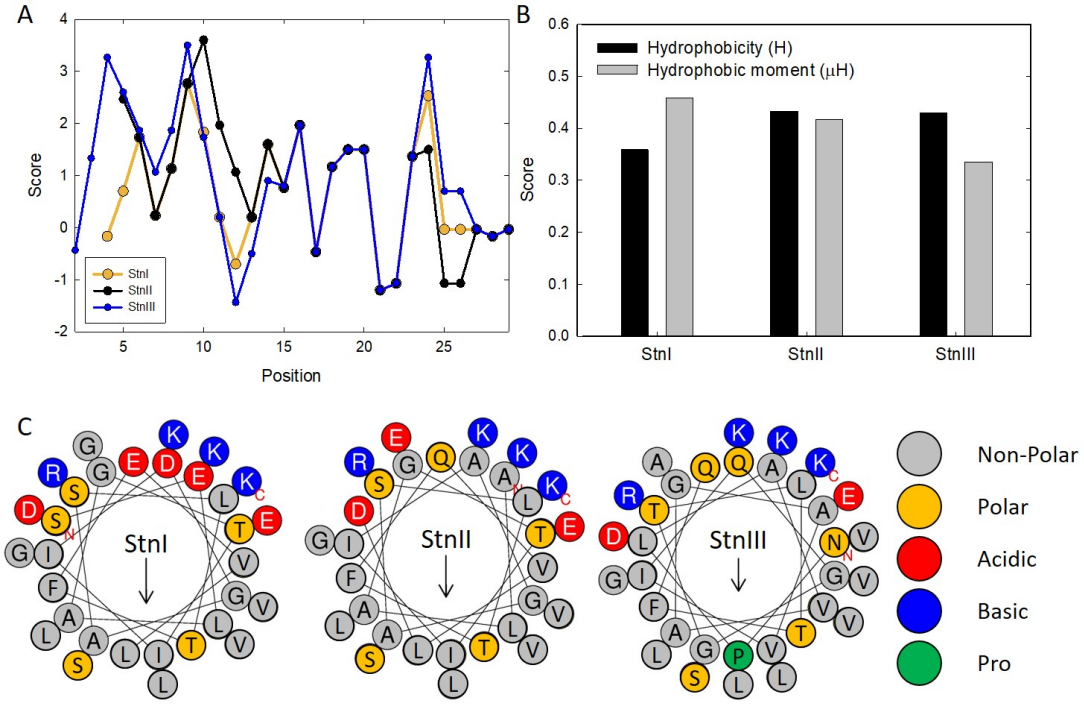

Figure 4. Hydrophobicity profile of sticholysin's N-terminal end(Kyte and Doolittle 1982) (A), calculated hydrophobicity (H)(Eisenberg 1984b) and hydrophobic moment (μH)(Eisenberg 1984b) (B) of the first 31, 30 and 33 residues of StnI, II and III respectively. The window size employed in (A) was 3 amino acids and the graph was made through simulation at Expasy ProScale web server tool (http://web.expasy.org/protscale/). (C) Helical wheel representation of the first 31, 30 and 33 N-terminal amino acid residues of StnI, II and III respectively. The arrow module indicates the hydrophobic moment and the direction marks the most hydrophobic face of the α-helix. N-termini and C-termini are indicated in red. Analysis were performed using the web server HELIQUEST(Gautier 2008).

Finally, and within this same N-terminal stretch the hydrophobicity of this region and its hydrophobic moment was *in silico* calculated based on sequence. The hydrophobicity profile calculated for the N-terminal domain of the three known Stns was highly similar (Figure 4A) and followed the same tendency even considering the amino acid variation among them. The hydrophobicity value measures the amphiphilicity of the region and hence its tendency to seek a surface between hydrophobic and hydrophilic phases. It was noticed that the hydrophobicity score of StnIII N-terminal 30 first residues (Kyte and Doolittle 1982), a critical feature for actinoporins' cytolytic properties (Rivera-de-Torre 2017), was very similar to the value obtained for StnII (Rivera-de-Torre 2017), therefore higher than the value calculated for StnI (Figure 4B). However, the hydrophobic moment, a magnitude that measures the affinity for the membrane core (Eisenberg 1984a), was lower than both values calculated for StnI and StnII (Rivera-de-Torre 2018, Rivera-de-Torre 2017, Ros 2012, Ros 2015) (Figure 4B), suggesting a lower tendency of this StnIII stretch to cross the membrane. Altogether, all these differences can have profound significance in explaining StnIII activity given the key role played by the stretch comprising the first 30 actinoporins' residues in penetrating the membrane to make a functional pore (Casallanovo 2006, Casallanovo 2004, Castrillo 2010, Cilli 2007, Rivera-de-Torre 2017, Rojko 2013, Ros 2012, Ros 2015).

All the other residues comprising important domains for the actinoporins function (García-Ortega 2011). are basically conserved or substituted by residues with similar

physicochemical properties (Figure 2) (García-Linares 2016a). The only exception would be Leu113 in StnIII, corresponding to W111 in StnI and W110 in StnII, which stands out because it belongs to the so-called cluster of aromatic residues, responsible for driving membrane binding and involved in maintaining the required hydrophobicity to achieve that goal. According to this observation, in actinoporins where there is not a Trp in this position, there is always Phe or Leu(García-Linares 2017), as it is also the case with StnIII.

Spectroscopic characterization

Far-UV CD characterization revealed that the three Stns display very similar spectra (Figure 5A), fully compatible with the canonical actinoporins structural fold (Athanasiadis 2001, García-Linares 2013, Hinds 2002, Mancheño 2003, Tanaka 2015), rich in β-sheet content. Differences in the near-UV spectra (Figure 5B) are easily explained by their different aromatic amino acid content (Table 1) and are also in agreement with the adoption of very similar conformational folds. Almost identical conclusions were reached after obtaining the fluorescence emission spectra (Figure 6), being a noticeable difference that the Trp quantum yields are almost identical between StnI and StnIII, despite their different Trp content (Table 1).

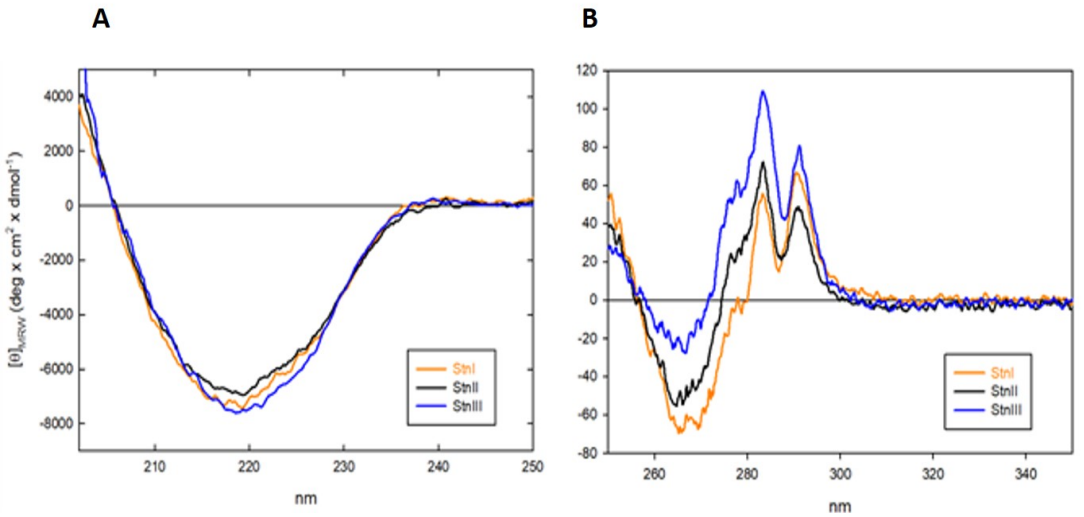

Figure 5. Circular dichroism spectra of the three Stns produced by S. helianthus. (A) Far- and (B) near-UV spectra of StnI (orange line), StnII (black line), and StnIII (blue line).

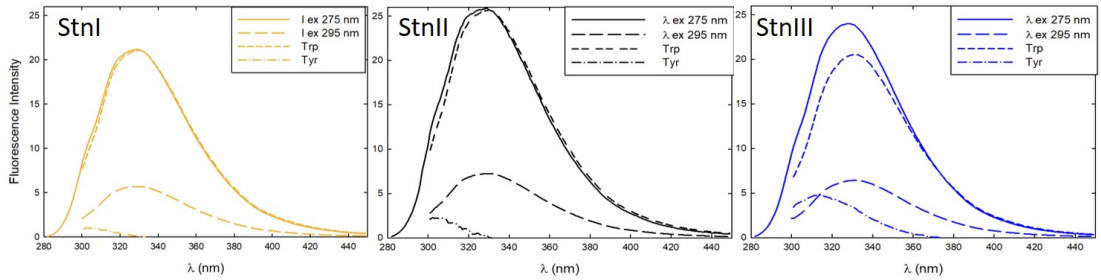

Figure 6. Fluorescence emission spectra of the three Stns produced by *S. helianthus*. StnI (orange), StnII (black), and StnIII (blue). All spectra were recorded at identical protein concentrations of 0.1 mg/mL. Experimental spectra resulted from excitation at 275 nm (solid lines) and 295 nm (long dashed lines). These spectra obtained upon excitation at 295 nm were normalized at wavelengths above 380 nm to obtain the Trp contributions (short dashed bold lines). Tyr contributions (dashed-dot-dashed bold lines) were calculated by subtracting the spectra that represent the Trp contribution from those obtained upon excitation at 275 nm. Fluorescence emission units are arbitrary.

The most remarkable difference between both StnI and II with StnIII is, however, its much higher Tyr emission quantum yield (Table 1 and Figure 6).

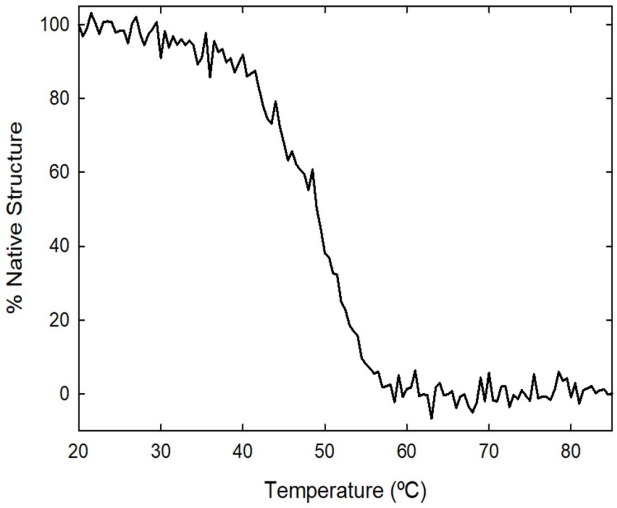

Figure 7. Thermal denaturation profile of StnIII. Measurements were performed by continuously recording the mean residue weight ellipticity at 220 nm (θMRW). These ellipticity values were used to calculate the percentage of native protein at each temperature.

Thermal unfolding analysis (Figure 7) revealed that StnIII was much less thermostable than the other two isotoxins, with a T_m value of 50°C. This value is 15 and 17 °C lower than those obtained for StnI and StnII (Table 1), respectively. Despite this lower thermostability of StnIII, the lyophilized protein remained intact and fully stable for months if stored at -20°C. However, if the protein was maintained in solution, some minor proteolysis was observed. Thus, StnIII aliquots were kept at 4, -20, or -80˚C for 1, 3, or 7 days and then were subjected to 0.1% (w/v) SDS−15% (w/v) PAGE analysis (Figure 8). The results obtained showed a similar behavior for the three different temperatures assayed. StnIII remained intact for at least 72 h and only some degradation was noticed in the samples stored for one week (Figure 8). Therefore, for the functional experiments herein described StnIII was always dissolved in previously autoclaved buffers and only used after storage at 4°C for no more than three days. On the other hand, StnI and II appear fully intact even after one week at room temperature in good agreement with their reported higher thermostability (Table 1).

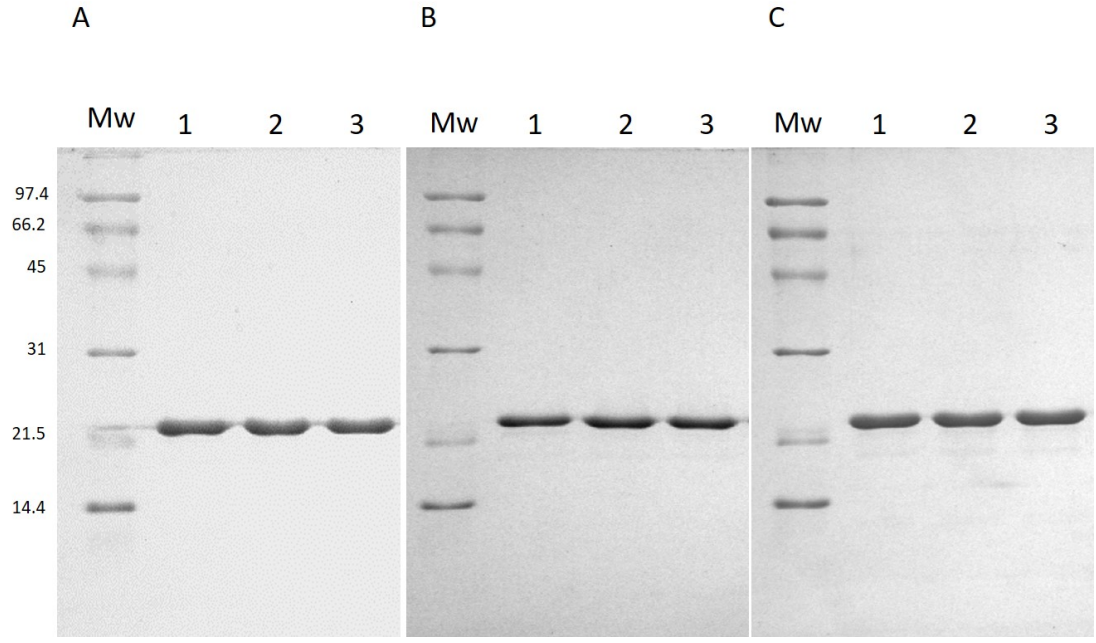

Figure 8. Stability study of StnIII. SDS-PAGE analysis of actinoporin solution preparations maintained at 4 ˚C(1), -20 ˚C (2), and -80 ˚C (3) for 24 h (A), 72 h (B), or 1 week (C). (Mw) Molecular weight standard (Low-Range SDS-PAGE Standards - Biorad) were also loaded, and the corresponding molecular masses are indicated in kDa at the left margin.

StnIII functional characterization

Functional characterization of StnIII by hemolysis showed an increased HC_{50} value in comparison with StnI and StnII (Table 1) and, consequently, much less relative hemolytic activity (Table 1). Interestingly, maximum initial rates of hemolysis showed that StnIII was completely inactive at concentration values below 10 nM (Figure 9), but upon reaching the critical value of 20 nM, StnIII was significantly faster than StnI at comparable concentrations (Figure 9). This stronger concentration dependence is probably related to the oligomerization step of the pore formation mechanism. Equivalent results were observed when calcein release from DOPC:SM:Chol (1:1:1) vesicles was evaluated (Figure 10). Both the effects of StnI and StnIII were negligible below 10 nM but, once reaching that critical concentration value, the maximal rate of calcein release was increased for both proteins, but this increment was sharper for StnIII (Figure 10).

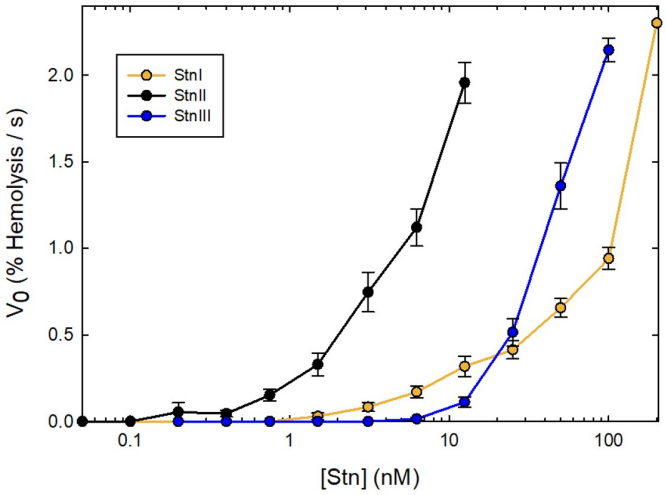

Figure 9. Hemolytic activity of StnI (orange), StnII (black) and StnIII (blue) expressed as the maximum initial hemolytic rate (% hemolysis/s) as a function of different Stn concentrations ranging from 0.1 nM to 100 nM. Values are average of n = 3 ± SEM.

Membrane binding affinity of StnIII to these model membranes was calculated by ITC (Figure 11). The thermodynamic parameters obtained after analysis of the thermograms are summarized in Table 2. StnIII membrane binding affinity for the DOPC:SM:Chol (1:1:1) model vesicles was only marginally smaller than for StnI, as revealed by their RMB values (Table 2), but almost seven-fold lower when compared to StnII (Table 2). Another significant difference was the smaller number of lipid molecules affected by StnIII binding when compared to the values obtained for the other two Stns (Table 2). This fact, in combination with the lower membrane binding affinity, could be related to the necessity of a higher StnIII concentration for erythrocytes or model vesicle

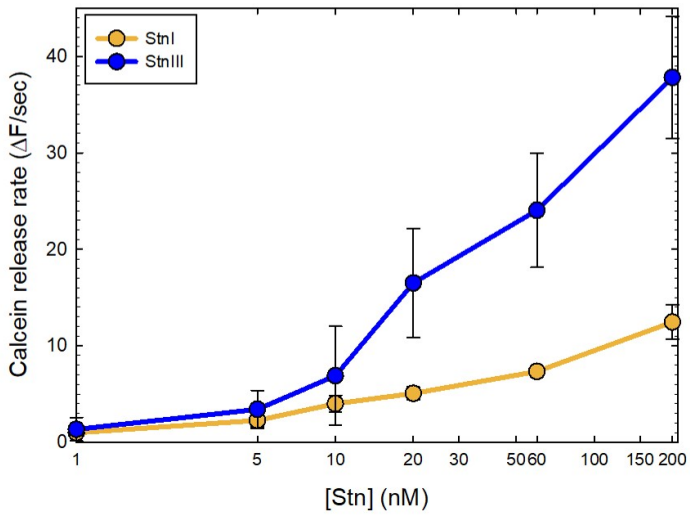

Figure 10. Maximum initial rates of calcein release from DOPS:SM:Chol (1:1:1) vesicles, showed as normalized fluorescence intensity increment/s, as a function of different concentrations of StnI (orange) and StnIII (blue). Values are average of n = 3 ± SEM.

disruption and suggests a different mechanism of action. All these results would agree with those from the hemolysis and calcein leakage experiments.

Finally, the potential synergistic effect in Stns mixtures containing StnIII was studied by hemolysis. Thus, StnII and StnIII were mixed in a 20:80 proportion and assayed as previously described (Rivera-de-Torre 2016). The total protein concentration range assayed was 1-10 nM, where both actinoporins show the highest hemolysis activity differences (Figure 9). As can be clearly observed in Figure 12A, actinoporins StnII and StnIII displayed a synergic hemolytic behavior, as had been previously described for mixtures composed by StnI and StnII(Rivera-de-Torre 2016). On the other hand, when StnI and StnIII were mixed in an 80:20 ratio and, following an identical approach, and assayed within the 5-40 nM concentration range to ensure both actinoporins were active and showing activity differences (Figure 9), synergy was not detected within the experimental error of the assays performed (Figure 12B).

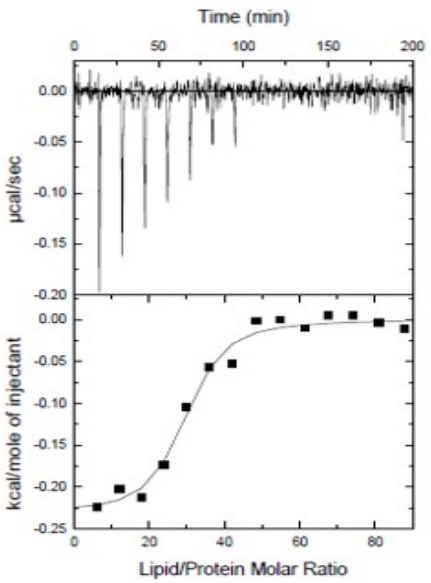

Figure 11. Binding of StnIII to DOPC:SM:Chol (1:1:1) vesicles studied by ITC. Reactant concentrations were 5 µM of StnIII and 3 mM of lipids. Binding isotherms were adjusted to a model in which protein membrane binding involves the participation of "n" lipid molecules as described (Alegre-Cebollada 2008). The c values ($c = K_a \times P_0$) for the graphs shown is within the range 1–1000.

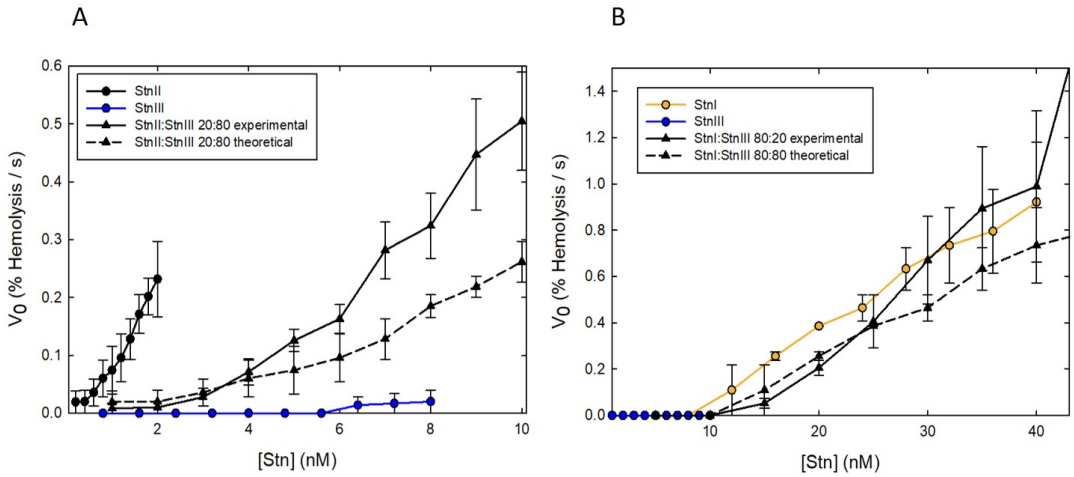

Figure 12. Synergic effect on hemolysis. Maximum hemolytic rate values (expressed as percentage of hemolysis per second) are represented versus the logarithm of total protein concentration. (A) StnII (black dots-solid line), StnIII (blue dots-solid line), the StnII:StnIII (20:80) mixture (black triangles-solid line). (B) Same as in (A), but now the proteins employed were StnI (orange dots-solid line), StnIII (blue dots-solid line), and StnI:StnIII (80:20) mixtures (black triangles-solid line). The black triangles-dashed lines were obtained as the arithmetical addition of the rates obtained with the individual proteins for the real concentration of each one in the different mixtures employed. Each of these experiments was made in triplicate. Values are average of n = 3 ± SEM.

Table 2. Binding to DOPC:SM:Chol (1:1:1) vesicles by StnI, II and III studied by ITC. All results shown are the average of at least three independent experiments.

	n	K_b (x10^{-6} M^{-1})	ΔG (kcal/mol)	ΔH (kcal/mol)	ΔS (cal mol^{-1} K^{-1})	RMB[a]
StnI[b]	49 ± 4	0.41 ± 0.03	-8.21 ± 0.03	-20.9 ± 2.1	-42.84 ± 6.78	1.00
StnII[b]	39 ± 4	1.70 ± 0.90	-9.10 ± 0.50	-44.0 ± 3.0	-115.00 ± 9.00	5.21
StnIII	26 ± 1	0.17 ± 0.40	-7.41 ± 0.22	-7.85 ± 0.31	-4.59 ± 1.78	0.78

[a]Relative membrane binding values calculated according to [n(StnI) × K_b(other actinoporin)]/[n(other actinoporin) × K_b(StnI)] as explained in(Alegre-Cebollada 2008).
[b]As reported before (Alegre-Cebollada 2008, Rivera-de-Torre 2016)

Discussion

Considering their synergistic interaction(Rivera-de-Torre 2016) and the multigenic character of the sticholysin's family (Leychenko 2018, Macrander and Daly 2016, Wang 2008), it was hypothesized that small amounts of other actinoporins, not yet detected, might also be produced to further expand whole venom versatility. Transcriptomic profiling of *S. helianthus* was performed as an effective approach for discovering new toxins produced by this sea anemone (Rivera-de-Torre 2018). After this transcriptome analysis was completed, it was concluded that *S. helianthus* produces at least one more actinoporin isoform, which was designated as StnIII. The phylogenetic analysis revealed that it was more closely related to other species' actinoporins rather than to the other well-studied isotoxins produced by *S. helianthus*. In fact, at the protein level StnIII is only 76% identical to StnI and 77% to StnII (Figure 1). A lower sequence conservation that was fully compatible with the small cross-reactivity observed in Western blot experiments. StnIII was, however, still detectable by polyclonal sera raised against StnI (Figure 3B), confirming that the three actinoporins share common epitopes. In fact, this lower sequence conservation was still high enough to allow a faithful prediction of StnIII's three-dimensional structure which resulted in a conformation perfectly compatible with the very well-known actinoporins' standard fold (García-Linares 2013, Mancheño 2003) and their far-UV CD spectra (Figure 5). Nevertheless, amino acid sequence comparison among the three proteins showed significant differences, especially at their N-terminal stretch.

StnIII N-terminal sequence is 2 and 3 residues longer than the corresponding region in StnI and StnII, respectively, and a particularly interesting detail is that the second residue of this region is a Pro, an imino acid that, although participating in extended protein segments, would not easily incorporate into a full α-helical structure when spanning the hydrophobic core of the membrane in order to constitute a pore (Figure 2). In addition, the hydrophobicity of this sequence stretch was also lower, suggesting a minor tendency to cross the membrane (Palacios-Ortega 2017, Rivera-de-Torre 2018, Rivera-de-Torre 2017) and maybe explaining its also lower hemolytic activity (Figure 9).

The observation that the N-terminal end of StnIII is three residues longer than this same stretch in StnII is especially relevant because it has been shown that bilayer thickness affects both functional and conformational aspects of Stns membrane binding and pore formation (Palacios-Ortega 2017). Accordingly, the length of StnII N-terminal α-helix, which penetrates the membrane to form a functional pore, appeared to be optimal for the membrane thickness represented by DOPC. Applying identical geometrical calculations to StnIII, the α-helical

transmembrane domain would be 49.5 Å long, instead of the 45.0 Å calculated for StnII (Palacios-Ortega 2017). Assuming a final pore octameric stoichiometry identical to the one found for the actinoporin from *Actinia fragacea*, FraC (Tanaka 2015), and taking into account the angle formed by the helix and the bilayer normal, the optimal thickness for StnIII would be 42.5 Å, instead of the 38.0 Å described for StnII (Palacios-Ortega 2017). This membrane thickness would correspond 1,2-dieicosenoyl-sn-glycero-3-phosphocholine (di-20:1-PC). Hence, just this length difference at the N-terminal end of StnIII suggests that its presence in *S. helianthus* venom would increase the range of possible targets, including the possibility of targeting cells with thicker membranes than the most common ones found in fishes, containing di-18:1-PC as its major phospholipid (Li 2011). Another possibility to explain StnIII's longer N-terminal end would be maintaining the di-18:1-PC membrane thickness but adopting a different stoichiometry for its final stable pore. Thus, if calculations are made without assuming any previous oligomerization stoichiometry, but fixing di-18:1-PC as representing the optimum membrane thickness, the results render the formation of a final pore with nine monomers. Interestingly, a nonameric structure has been also described for FraC (Mechaly 2011). Finally, the presence of Pro in the second position also opens the possibility that StnIII uses a slightly different conformation, other than a 100% α-helix, to penetrate the membrane.

All the other residues comprising important domains for the actinoporins function(García-Ortega 2011) are conserved or substituted by residues with similar physicochemical properties (Figure 1) (García-Linares 2016a). Within this context, StnIII L113, corresponding to W111 in StnI and W110 in StnII, stands out as a remarkable difference because this residue belongs to the so-called cluster of aromatic residues, responsible for driving membrane binding and involved in maintaining the required hydrophobicity to achieve that goal. In agreement with this observation, StnII W110 has been recently described as penetrating the hydrophobic membrane core (García-Linares 2016a). In fact, its substitution by another highly hydrophobic amino acid such as Phe barely affected membrane binding (García-Linares 2016a). Accordingly, substitution by another highly hydrophobic amino acid, as is the case with L113, would be expected to have only minor influence on StnIII membrane interaction ability, as occurs with some other less studied actinoporins[25]. However, this substitution leaves StnIII as a sticholysin with only four Trp residues, instead of five as in the other two Stns. Five Trp residues, which appear quite conserved within the actinoporin's family and which, when not, are preferentially substituted by Phe or Leu residues (García-Linares 2017).

The role played by the different StnII Trp residues has been previously analyzed in detail using a quite complete set of Trp to Phe mutants (García-Linares 2016a). Apart from its role in membrane binding, in its monomeric water-soluble conformation, StnII W110 is a fully exposed residue that does not contribute significantly to fluorescence emission, explaining why its substitution by Leu in StnIII does not involve major significant differences in terms of Trp fluorescence emission, when compared to StnII (Figure 6; Table 1), despite of having one less Trp residue.

On the other hand, the most remarkable feature that emerges from Figure 6 is the much higher Tyr quantum yield. For example StnIII's Tyr emission is about four-fold higher than StnII's (Table 1). This is even more noticeable considering that StnI and StnII contain 13 and 12 Tyr residues, respectively, while StnIII contains only 11 (García-Linares 2016a).It was found that replacement of W110 (the StnII equivalent residue of StnIII L113; Figure 1B) yielded mutants

showing a significant increase in Tyr emission. This was interpreted as StnII Y114 being quenched through non-radiative energy transfer to StnII W110. This non-radiative energy transfer phenomenon could not take place in StnIII due to the presence of Leu in that critical position (Figure 1B), possibly explaining the high Tyr quantum yield increment observed (Figure 6).

Finally, comparison between StnII and StnIII sequences reveals that StnII Y140 is in a position equivalent to StnIII F143 (Figures 1 and 2). StnII Y140 seems to be quenched by W115 (Figure 1C) supporting another event of non-radiative energy transfer between Tyr and Trp residues (García-Linares 2016a). This interpretation explains why Y140 does not contribute significantly to StnII fluorescence emission (García-Linares 2016a). Consequently, the change of this residue by Phe in the equivalent position of StnIII has a negligible effect on the StnIII fluorescence emission while Phe is still an amino acid with the properties needed to establish the required stabilizing interaction with StnIII W118 (Figure 1C).

StnI and III showed very similar relative binding affinity values (Table 2) but StnIII's relative hemolytic activity was four-fold lower (Table 1). Both proteins are significantly much less efficient than StnII in terms of membrane binding and lytic activity (Tables 1 and 2). These results suggest that StnI and StnIII functional differences would reside rather on the membrane diffusion and oligomerization steps needed to form the final pore than on their ability to recognize and bind to the membrane surface. Accordingly, inspection of their hemolytic behavior in kinetic terms reveals that both hemolytic curves of StnI and III (Figure 9) are quite different. Apparently, the critical concentration for StnIII to become hemolytic is higher in comparison with StnI but, once reached, StnIII displays higher activity than StnI. This observation agrees with the interpretation that both proteins would mostly differ in their oligomerization mechanism. Furthermore, it could also be speculated that it agrees with the above mentioned hypothesis that the final pore assembly of StnIII might display a different stoichiometry other than an octamer, as described for the pore crystalline structure of FraC (Tanaka 2015).

Finally, the remaining question would be if this newly discovered StnIII can establish synergistic interactions with the other two very well-known Stns. This question arises from the previously established observation that StnI and II can act synergistically and even assemble into functionally active heteropores (Rivera-de-Torre 2016). The results show quite clearly that such synergy takes place, at least between StnII and III (Figure 12). The synergy between StnI and III, if still possible, is almost impossible to show by looking only at the combination of their hemolytic activities, given that these two actinoporins show very similar hemolysis rates within all the range of protein concentrations studied. Thus, StnII and StnIII show synergy, and we can speculate that they most probably form mixed heteropores, but the potential synergy between StnI and StnIII remains to be studied using a different approach. The synergistic effect between StnII and III would occur at the membrane binding step, with StnII facilitating StnIII binding. An observation that reinforces the more general hypothesis that the main reason for the presence of several actinoporin isoforms in all sea anemone venoms would be to improve their versatility in defense and/or attack responses in their natural environment.

Conclusions

StnIII is a new actinoporin isoform produced by *S. helianthus*, discovered through transcriptomic analysis. This protein has been cloned and produced in the heterologous system

E. coli. Its successful purification allowed its spectroscopic and functional characterization. Its spectroscopic features are compatible with the protein adopting a globular β-sheet rich conformation that resembles the common actinoporin fold. StnIII is active against sheep red blood cells, but significantly less hemolytic than StnII and quite similar to StnI in spite of its much higher HC_{50} value which, in this case, could be attributed to a different oligomerization behavior on the membrane rather than to a less hemolytic efficiency. This behavior was also consistent with the calcein release and model membranes binding experiments. The results, altogether with its longer N-terminal end and the presence of Pro as its second amino acid, suggest the possibility of StnIII oligomerizing into a final membrane structure whose stoichiometry would be larger. Finally, mixtures composed by StnII and StnIII show synergistic activity, probably because StnII eases StnIII binding to the membrane, reinforcing the hypothesis that the presence of different actinoporin isoforms plays a key role in regulating and expanding the range of targets the venom can act against.

Acknowledgements

This research was supported by the Sigrid Juselius Foundation, the Jane and Aatos Erkko Foundation, and the Magnus Ehrnrooth Foundation (to J.P.S.), and by UCM-Banco Santander grant PR75/18-21561 (to A.M.-d.-P.). J.P.-O. has a funded doctoral student position from ISB/ÅA. UCM-Banco Santander fellowship was granted to E.R.-d.-T.

References

Alegre-Cebollada, J., Clementi, G., Cunietti, M., Porres, C., Oñaderra, M., Gavilanes, J.G., and Martínez-del-Pozo, A. (2007a) "Silent Mutations at the 5'-End of the Cdna of Actinoporins from the Sea Anemone *Stichodactyla Helianthus* Allow Their Heterologous Overproduction in *Escherichia Coli*." *J Biotechnol* 127, 2: 211-221.

Alegre-Cebollada, J., Cunietti, M., Herrero-Galán, E., Gavilanes, J.G., and Martínez-del-Pozo, A. (2008) "Calorimetric Scrutiny of Lipid Binding by Sticholysin Ii Toxin Mutants." *J Mol Biol* 382, 4: 920-930.

Alegre-Cebollada, J., Lacadena, V., Oñaderra, M., Mancheño, J.M., Gavilanes, J.G., and Martínez-del-Pozo, A. (2004) "Phenotypic Selection and Characterization of Randomly Produced Non-Haemolytic Mutants of the Toxic Sea Anemone Protein Sticholysin Ii." *FEBS Lett* 575, 1-3: 14-18.

Alegre-Cebollada, J., Martínez-del-Pozo, A., Gavilanes, J.G., and Goormaghtigh, E. (2007b) "Infrared Spectroscopy Study on the Conformational Changes Leading to Pore Formation of the Toxin Sticholysin Ii." *Biophys J* 93, 9: 3191-3201.

Alegre-Cebollada, J., Oñaderra, M., Gavilanes, J.G., and Martínez-del-Pozo, A. (2007c) "Sea Anemone Actinoporins: The Transition from a Folded Soluble State to a Functionally Active Membrane-Bound Oligomeric Pore." *Curr Protein Pept Sci* 8, 6: 558-572.

Alegre-Cebollada, J., Rodríguez-Crespo, I., Gavilanes, J.G., and Martínez-del-Pozo, A. (2006) "Detergent-Resistant Membranes Are Platforms for Actinoporin Pore-Forming Activity on Intact Cells." *FEBS J* 273, 4: 863-871.

Alm, I., Garcia-Linares, S., Gavilanes, J.G., Martinez-Del-Pozo, A., and Slotte, J.P. (2015a) "Cholesterol Stimulates and Ceramide Inhibits Sticholysin Ii-Induced Pore Formation in Complex Bilayer Membranes." *Biochim Biophys Acta* 1848, 4: 925-931.

Alm, I., García-Linares, S., Gavilanes, J.G., Martínez-del-Pozo, A., and Slotte, J.P. (2015b) "Cholesterol Stimulates and Ceramide Inhibits Sticholysin Ii-Induced Pore Formation in Complex Bilayer Membranes." *Biochim Biophys Acta - Biomembranes* 1848925-931.

Anderluh, G., and Lakey, J.H. (2008) "Disparate Proteins Use Similar Architectures to Damage Membranes." *Trends Biochem Sci* 33, 10: 482-490.

Anderluh, G., and Maček, P. (2002) "Cytolytic Peptide and Protein Toxins from Sea Anemones (Anthozoa: Actiniaria)." *Toxicon* 40, 2: 111-124.

Athanasiadis, A., Anderluh, G., Maček, P., and Turk, D. (2001) "Crystal Structure of the Soluble Form of Equinatoxin Ii, a Pore-Forming Toxin from the Sea Anemone *Actinia Equina*." *Structure* 9, 4: 341-346.

Bartlett, G.R. (1959) "Colorimetric Assay Methods for Free and Phosphorylated Glyceric Acids." *J Biol Chem* 234, 3: 469-471.

Casallanovo, F., de Oliveira, F.J., de Souza, F.C., Ros, U., Martínez, Y., Penton, D., Tejuca, M., Martínez, D., Pazos, F., Pertinhez, T.A., Spisni, A., Cilli, E.M., Lanio, M.E., Álvarez, C., and Schreier, S. (2006) "Model Peptides Mimic the Structure and Function of the N-Terminus of the Pore-Forming Toxin Sticholysin Ii." *Biopolymers* 84, 2: 169-180.

Casallanovo, F., de Oliveira, F.J.F., Souto, A.L.C.F., de Souza, F.C., Cilli, E.M., Martínez, Y., Lanio, M.E., and Álvarez, C. "Peptides from the N-Terminal Domain of a Pore-Forming Toxin, Sticholysin Ii. Conformation and Activity." Paper presented at the 48th Annual Meeting of the Biophysical Society, Baltimore, MD 2004.

Castrillo, I., Araujo, N.A., Alegre-Cebollada, J., Gavilanes, J.G., Martínez-del-Pozo, A., and Bruix, M. (2010) "Specific Interactions of Sticholysin I with Model Membranes: An Nmr Study." *Proteins* 78, 8: 1959-1970.

Cilli, E.M., Pigossi, F.T., Crusca, E., Jr., Ros, U., Martinez, D., Lanio, M.E., Alvarez, C., and Schreier, S. (2007) "Correlations between Differences in Amino-Terminal Sequences and Different Hemolytic Activity of Sticholysins." *Toxicon*.

De Antonio, C., Martínez-del-Pozo, A., Mancheño, J.M., Oñaderra, M., Lacadena, J., Martínez-Ruiz, A., Pérez-Cañadillas, J.M., Bruix, M., and Gavilanes, J.G. (2000) "Assignment of the Contribution of the Tryptophan Residues to the Spectroscopic and Functional Properties of the Ribotoxin α-Sarcin." *Proteins* 41, 3: 350-361.

De los Ríos, V., Mancheño, J.M., Lanio, M.E., Oñaderra, M., and Gavilanes, J.G. (1998) "Mechanism of the Leakage Induced on Lipid Model Membranes by the Hemolytic Protein Sticholysin Ii from the Sea Anemone *Stichodactyla Helianthus*." *Eur J Biochem* 252284-289.

De los Ríos, V., Oñaderra, M., Martínez-Ruiz, A., Lacadena, J., Mancheño, J.M., Martínez-del-Pozo, A., and Gavilanes, J.G. (2000) "Overproduction in *Escherichia Coli* and Purification of the Hemolytic Protein Sticholysin Ii from the Sea Anemone *Stichodactyla Helianthus*." *Protein Expr Purif* 18, 1: 71-76.

Eisenberg, D., Schwarz, E., Komaromy, M., and Wall, R. (1984a) "Analysis of Membrane and Surface Protein Sequences with the Hydrophobic Moment Plot." *J Mol Biol* 179125-142.

Eisenberg, D., Schwarz, E., Komaromy, M., and Wall, R. (1984b) "Analysis of Membrane and Surface Protein Sequences with the Hydrophobic Moment Plot." *J Mol Biol* 179, 1: 125-142.

García-Linares, S., Alm, I., Maula, T., Gavilanes, J.G., Slotte, J.P., and Martínez-Del-Pozo, A. (2015) "The Effect of Cholesterol on the Long-Range Network of Interactions Established among Sea Anemone Sticholysin Ii Residues at the Water-Membrane Interface." *Mar Drugs* 13, 4: 1647-1665.

García-Linares, S., Castrillo, I., Bruix, M., Menéndez, M., Alegre-Cebollada, J., Martínez-del-Pozo, A., and Gavilanes, J.G. (2013) "Three-Dimensional Structure of the Actinoporin Sticholysin I. Influence of Long-Distance Effects on Protein Function." *Arch Biochem Biophys* 532, 1: 39-45.

García-Linares, S., Maula, T., Rivera-de-Torre, E., Gavilanes, J.G., Slotte, J.P., and Martínez-del-Pozo, A. (2016a) "Role of the Tryptophan Residues in the Specific Interaction of the Sea Anemone *Stichodactyla Helianthus*'s Actinoporin Sticholysin Ii with Biological Membranes." *Biochemistry* 55, 46: 6406-6420.

García-Linares, S., Palacios-Ortega, J., Yasuda, T., Astrand, M., Gavilanes, J.G., Martínez-del-Pozo, A., and Slotte, J.P. (2016b) "Toxin-Induced Pore Formation Is Hindered by Intermolecular Hydrogen Bonding in Sphingomyelin Bilayers." *Biochim Biophys Acta* 1858, 6: 1189-1195.

García-Linares, S., Richmond, R., García-Mayoral, M.F., Bustamante, N., Bruix, M., Gavilanes, J.G., and Martínez-del-Pozo, A. (2014) "The Sea Anemone Actinoporin (Arg-Gly-Asp) Conserved Motif Is Involved in Maintaining the Competent Oligomerization State of These Pore-Forming Toxins." *FEBS J* 281, 5: 1465-1478.

García-Linares, S., Rivera-de-Torre, E., Morante, K., Tsumoto, K., Caaveiro, J.M., Gavilanes, J.G., Slotte, J.P., and Martínez-del-Pozo, Á. (2016c) "Differential Effect of Membrane Composition on the Pore-Forming Ability of Four Different Sea Anemone Actinoporins." *Biochemistry* 55, 48: 6630-6641.

García-Linares, S., Rivera-de-Torre, E., Palacios-Ortega, J., Gavilanes, J.G., and Martínez-del-Pozo, A. "The Metamorphic Transformation of a Water-Soluble Monomeric Protein into an Oligomeric Transmembrane Pore." In *Advances in Biomembranes and Lipid Self-Assembly*, edited by A. Iglič, M. Rappolt and A. J. García-Sáez, 51-97, 2017.

García-Ortega, L., Alegre-Cebollada, J., García-Linares, S., Bruix, M., Martínez-del-Pozo, A., and Gavilanes, J.G. (2011) "The Behavior of Sea Anemone Actinoporins at the Water-Membrane Interface." *Biochim Biophys Acta* 1808, 9: 2275-2288.

Gautier, R., Douguet, D., Antonny, B., and Drin, G. (2008) "Heliquest: A Web Server to Screen Sequences with Specific Alpha-Helical Properties." *Bioinformatics* 24, 18: 2101-2102.

Hinds, M.G., Zhang, W., Anderluh, G., Hansen, P.E., and Norton, R.S. (2002) "Solution Structure of the Eukaryotic Pore-Forming Cytolysin Equinatoxin Ii: Implications for Pore Formation." *J Mol Biol* 315, 5: 1219-1229.

Hong, Q., Gutiérrez-Aguirre, I., Barlič, A., Malovrh, P., Kristan, K., Podlesek, Z., Maček, P., Turk, D., González-Mañas, J.M., Lakey, J.H., and Anderluh, G. (2002) "Two-Step Membrane Binding by Equinatoxin Ii, a Pore-Forming Toxin from the Sea Anemone, Involves an Exposed Aromatic Cluster and a Flexible Helix." *J Biol Chem* 277, 44: 41916-41924.

Kelley, L.A., Mezulis, S., Yates, C.M., Wass, M.N., and Sternberg, M.J. (2015) "The Phyre2 Web Portal for Protein Modeling, Prediction and Analysis." *Nat Protoc* 10, 6: 845-858.

Kristan, K., Podlesek, Z., Hojnik, V., Gutiérrez-Aguirre, I., Guncar, G., Turk, D., González-Mañas, J.M., Lakey, J.H., Maček, P., and Anderluh, G. (2004) "Pore Formation by Equinatoxin, a Eukaryotic Pore-Forming Toxin, Requires a Flexible N-Terminal Region and a Stable B-Sandwich." *J Biol Chem* 279, 45: 46509-46517.

Kyte, J., and Doolittle, R.F. (1982) "A Simple Method for Displaying the Hydropathic Character of a Protein." *J Mol Biol* 157, 1: 105-132.

Laemli, U.K. (1970) "Cleavage of Structural Proteins During the Assembly of the Head of Bacteriophage T4." *Nature* 227680-685.

Lanio, M.E., Morera, V., Álvarez, C., Tejuca, M., Gómez, T., Pazos, F., Besada, V., Martínez, D., Huerta, V., Padrón, G., and Chavez, M.A. (2001) "Purification and Characterization of Two Hemolysins from *Stichodactyla Helianthus*." *Toxicon* 39, 2-3: 187-194.

Leychenko, E.V., Isaeva, M., Tkacheva, E., Zelepuga, E., Kvetkina, A., Guzev, K., Monastyrnaya, M., and Kozlovskaya, E. (2018) "Multigene Family of Pore-Forming Toxins from Sea Anemone *Heteractis Crispa*." *Mar Drugs* 16, 6.

Li, G., Sinclair, A.J., and Li, D. (2011) "Comparison of Lipid Content and Fatty Acid Composition in the Edible Meat of Wild and Cultured Freshwater and Marine Fish and Shrimps from China." *J Agric Food Chem* 59, 5: 1871-1881.

Macrander, J., and Daly, M. (2016) "Evolution of the Cytolytic Pore-Forming Proteins (Actinoporins) in Sea Anemones." *Toxins (Basel)* 8, 12.

Malovrh, P., Viero, G., Serra, M.D., Podlesek, Z., Lakey, J.H., Maček, P., Menestrina, G., and Anderluh, G. (2003) "A Novel Mechanism of Pore Formation: Membrane Penetration by the N-Terminal Amphipathic Region of Equinatoxin." *J Biol Chem* 278, 25: 22678-22685.

Mancheño, J.M., Martín-Benito, J., Martínez-Ripoll, M., Gavilanes, J.G., and Hermoso, J.A. (2003) "Crystal and Electron Microscopy Structures of Sticholysin Ii Actinoporin Reveal Insights into the Mechanism of Membrane Pore Formation." *Structure* 11, 11: 1319-1328.

Martínez-Ruiz, A., García-Ortega, L., Kao, R., Lacadena, J., Oñaderra, M., Mancheño, J.M., Davies, J., Martínez-del-Pozo, A., and Gavilanes, J.G. (2001) "Rnase U2 and α-Sarcin: A Study of Relationships." *Methods Enzymol* 341335-351.

Martínez-Ruiz, A., García-Ortega, L., Kao, R., Oñaderra, M., Mancheño, J.M., Davies, J., Martínez-del-Pozo, A., and Gavilanes, J.G. (2000) "Ribonuclease U2: Cloning, Production in *Pichia Pastoris* and Affinity Chromatography Purification of the Active Recombinant Protein." *FEMS Microbiol Lett* 189, 2: 165-169.

Maula, T., Isaksson, Y.J., García-Linares, S., Niinivehmas, S., Pentikainen, O.T., Kurita, M., Yamaguchi, S., Yamamoto, T., Katsumura, S., Gavilanes, J.G., Martínez-del-Pozo, A., and Slotte, J.P. (2013) "2nh and 3oh Are Crucial Structural Requirements in Sphingomyelin for Sticholysin Ii Binding and Pore Formation in Bilayer Membranes." *Biochim Biophys Acta* 1828, 5: 1390-1395.

Mechaly, A.E., Bellomio, A., Gil-Carton, D., Morante, K., Valle, M., González-Mañas, J.M., and Guerin, D.M. (2011) "Structural Insights into the Oligomerization and Architecture of Eukaryotic Membrane Pore-Forming Toxins." *Structure* 19, 2: 181-191.

Monastyrnaya, M., Leychenko, E., Isaeva, M., Likhatskaya, G., Zelepuga, E., Kostina, E., Trifonov, E., Nurminski, E., and Kozlovskaya, E. (2010) "Actinoporins from the Sea Anemones, Tropical *Radianthus Macrodactylus* and Northern *Oulactis Orientalis*: Comparative Analysis of Structure-Function Relationships." *Toxicon* 56, 8: 1299-1314.

Palacios-Ortega, J., García-Linares, S., Astrand, M., Al Sazzad, M.A., Gavilanes, J.G., Martínez-del-Pozo, A., and Slotte, J.P. (2016) "Regulation of Sticholysin Ii-Induced Pore Formation by Lipid Bilayer Composition, Phase State, and Interfacial Properties." *Langmuir* 32, 14: 3476-3484.

Palacios-Ortega, J., García-Linares, S., Rivera-de-Torre, E., Gavilanes, J.G., Martínez-del-Pozo, A., and Slotte, J.P. (2017) "Differential Effect of Bilayer Thickness on Sticholysin Activity." *Langmuir* 33, 41: 11018-11027.

Palacios-Ortega, J., García-Linares, S., Rivera-de-Torre, E., Gavilanes, J.G., Martínez-del-Pozo, A., and Slotte, J.P. (2019) "Sticholysin, Sphingomyelin, and Cholesterol: A Closer Look at a Tripartite Interaction." *Biophys J* 116, 12: 2253-2265.

Pardo-Cea, M.A., Castrillo, I., Alegre-Cebollada, J., Martínez-del-Pozo, A., Gavilanes, J.G., and Bruix, M. (2011) "Intrinsic Local Disorder and a Network of Charge-Charge Interactions Are Key to Actinoporin Membrane Disruption and Cytotoxicity." *FEBS J* 278, 12: 2080-2089.

Parker, M.W., and Feil, S.C. (2005) "Pore-Forming Protein Toxins: From Structure to Function." *Prog Biophys Mol Biol* 88, 1: 91-142.

Rivera-de-Torre, E., García-Linares, S., Alegre-Cebollada, J., Lacadena, J., Gavilanes, J.G., and Martínez-del-Pozo, A. (2016) "Synergistic Action of Actinoporin Isoforms from the Same Sea Anemone Species Assembled into Functionally Active Heteropores." *J Biol Chem* 291, 27: 14109-14119.

Rivera-de-Torre, E., Martínez-del-Pozo, A., and Garb, J.E. (2018) "*Stichodactyla Helianthus*' De Novo Transcriptome Assembly: Discovery of a New Actinoporin Isoform." *Toxicon* 150105-114.

Rivera-de-Torre, E., Palacios-Ortega, J., García-Linares, S., Gavilanes, J.G., and Martínez-del-Pozo, A. (2017) "One Single Salt Bridge Explains the Different Cytolytic Activities Shown by Actinoporins Sticholysin I and Ii from the Venom of *Stichodactyla Helianthus*." *Arch Biochem Biophys* 63679-89.

Rojko, N., Kristan, K.C., Viero, G., Zerovnik, E., Maček, P., Dalla Serra, M., and Anderluh, G. (2013) "Membrane Damage by an α-Helical Pore-Forming Protein, Equinatoxin Ii, Proceeds through a Succession of Ordered Steps." *J Biol Chem* 288, 33: 23704-23715.

Ros, U., Pedrera, L., Diaz, D., Karam, J.C., Sudbrack, T.P., Valiente, P.A., MartInez, D., Cilli, E.M., Pazos, F., Itri, R., Lanio, M.E., Schreier, S., and Avarez, C. (2012) "The Membranotropic Activity of N-Terminal Peptides from the Pore-Forming Proteins Sticholysin I and Ii Is Modulated by Hydrophobic and Electrostatic Interactions as Well as Lipid Composition." *J Biosci* 36, 5: 781-791.

Ros, U., Rodríguez-Vera, W., Pedrera, L., Valiente, P.A., Cabezas, S., Lanio, M.E., García-Saez, A.J., and Álvarez, C. (2015) "Differences in Activity of Actinoporins Are Related with the Hydrophobicity of Their N-Terminus." *Biochimie* 11670-78.

Tanaka, K., Caaveiro, J.M., Morante, K., González-Mañas, J.M., and Tsumoto, K. (2015) "Structural Basis for Self-Assembly of a Cytolytic Pore Lined by Protein and Lipid." *Nat Commun* 66337.

Wang, Y., Yap, L.L., Chua, K.L., and Khoo, H.E. (2008) "A Multigene Family of *Heteractis* Magnificalysins (Hmgs)." *Toxicon* 51, 8: 1374-1382.

BLOCK II:

The membrane pore-forming *latrotoxin macromolecular complex*: latrodectins and latroinsectotoxins produced by black widow spiders

Article V

Structural and functional characterization of Latrodectins I and II, low molecular weight components from black widow spider venom

Esperanza Rivera-de-Torre[1], Javier Narbona[1], David Pantoja-Uceda[2], Gustavo Titaux[2], Miguel A. Treviño[2], Belén Patiño[3], Pilar Medina[4], Javier Maraver-de-Paz[1], Sara García-Linares[1], José G. Gavilanes[1], Jessica E. Garb[5], María Ángeles Jiménez[2], Álvaro Martínez-del-Pozo[1]

[1]Department of Biochemistry and Molecular Biology, Faculty of Chemistry, Complutense University, 28040 Madrid, Spain.
[2]Department of Biological Physical Chemistry, Institute of Physical Chemistry Rocasolano, CSIC, Serrano 119, 28006 Madrid, Spain.
[3]Department of Genetics, Physiology and Microbiology, Faculty of Biology, Complutense University of Madrid, 28040 Madrid, Spain.
[4]Unidad de Protección de Cultivos, E.T.S. I. Agronómica, Alimentaria y de Biosistemas, Universidad Politécnica de Madrid, 28040 Madrid, Spain.
[5]Department of Biological Sciences, University of Massachusetts Lowell, Lowell, MA, USA.

Las viudas negras (*Latrodectus* spp.) son unas de las pocas arañas capaces de causar envenenamiento en los humanos. Las consecuencias de su mordedura varían desde el dolor local hasta un severo síndrome sistémico llamado "latrodectismo" que implica dolor deslocalizado, parálisis y dificultad respiratoria y que puede requerir hospitalización. Las principales toxinas presentes en el veneno de las arañas del género *Latrodectus*, responsables de la sintomatología mencionada, son unas proteínas de elevada masa molecular (110-140kDa) denominadas Latrotoxinas (LTXs). Su actividad tóxica reside en la formación de poros a través de las presinapsis neuronales, conduciendo a la liberación masiva de neurotransmisores. Las LTXs purificadas del veneno crudo siempre aparecen asociadas con péptidos llamados Latrodectinas (Ltds). LTXs y Ltds se unen con gran afinidad y, debido a esta fuerte asociación, algunos autores han propuesto su ensamblaje conjunto en un complejo macromolecular que denominan "*el complejo macromolecular latrotoxina*". Estas Ltds son péptidos de 6-8 kDa con un punto isoeléctrico ácido, y un alto contenido de enlaces disulfuro. A diferencia del papel tóxico ya descrito de las LTXs, la función de las Ltds no se conoce todavía. Los escasos datos disponibles sugieren que refuerzan la actividad neurotóxica de las LTXs al aumentar su afinidad de unión a la membrana neural presináptica. El objetivo principal de esta investigación fue entonces producir, purificar y caracterizar las Ltds más abundantes en el veneno de *L. hesperus* mediante la utilización de un sistema recombinante. El objetivo final era dilucidar su papel específico en la toxicidad del veneno de la araña viuda negra. De acuerdo con este planteamiento, LtdI y LtdII se clonaron y expresaron en la levadura *Pichia pastoris*. Ambas proteínas se purificaron a homogeneidad mediante sucesivas etapas cromatográficas, si bien sólo LtdII se llegó a caracterizar con suficiente detalle a nivel funcional y estructural. Mediante espectrometría de masas, se demostró que los seis residuos de cisteína de LtdII estaban dispuestos formando tres enlaces disulfuro. Su caracterización por dicroísmo circular indicó que ambas toxinas eran proteínas globulares, termoestables y totalmente plegadas con un alto contenido en hélice α. La espectroscopia de resonancia magnética nuclear (RMN) se usó para la

determinación parcial de la estructura tridimensional de LtdII, lo que también implicó su producción previa etiquetada con los isótopos estables ^{15}N y ^{13}C. Finalmente, una caracterización funcional de LtdII sugirió que, al menos en condiciones aisladas, este péptido no muestra propiedades insecticidas, ni antifúngicas.

PhD candidate contributions

Esperanza Rivera de Torre conceived, designed and conducted most of the experiments, except those regarding with the NMR and the antifungal and insecticidal experiments. She also significantly contributed to analyzing and discussing all the results, writing and correcting the manuscript, and suggesting modifications.

Abstract

Black widow spiders (*Latrodectus* spp.) are one of the few spiders known to cause poisoning in humans. Their bite consequences vary from local pain to a severe systemic syndrome called *latrodectism* which symptoms include systemic pain, paralysis and respiratory distress that may even require hospitalization. The major toxins present in *Latrodectus* spp's venom, and responsible of this symptomatology, are high molecular weight proteins (110-140kDa) known as latrotoxins (LTXs). Their toxic activity relies on the formation of pores through presynaptic neurons, leading to massive neurotransmitter release. LTXs purified from crude venom always appear associated with high affinity to peptides called latrodectins (Ltds). Due to this strong association, some authors have proposed their mutual functional assembly into a macromolecular complex known as the "*latrotoxin macromolecular complex*". On the other hand, Ltds are rather small peptides (6-8 kDa), also with an acidic pI value and a high content of disulphide bonds. Unlike the already described toxic role of LTXs, the function of Ltds is not known yet. The limited data available suggest that Ltds enhance the neurotoxic activity of LTXs by increasing their affinity for binding to the presynaptic neural membrane. The main objective of this research was then to produce, purify and characterize the most abundant Ltds in *L. hesperus* venom, using a recombinant expression system, in order to elucidate their specific role in the toxicity of black widow spider venom. According to this approach, LtdI and LtdII from *L. hesperus* were cloned and produced using the *Pichia pastoris* yeast. Both proteins were purified to homogeneity by successive chromatographic steps, although only LtdII was characterized in enough detail at the functional and structural level. By mass spectrometry, it was shown that the six cysteine residues of LtdII were arranged to form three disulfide bonds. Their characterization by circular dichroism indicated that both toxins were globular, heat-stable, fully folded proteins with a high α-helix content. Nuclear magnetic resonance spectroscopy (NMR) was used for structural characterization of LtdII, which required its production labeled with the stable isotopes ^{15}N and ^{13}C. Finally, a functional characterization of LtdII suggested that, at least under isolated conditions, this peptide does not show insecticidal, nor antifungal properties.

Introduction

Latrodectus is a medically important spider genera with a worldwide widespread distribution, more well-known as black widow spiders. Their venomous injection in vertebrates causes localized acute manifestations like intense pain and local paralysis but it can also cause a long-term highly disturbing syndrome called "*latrodectism*". This pathology is characterized by systemic symptoms like nausea, paresthesia and muscle rigidity (Camp 2014, Grishin 1998), which respond to the action of huge toxic polypeptides (≈130kDa) known as α-Latrotoxins (α-LTX). The molecular mechanism behind these clinical symptoms is hardly known but, at least, it seems to involve initial binding to the presynaptic membrane receptors neurexin and latrophilin (Sudhof 2001, Ushkaryov 2008). Upon binding, the toxin elements assemble into a cation selective pore which induces calcium imbalance, stimulating massive neurotransmitters release at synapses of both peripherical and central nervous systems (Frontali 1976, Orlova 2000, Ushkaryov 2002).

Frequently, characterization of α-LTXs purified from crude venom reveals the presence of Low Molecular Weight Protein (LMWP) components. These peptides of around 70 amino

acids long appear to associate with LTXs (Gasparini 1994, Kiyatkin 1992) and were lately named as latrodectins (Ltds). This conserved association between these two groups of proteins (Ltds and LTXs) has even driven some authors to use the concept of what is now called the *latrotoxin macromolecular complex* (Orlova 2000). It is, however, still unknown the relevance of this association and its biological implications. The only structural information known so far is that the sequences of these Ltds are very similar to peptides from the crustacean hyperglycemic hormone family (CHHs), which contains neuropeptides involved in ionic metabolism and osmoregulation. This family is also present in insects as ion transport peptides (ITPs) and it is also possible to find similar polypeptides in ticks and nematodes (Montagne 2010). Considering that ticks are arachnids, it seems feasible to speculate that latrodectins genes were recruited for venom gland expression from ancient spider CHH/ITP homologs. However, the potential relationship between latrodectins and the CHH/ITP family of peptides has not been even studied yet (McCowan and Garb 2014).

As stated above, Ltds are small proteins with a highly acidic isoelectric point value (around 4) which are importantly expressed in venom glands (Haney 2014). Their function is still unknown and, because they do not have been shown to exert any antibiotic or insecticidal activity so far, some authors propose that their function is related to their necessary presence in the aforementioned *latrotoxin macromolecular complex* (Volkova 1995).

In order to understand Ltds role in this complex, in particular, and in the *Latrodectus* venom, in general, we aimed to clone and produce them in the heterologous *Pichia pastoris* yeast system. cDNA selected sequences were obtained from *Latrodectus hesperus* transcriptomic results, considering those contigs that had been confirmed regarding the corresponding proteomic profile (Haney 2014, Haney 2016). Finally, it is also relevant for the purpose of this work to remark that the two Ltds selected seem to be produced as immature propeptide products that need to be processed at their N-terminal end for obtaining the mature, presumably active, toxic peptides (Pescatori 1995).

Materials and methods

cDNA synthesis from L. hesperus' venom gland mRNA

Western black widow venom glands from two female individuals collected in Riverside (Riverside County, California, USA) were dissected according to (Garb 2014). Tissue was dissolved in TRIzol /Ambion, Life Technologies). Total RNA was extracted following TRIzol recommended protocol (Chomczynski 1993). Briefly, homogenized tissue was incubated at room temperature for 5 min and then chloroform was added. After vortex shaking, samples were centrifuged at 12000 x g for 15 min at 4°C. Aqueous phase was recovered, and RNA was precipitated with isopropanol, followed by three washing steps with 75% ethanol. Dried RNA was dissolved in RNase free water. Potentially contaminating DNA was removed with TURBO DNA-free kit (Ambion, Life Technologies). RNA was stored at -80°C upon utilization until using it as template for cDNA synthesis with SuperScript III First-Strand Synthesis SuperMix kit (Thermo Fisher).

Cloning mature Ltds

Selected contigs 6065 and 11185 from *L. hesperus* transcriptome assembly (BioProject PRJNA242358) were translated to protein sequences. Signal peptides were predicted using SpiderP tool from ArachnoServer (Pineda 2018) (Figure 1). Oligonucleotides were designed for amplification of the fragments from cDNA through PCR with proofreading Pfu DNA polymerase (Thermo Scientific) following these instructions: 60 s at 95°C initial denaturation, followed by 30 cycles of 45 s denaturation at 95°C, 30 s of annealing at 50°C, 60s of elongation at 72°C, finally remaining fragments annealed fragments were elongated for 300 s at 72°C. Samples were subcloned in a modified version of pPICZαA expression vector for the yeast *P. pastoris*, which have suffered a deletion within the yeast α-factor signal-sequence to remove Ste13 clevage site (López-García 2009). During PCR, restriction sites EcoRI and XhoI sites were also introduced into the fragment. Next, amplified cDNAs and pPICZαA plasmid were digested with the corresponding restriction enzymes (Roche), purified via Wizard PCR Preps DNA purification system (Promega) and ligated using T4 DNA ligase (Promega). This way, Ltds were inserted in frame with the complete yeast α-factor signal sequence, including Kex2 signal cleavage sites. Purification of plasmids were carried out by Minipreps and their sequences were determined by Sanger sequencing.

Contig	Name	Abbreviation	Designed oligonucleotides 5'→3'	
6065	Latrodectin I	LtdI	Forward	GTATCT **CTCGAG** AAAAGA ACCACACCAGATGAAATAG XhoI Kex2
			Reverse	TTTTGT **TCTAGA** *CTA* TTCCTTAGCTGGAGG XbaI STOP
11185	Latrodectin II	LtdII	Forward	GTATCT **CTCGAG** AAAAGA GAGGACTCTCTGGACCCAG XhoI Kex2
			Reverse	TTTTGT **TCTAGA** *TTA* TTCAGGTGGTTCTTTTTC XbaI STOP

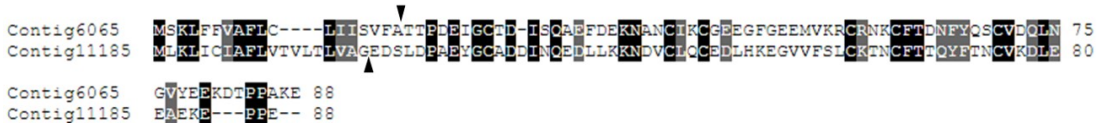

Figure 1. Correspondence between selected contigs from transcriptomic information (Haney 2014, Haney 2016)the protein name as well as its abbreviation. Oligonucleotides desgined for PCR amplification from cDNA are also shown. In bold, restriction sites for cloning in pPICZαA expression vector, the Kex2 site is underlined and the STOP codon is highlighted in italics. The selected contigs sequences alignments shows conservation of the cysteine pattern arrangement. Black arrows indicate the predicted cleavage site of the signal peptide, (SignalP, Arachnoserver (Pineda 2018)). Conserved residues are backgrounded in black, conservative substitutions appear in grey and non-conserved residues remain with white blackground.

Protein production and purification

To produce recombinant versions of LtdI and II, 10 µg of each plasmid were digested using PmeI (New England Biolabs, Boston-MA) and used to transform electrocompetent KM71 cells by electroporation on a Bio-Rad Gene-Pulser apparatus as described (Martínez-Ruiz 1998). pPICZα plasmid confers resistance to zeocin. Upon electroporation, 1mL of cold 1M sorbitol was added to cells and incubated for 1h on ice followed by 4h incubation at 30°C 200rpm, after addition of 1mL of YPD media (1% yeast extract, 2%peptone and 2% dextrose). Yeasts were plated in YPD medium plates containing 1M sorbitol and different concentration of zeocin ranging 100-1500µg/mL. Plates were incubated 3 days at 30°C until resistant colonies appeared. In each case, best producing colony among 4 tested by small production experiments and SDS-

PAGE analysis of extracellular media at different culture times. Selected colonies were used for large-scale production of both LtdI and LtdII in minimal media. 1L of buffered minimal medium containing glycerol (BMG) was used for yeast growth for 24h. Then, culture was concentrated in 200mL of buffered minimal medium containing methanol (BMM) Incubation was carried out at 30°C for 4 days in baffled Erlenmeyer flaks to ensure high aeration and 1mL of pure methanol was added every 12 hours. After protein production, extracellular media was harvested by centrifugation and used to purify the recombinant proteins. After addition of 800 mL of Tris 50mM pH 7.5 to extracellular media, it was incubated at 4°C with soft overnight stirring with 200mL of DEAE-cellulose (Whatman) equilibrated in the same buffer. After collecting non-retained fraction and the chromatographic matrix was loaded onto a 4 cm x 18 cm glass column and washed with the equilibration buffer. Proteins were then eluted with an ionic strength gradient from 0 M to 2 M NaCl. Fractions containing the desired proteins were desalted with a Bio-Gel P2 chromatography, equilibrated in 50mM NH_4HCO_3 pH 7.0 buffer, and then lyophilized. Finally, these proteins were dissolved in 50mM NH_4HCO_3 pH 7.0 buffer to an approximate final concentration of 4mg/mL and further purified by size-exclusion FPLC system ÄKTA Purifier (GE Healthcare Life Sciences) using a Superdex 75 10/300 GL prepacked column (GE Healthcare Life Sciences. Samples containing the protein of interest were evaluated by SDS-PAGE, aliquoted and lyophilized until used.

To produce uniformly labelled $^{13}C/^{15}N$ proteins, the procedure was as described above, but carbon and nitrogen sources were substituted by uniformly ^{13}C and ^{15}N labeled compounds. *P. pastoris* growth step was carried out in BMG containing 2% (w/v) of ^{13}C-glucose (Cambridge Isotope Laboratories (Cambridge, MA)) instead of glycerol as carbon source. For induction phase, BMM was prepared with yeast nitrogen base (YNB) variant without amino acids and supplemented with 1% (w/v) of ^{15}N-$(NH_4)_3SO_4$ (Cambridge Isotope Laboratories (Cambridge, MA)), as nitrogen source, and 0.5% (v/v) ^{13}C-methanol ((Cambridge Isotope Laboratories (Cambridge, MA)) as carbon source. ^{13}C-methanol was also added every 24h of culture. Purification was carried out as previously described.

Characterization of the purified proteins

SDS-PAGE was developed to asses purity of the purified proteins. Protein hydrolysis (5.7M HCl, 24 h, 110°C) and amino acid analyses were carried out as previously described (Álvarez-García 2009, García-Ortega 2005, Lacadena 1995, Martínez-Ruiz 1997, Martínez-Ruiz 1998). These amino acid analyses were performed on a Biochrom 20 automatic analyzer (Pharmacia). Molecular weights of proteins were determined in purified samples dissolved in the same conditions as NMR samples (see below) by matrix-assisted laser desorption ionization time-of-flight (MALDI-TOF) mass spectrometry (Voyager-DE PRO (Applied Biosystems)). Absorbance measurements were performed on a Shimadzu UV-1800 (Tokyo, Japan) at 100nm/min scanning speed, at room temperature in 1 or 0.1 cm optical path cells. Using UV absorbance spectra and the aforementioned amino acid analysis, individual E0.1% were calculated for every single protein. Circular Dichroism (CD) spectra were obtained on a Jasco (Easton, MD) 715 spectropolarimeter. Near and far-UV CD spectra were recorded at 1.0 and 0.2 mg/mL, respectively, in 0.1 M NaCl and 15 mM Mops (pH 7.5). At least six spectra were averaged to obtain the final spectrum. CD measurements were also employed to study the thermal stability of the peptides, by following the ellipticity variation at a characteristic wavelength

determined on the spectra at (207 nm), temperature was constantly increased from 25°C to 85°C at a constant rate of 20°C/hour. Next, the reverse path was taken, cooling the sample at the same speed. Far-UV CD spectra were recorded at 25°C, at 85°C and then again at 25°C after cooling the sample. An identical buffer was used for the fluorescence emission spectra with the proteins at concentrations of 0.2 mg/mL). Their fluorescence emission spectra on an SLM Aminco (Urbana, IL) model 8000 spectrofluorimeter, also as previously described (García-Linares 2014, Pardo-Cea 2011). Briefly, emission spectra was recorded upon excitation at 275nm (for Tyr and Trp emission) and 295 nm (Trp emission). Thermostated cells with 0.2 and 1.0 cm optical paths for the excitation and emission beams, respectively, were used. The temperature was controlled with a circulating water bath (Huber Polystat).

FPLC calibration for molecular weight determination. To determine possible Ltd oligomerization state, a mixtures of proteins (BSA (Sigma-Aldrich), Ova (Sigma-Aldrich), RNase (Sigma-Aldrich) and Pher *S. cerevisiae* (Vitale 2017)) with known molecular weight were loaded in a Superdex G75 10/300 GL prepacked column (GE Healthcare Life Sciences) and were eluted following manufacturer recommendation with sodium phosphate 50mM pH 7.0 NaCl 150mM. Then, a 0.1mg/mL aliquot of LtdII was loaded in the same equilibrated column. Calibration curve was built plotting elution volume of known proteins against their corresponding molecular weight logarithm. LtdII elution volume was interpolated in the calibration curve to obtain its apparent molecular weight.

NMR

NMR samples of LtdII and $^{13}C,^{15}N$-LtdII were prepared at 0.5-1.0 mM protein concentration in H_2O/D_2O 9:1 v/v at pH ~4.0. The pH was measured with a glass microelectrode and was not corrected for isotope effects. Spectra were recorded at 25 °C on a Bruker AV800 spectrometer equipped with a TCI cryoprobe and operating at 800.1 MHz for the proton. Using $^{13}C,^{15}N$-LtdII samples, the following experiments were acquired: 2D ^{1}H-^{15}N HSQC and 3D HNCO, HNcaCO, HNCA, HNcoCA, CBCANH, CBCAcoNH, HcccoNH and CccoNH experiments. Using LtdII samples, 2D homonuclear 2D ^{1}H-^{1}H TOCSY, ^{1}H-^{1}H NOESY and ^{1}H-^{13}CHSQC were recorded. Spectra were processed using either TOPSPIN v2.1 pl6 (Bruker, Inc) or NMRpipe (Delaglio 1995) and the istHMS reconstruction method was used to process the 3D spectra acquired using NUS (Hyberts 2009). The spectra were analyzed with the help of the SPARKY software (Goddard and Kneller 2005).

Insecticidal activity

Insecticidal activity of LtdII was evaluated by means of tests performed by injection into the beet armyworm *Spodoptera exigua* (Hübner) (Lepidoptera: Noctuidae) (Figure 2) commonly known as gardama or green doughnut. The aim of the study was to evaluate the lethal effect of LtdII on the last instar larvae (L5) of this insect which is a major polyphagous pest of numerous crops in greenhouses and open fields, such as tomato, pepper, lettuce, cabbage, cotton and

Figure 2. *Spodoptera exigua* (Hübner) larvae.

alfalfa (Smagghe 2003). Two different protein concentrations were evaluated, 25 and 50 µM, and a 0.9% (w/v) NaCl solution was used as a control. Apparently healthy larvae with similar size were selected and individually weighed on a precision scale before being injected to ensure did not show any significant difference among them. All experiments were made by duplicate, by injecting 4µL of each of each protein solutions and the same volume of the control into 20 larvae per treatment with a Hamilton microsyringe (Burkard, UK). ProGel® food-grade blue dye added to the corresponding solutions of proteins or NaCl was used as color indicator, in order to check that the entire volume loaded into the syringe had completely penetrated the larvae. Upon injection, the percentage of dead larvae, the number of days until they died, the time it took for the survivors to reach adulthood and, in this case, the number of days they were in pupation were all evaluated.

Antifungal activity

The fungal strains used were deposited in the collection of the laboratory of fungi and mycotoxins of the Teaching Unit of Microbiology at the Faculty of Biology (Complutense University of Madrid). They were isolated from oat and corn samples, and their classification was confirmed by molecular techniques (Garcia-Diaz 2020). They included *Fusarium proliferatum* (F2, maize; F47, maize), *F. verticillioides* (F1, maize; F48, oat), *F. graminearum* (F61, maize), *F. langsethiae* (F23, oats), *Aspergillus niger* (N1, oats), *A. welwitschiae* (N6, maize), *A. flavus* (A10, oats), and *A. parasiticus* (A19, maize). All of them were maintained by regular subculturing on Czapek Dox Modified Agar (Pronadisa, Madrid, Spain). Spore suspensions of 10^5 spores/mL in 0.9% (w/v) NaCl were obtained from a sporulating culture (7 day-old) on Czapek-Dox Modified Agar, and filtered through Whatman #1 paper. Spore concentrations were measured by microscopy using a Thoma counting chamber and the suspension was diluted to the final concentration

The effect of LtdII at different concentrations on fungal growth were evaluated using the method previously described (Patiño 2018). Briefly, 200µL of spore suspension of each fungal strain were inoculated in 90 mm diameter plates with Czapek Dox Modified Agar. Subsequently, 6 mm diameter cellulose discs containing 10 µL of LtdII at different protein concentrations (7 µg/µL, 3.5 µg/µL, 1.4 µg/µL and 0.7 µg/µL) were deposited on the plated and incubated for 3 days at 25°C. The effect of the protein was evaluated by the appearance of clear growth inhibition halos around the protein disks. All assays were carried out in triplicate. As a positive control of antifungal activity, the very well-known antifungal protein from *Fusarium graminearum* (FgAFP) (Patiño 2018) was also employed.

After this preliminary screening, only the four species of great importance in maize crops were further analysed: F2, F48, N1 and A10. They were inoculated on 55 mm diameter plates containing 30 µL of the proteins, at a concentration of 1.5 µg/µL, which had been spread over the surface of the Modified Czapek Dox Agar. In the centre of the plate 2 µL of spore suspensions were inoculated (10^5 spores/mL). For each species, a control without protein was performed. These plates were maintained at 25°C and the diameter of the surface grown by each fungus was measured 8 times along 121 h. After the test, these values representing fungal growth were plotted against time. The slope of the resulting curve was considered as the specific growth rate. The lag phase of each fungus was also estimated. Measurements were then analysed with the

Microsoft Excel® software version 15.32 (Microsoft Corporation, USA). All tests were carried out in triplicate.

Statistical analyses were performed with the StatGraphics Centurion XVII® software (Statpoint Technologies, Inc., USA). The data, both growth rate and lag phase, were first found to be normally distributed and homoscedastic. The Shapiro-Wilk and Levene tests were used for this purpose, respectively. Once these two criteria were checked, an analysis of variance (ANOVA) was performed. Fisher's LSD was used for the POST HOC analysis and a significance level p≤0,05 was established in all cases. The growth rate and the lag phase time were taken as dependent variables, with each treatment being independent, and compared with each other and with the control.

Results and Discussion

LtdI and II were successfully cloned, produced and purified

Ltds were successfully cloned from cDNA and inserted into the pPICZαA expression vector. Sanger sequencing revealed amino acid changes with respect to the expected sequence regarding transcriptomic information (Figure 3). Computed parameters for protein cloned sequences were obtained by ProtParam (ExPASy Server) (Gasteiger 2003)(Table 1).

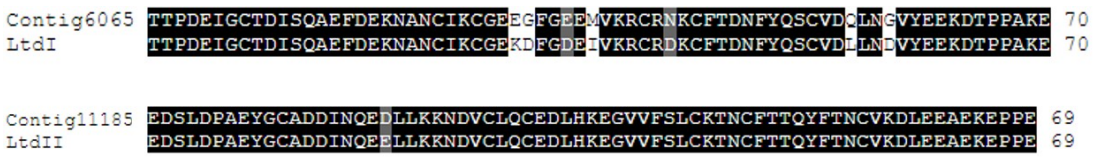

Figure 3. Sequence alignment between selected *L. hesperus* contigs obtained from transcriptomic information (Haney 2014) and the corresponding Sanger sequenced cDNAs cloned in the pPICZαA production vector. Contig6065 and Contig 11185 are the original sequences from the transcriptomic assembly whereas LtdI and LtdII are the cDNA sequences which were finally cloned.

The small-scale production of four colonies selected for each Ltd revealed in both cases the production of a very predominant protein in the yeast's extracellular medium. For no reason in particular, other than it was more quickly cloned, LtdII was the peptide that was studied first and, so far, it is known in higher detail. This explains why many of the data shown in this manuscript mostly refer to LtdII. An identical characterization of LtdI is in progress, but only the already well-proven results obtained so far for LtdII are reported here.

Table 1. Computed physicochemical parameters of LtdI and LtdII obtained via ProParam ExPASy analysis tool (Gasteiger 2005)

	Number of amino acids	Molecular weight (Da)	Theoretical pI value	Tyr	Trp	$E^{0.1\%}$ *
LtdI	70	7990	4.24	2	0	0.420
LtdII	69	7877	4.11	2	0	0.426

*Absorbance for a solution at 0.1 mg/mL assuming all pairs of Cys residues form cystines

After applying the protocol designed (see Materials and Methods section and Table 1), previously designed considering their acidic character and small size, both LtdI and II were purified to homogeneity according to their electrophoretic analysis in 0.1% SDS-17% PAGE. Electrophoretic mobility was however blurred and slower than expected for their molecular weight, what it is easily explained because it is known that proteins with such acidic isoelectric point values display anomalous electrophoretic migration [23] (Figure 4). Nevertheless, the correct molecular mass of LtdII was then confirmed by mass spectrometry analysis. This spectrum showed a good signal to noise ratio that allowed distinguishing a major intense peak at 7876.3 m/z, compatible not only with the expected molecular weight of LtdII, but also that all Cys residues were oxidized forming disulfide bonds (Figure 5).

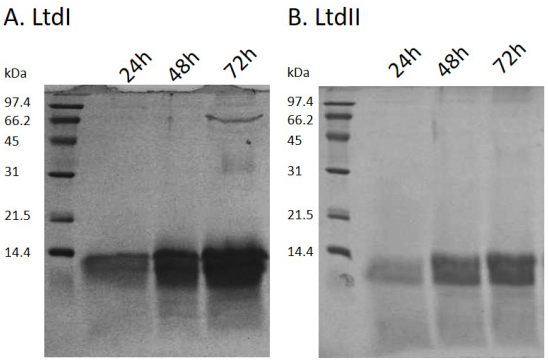

Figure 4. Small scale production of LtdI (A) and LtdII (B) by *P. pastoris* KM71H. Induction was maintained for 72h by adding methanol (5.0%) every 24 h.

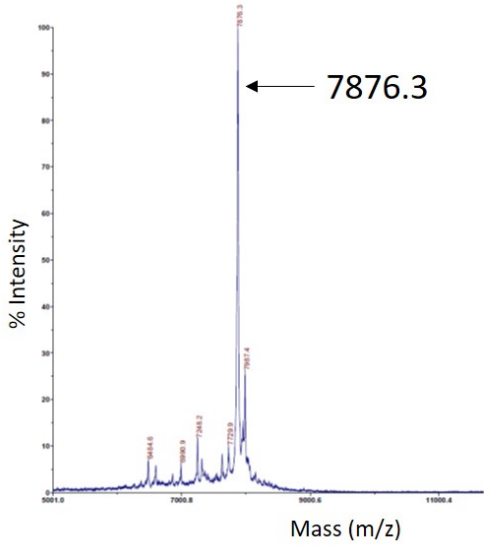

Figure 5. Mass spectrometry spectrum of purified LtdII. The most intense peak at 7876.3 m/z corresponds to the expected size of 7877 Da for LtdII if all its Cys residues are oxidized.

LtdI and II are dimeric and highly thermostable α-helical rich peptides

Size-exclusion chromatography behavior of both LtdI (not shown) and LtdII (Figure 6) yielded molecular weight values for the native peptides of around 13000 Da. The expected molecular weights for the monomeric species were about 7.99 KDa for LtdI and 7.87 for LtdII (Table 1). This latter value was indeed confirmed for LtdII in mass spectrometry analysis (Figure 5), as mentioned above. Around half the size calculated for their chromatographic elution volumes. Therefore, it was safe to conclude that both native LtdI and II structures are homodimeric.

Far-UV CD spectra of both peptides was also consistent with an α-helical rich secondary structure showing two characteristic minima centered around 208 nm and 222 nm (Figure 7 Near-FarUV+Tm). Near-UV CD spectrum of LtdII showed a minimum value centered at 275 nm (Figure 7), attributable to a net contribution of its two Tyr residues (Figure 3) which most probably show a very low degree of rotational freedom.

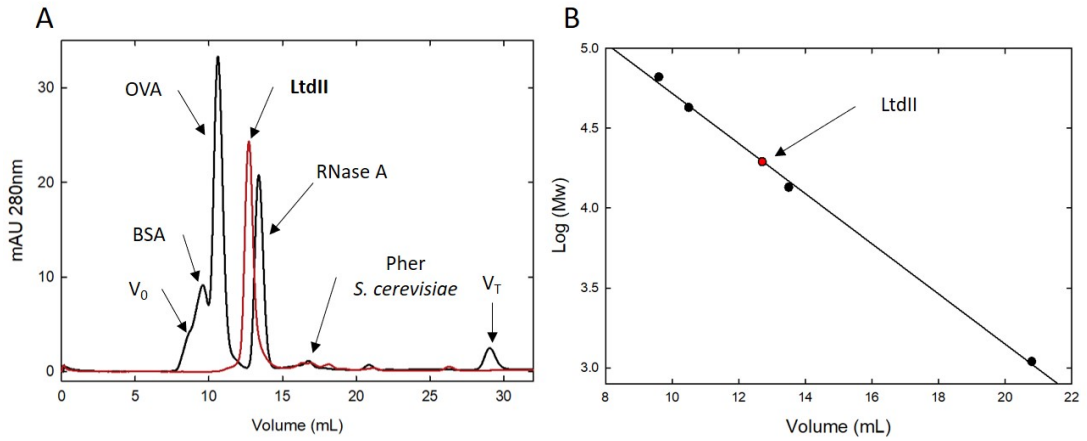

Figure 6. (A) Size-exclusion chromatography elution profile on Superdex G75 column of LtdII (red line)and other proteins of known size (black line) used as standards to calibrate the chromatographic column. V_0 corresponds with the exclusion volume of the column while V_T represents its total volume of the column. (B) Log molecular weight of the proteins used as standards is represented versus elution position yields a straight line from which molecular weight for native conformation of LtdII could be estimated. The red dot represents the interpolated value for LtdII. LtdI shows identical behavior as LtdII (data not shown).

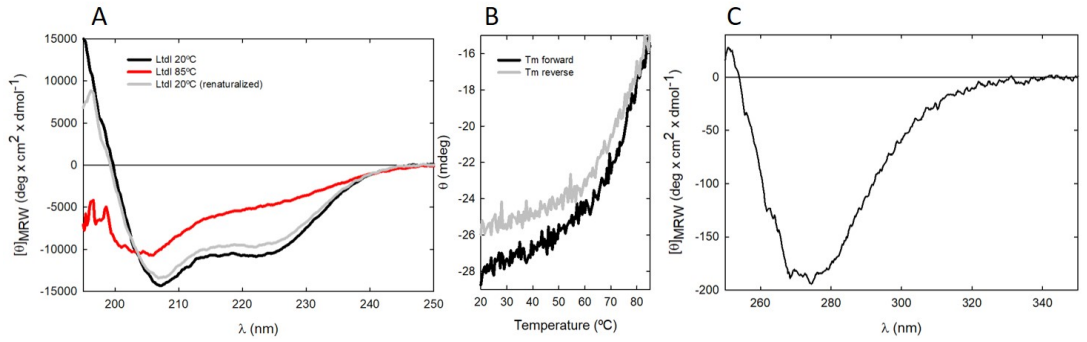

Figure 7. Spectroscopic characterization of LtdII. (A) Far -UV CD spectra at 20 ˚C (black) at 85 ˚C (red) and at 20 ˚C after denatutarion (grey). (B) T_m denaturation represented as ellipticity (Θ – mdeg) against temperature black line represent the denaturation progress by rising the temperature and grey line represent the renaturation process by cooling. (C) Near-UV CD spectra.

The LtdII thermal denaturation curve (Figure 7) showed that at temperatures as high as 85°C the protein is not yet fully unfolded, in good agreement with the presence of three disulfide bonds within its only 70 amino acids long sequence. An assertion which was confirmed by the almost complete renaturation of the protein after slowly cooling to 25 ˚C, as deduced from almost complete recovery of the original far-UV CD spectrum (Figure 7). Preliminary results indicate that LtdI is highly thermostable too (data not shown).

Fluorescence emission spectra did also confirm the complete absence of Trp residues within the LtdI and LtdII amino acid sequences.

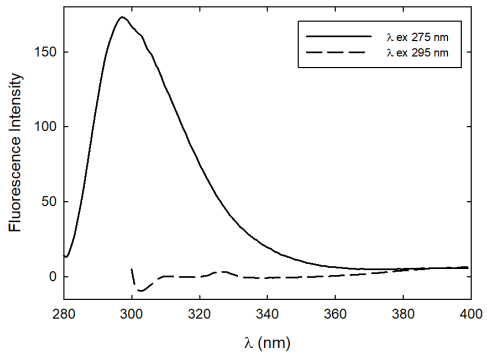

Figure 8. Fluorescence emission spectra of LtdII. Solid and dashed line represents emission upon excitation at 275 and 295 nm respectively. By excitatng at 295 nm only Trp residues would emit fluorescence, since that contribution is null, the peptide lacks such residue as expected.

Not only a single band, centered at 300 nm, was the only emission observed when the protein solutions were excited at 275 nm, but also negligible fluorescence was obtained when using 295 nm as the excitation wavelength (Figure 8 Fluorescence emission). This absence of Trp residues was also consisted with their calculated $E^{0.1\%}$ (280 nm, 1 cm) values of 0.50 and 0.38 for LtdI and LtdII, respectively. Both values were very close to the predicted values taking into consideration their content in aromatic amino acids and disulfide bonds (Pace 1995).

NMR structural characterization of LtdII

The 2D ^{1}H-^{15}N HSQC spectrum of LtdII (Figure 9), in which each residue give rise to a cross-peak corresponding to is ^{1}H and ^{15}N amide nuclei, shows a good signal dispersion, indicating that the protein is well-folded. Combined analyses of a series of 3D NMR spectra (HNCO, HNcaCO, HNCA, HNcoCA, CBCANH, CBCAcoNH) allowed us to achieve the assignment of backbone nuclei (^{1}HN, ^{15}N, $^{13}C'$, $^{13}C\alpha$ and $^{13}C\beta$) for residues 1-30 and 42-69. The low intensity cross-peaks present in the 2D ^{1}H-^{15}N HSQC spectrum do not correspond to the unassigned residues. The reason why the NMR signals for residues 31-41 are not observed remains to be clarified. A plausible explanation might be line broadening due to exchange among interconverting conformations.

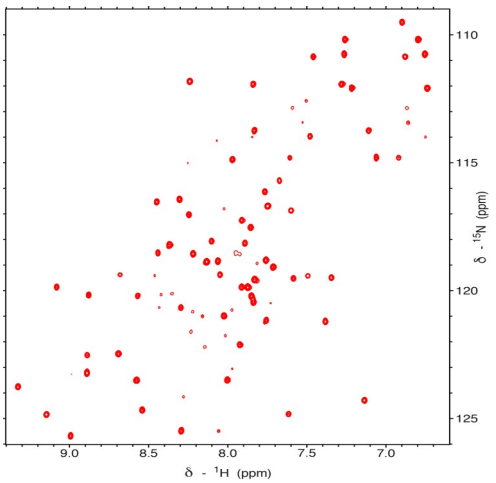

Figure 9. 2D ^{1}H-^{15}N HSQC spectrum of LtdII at pH 4.0 and 25 °C. One backbone amide ^{15}N–^{1}H correlation peak is observed per residue.

In any case, secondary structure can be analysed for the assigned regions from the $^{13}C\alpha$ and $^{13}C\beta$ chemical shift deviations from the reference random coil values (Wishart 1995) ($\Delta\delta = \delta^{observed} - \delta^{random\ coil}$, ppm), which are plotted as a function of sequence in Figure 10. In these plots, the 16-30 and 51-63 segments show positive values for the $^{13}C\alpha$ chemical shift deviations and negative values for the $^{13}C\beta$ chemical shift deviations (Figure 10), which evidences that these two regions are helical. This agrees with the secondary structure predicted from LtdII sequence by the program Psipred (http://bioinf.cs.ucl.ac.uk/psipred/; (Figure 11). The 3D structure was not calculated because of the unassigned residues. Instead, NMR study of the ^{13}C,^{15}N-LtdI protein is currently underway to see if the line broadening of residues 31-41 persists or, hopefully, disappears.

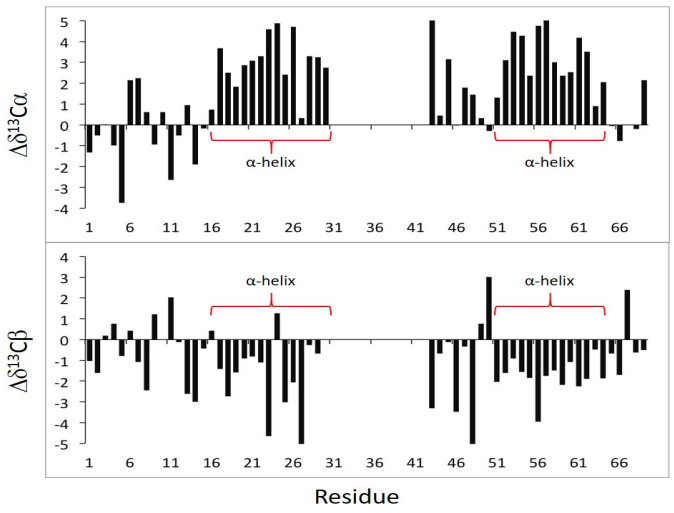

Figure 10. Chemical shift deviations of ^{13}Cα (up) and ^{13}Cβ (down) nucleus of LtdII protein backbone residues. Δδ^{13}Cα positive values and Δδ^{13}Cβ plot negative values corresponding with an α-helical secondary structure are bracket in red. The values for the 31-42 residues are missing because their chemical shift could not be assigned due to signal broadening under the experimental conditions used up to now.

In the meantime, it is interesting to notice that the only available Ltds orthologue peptide structure, from crustacean hyperglycemic hormone (CHH-L) from the crab Scylla olivacea, greatly resembles the secondary structure experimentally determined for LtdII (Figure 12). Three-dimensional structure prediction with the on-line software Phyre2 (Kelley 2015) returned a structure compatible with NMR elucidations and estimated three disulfide bonds with the CHH-L distribution (Figure 12).

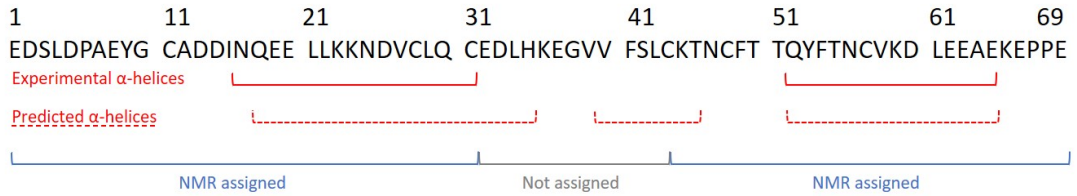

Figure 11. Solid red brackets under LtdII sequence highlights α-helical secondary structure regions according to ^{13}C chemical shifts. Dashed red brackets indicates predicted ordered secondary structure by PsiPred server. Finally, blue brackets indicated already assigned residues by three-dimensional ^{1}H, ^{13}C, ^{15}N NMR spectra and the grey bracket indicates the unassigned region.

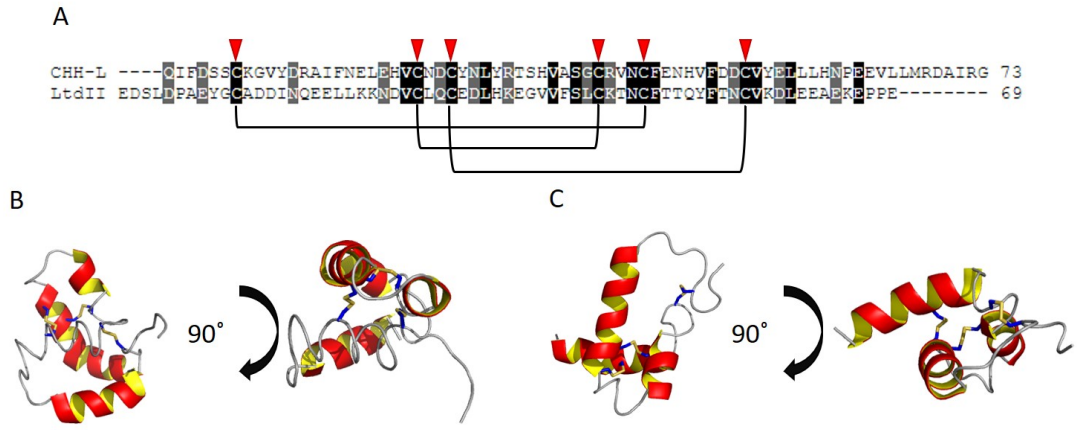

Figure 12. (A) Sequence alignment between LtdII and its orthologue peptide CHH-L (5XS1_A). Cys residues are indicated with red arrows. Brackets under the alignment indicate the disulfide bonds observed for CHH-L and predicted for LtdII. Conserved residues are backgrounded in black, conservative substitutions appear in grey and non-conserved residues remain with white blackground. (B) CHH-L three-dimensional structure solved by NMR method (PDB: 5XS1). (C) LtdII predicted structure with Phyre2 software (Kelley 2015). α-helices in red-yellow and disordered loops are grey. Cys residues forming disulfide bonds are highlighted in blue-yellow.

LtdII does not show insecticidal activity

Only at the higher tested concentration LtdII caused more mortality (50%) than the control individua (32%) when this peptide was assayed against *S. exigua* (Hübner) larvae (Table 2). The number of days until death, did also showed statistically significant differences (F = 9.00; df= 2,18; P< 0.0001) between LdtII at 25 µM and the rest of treatments, which can be purely coincidental, as it has no rational explanation and all the other parameters measured showed lack of activity on the insect. Survivors pupated (F = 0.34; df = 2,33; P = 0.71) and reached the adult stage (F = 0.79; df = 2,33; P = 0.46) irrespective of treatment. Identical results were obtained when evaluating the length of the time the larvae remained in their pupal stage (Table 4). Overall, this set of results was interpreted as LtdII not displaying insecticidal activity, at least in the above described conditions assayed against *S. exigua* larvae.

Table 2. Mortality and days to death of *Spodoptera exigua* fifth instar larvae after injection with LtdII (25 and 50 µM) or the control solution (0.9 % (w/v) NaCl), and pupation time and time to reach adulthood of survivors.

	Concentration (µM)	Mortality (%)	Days to death (d)	Pupation time (d)	Time to adulthood (d)
Control	-	32	$2.17_a \pm 0.17$	$7.69_a \pm 0.17$	$12.85_a \pm 0.39$
LtdII	25	28	$4.20_b \pm 0.66$	$7.69_a \pm 0.17$	$13.08_a \pm 0.31$
	50	50	$2.30_a \pm 0.21$	$7.50_a \pm 0.22$	$12.40_a \pm 0.43$

Data (mean ± standard error) in the same column followed by the same letter are not significantly different (ANOVA, LSD. P≥0.05).

LtdII does not show antifungal activity

After incubating the plates at 25°C for 3 days with the cellulose protein containing discs, no growth inhibition was observed. However, around the cellulose discs appeared areas with higher sporulation, in all cases except in strains F61 and F48 (*F. graminearum* and *F. verticillioides*). Unfortunately, these areas did not appear to be related either to the amount of protein within the disc assayed (Figure 13C and 13D). For example, the most obvious effects appeared mostly around discs with a concentration of 3.5 µg/µL. Furthermore, in the specific case of the A19 strain, which produces aflatoxins of the *A. parasiticus* species, a notable change in pigmentation appeared at different

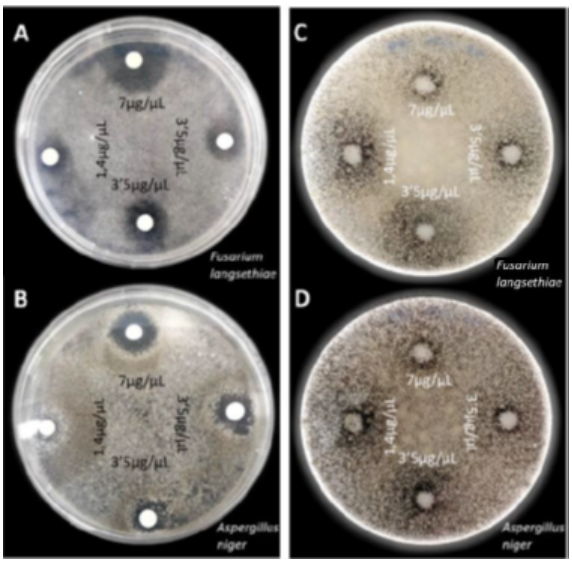

Figure 13. Representative examples of the growth inhibition effect of FgAFP (A and B) and LtdII (C and D) on two different fungal species, *F. langsethiae* and *A. niger*.

concentrations, with green aspect at 7 µg/µL and 1.4 µg/µL; and yellow at 3.5 µg/µL and 0.7 µg/µL (Figure 14).

The results of the effect of surface spread proteins on the growth of *A. flavus*, *F. proliferatum*, *F. verticillioides*, and *A. niger* are shown in Figure 15. While the antifungal control peptide FgAFP showed a strong inhibitory effect against all four different fungi species assayed, as described before(Patiño 2018), LtdII kept on showing no signs of antifungal activity at all the protein concentrations assayed. All data presented normality and homoscedastic it under Levene and Shapiro-Wilk tests.

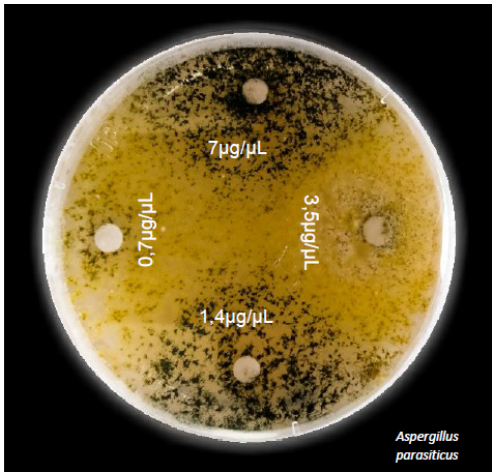

Figure 14. Effect of LtdII on *A. parasiticus* growth.

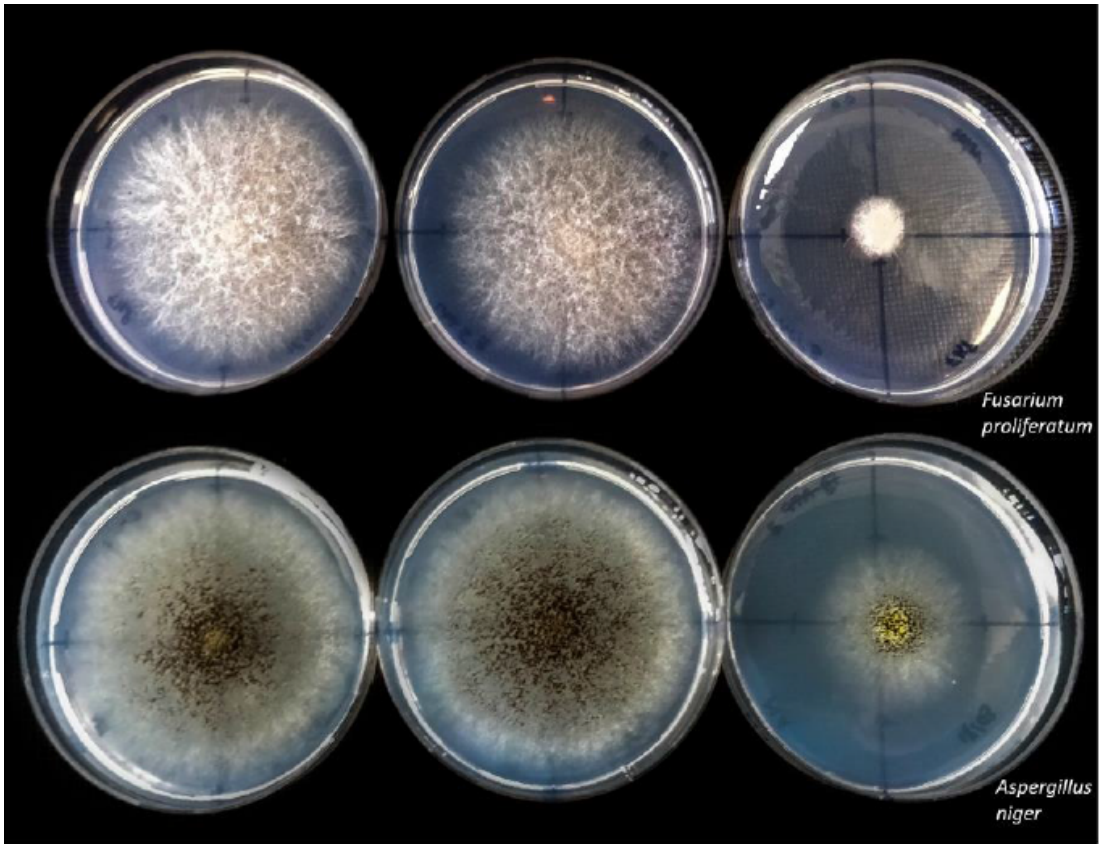

Figure 15. Representative examples of the growth inhibition effect of surface spread FgAFP (right plates) and LtdII (central plates) on two different fungal species, *F. proliferatum* and *A. niger*. Left plates: controls without protein.

Overall, the antimicrobial assays performed showed that neither in the initial screening, nor in later trials, did the LtdII spider toxin inhibit the growth of any of the fungi assayed, although areas with greater sporulation did appear. This observation, as well as the pigmentation changes observed in *Aspergillus parasiticus* (Han 1998), suggest that the fungi were however under stress conditions (Adams 1998) in the presence of LtdII. Therefore, it seems

that this protein, although it does not impede the growth of the fungi, can interact with them affecting the sporulation and the production of secondary metabolites. Further studies are however needed in order to clarify the potential role of Ltds on fungal growth and metabolism.

Conclusions

Latrodectins are one of the most highly expressed toxins in *L. hesperus* venom. Cloned sequences from cDNA included minor amino acid changes in comparison with transcriptomic data which can be easily explained because last generation high-throughput transcriptome assembly is performed by overlapping small fragments which were obtained after massively sequencing the venom mRNA [28, 29]. This process is especially difficult when determining the sequence of small mRNAs and assembly is performed *de novo* instead of using an available genome as template. Overall, this procedure can lead to small differences between the sequences deposited in databases and those actually found in the cDNA extracted from animals. Finally, it cannot be either discarded the existence of intrinsic polymorphic variations between individuals which could also explain the sequence changes observed.

LtdI and LtdII were successfully cloned and overproduced in the yeast *P. pastoris* and their purification was performed using a protocol designed according to their physicochemical characteristics. Their chromatographic behavior and spectra were compatible with α-helical rich structures, whose existence has been confirmed for LtdII after the analysis of its three-dimensional structure by NMR. Both proteins, LtdI and II are highly thermostable, most probably due to the presence of their three disulfide bonds. Unfortunately, Ltds function remains obscure since they do not seem to show either insecticidal or antifungal activity, at least in the case of LtdII. Therefore, after all these results, the original hypothesis that the role of these small proteins would be to collaborate with latrotoxins in the formation of a complex macromolecular toxic structure on the surface of neuronal synapses gains strength. A hypothesis that, in any case, still awaits direct, unequivocal demonstration when producing and purifying any of the giant membrane pore-forming *L. hesperus* LTXs.

References

Adams, T.H., Wieser, J.K., and Yu, J.H. (1998) "Asexual Sporulation in Aspergillus Nidulans." *Microbiol Mol Biol Rev* 62, 1: 35-54.

Álvarez-García, E., García-Ortega, L., De los Ríos, V., Gavilanes, J.G., and Martínez-del-Pozo, A. (2009) "Influence of Key Residues on the Heterologous Extracellular Production of Fungal Ribonuclease U2 in the Yeast *Pichia Pastoris*." *Protein Expr Purif* 65, 2: 223-229.

Camp, N.E. (2014) "Black Widow Spider Envenomation." *J Emerg Nurs* 40, 2: 193-194.

Chomczynski, P. (1993) "A Reagent for the Single-Step Simultaneous Isolation of Rna, DNA and Proteins from Cell and Tissue Samples." *Biotechniques* 15, 3: 532-534, 536-537.

Delaglio, F., Grzesiek, S., Vuister, G.W., Zhu, G., Pfeifer, J., and Bax, A. (1995) "Nmrpipe: A Multidimensional Spectral Processing System Based on Unix Pipes." *J Biomol NMR* 6, 3: 277-293.

Frontali, N., Ceccarelli, B., Gorio, A., Mauro, A., Siekevitz, P., Tzeng, M.C., and Hurlbut, W.P. (1976) "Purification from Black Widow Spider Venom of a Protein Factor Causing the Depletion of Synaptic Vesicles at Neuromuscular Junctions." *J Cell Biol* 68, 3: 462-479.

Garb, J.E. (2014) "Extraction of Venom and Venom Gland Microdissections from Spiders for Proteomic and Transcriptomic Analyses." *J Vis Exp*, 93: e51618.

Garcia-Diaz, M., Gil-Serna, J., Vazquez, C., Botia, M.N., and Patino, B. (2020) "A Comprehensive Study on the Occurrence of Mycotoxins and Their Producing Fungi During the Maize Production Cycle in Spain." *Microorganisms* 8, 1.

García-Linares, S., Richmond, R., García-Mayoral, M.F., Bustamante, N., Bruix, M., Gavilanes, J.G., and Martínez-del-Pozo, A. (2014) "The Sea Anemone Actinoporin (Arg-Gly-Asp) Conserved Motif Is Involved in Maintaining the Competent Oligomerization State of These Pore-Forming Toxins." *FEBS J* 281, 5: 1465-1478.

García-Ortega, L., Lacadena, J., Villalba, M., Rodríguez, R., Crespo, J.F., Rodríguez, J., Pascual, C., Olmo, N., Oñaderra, M., Martínez-del-Pozo, A., and Gavilanes, J.G. (2005) "Production and Characterization of a Noncytotoxic Deletion Variant of the *Aspergillus Fumigatus* Allergen Asp F 1 Displaying Reduced Ige Binding." *FEBS J* 272, 10: 2536-2544.

Gasparini, S., Kiyatkin, N., Drevet, P., Boulain, J.C., Tacnet, F., Ripoche, P., Forest, E., Grishin, E., and Menez, A. (1994) "The Low Molecular Weight Protein Which Co-Purifies with Alpha-Latrotoxin Is Structurally Related to Crustacean Hyperglycemic Hormones." *J Biol Chem* 269, 31: 19803-19809.

Gasteiger, E., Gattiker, A., Hoogland, C., Ivanyi, I., Appel, R.D., and Bairoch, A. (2003) "Expasy: The Proteomics Server for in-Depth Protein Knowledge and Analysis." *Nucleic Acids Res* 31, 13: 3784-3788.

Goddard, T.D., and Kneller, D.G. (2005) "Sparky 3, University of California, San Francisco."

Grishin, E.V. (1998) "Black Widow Spider Toxins: The Present and the Future." *Toxicon* 36, 11: 1693-1701.

Han, S.J., Lee, B.J., and Kang, H.S. (1998) "Purification and Characterization of the Nuclear Ribonuclease P of *Aspergillus Nidulans*." *European Journal of Biochemistry* 251244-251.

Haney, R.A., Ayoub, N.A., Clarke, T.H., Hayashi, C.Y., and Garb, J.E. (2014) "Dramatic Expansion of the Black Widow Toxin Arsenal Uncovered by Multi-Tissue Transcriptomics and Venom Proteomics." *Bmc Genomics* 15366.

Haney, R.A., Clarke, T.H., Gadgil, R., Fitzpatrick, R., Hayashi, C.Y., Ayoub, N.A., and Garb, J.E. (2016) "Effects of Gene Duplication, Positive Selection, and Shifts in Gene Expression on the Evolution of the Venom Gland Transcriptome in Widow Spiders." *Genome Biol Evol* 8, 1: 228-242.

Hyberts, S.G., Frueh, D.P., Arthanari, H., and Wagner, G. (2009) "Fm Reconstruction of Non-Uniformly Sampled Protein Nmr Data at Higher Dimensions and Optimization by Distillation." *J Biomol NMR* 45, 3: 283-294.

Kelley, L.A., Mezulis, S., Yates, C.M., Wass, M.N., and Sternberg, M.J. (2015) "The Phyre2 Web Portal for Protein Modeling, Prediction and Analysis." *Nat Protoc* 10, 6: 845-858.

Kiyatkin, N., Dulubova, I., Chekhovskaya, I., Lipkin, A., and Grishin, E. (1992) "Structure of the Low Molecular Weight Protein Copurified with α-Latrotoxin." *Toxicon* 30, 7: 771-774.

Lacadena, J., Martínez-del-Pozo, A., Gasset, M., Patiño, B., Campos-Olivas, R., Vázquez, C., Martínez-Ruiz, A., Mancheño, J.M., Oñaderra, M., and Gavilanes, J.G. (1995) "Characterization of the Antifungal Protein Secreted by the Mould *Aspergillus Giganteus*." *Arch Biochem Biophys* 324, 2: 273-281.

López-García, B., Moreno, A.B., San Segundo, B., De los Ríos, V., Manning, J.M., Gavilanes, J.G., and Martínez-del-Pozo, A. (2009) "Production of the Biotechnologically Relevant Afp from *Aspergillus Giganteus* in the Yeast *Pichia Pastoris*." *Protein Expr Purif* 70, 2: 206-210.

Martínez-Ruiz, A., Martínez-del-Pozo, A., Lacadena, J., Mancheño, J.M., Oñaderra, M., and Gavilanes, J.G. (1997) "Characterization of a Natural Larger Form of the Antifungal Protein (Afp) from *Aspergillus Giganteus*." *Biochimica et Biophysica Acta - Protein Structure and Molecular Enzymology* 134081-87.

Martínez-Ruiz, A., Martínez-del-Pozo, A., Lacadena, J., Mancheño, J.M., Oñaderra, M., López-Otín, C., and Gavilanes, J.G. (1998) "Secretion of Recombinant Pro- and Mature Fungal α-Sarcin Ribotoxin by the Methylotrophic Yeast *Pichia Pastoris*: The Lys-Arg Motif Is Required for Maturation." *Protein Expr Purif* 12315-322.

McCowan, C., and Garb, J.E. (2014) "Recruitment and Diversification of an Ecdysozoan Family of Neuropeptide Hormones for Black Widow Spider Venom Expression." *Gene* 536, 2: 366-375.

Montagne, N., Desdevises, Y., Soyez, D., and Toullec, J.Y. (2010) "Molecular Evolution of the Crustacean Hyperglycemic Hormone Family in Ecdysozoans." *BMC Evol Biol* 1062.

Orlova, E.V., Rahman, M.A., Gowen, B., Volynski, K.E., Ashton, A.C., Manser, C., van Heel, M., and Ushkaryov, Y.A. (2000) "Structure of α-Latrotoxin Oligomers Reveals That Divalent Cation-Dependent Tetramers Form Membrane Pores." *Nat Struct Biol* 7, 1: 48-53.

Pace, C.N., Vajdos, F., Fee, L., Grimsley, G., and Gray, T. (1995) "How to Measure and Predict the Molar Absorption Coefficient of a Protein." *Protein Science* 42411-2423.

Pardo-Cea, M.A., Castrillo, I., Alegre-Cebollada, J., Martínez-del-Pozo, A., Gavilanes, J.G., and Bruix, M. (2011) "Intrinsic Local Disorder and a Network of Charge-Charge Interactions Are Key to Actinoporin Membrane Disruption and Cytotoxicity." *FEBS J* 278, 12: 2080-2089.

Patiño, B., Vázquez, C., Manning, J.M., Roncero, M.I.G., Córdoba-Canero, D., Di Pietro, A., and Martínez-del-Pozo, A. (2018) "Characterization of a Novel Cysteine-Rich Antifungal Protein from *Fusarium Graminearum* with Activity against Maize Fungal Pathogens." *Int J Food Microbiol* 28345-51.

Pescatori, M., Bradbury, A., Bouet, F., Gargano, N., Mastrogiacomo, A., and Grasso, A. (1995) "The Cloning of a Cdna Encoding a Protein (Latrodectin) Which Co-Purifies with the Alpha-Latrotoxin from the Black Widow Spider Latrodectus Tredecimguttatus (Theridiidae)." *Eur J Biochem* 230, 1: 322-328.

Pineda, S.S., Chaumeil, P.A., Kunert, A., Kaas, Q., Thang, M.W.C., Le, L., Nuhn, M., Herzig, V., Saez, N.J., Cristofori-Armstrong, B., Anangi, R., Senff, S., Gorse, D., and King, G.F. (2018) "Arachnoserver 3.0: An Online Resource for Automated Discovery, Analysis and Annotation of Spider Toxins." *Bioinformatics* 34, 6: 1074-1076.

Smagghe, G., Pineda, S., Carton, B., Del Estal, P., Budia, F., and Vinuela, E. (2003) "Toxicity and Kinetics of Methoxyfenozide in Greenhouse-Selected Spodoptera Exigua (Lepidoptera: Noctuidae)." *Pest Manag Sci* 59, 11: 1203-1209.

Sudhof, T.C. (2001) "Alpha-Latrotoxin and Its Receptors: Neurexins and Cirl/Latrophilins." *Annu Rev Neurosci* 24933-962.

Ushkaryov, Y. (2002) "A-Latrotoxin: From Structure to Some Functions." *Toxicon* 40, 1: 1-5.

Ushkaryov, Y.A., Rohou, A., and Sugita, S. (2008) "A-Latrotoxin and Its Receptors." *Handb Exp Pharmacol*, 184: 171-206.

Vitale, S., Partida-Hanon, A., Serrano, S., Martínez-del-Pozo, A., Di Pietro, A., Turrà, D., and Bruix, M. (2017) "Structure-Activity Relationship of A Mating Pheromone from the Fungal Pathogen *Fusarium Oxysporum*." *J Biol Chem* 292, 9: 3591-3602.

Volkova, T.M., Pluzhnikov, K.A., Woll, P.G., and Grishin, E.V. (1995) "Low Molecular Weight Components from Black Widow Spider Venom." *Toxicon* 33, 4: 483-489.

Wishart, D.S., Bigam, C.G., Holm, A., Hodges, R.S., and Sykes, B.D. (1995) "1h, 13c and 15n Random Coil Nmr Chemical Shifts of the Common Amino Acids. I. Investigations of Nearest-Neighbor Effects." *J Biomol NMR* 5, 1: 67-81.

Article VI

Heterologous production and characterization of δ-latroinsectotoxin, a huge insecticidal protein from black widow spider venom

Esperanza Rivera-de-Torre[1], Sara García-Linares[1], José G. Gavilanes[1], Jessica E. Garb[2] and Álvaro Martínez-del-Pozo[1]

[1]Department of Biochemistry and Molecular Biology, Faculty of Chemistry, Complutense University, 28040 Madrid, Spain.

[2]Department of Biological Sciences, University of Massachusetts Lowell, Lowell, MA, USA.

La población mundial ha ido aumentando exponencialmente desde principios del siglo XX. Las Naciones Unidas estiman que alcanzaremos los 9.000 millones para 2050. Dicho incremento viene acompañado de una demanda de alimentos creciente. Por lo tanto, las pérdidas de cosechas por plagas, o por el cambio climático, suponen un problema mundial al que hay que hacer frente. Los venenos animales son mezclas complejas de moléculas tóxicas altamente especializadas. La arañas viuda negra (*Latrodectus* spp.) son cazadoras profesionales de insectos que, como parte de su cóctel tóxico, producen una familia de enormes proteínas tóxicas (110-140kDa), conocidas como latrotoxinas (LTXs), que, cuando son purificadas a partir del veneno crudo, aparecen en asociación con otras proteínas, éstas de bajo peso molecular (7-8kDa), conocidas como latrodectinas (Ltds). La actividad tóxica de las LTXs se basa en la formación de poros oligoméricos en las membranas de las células de las uniones neuromusculares, que provocan una liberación masiva de neurotransmisores que se traduce en intenso dolor y parálisis. Aún no se conoce si sólo la presencia de LTX es suficiente para formar un poro, o si también se necesita la presencia de otros componentes del veneno como las mencionadas Ltds. Tampoco se conoce si realmente hace falta en todos los casos la presencia de receptores proteicos específicos en las membranas que constituyen su diana, si bien lo razonable es pensar que así sea. Las LTXs se clasifican según la especificidad de presa. Dentro de este grupo, las latroinsectotoxinas (LITs) constituyen una subfamilia de toxinas que afectan exclusivamente a los insectos. Con el fin de estudiar las relaciones estructurales y funcionales dentro del presumible complejo macromolecular formado por LITs, y poder hacerlo además en condiciones controladas y sin la contaminación cruzada inherente a la purificación de proteínas a partir del veneno crudo, se abordó la clonación y producción heteróloga de una de estas proteínas. Concretamente, se planteó producir la δ-LIT de *L. hesperus* en el sistema de producción recombinante que constituye la levadura *Pichia pastoris*. Este sistema, además de ser especialmente adecuado para la producción de proteínas de eucariotas ricas en enlaces disulfuro, tiene la ventaja adicional de ser un organismo considerado como GRAS (*Generally Regarded As Safe*). Con este propósito, δ-LIT se clonó en un vector adecuado a partir de cDNA de *L. hesperus* y se consiguió producir en cantidad suficiente como para llevar a cabo su purificación a homogeneidad, si bien el protocolo diseñado todavía debe ser optimizado. Eventualmente, esta optimización, así como su posterior caracterización detallada, permitirá

plantear su utilización, sola o en combinación con otras proteínas de araña, como bioinsecticida ecológicamente sostenible.

PhD candidate contributions

Esperanza Rivera de Torre conceived, designed and conducted most of the experiments as well as significantly contributed to analyze and discuss the results, writing and correcting the manuscript, and suggesting modifications.

Abstract

The world's population has been increasing exponentially since the beginning of the 20th century. The United Nations estimates that we will reach 9 billion by 2050. This increase is accompanied by a growing demand for food. Crop losses due to pests, or climate change, are therefore a global problem that must be addressed. Animal venoms are complex mixtures of highly specialized toxic molecules. Black widow spiders (Latrodectus spp.) are professional insect hunters that, as part of their toxic cocktail, produce a family of huge toxic proteins (110-140kDa), known as latrotoxins (LTXs), which, when purified from raw venom, appear in association with other proteins of much lower molecular weights (7-8kDa), known as latrodectins (Ltds). The toxic activity of LTXs is based on the formation of oligomeric pores in the cell membranes of neuromuscular junctions, which cause a massive release of neurotransmitters that results in intense pain and paralysis. It is not yet known if only the presence of LTX is enough to form a pore, or if the presence of other components of the poison, such as the mentioned Ltds, is also needed. It is also not known if the presence of specific protein receptors in the target membranes is necessary in all cases, although it is reasonable to think so. LTXs are classified according to prey specificity. Within this group, latroinsectotoxins (LITs) constitute a subfamily of toxins that affect exclusively insects. In order to study the structural and functional relationships within the presumed macromolecular complex formed by LITs, and also to be able to do so under controlled conditions, and without the cross-contamination inherent to the purification of proteins from raw venom, the cloning and heterologous production of one of these proteins was intended. Specifically, it was proposed to produce the δ-LIT of L. hesperus in the recombinant production system that constitutes the yeast Pichia pastoris. This system, besides being especially suitable for the production of eukaryotic proteins rich in disulfide bonds, has the additional advantage of being an organism considered as GRAS (Generally Regarded As Safe). For this purpose, δ-LIT was cloned in a suitable vector from cDNA of L. hesperus and then was produced in enough amount as to carry out its purification to homogeneity, although the used procedure still needs to be optimized. Eventually, this optimization, as well as the subsequent detailed characterization of this δ-LIT, will allow to consider its use, alone or in combination with other spider proteins, as an ecologically sustainable bioinsecticide.

Introduction

Black widow spiders (*Latrodectus spp.*) venom is a complex neurotoxic cocktail composed by proteins, peptides, salts and small metabolites that interfere with the physiological nervous transmission (Garb and Hayashi 2013, Grishin 1999, Grishin 1998, Jelinek 1997, Matsumura 2018, Vetter and Isbister 2008, Yan and Wang 2015). Latrotoxins (LTXs) are toxic proteins specific from *Latrodectus* genera venom that trigger neurotransmitter release by forming Ca^{2+} selective pores within presynaptic neuron membranes (Deak 2009, Fritz 1980, Orlova 2000). LTXs are a superfamily of huge (>100 kDa) acidic (pI ≈4) toxins which are classified attending to their prey specificity. In fact, the general name of the family, latrotoxins, is generally used to refer to those affecting vertebrates, even though it contains only one known member, called α-LTX. Latrocrustaceatoxins (LCTs), with also one single representant known so far (α-LCT), attack crustaceans. Latroinsectotoxins (LITs) are however the biggest group, with five

members (α, β, γ, δ and ε-LIT) targeting specifically insects (Grishin 1998, Kiyatkin 1990, Kiyatkin 1995, Krasnoperov 1990a, b, Rohou 2007, Ushkaryov 2004). Not surprisingly, LITs are the most numerous group, since insects are the most common prey of black widow spiders.

LTXs mechanism of action at the neuromuscular junctions level seems to be very similar for all the members of the family mentioned above (Cull-Candy 1973, Magazanik 1992), although they of course keep their strong prey specificity. The first amino acid sequences of LTXs from certain *Latrodectus* species were yet determined in the 90's (Kiyatkin 1993, Kiyatkin 1990), but during these last years this sequences information has grown exponentially. This is mostly due to the application of high-throughput methods, such as genomics, proteomics and transcriptomics, which have become highly reliable and sensitive, altogether with the facts that scientists make this information accessible at different public repositories or databases (Calvete 2017, Macrander 2018).

LTXs share a common genetic structure and are synthesized as single long mRNA products of intronless genes (Gendreau 2017, Haney 2014, Haney 2016), which are translated into a polypeptide chain ranging from approximately 990 amino acids for δ-LIT up to the more than 1300 residues of fully functional α-LTX. These large products undergo proteolytic processing on both N- and C-terminal ends to deliver the final mature active polypeptide (Dulubova 1996), where two very different regions can be clearly distinguished. The first 450

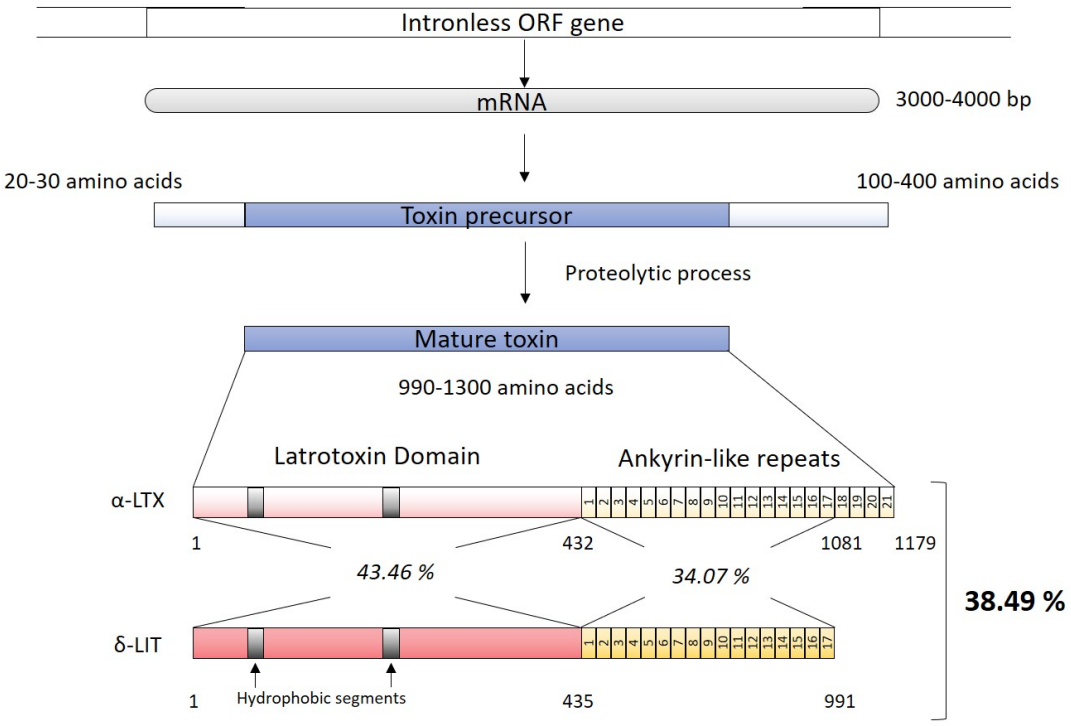

Figure 1. Genetic structure of LTXs. A single mRNA from an intronless gene is translated (ORF stands for *Open Reading Frame*). This protein precursor suffers proteolytic processing on both N and C-termini to obtain the active toxin. Mature proteins have two well-differentiated domains as exemplified in the figure for α-LTX and δ-LIT. The N-terminal fraction characteristic latrotoxin domain, with two conserved hydrophobic segments, followed by ankyrin-like repeats along the C-terminal portion. Numbers in italic correspond to the identity percentage between the indicated domains. The global identity between both full length mature proteins is 38.49% as indicated at the right margin of the figure.

amino acids represent a latrotoxin specific domain, conserved among all LTXs. The remaining C-terminal domain is composed of many ankyrin-like domain repetitions (Figure 1). α-LTX is the most well studied member of the family probably just because is the only one affecting vertebrates. Therefore it has clinical importance, as it is responsible of the severe symptoms of envenomation in humans (Jelinek 1997). It has been purified from *L. mactans tredecimguttatus* crude venom and its membrane bound, very low resolution, structure has been solved by means of cryo-EM using phosphatidylcholine as the membrane mimetic support (Orlova 2000). This structure shows a tetrameric assembly with a Ca^{2+} permeable pore in its center (Figure 2). The resulting three-dimensional structure does not allow, however, definition at the atomic level and thus the detailed structure of any LTX with atomic resolution is still pending. In addition, as explained in previous chapters of this Thesis, LTXs co-purify with acidic low molecular weight peptides known as latrodectins (Kiyatkin 1992), whose presence cannot be discarded in the mentioned solved structure.

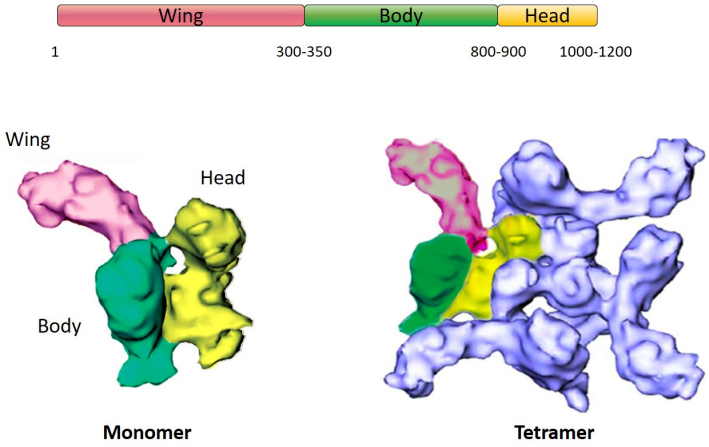

Figure 2. Schematic representation of the structural organization of α-LTX from *L. mactans tredecimguttatus* (*up*). Low-resolution three-dimensional structure of α-LTX monomer, obtained by cryo-EM (*down left*). Three different domains can be differentiated: the wing (pink), the body (green), and the head (yellow). The final pore, assembled onto a dipalmitoylphospatidylcholine bilayer is a homotetramer, combined in an assembly known as the "four-bladed propeller" (*down right*). The head and the body would be responsible of membrane binding and pore-formation, whereas the wing domain seems to be implicated in receptor recognition (Orlova 2000). Adapted from (Rivera-de-Torre 2019)

World population is growing exponentially, which is accompanied by an increase in the demand for food. Simultaneously, crop losses due to insect pests threaten food supplies Within this context, LITs isoforms stand out as quite interesting proteins from the biotechnological point of view. Given LITs specific insecticidal activity, and the fact that they are completely harmless for vertebrates, they could probably be produced to become part of ecofriendly bioinsecticide formulations aimed against specific agriculture damaging pests (Rivera-de-Torre 2019). Within the LIT group, δ-LIT is the smaller isoform, with also the fewer number of ankyrin repeats on its C-terminal domain (Figure 1). Both features suggest that this protein is the best candidate to try to achieve its heterologous production and purification. Characterizing this toxin from structural and functional points of view will probably provide enough information to approach the more general project of designing a new, biodegradable and safe insecticide. With this purpose in mind, we aimed to clone and produce δ-LIT from *L. hesperus* using the *Pichia pastoris* yeast system. In order to understand its mechanism of action, this approach will also completely avoid cross contamination of other components present in the crude venom, such as the Ltds mentioned above. It is also remarkable that these small proteins, presumably integrated within the latrotoxin macromolecular complex, have been already purified in milligram amounts using the same yeast production system (see Article V of this Thesis).

Therefore, eventually we will be able to study the toxic mechanism of δ-LIT in isolation or in combination with LtdI, LtdII or both.

Materials and methods

cDNA synthesis from *L. hesperus*' venom gland mRNA

The sequence to be amplified and cloned was obtained from *L. hesperus* venom gland transcriptomic assembly (Haney 2014, Haney 2016) (BioProject PRJNA242358), which had been deposited in NCBI GenBank database under GBCS01004653.1 accession code. Considering that it has been described that full-length LITs are not active (Dulubova 1996), only the sequence corresponding to the mature functional form of δ-LIT was selected to be cloned. Western black widow venom glands from two female individuals collected in Riverside (Riverside County, California, USA) were dissected according to (Garb 2014). Tissue was dissolved in TRIzol /Ambion, Life Technologies). Total RNA was extracted following TRIzol recommended protocol (Chomczynski 1993). Briefly, homogenized tissue was incubated at room temperature for 5 min and then chloroform was added. After vortexing, samples were centrifuged at 12000 x g for 15 min at 4°C. Aqueous phase was recovered, and RNA was precipitated with isopropanol, followed by three washing steps with 75% ethanol. Dried RNA was dissolved in RNase free water. Potentially contaminating DNA was removed with TURBO DNA-free kit (Ambion, Life Technologies). RNA was stored at -80°C until using it as template for cDNA synthesis with SuperScript III First-Strand Synthesis SuperMix kit (Thermo Fisher).

Cloning cDNA corresponding to mature δ-LIT

δ-LIT cDNA sequence was translated into its corresponding protein sequence. Its N-terminal signal peptide was then predicted using SpiderP tool from arachnoserver (Pineda 2018). The C-terminal immature region was determined by comparison with the sequences determined for δ-LIT from *L. mactans thedecimguttatus* (Dulubova 1996) and other members from LTX superfamily (Garb and Hayashi 2013). Oligonucleotides were designed to include new initiation and STOP codons as well as XhoI and NotI restriction sites for future ligation with pPICZαA expression vector (Table 1). Fragment amplification of the from *L. hesperus* venom gland's cDNA was performed by PCR with proofreading Pfu DNA polymerase (Thermo Scientific)

Table 1. Designed oligonucleotides for δ-LIT amplification from cDNA and Sanger sequencing on pPICZαA expression vector. Restriction sites are highlighted in bold letter, Kex2 proteolytic site is underlined and STOP codon is indicated in italic.

Abbreviation	Name	Sense	Designed oligonucleotides 5'→3'
Amplification from cDNA	498	Forward	GTATCT **CTCGAG** AAAAGA GTAGAAGAAGATGGAG **XhoI** Kex2
	499	Reverse	TTTTGT **GCGGCCGC** *CTA* TTCCGGTAAAGTACGACG **NotI** *STOP*
Sanger sequencing on pPICZαA vector	3AOX	Forward	GCAAATGGCATTCTGACATCC
	5AOX	Reverse	GACTGGTTCCAATTGACAAGC
	514	Forward	GAACAACATTCTTATCTGGC
	511	Reverse	GATTACCATCTGCAGC

following these instructions: 60 s at 95 °C initial denaturation, followed by 30 cycles of 45 s denaturation at 95°C, 30 s of annealing at 50 °C, 60s of elongation at 72 °C. The resulting final

mixture was elongated for 300 s at 72 °C to complete all intermediate DNA molecules. This PCR product was incubated with Taq Polymerase (rTaq, Takara) for 10 min at 72 °C to obtain adenine overhands in both 5' edges. After a purification step performed with Wizard PCR Preps DNA purification system (Promega), ligation reaction was performed between TOPO vector (pCR™2.1 TOPO®) (Invitrogen) and the PCR fragment. TOP10 *E. coli* competent cells were then transformed with the ligation mixture by thermal shock for 20 s at 42 °C, following a the standard protocol recommended by the manufacturer (Invitrogen). Transformant white colonies were selected in LB-Amp (50 µg/mL) plates supplemented with 40 µL of 2 % (w/v) X-Gal and 40 µL of 100 mM IPTG. Plasmids were isolated using a standard Minipreps-kit protocol (Sigma-Aldrich) and analyzed by agarose electrophoresis. Those plasmids with a size compatible with the desired cloned product (≈ 8000 bp) were digested with XhoI and NotI and subcloned into pPICZαA production vector with compatible ends. Ligation was using T4 ligase (Promega) over-night at 20 °C. DH5-α *E.coli* competent cells were transformed by thermal shock for 4 min at 37 °C, followed by addition of ψ-Broth medium. Transformant colonies were selected in Low salt LB-Amp (100 µg/mL) plates and plasmids were again isolated through the aforementioned Minipreps-kit. Sanger sequencing , using oligonucleotides designed to cover the whole 5' to 3' cDNA sequence, confirmed the correctness of the DNA fragment cloned (Table 1 and Figure 3).

Pichia pastoris electroporation

In order to produce the recombinant version δ-LIT, 10 µg of each plasmid were digested using PmeI (New England Biolabs, Boston-MA) and used to transform electrocompetent KM71H or SMD1168 cells by electroporation on a Bio-Rad Gene-Pulser apparatus as described (Martínez-Ruiz 1998). pPICZα plasmid confers resistance to zeocin. Upon electroporation, 1mL of cold 1M sorbitol was added to cells and incubated for 1h on ice followed by 4h of incubation at 30°C, 200rpm, after addition of 1mL of YPD media (1% yeast extract, 2%peptone and 2% dextrose). Yeasts were plated in YPD medium plates containing 1M sorbitol and different concentration of zeocin ranging 100-1500µg/mL. Plates were incubated 3 more days at 30°C until colonies appeared.

δ-LIT small-scale production

Individual colonies were tested for production in small scale cultures as follows. First, 100 mL of Buffered Glycerol-Complex Medium (BMGY) was used to grow yeasts for 24 h. Then, cultures were concentrated in 20 mL of Buffered Methanol-Complex Medium (BMMY). Concentration was made by centrifugation and subsequent resuspension of the cellular pellet. Production incubation was carried out at 20 °C for 72 h in baffled Erlenmeyer flaks to ensure high aeration. With the aim of ensuring the induction conditions, 100 µL of pure methanol were added every 12 hours. δ-LIT production was monitored by SDS-PAGE analysis of aliquots harvested extracellular media at different culture times.

δ-LIT large-scale production

Best producing colony was selected to grow in 1 L of BMGY overnight at 30 °C. Then, this culture was concentrated in 200 mL of BMMY. Production incubation was carried out at 20 °C for 48 h in baffled Erlenmeyer flaks to ensure high aeration and 1 mL of pure methanol was added every 12 hours to maintain production induction. After stopping the culture, extracellular

media was harvested by centrifugation and dialyzed in 6-8000 Da cut-off membranes for 6 hours against 500 mL of 50 mM Tris-HCl pH 7.4 containing 10 mM EDTA, followed by overnight dialysis in the same conditions but in the absence of EDTA. This dialyzed culture media was maintained overnight at 4°C with continuous soft stirring and 200 mL of DEAE-cellulose (Whatman), equilibrated in 50 mM HCl-Tris pH 7.4 buffer. After collecting the non-retained fraction , the chromatographic matrix was loaded onto a 4 cm x 18 cm glass column and washed with the same buffer. Proteins were then eluted with an ionic strength gradient from 0 M to 2 M NaCl. Fractions containing the desired protein were desalted using a Bio-Gel P2 chromatography, equilibrated in 50mM NH_4HCO_3 pH 7.0 buffer, and then lyophilized. Finally, these proteins were dissolved in 50mM NH_4HCO_3 pH 7.0 buffer and further purified by size-exclusion FPLC system ÄKTA Purifier (GE Healthcare Life Sciences) using a Superdex 200 10/300 GL prepacked column (GE Healthcare Life Sciences). Samples containing the protein of interest were evaluated by SDS-PAGE, aliquoted and lyophilized until used.

Characterization of purified proteins

Absorbance measurements were performed on a Shimadzu UV-1800 (Tokyo, Japan) at 100 nm/min scanning speed, at room temperature in 1 or 0.1 cm optical path cells. Protein concentrations were estimated using UV absorbance spectra and the theoretical $E^{0.1\%}$ obtained through computational analysis performed through ProParam Expasy tool (Table 2). Circular dichroism (CD) spectra were obtained on a Jasco (Easton, MD) 715 spectropolarimeter. Far-UV CD spectra were recorded at approximately 0.1 mg/mL, in FPLC elution buffer. At least six spectra were averaged to obtain the final spectrum.

Table 2. Computed physicochemical parameters of LtdI and LtdII obtained via ProtParam ExPASy analysis tool (Gasteiger 2003).

	Number of amino acids	Molecular weight (Da)	Theoretical pI value	Tyr	Trp	$E^{0.1\%}$ *
δ-LIT	991	110418	5.36	26	2	0.454

*Absorbance for a solution at 0.1 mg/mL assuming all pairs of Cys residues form cystines

Results and Discussion

δ-LIT was successfully cloned in the pPICZαA production vector

A single resulting PCR product around 3000 bp was obtained by the PCR protocol utilized. Such product was successfully cloned in the pCR™2.1 TOPO®vector (Invitrogen) using the commercially available protocol. Finally, the purified plasmid, with the correct expected size (around ≈8000 bp), was digested with the corresponding restriction enzymes for subcloning in pPICZαA. Resulting pPICZαAδLIT plasmid was -sequenced (Figure 3). There were 11 nucleotide differences with the original sequence assembled in the transcriptome analysis (NCBI GenBank: GBCS01004653.1). However, discrepancies can be easily explained since the spider individual used to obtain departing cDNA for cloning was not the same used for transcriptome assembly, and single nucleotide polymorphism is possible between individuals. Much more considering the enormous size of the protein considered. In addition, *de novo* transcriptome assemblies are

based on overlapping sequenced sequences and then, depending on the fragments abundance, it is possible to find some differences between actual and assembled sequences.

δ-LIT was produced in P. pastoris KM71H yeast system

Small-scale cultures revealed positive production under methanol induction of *P. pastoris* KM71H strain. Maximum expression was reached after 48 h of induction at 20 °C (Figure 4). Very similar results were obtained with the protease deficient *P. pastoris* SMD1168 strain (data not shown). Then, the KM71H strain was used for large-scale production in identical conditions as those describe for the small-scale experiments. After 48 h of culture, the culture medium was collected by centrifugation and subjected to the three chromatographic steps described in the Materials and Methods section.

Once finished this procedure, δ-LIT was purified to homogeneity according to its SDS-PAGE behavior (Figure 5). Visualization of the protein using a Coomassie Blue staining standard protocol did not render a signal intensity proportional to the protein quantity present in the gel. Furthermore, the δ-LIT band quickly faded when the gel was subjected to the traditional washing procedure of immersing it in a solution of water:methanol: acetic acid (80:20:7.5). This observation, as well as a rather anomalous electrophoretic behavior, has been described before for highly acidic such as the case of δ-LIT(García-Ortega 2005).

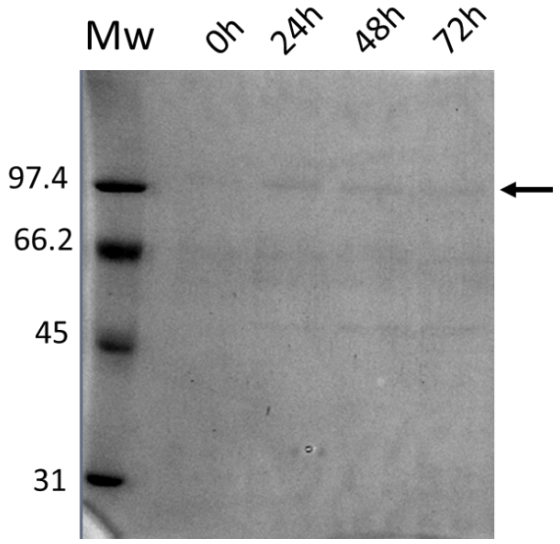

Figure 4. Small-scale production of δ-LIT by *P pastoris* KM71H. 0.1% SDS-10%PAGE analysis of aliquots from the extracellular media taken after 0, 24, 48 and 72 hours of culture. Induction was maintained for 72h by adding methanol every 12 hours to maintain a stable concentration of approximately 5.0 % (v/v) during all the experiment. (Mw) Molecular weight standard (Low-Range SDS-PAGE Standards - Biorad) were also loaded, and the corresponding molecular masses are indicated in kDa at the left margin. The black arrow at the right indicates the position of the band corresponding to δ-LIT molecular weight.

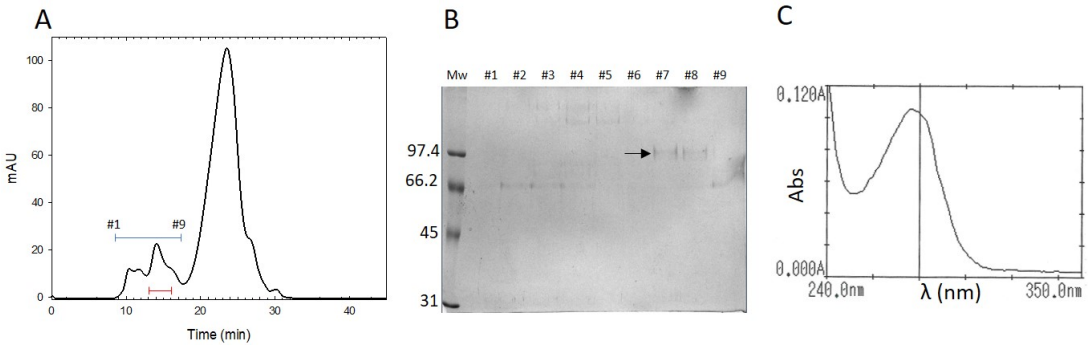

Figure 5. (A) Size exclusion FLPC elution profile on Superdex 200 column. Blue bar indicates the fractions analyzed in (B). Red bar indicates de pooled fractions #7 and #8. (B) SDS-PAGE (0.1%-10%) of the fractions indicated with blue a blue bar in (A). The arrow indicates δ-LIT band according to its electrophoretic mobility. (C) Absorbance spectra of the pooled fractions indicated in (A) and analyzed in (B).

Purified δ-LIT appears to be unstructured

Far-UV CD spectrum of the purified δ-LIT (Figure 6) was compatible with that one of an unstructured protein, though there is not any previous reference to compare with of any LTX characterized by this spectroscopic approach. Previous studies with α-LTX have shown that Ca^{2+} was necessary for its function (Orlova 2000). However, adding $CaCl_2$ to a final 100 nM concentration did not affect the far-UV CD spectrum (Figure 6).

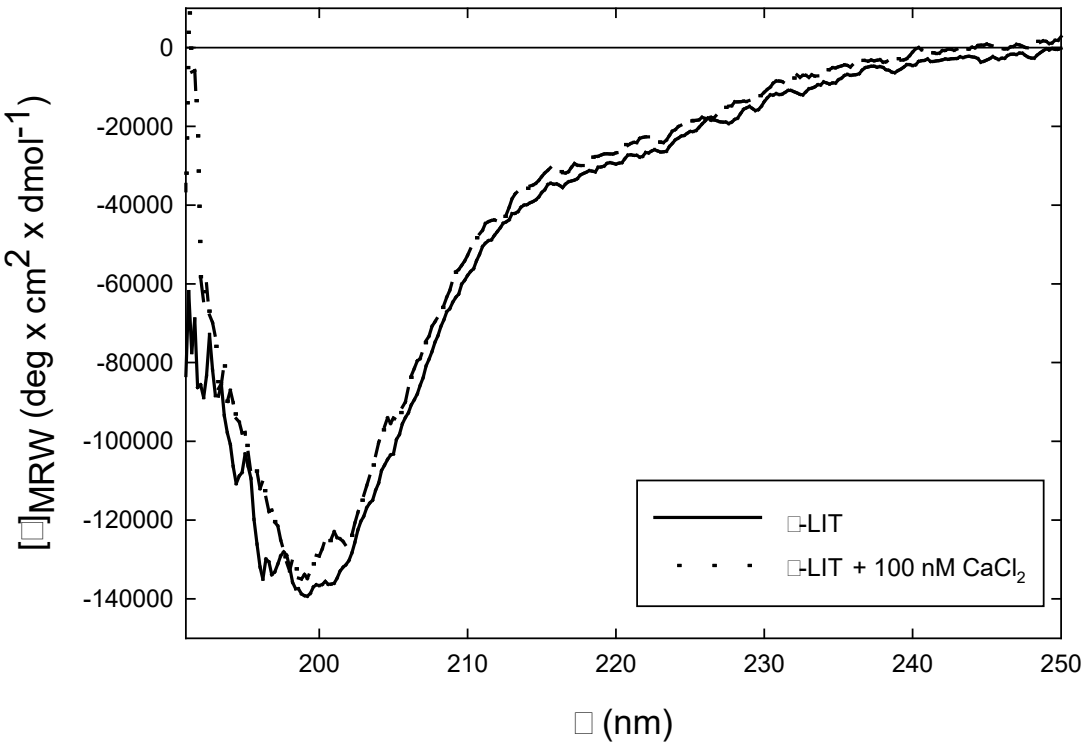

Figure 6. Far-UV circular dichroism spectra of δ-LIT in the absence (solid line) or in the presence of 100 nM $CaCl_2$ (dashed line).

Conclusions and future perspectives

δ-LIT from *L. hesperus* has been cloned from cDNA into a *P* pastoris production vector. Sequencing has revealed some differences between the *de novo* assembled sequence and the cloned one, although such differences are easily accountable considering that the process used for assembly relies on overlapping sequence fragments, whose abundance is critical for optimal coverage. The protein was successfully produced and purified, although yields were low. CD spectroscopic characterization was compatible with a rather unfolded protein.

The results are still preliminary and in need of high effort investment in the optimization of the purification protocols used. To avoid unexpected protein degradation, which maybe an issue for such a big protein, which also could explain the presence of some bands of higher electrophoretic mobility (Figure 4) along the production and purification procedures, some modifications will have to be introduced. For example, we will revisit the employment of protease deficient strains, or the addition of protease inhibition cocktails during the first purification steps. This purification procedure will be developed at 4°C, using autoclaved buffers and in the absence of EDTA. It has not escaped to our attention that the use of a chelating agent such as EDTA might have removed the calcium required for the protein to maintain its folded conformation. Different polyacrylamide gel staining methods will also be assayed in order to provide more sensitivity and stability of the protein bands detected.

Once all these methodologies are improved, we will move forward to purify larger amounts of recombinantly produced δ-LIT and proceed with the originally intended structural and functional characterization of this interesting and huge toxic protein.

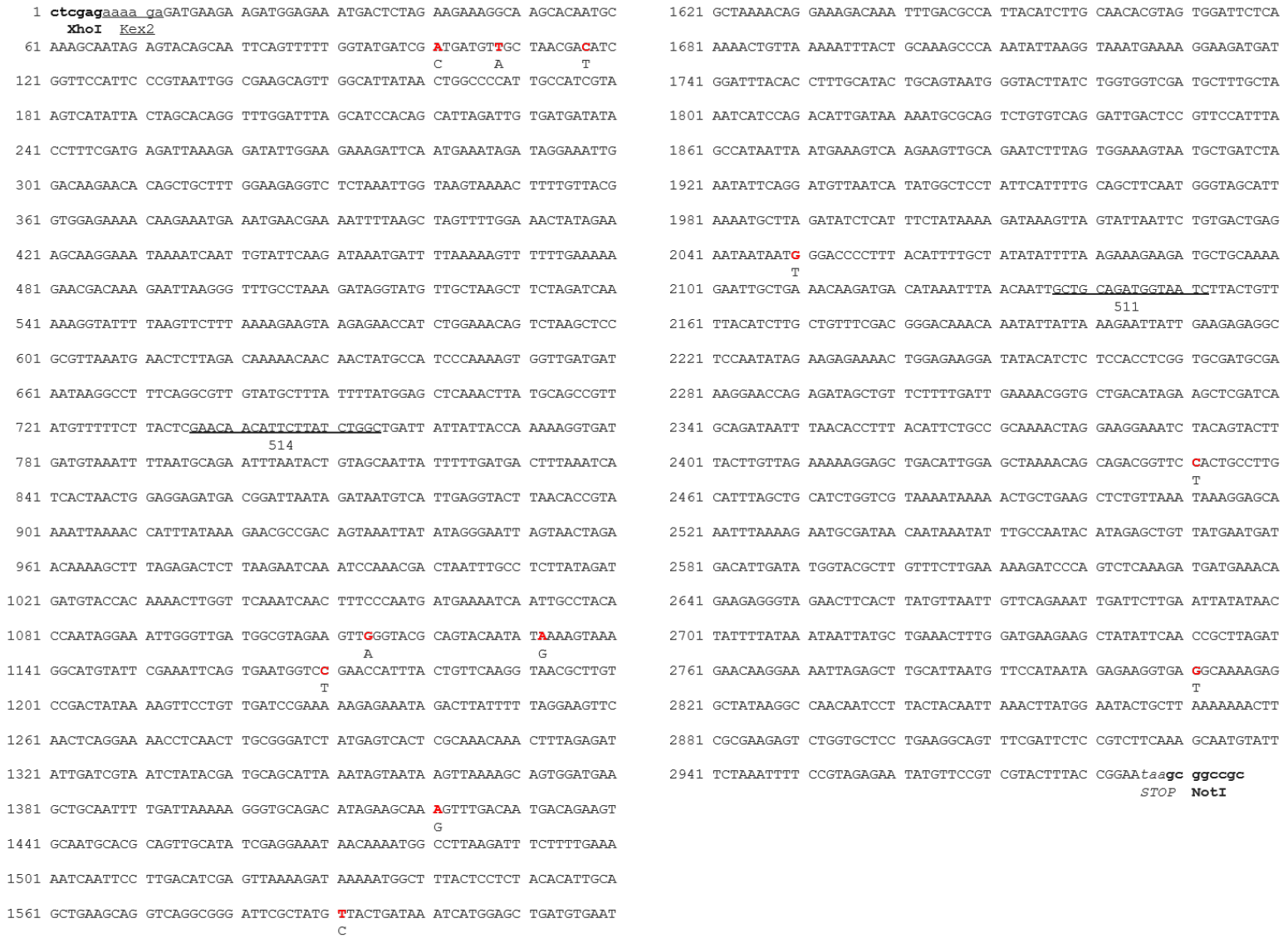

Figure 3. δ-LIT sequence obtained by Sanger sequencing. Introduced restriction sites are indicated in bold letter, Kex 2 site for proteolytic processing is underlined and STOP codon is indicated in italics. In red, nucleotide changes in comparison with the sequence obtained in the transcriptome assembly procedure (GBCS01004653.1) Oligonucleotide sequences used for internal sequencing are also underlined.

References

Calvete, J.J. (2017) "Venomics: Integrative Venom Proteomics and Beyond." Biochem J 474, 5: 611-634.

Cull-Candy, S.G., Neal, H., and Usherwood, P.N. (1973) "Action of Black Widow Spider Venom on an Aminergic Synapse." Nature 241, 5388: 353-354.

Chomczynski, P. (1993) "A Reagent for the Single-Step Simultaneous Isolation of Rna, DNA and Proteins from Cell and Tissue Samples." Biotechniques 15, 3: 532-534, 536-537.

Deak, F., Liu, X.R., Khvotchev, M., Li, G., Kavalali, E.T., Sugita, S., and Sudhof, T.C. (2009) "A-Latrotoxin Stimulates a Novel Pathway of Ca2+-Dependent Synaptic Exocytosis Independent of the Classical Synaptic Fusion Machinery." Journal of Neuroscience 29, 27: 8639-8648.

Dulubova, I.E., Krasnoperov, V.G., Khvotchev, M.V., Pluzhnikov, K.A., Volkova, T.M., Grishin, E.V., Vais, H., Bell, D.R., and Usherwood, P.N. (1996) "Cloning and Structure of D-Latroinsectotoxin, a Novel Insect-Specific Member of the Latrotoxin Family: Functional Expression Requires C-Terminal Truncation." J Biol Chem 271, 13: 7535-7543.

Fritz, L.C., Tzen, M.C., and Mauro, A. (1980) "Different Components of Black Widow Spider Venom Mediate Transmitter Release at Vertebrate and Lobster Neuromuscular Junctions." Nature 283, 5746: 486-487.

Garb, J.E. (2014) "Extraction of Venom and Venom Gland Microdissections from Spiders for Proteomic and Transcriptomic Analyses." J Vis Exp, 93: e51618.

Garb, J.E., and Hayashi, C.Y. (2013) "Molecular Evolution of Alpha-Latrotoxin, the Exceptionally Potent Vertebrate Neurotoxin in Black Widow Spider Venom." Mol Biol Evol 30, 5: 999-1014.

García-Ortega, L., de los Ríos, V., Martínez-Ruiz, A., Oñaderra, M., Lacadena, J., Martínez-del-Pozo, A., and Gavilanes, J.G. (2005) "Anomalous Electrophoretic Behavior of a Very Acidic Protein: Ribonuclease U2." Electrophoresis 26, 18: 3407-3413.

Gasteiger, E., Gattiker, A., Hoogland, C., Ivanyi, I., Appel, R.D., and Bairoch, A. (2003) "Expasy: The Proteomics Server for in-Depth Protein Knowledge and Analysis." Nucleic Acids Res 31, 13: 3784-3788.

Gendreau, K.L., Haney, R.A., Schwager, E.E., Wierschin, T., Stanke, M., Richards, S., and Garb, J.E. (2017) "House Spider Genome Uncovers Evolutionary Shifts in the Diversity and Expression of Black Widow Venom Proteins Associated with Extreme Toxicity." BMC Genomics 18, 1: 178.

Grishin, E. (1999) "Polypeptide Neurotoxins from Spider Venoms." Eur J Biochem 264, 2: 276-280.

Grishin, E.V. (1998) "Black Widow Spider Toxins: The Present and the Future." Toxicon 36, 11: 1693-1701.

Haney, R.A., Ayoub, N.A., Clarke, T.H., Hayashi, C.Y., and Garb, J.E. (2014) "Dramatic Expansion of the Black Widow Toxin Arsenal Uncovered by Multi-Tissue Transcriptomics and Venom Proteomics." BMC Genomics 15366.

Haney, R.A., Clarke, T.H., Gadgil, R., Fitzpatrick, R., Hayashi, C.Y., Ayoub, N.A., and Garb, J.E. (2016) "Effects of Gene Duplication, Positive Selection, and Shifts in Gene Expression on the Evolution of the Venom Gland Transcriptome in Widow Spiders." Genome Biol Evol 8, 1: 228-242.

Jelinek, G.A. (1997) "Widow Spider Envenomation (Latrodectism): A Worldwide Problem." Wilderness Environ Med 8, 4: 226-231.

Kiyatkin, N., Dulubova, I., Chekhovskaya, I., Lipkin, A., and Grishin, E. (1992) "Structure of the Low Molecular Weight Protein Copurified with a-Latrotoxin." Toxicon 30, 7: 771-774.

Kiyatkin, N., Dulubova, I., and Grishin, E. (1993) "Cloning and Structural Analysis of Alpha-Latroinsectotoxin Cdna. Abundance of Ankyrin-Like Repeats." Eur J Biochem 213, 1: 121-127.

Kiyatkin, N.I., Dulubova, I.E., Chekhovskaya, I.A., and Grishin, E.V. (1990) "Cloning and Structure of Cdna Encoding Alpha-Latrotoxin from Black Widow Spider Venom." FEBS Lett 270, 1-2: 127-131.

Kiyatkin, N.I., Kulikovskaya, I.M., Grishin, E.V., Beadle, D.J., and King, L.A. (1995) "Functional Characterization of Black Widow Spider Neurotoxins Synthesised in Insect Cells." Eur J Biochem 230, 3: 854-859.

Krasnoperov, V.G., Shamotienko, O.G., and Grishin, E.V. (1990a) "A Crustacean-Specific Neurotoxin from the Venom of the Black Widow Spider Latrodectus Mactans Tredecimguttatus." Bioorg Khim 16, 11: 1567-1569.

Krasnoperov, V.G., Shamotienko, O.G., and Grishin, E.V. (1990b) "Isolation and Properties of Insect-Specific Neurotoxins from Venoms of the Spider Lactodectus Mactans Tredecimguttatus." Bioorg Khim 16, 8: 1138-1140.

Macrander, J., Panda, J., Janies, D., Daly, M., and Reitzel, A.M. (2018) "Venomix: A Simple Bioinformatic Pipeline for Identifying and Characterizing Toxin Gene Candidates from Transcriptomic Data." PeerJ 6e5361.

Magazanik, L.G., Fedorova, I.M., Kovalevskaya, G.I., Pashkov, V.N., Bulgakov, O.V., and Grishin, E.V. (1992) "Selective Presynaptic Insectotoxin (Alpha-Latroinsectotoxin) Isolated from Black Widow Spider Venom." Neuroscience 46, 1: 181-188.

Martínez-Ruiz, A., Martínez-del-Pozo, A., Lacadena, J., Mancheño, J.M., Oñaderra, M., López-Otín, C., and Gavilanes, J.G. (1998) "Secretion of Recombinant Pro- and Mature Fungal a-Sarcin Ribotoxin by the Methylotrophic Yeast Pichia Pastoris: The Lys-Arg Motif Is Required for Maturation." Protein Expr Purif 12315-322.

Matsumura, T., Mashiko, R., Sato, T., Itokawa, K., Maekawa, Y., Ogawa, K., Isawa, H., Yamamoto, A., Mori, S., Horita, A., Ginnaga, A., Miyatsu, Y., Takahashi, M., Taki, H., Hifumi, T., Sawabe, K., and Ato, M. (2018) "Venom and Antivenom of Redback Spider (Latrodectus Hasseltii) in Japan." Jpn J Infect Dis.

Orlova, E.V., Rahman, M.A., Gowen, B., Volynski, K.E., Ashton, A.C., Manser, C., van Heel, M., and Ushkaryov, Y.A. (2000) "Structure of Alpha-Latrotoxin Oligomers Reveals That Divalent Cation-Dependent Tetramers Form Membrane Pores." Nat Struct Biol 7, 1: 48-53.

Pineda, S.S., Chaumeil, P.A., Kunert, A., Kaas, Q., Thang, M.W.C., Le, L., Nuhn, M., Herzig, V., Saez, N.J., Cristofori-Armstrong, B., Anangi, R., Senff, S., Gorse, D., and King, G.F. (2018) "Arachnoserver 3.0: An Online Resource for Automated Discovery, Analysis and Annotation of Spider Toxins." Bioinformatics 34, 6: 1074-1076.

Rivera-de-Torre, E., Palacios-Ortega, J., Gavilanes, J.G., Martínez-del-Pozo, A., and García-Linares, S. (2019) "Pore-Forming Proteins from Cnidarians and Arachnids as Potential Biotechnological Tools." Toxins (Basel) 11, 6.

Rohou, A., Nield, J., and Ushkaryov, Y.A. (2007) "Insecticidal Toxins from Black Widow Spider Venom." Toxicon 49, 4: 531-549.

Ushkaryov, Y.A., Volynski, K.E., and Ashton, A.C. (2004) "The Multiple Actions of Black Widow Spider Toxins and Their Selective Use in Neurosecretion Studies." Toxicon 43, 5: 527-542.

Vetter, R.S., and Isbister, G.K. (2008) "Medical Aspects of Spider Bites." Annu Rev Entomol 53409-429.

Yan, S., and Wang, X. (2015) "Recent Advances in Research on Widow Spider Venoms and Toxins." Toxins (Basel) 7, 12: 5055-5067.

Summary and future perspectives

Article VIII

Pore-Forming Proteins from Cnidarians and Arachnids as Potential Biotechnological Tools

Esperanza Rivera-de-Torre[1], Juan Palacios-Ortega[1,2], José G. Gavilanes[1], Álvaro Martínez-del-Pozo[1], and Sara García-Linares[3]

[1] Departamento de Bioquímica y Biología Molecular, Facultades de Química y Biología, Universidad Complutense, 28040 Madrid
[2] Biochemistry, Faculty of Science and Engineering, Åbo Akademi University, 20500 Turku, Finland
[3] Cell Biology Department, Harvard Medical School, Boston, MA 02115, USA

Toxins. 2019, 11 (6), 370

DOI: https://doi.org/10.3390/toxins11060370

Los venenos animales son mezclas complejas de moléculas tóxicas altamente especializadas. Tanto el veneno de los cnidarios como el de los arácnidos contiene proteínas formadoras de poros (PFPs) dirigidas contra la membrana plasmática de sus células diana. Entre las de cnidarios, destacan las actinoporinas por su pequeño tamaño y su simplicidad molecular. Ello explica que algunas de ellas se hayan estudiado en profundidad y se conozcan con gran detalle molecular, tanto a nivel estructural como funcional. Mientras las actinoporinas nativas sólo requieren esfingomielina para unirse a la membrana, quimeras sintéticas formadas por dominios de reconocimiento derivadas de anticuerpos fusionadas a una isoforma de actinoporina pueden servir como inmunotoxinas altamente específicas. De hecho, algunos ejemplos de este tipo de construcción, dirigida contra células malignas, han sido ya descritos. Por otro lado, las PFPs producidas por arácnidos han sido mucho menos estudiadas. Por este motivo, es destacable cómo las arañas del género *Latrodectus*, que son cazadoras profesionales de insectos, también producen PFPs como parte de su arsenal tóxico. Se trata, además, de proteínas enormes que se conocen con el nombre de latrotoxinas. Es también interesante que algunas de estas latrotoxinas hayan sido identificadas como insecticidas potentes y altamente específicos. Dada la naturaleza proteica de estas toxinas, se prevé que en un futuro puedan ser utilizadas como eficientes y sostenibles bioinsecticidas. La ingeniería de proteínas, y su producción recombinante a gran escala en sistemas heterólogos, son pasos críticos necesarios para avanzar en la dirección de poder utilizar estas PFPs como herramientas en el control de importantes plagas agrícolas de insectos. En resumen, ambas familias de PFPs, tanto de cnidarios como de arácnidos, son moléculas con prometedoras aplicaciones biotecnológicas.

PhD candidate contributions

Esperanza Rivera de Torre wrote, read, and, together with the other authors, revised it and suggested changes and modifications.

toxins

MDPI

Perspective

Pore-Forming Proteins from Cnidarians and Arachnids as Potential Biotechnological Tools

Esperanza Rivera-de-Torre [1], Juan Palacios-Ortega [1,2], José G. Gavilanes [1], Álvaro Martínez-del-Pozo [1,*] and Sara García-Linares [3,*]

1 Departamento de Bioquímica y Biología Molecular, Facultad de CC. Químicas, Universidad Complutense de Madrid, 28040 Madrid, Spain; esperanza.rivera.detorre@gmail.com (E.R.-d.-T.); juan.palaciosb1a@gmail.com (J.P.-O.); jggavila@ucm.es (J.G.G.)
2 Biochemistry, Faculty of Science and Engineering, Åbo Akademi University, 20500 Turku, Finland
3 Cell Biology Department, Harvard Medical School, Boston, MA 02115, USA
* Correspondence: alvaromp@quim.ucm.es (Á.M.-d.-P.); sara_garcialinares@hms.harvard.edu (S.G.-L.)

Received: 29 May 2019; Accepted: 21 June 2019; Published: 25 June 2019

Abstract: Animal venoms are complex mixtures of highly specialized toxic molecules. Cnidarians and arachnids produce pore-forming proteins (PFPs) directed against the plasma membrane of their target cells. Among PFPs from cnidarians, actinoporins stand out for their small size and molecular simplicity. While native actinoporins require only sphingomyelin for membrane binding, engineered chimeras containing a recognition antibody-derived domain fused to an actinoporin isoform can nonetheless serve as highly specific immunotoxins. Examples of such constructs targeted against malignant cells have been already reported. However, PFPs from arachnid venoms are less well-studied from a structural and functional point of view. Spiders from the *Latrodectus* genus are professional insect hunters that, as part of their toxic arsenal, produce large PFPs known as latrotoxins. Interestingly, some latrotoxins have been identified as potent and highly-specific insecticides. Given the proteinaceous nature of these toxins, their promising future use as efficient bioinsecticides is discussed throughout this Perspective. Protein engineering and large-scale recombinant production are critical steps for the use of these PFPs as tools to control agriculturally important insect pests. In summary, both families of PFPs, from Cnidaria and Arachnida, appear to be molecules with promising biotechnological applications.

Keywords: venomics; transcriptomics; pore-forming proteins; actinoporin; latrotoxin; immunotoxin; bioinsecticides

Key Contribution: Pore-forming proteins from Cnidaria and Arachnida venoms are interesting toxins to develop biotechnological applications such as immunotoxins or bioinsecticides.

1. Introduction

Venomous organisms have fascinated humankind throughout history. This has been, in great part, due to their inherent danger and the fatal consequences exerted by a usually small but envenomed injury. Venomous animals use their venoms for competitive, defensive, and predatory purposes and comprise a phylogenetically diverse set of organisms: from vertebrates like amphibians, reptiles, or even mammals, to invertebrates like insects, arachnids, or cnidarians. Most of these venomous animals are small in size compared to their natural predators and, in many instances, do not seem to be dangerous at first sight.

Venoms are complex mixtures of bioactive compounds such as peptides, proteins, salts, and neurotoxins [1]. Thus, venoms balance the predator–prey relationship. A continuous race is

established between both actors: prey are evolutionarily selected for venom resistance, which is achieved through different mechanisms [1–3]; to work within the new evolutionary landscape, venoms must adapt quickly to keep harming their prey. How do new venoms appear in a species? One hypothesis is that a proto-toxin gene is first duplicated, and then one copy becomes expressed in the organism's venom gland. Additional amplification of the venom gland-expressed gene can generate variants that produce a toxic protein product or compound. Due to this duplication–neofunctionalization mechanism, it is common to find venom toxins genetically structured as multigene families [2,4–6].

When venoms are delivered, they must interact with their prey at the molecular level in order to cause cellular damage. Venoms must breach multiple barriers to reach their targets, including skin, the intricate network of the extracellular matrix, and, eventually, the cell membrane. Delivery systems like chelicerae, nematocysts, and other piercing structures have an initial harmful physical activity, overtaking the barriers and bringing toxins closer to their final target [3] (Figure 1). Within the injected cocktail, metalloproteases, for example, are very effective in attacking the interstitial space between cells, by digesting extracellular matrix components and facilitating the activity of other toxins on the cells. Non-proteinaceous components of the venom, like serotonin and histamine, produce fast and sharp pain and increase vasodilatation. As cells are defined by the plasma membrane [7], the first cellular structures encountered by the venomous cocktail are the transmembrane and peripheral receptor proteins as well as the lipid membrane itself. Therefore, venoms also contain proteins that remodel and directly attack the lipid membrane, such as neurotoxins, phospholipases, and pore-forming toxins (PFTs), which finally destroy this key structure defining the cell.

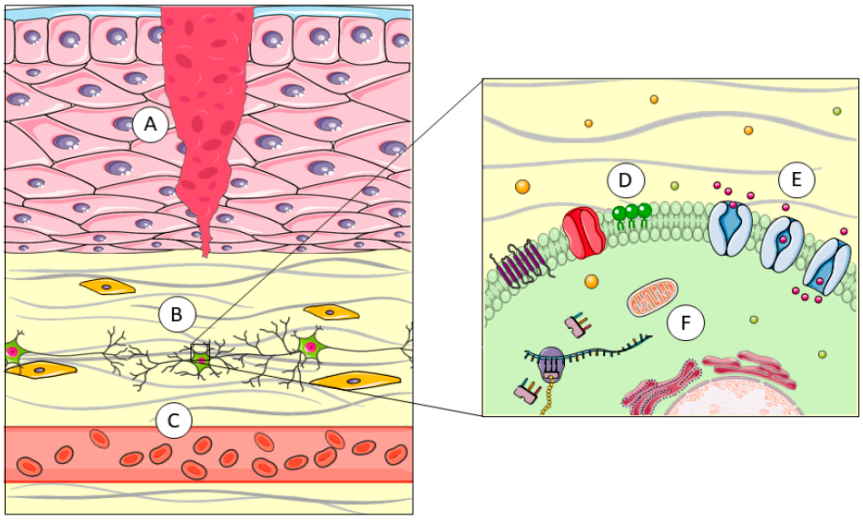

Figure 1. Piercing delivery systems cross the skin, the first barrier encountered by venom (**A**). Specific extra-cellular matrix proteases, like metalloproteases, digest scaffold proteins (**B**). Non-proteinaceous components, like serotonin, promote vasodilatation (**C**). The plasma membrane is the most widespread structure in nature and, therefore, a suitable target of attack by enzymes like phospholipases or cytolysins (**D**). Neurotoxins interact with membrane receptors and channels, leading to imbalance in ion distribution across the membrane (**E**). Some toxins develop their harmful effects once they are internalized, blocking protein production or oxidative respiration in mitochondria (**F**). This image was created using Servier Medical Art free images database (SERVIER, Paris, France).

2. Pore-Forming Proteins (PFPs)

PFPs are the perfect example of toxins whose activity relies on the disruption of a lipid membrane. In general terms, they violate the standard classification of proteins—into water-soluble or membrane proteins—that can be found in any basic Biochemistry textbook. PFPs remain stably folded and soluble in water but, upon interaction with the membrane of their target cells—and after recognition of a

receptor that can be a sugar, a protein, or even a specific lipid—they polymerize into an oligomeric transmembrane protein that makes a pore. We, and other authors, even speak of a molecular metamorphosis transforming these toxins from water-soluble to transmembrane proteins, escaping the aforementioned classification [8–10]. Attachment to the membrane increases the local concentration of the toxin, reducing protein diffusion to a bidimensional system, and thus facilitating the oligomerization that leads to pore formation. Depending on the toxin, pore size and permeability selectivity vary, allowing the passage of species ranging in size from small ions to medium-size proteins. In most cases, the final outcome of the formation of a pore is cell death by osmotic shock. Based on the protein structure that forms the final pore, these proteins are classified either as α-PFPs, if the pore walls are defined by α-helices, or β-PFPs, if the pore walls are β-sheets [11,12].

PFPs attack the plasma membrane, the primordial structure that defines a cell. As stated, some of them only need a lipidic receptor, like cholesterol [13] or sphingomyelin [14–18]. But others seem to need protein receptors, such as the understudied latrotoxin macrocomplexes from black widow spiders (*Latrodectus* spp.) [19]. Especially when targeting a particular lipid or lipidic composition, PFPs are not specific enough. However, since they constitute a component of a complex cocktail (the venom), they can be used to target a wide range of animals. These toxins act very quickly [10,12,14], so they are used for both predatory and defensive purposes [1].

In this Perspective, we focus on PFPs produced by two different groups of animals, which constitute our major areas of research in the field. Cnidarians, given their privileged evolutionary position and their wide-range spectrum of attack, and arachnids, whose powerful PFP collection is usually aimed, with high specificity, at insects. Taking into account the above outlined possibilities on toxin biotechnological applications, both groups of proteins display different interesting characteristics to turn them into powerful weapons.

2.1. Pore-Forming Proteins in Cnidaria

Cnidaria is an ancient clade of animals, whose genetic analysis is interesting from the evolutionary and phylogenetic point of view because they also are the oldest lineage of venomous animals [2]. Cnidaria includes about 10,000 species, most of them living in saltwater. The Cnidaria phylum is phylogenetically divided in two subdivisions: the class Anthozoa (anemones and corals) and the subphylum Medusozoa, which includes the classes Cubozoa (jellyfishes) and Hydrozoa (hydras), among others. Although they exhibit very simple anatomy, they are able to defend themselves with high rate of success [2]. This animal group has clinical relevance from the point of view of envenomation, and its hazard for humans fluctuates from non-hazardous to extremely dangerous like the Australian box jellyfish (*Chironex fleckeri*) [20] or the Atlantic Portuguese Man o' War (*Physalia physalis*) [21]. Most sea anemones, however, are harmless to humans or just cause skin burning after contact with tentacles [22].

Sea anemones inject venom into their prey through nematocysts, specialized penetrant structures that discharge upon activation of cnidocytes [1,2]. Nematocysts are mostly located in the tentacles, structures that cover a large area of anemones' bodies and contain the venomous weapon needed not only to protect the animal, but also to attack and entrap the prey. However, it is also possible to find nematocysts surrounding the oral disc, in order to paralyze the prey, or in the ring surrounding the base of the column, specialized for inter- and intraspecific competition. In fact, Cnidaria is the only venomous lineage that lacks a centralized venom system [23,24].

Like most animal venoms, sea anemones' venoms can be largely classified as non-proteinaceous toxins, neurotoxins, enzymes, or cytolysins [3,4,6]. Among the latter, actinoporins are a family of α-PFTs produced by sea anemones as part of their venomous arsenal. They are small (around 20 kDa/175 amino acids), cysteineless, and basic (pI ≈ 9) [10,12,25]. It has been largely accepted that actinoporins do not need a protein receptor to exert their toxicity, but instead require sphingomyelin as a specific lipidic receptor [16,17,26–28]. Furthermore, cholesterol, though not indispensable, plays a key role in their pore-forming mechanism [14,29–34], a mechanism still not fully understood, especially with

regard to the sequence of events during pore formation and the final stoichiometry of the pore [35–42]. Overall, actinoporins represent a simple and optimal model to study the challenging biophysical transition from a water-soluble conformation to an integral transmembrane state.

So far, actinoporins have been detected in at least 20 different species of anemones [10,12,25], constituting multigenic families in practically all cases [6,43–45]. All of them show a remarkable sequence identity that reaches values as high as 90% [12,25]. But despite this great structural similarity, they also show notable functional differences [14,46]. This identity of sequence is logically manifested in its three-dimensional structure [36,37,42,47–49]. All studied actinoporins contain a core consisting of a stranded β-sandwich which is flanked by two short α-helixes. This sandwich contains a motif that anchors the protein to the membrane and remains virtually unchanged during the process of pore formation; in contrast, the N-terminal end, in association with the N-terminal ends of adjacent monomers, is the portion that undergoes a conformational change and finally pierces through the membrane [50] (Figure 2).

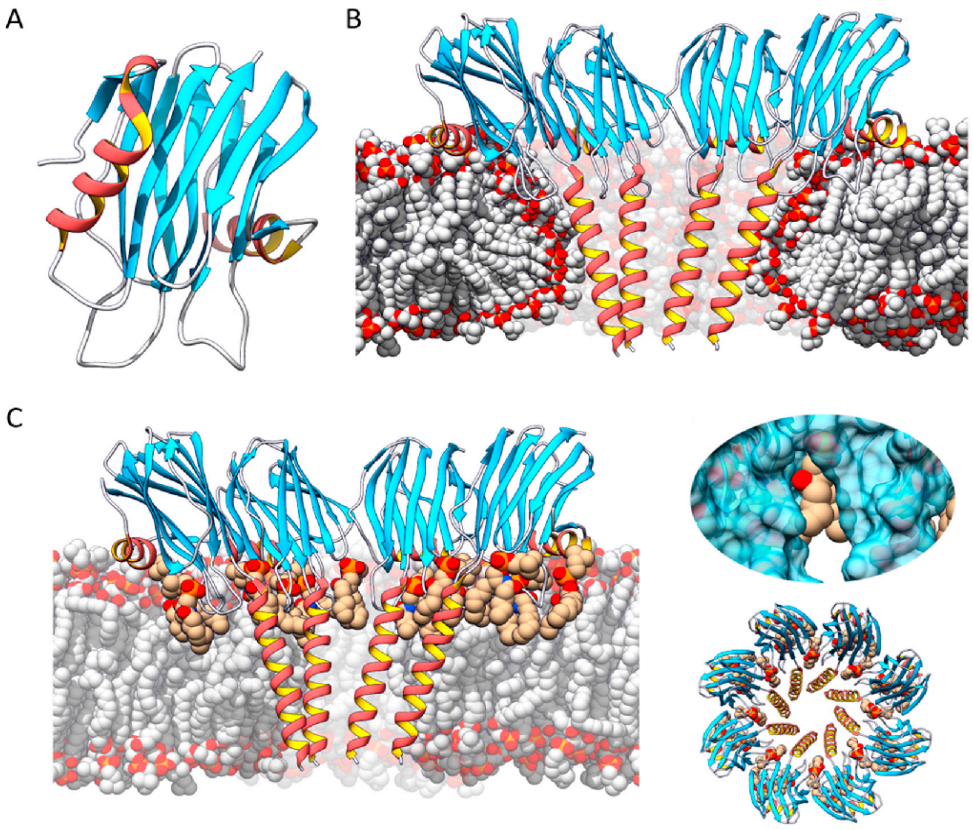

Figure 2. (**A**) Actinoporin monomers share a common fold: a stranded β-sandwich flanked by two short α-helixes. With regard to pore structure, two models have been proposed: (**B**) a tetrameric structure in which the lipid membrane adopts a toroidal shape around the pore walls, and (**C**) an octameric lipid-protein mixed structure in which lipids (in tan color) are accommodated in pore-wall fenestrations (see inserts on the right).

The mechanism by which actinoporins carry out their action has been studied in detail and, while some aspects remain controversial, there is at least a general consensus about the stages leading to pore formation [10,12,16,25,51,52]. According to the commonly accepted model, the monomeric units of the protein bind to its target membrane, initiating an oligomerization process followed by separation and elongation of the α-helix located at the N-terminal end of the actinoporin [53–55]. It is approximately the first 30 amino acids that adopt a helical amphipathic structure, insert into the membrane, and,

in association with other actinoporin molecules, form a pore in the lumen of which the polar heads of some lipids would also participate (Figure 2) [23,36,38,42,50,56,57]. However, there are still aspects of this mechanism to be elucidated: mainly, the order in which these stages occur [8,41,42,51,58], the need for 'pre-pore' type intermediates [38,58], and, above all, the stoichiometry and composition of the final functionally active structure [36,37,41,42,51].

At least three different models have been proposed to explain the actinoporins' transmembrane pore. The first proposed model suggested the existence of a toroidal tetrameric protein-lipidic structure [35,38,59]. However, a non-toroidal nonameric pore of fragaceatoxin C (FraC), produced by the sea anemone *Actinia fragacea*, was proposed based on a detergent-containing crystalline structure [37]. The most detailed structural study carried out in the field is a crystalline lipid-containing octameric pore, solved with atomic resolution [42]. In fact, none of these models is fully accepted and, in our opinion, most probably all of them describe different aspects of the mechanism of pore formation and cell lysis employed by actinoporins. The different conformations detected are just static images of a dynamic process (Figure 2).

2.2. Pore-Forming Proteins in Arachnids

Araneae (spiders) is the largest order within the Arachnida class, which also includes scorpions, mites, and harvestmen. Most adult arachnids have eight legs and they also count with other mobile appendages like pedipalps, which are adapted for a wide variety of functions from feeding to reproduction, and chelicerae, involved in feeding and defense. In most venomous arachnid species (*Latrodectus* spp. are just one of the few exceptions), chelicerae are only connected to glands where venom is produced, as opposed to Cnidaria, where it is usually more homogeneously distributed within their bodies. Production of the venom is mediated by a process called holocrine secretion, in which the toxic compounds are produced in the cytosol of the gland cells and, then, these productive cells disintegrate, dumping the cytosol content into the venom gland lumen.

Most of natural spiders' prey are insects. Consequently, their venoms have been selected during evolution so that they immobilize and kill this particular kind of invertebrate. However, spider venom can be also harmful for vertebrates, a feature most probably 'developed' as a protective weapon against predation. Species from the *Latrodectus* genus, commonly known as black widow spiders, constitute a group of around 40,000 different spider species. Their bite causes acute pain and severe secondary conditions in humans, called 'latrodectism' [60], which involves a complex symptomatology from nausea to body rigidity and widespread intense pain [61]. Because of the frequency of envenomation events on humans, severity of clinical symptoms, and the frequent serious clinical consequences of their bite, black widow spiders are classified as medically important [62].

2.2.1. Latrotoxins

From the point of view of this Perspective, the most interesting group of toxic proteins from the venom of species belonging to the *Latrodectus* genus are latrotoxins. They are high molecular weight (110–140 kDa) and acidic proteins whose toxic activity relies on the formation of pores through biological membranes [63–66]. The latrotoxin family includes 3 different subclasses based on their prey specificity: vertebrates (LTX), crustaceans (LTC), or insects (LIT). LTX and LCT subclasses contain only one member each, α-latrotoxin (α-LTX) and α-latrocrustaceatoxin (α-LCT), respectively. So far, five latrotoxins have been identified as insect specific and, consequently, they are known as α, β, γ, δ and ε-latroinsectotoxins (LITs) [67,68]. Therefore, the main difference between α-LTX and the different LITs is prey selectivity. From the evolutional point of view, the presence of different LIT isoforms is related to hunt specialization. Nevertheless, only α-LTX is specific for mammals, which can be associated with the evolution of a defensive weapon against other attackers, like rodents.

α-LTX is the best characterized member of the latrotoxin family and neurexins and latrophilins have been identified as its potential protein receptors [19,63,64]. Although no specific information about LIT receptors has been reported so far, there are orthologs of the above receptors in insects,

suggesting that these similar insect proteins could be involved in recognition. However, both α-LTX and LITs have been proven to produce pores not only in cells expressing these receptors, but also in artificial bilayers [19,69]. Interestingly, although very little is known about the physiological activity of δ-LIT, it seems to be receptor-independent, showing a lack of neuronal selectivity.

LTXs are synthetized as large inactive polypeptide precursors which undergo post-translational processing on both their N- and C-termini [63,67,69,70]. The mature versions show a modular structure with three well-differentiated domains: the 'wing', the 'body', and the 'head' [19] (Figure 3). The wing corresponds to a unique N-terminal domain which seems to be involved in receptor recognition, while the C-terminal domain is composed by a high number of consecutive ankyrin repeats and comprises the body and the head. A low-resolution three-dimensional structure was obtained for α-LTX by cryo-electron microscopy (cryo-EM). It appeared as a dimer in the absence of cations but, in the presence of Ca^{2+} or Mg^{2+}, ankyrin-repeats probably mediate protein-protein interactions that led to the formation of water-soluble homotetramers with a well-defined central channel. This type of assembly is known as the 'four-bladed propeller' model [19] (Figure 3). In fact, this four-bladed structure, which is amphipathic, appears to be inserted into the membrane, forming pores that could also be detected by cryo-EM [19,63]. The reconstruction published had very low resolution [19] but, even so, the presence of 'windows' (fenestrations) was observed in the pore lumen. The polar heads of some phospholipids would presumably show up through those fenestrations, providing stability and selectivity to the channel. This situation is far from being solved, but it has also been detected in other PFPs such as the actinoporin FraC [42] (Figure 2). These cryo-EM experiments were carried out, however, not only in the absence of the corresponding membrane protein receptors, but also using palmitoyl-oleyl-phosphatidylcholine (POPC) as the sole support. Plasma membranes also contain large amounts of other key lipids for the physiological behavior of a biological membrane, such as cholesterol (50%), phosphatidylserine (7%), sphingomyelin (4%), and phosphatidylinositols (1%). To date, the role of lipids in the mechanism of action of LTXs is still not fully known. Thus, although the authors of the paper concluded that the toxin itself was capable of forming pores in the membrane in the absence of any other protein component of neuronal origin it is far from proven that another component of spider venom, for example, is not needed to carry out this insertion. The structure-function relationship of these proteins is still mostly unknown at the molecular level. Furthermore, there is no three-dimensional structural information about LITs. However, α-LTX and LIT share the same genetic domain structure; they are around 50% identical, so it can be assumed that they probably exhibit a similar fold.

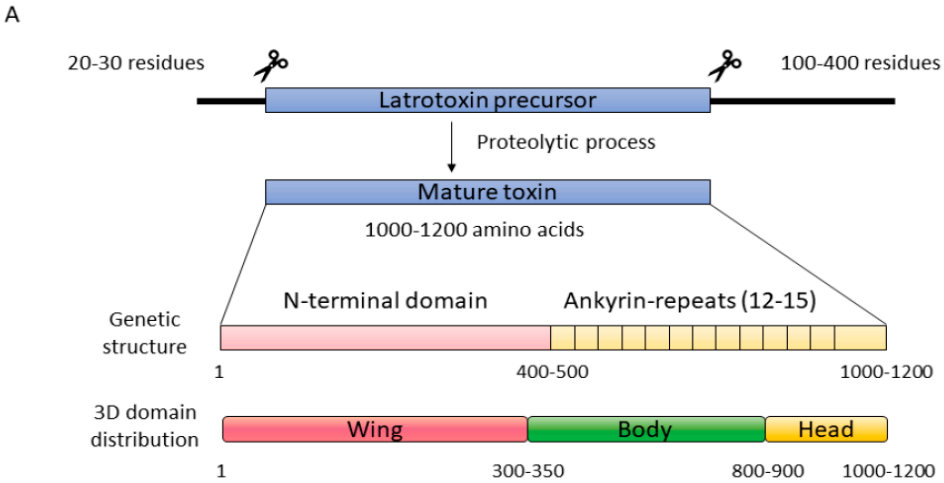

Figure 3. *Cont.*

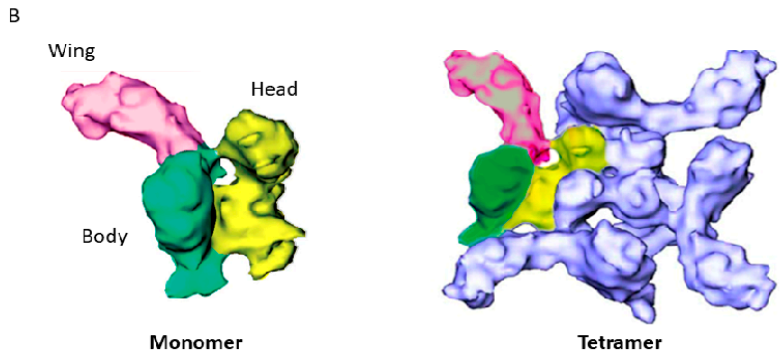

Figure 3. (**A**) Latrotoxins are produced as inactive precursor activated upon proteolytic digestion in both the N- and C-termini. The genetic structure comprises a unique N-terminal domain and a C-terminal domain rich in ankyrin repeats. Within a low-resolution three-dimensional structure of α-LTX obtained by cryo-EM, three different domains can be differentiated: the wing (pink), the body (green), and the head (yellow). (**B**) The final pore is composed by four α-LTX monomers, combined in a so called 'four-bladed propeller'. The head and the body are responsible for membrane binding and pore formation, while the wing seems to be implicated in receptor recognition. Reproduced from Ushkaryov, Y.A., Volynski, K.E., Ashton, A.C., The multiple actions of black widow spider toxins and their selective use in neurosecretion studies. *Toxicon* 2004, Elsevier.

The physiological effect observed regarding the toxicity of LTXs or LITs in insect tissues includes the increase in the frequency of glutamatergic and GABA-ergic potential at the neuromuscular junctions and the asynchronous release of these neurotransmitters [67,69]. The cholinergic sensory nervous system of the insects is also affected. All these events seem to be related with the major molecular event of LTX toxicity: the formation of cation selective pores in membranes. Thus, in the presynaptic space, pore formation leads to Ca^{2+} fluctuations, promoting massive neurotransmitter release. However, it is still necessary to study LITs in deeper detail in order to understand their toxicity and structure-function relationships. Actually, all the aforementioned LITs have been tested for toxicity against *Galleria mellonella* larvae [71], a model system where they showed very different LD_{50} values (mg of toxin necessaries to kill 50% of the tested animals expressed per kg of body weight).

2.2.2. Latrodectins

Low molecular weight proteins (originally called LMW, or black widow low molecular weight venom components) of around 70 amino acids long and with a high content of disulfide bridges have also been detected within the venomous black widow spider cocktail, and even isolated in small quantities. Nowadays, these proteins are known as latrodectins (Ltds) [72]. Their natural function is not yet known, but the few available results suggest that they are essential for increasing the neurotoxic capacity of LTXs, most likely by cooperating with them and increasing their affinity for the membrane. Paradoxically, their participation seems to be also key in diminishing the specificity of this interaction, thus facilitating an insecticidal activity of α-LTX [72], a toxicity which, in the absence of Ltds, seems to be only restricted to vertebrates. The association between LTXs and Ltds is presumed to be crucial, given that it seems practically impossible to purify LTXs to homogeneity by conventional methods [73–75], as they seem to be always contaminated with Ltds. Some authors even consider them as mere subunits of what is called the *latrotoxin macromolecular complex* [74], given that, separately, they do not appear to be toxic neither against insects or vertebrates [75–78]. As for their structure, apart from their sequences, there is only one spectroscopic characterization, by means of circular dichroism, which suggests that they should have a high α-helix content [79]. Thus, although they are not proven to be PFPs, they could be determinant for the final pore formation of LTXs, forming a macromolecular complex, and their presence should be taken into account when designing biotechnological application of LTXs.

3. Biotechnological Applications of PFPs

The obvious benefit of studying venoms in detail is finding the means to block their deleterious effects. Although envenomation is a neglected public health problem in many of developed countries [80], it frequently causes intense pain and, when complicated symptoms occur, can even lead to death of the affected individual. This Perspective, however, focuses on the potential of some venom components as biotechnological tools.

The study of venoms can then open the gate to not-so-obvious venues. For example, detailed knowledge about the mechanism of action of many toxins offers the possibility of using them for at least three different approaches: detecting, inactivating, or modulating different cellular or metabolic pathways. As mentioned above, toxins co-evolve with their targets. During this intense competition, toxic compounds become highly specific to their target. Such a great specificity can be used to fight different pests with the employment of the corresponding venomous natural product. In addition, venom can interfere with the immune system regulating signaling pathways, tuning cytokine secretion or promoting cell migration. Understanding how they work can put toxins on the radar of new immunotherapies with venom or venom-derived products [61,62,81,82].

Given the high specificity and binding affinity of some toxins, they can be also used as molecular probes, after the appropriate modifications such as conjugation to fluorophores. In fact, one of the most successful and best systems for cellular in situ detection of sphingomyelin and cholesterol-rich domains is based on the employment of modified versions of actinoporins, PFTs from sea anemones [83,84].

On the other hand, if the target cellular components or metabolic pathways are dysregulated during a disease, having a molecule with high binding affinity is a perfect starting point to make the appropriate modifications and modulate the target activity, regulating its biological function. Our present knowledge allows molecular mimicry of natural products which appear promising in order to find new therapeutic treatments.

Another possibility would be providing proteinaceous toxins with the means to change their specificity without losing their lethal properties, as in the case of immunotoxins (IMTXs). This approach takes advantage of toxins' highly specific and potentially deadly activity, but it drives it toward aberrant cells like cancer, metastatic, or cancer stem cells, for example. IMTXs are chimeric constructions built from a target domain, which recognizes the harmful cell, and a toxic domain, which kills it [81,85–91].

3.1. The Biotechnological Potential of Cnidaria PFTs as IMTXs

Immunotoxins are hybrid artificial molecules in which the killer action of a toxin is directed to a target cell through a binding domain (Figure 4). The binding domain can be a monoclonal antibody or, in order to improve the penetration capacity of the construct, a smaller engineered version such as the single-chain variable fraction of the selected antibody. Regarding the toxic moiety, most IMTXs use toxic proteins which, acting intracellularly, lead to cell death by different means. The translocation of this IMTX is then necessary to achieve the internalization of this toxin moiety into the cytosol. This approach is especially successful against hematological tumors [92]. However, IMTXs have trouble attacking solid tumors due to difficult penetration in tumor masses.

One of the advantages of using PFPs as the toxic moiety of IMTXs be is that they do not need internalization to exert their toxic activity. Some examples can be found in recent scientific literature, which use actinoporins [39], melittin peptide from bee venom [93], or the N-terminal domain of the human perforin [94]. Since PFPs increase membrane permeabilization, in addition to their lethal membrane altering properties, they can also facilitate the action of regular chemotherapies by facilitating the entrance to the cytosol [95].

The first IMTX built with an actinoporin was developed by Avila et al. [96] conjugating a monoclonal antibody recognizing IOR-T6, a specific antigen expressed on the surface of immature T-lymphocytes, and a hemolytic toxin from *Stichodacthyla helianthus*. Later, the same group developed a new chimera with a monoclonal antibody against carcinoembryonic antigen (CEA) [97]. One of the latest approximations was linking, again, an actinoporin from *S. helianthus* with a monoclonal antibody

recognizing a colorectal cancer-associated antigen (IOR-C2) [98]. Although the chimeras recognized the corresponding antigens preferentially through the monoclonal antibody fraction, the non-specific toxicity against cell lines not expressing the targeted antigen was still relatively high. Thus, the greater advantage of these toxins (attacking the membrane, which is the most widespread target in the living cells), is also their greatest weakness. Further research is required in order to eliminate the off-target effects of the actinoporin-based chimeras.

In addition, once bound, actinoporins need to diffuse within the membrane in order to oligomerize and form a pore. Being attached to an antibody recognizing a surface antigen is probably an obstacle for the final pore formation. However, actinoporins are very well studied from the structure-function point of view, allowing protein engineering to overcome these hurdles. Several research studies delve into the details of the protein-lipid interactions [10,15,30,31,33,42,99–103], making possible the application of different strategies directed to improve toxin specificity: for example, protecting the toxin region responsible for membrane binding or blocking the N-terminal domain directly implicated in pore formation. Actinoporins can be engineered to protect their key regions with polypeptide domains, which can later be released by tumor specific proteases. Actinoporins are quite resistant to protease activity and are cysteineless. This last feature makes them suitable for site directed mutagenesis followed by modification through conjugation. Matrix metalloproteases (MMPs) are extracellular proteases that remodel the extracellular matrix and whose expression is increased in the cells surrounding tumors [104], along with other proteinases like catepsin B [105] or furin [106] (Figure 4). High expression of extracellular matrix proteases is correlated with the invasion capacity of the tumor. Protective domains could be linked to the protein by sites suitable for tumor-specific protease digestion. Conjugating the specificity of the antigen recognition provided by the monoclonal antibody moiety and the proteinase-activated toxic activity could improve the specificity of cytolysin-based IMTXs [95,107,108].

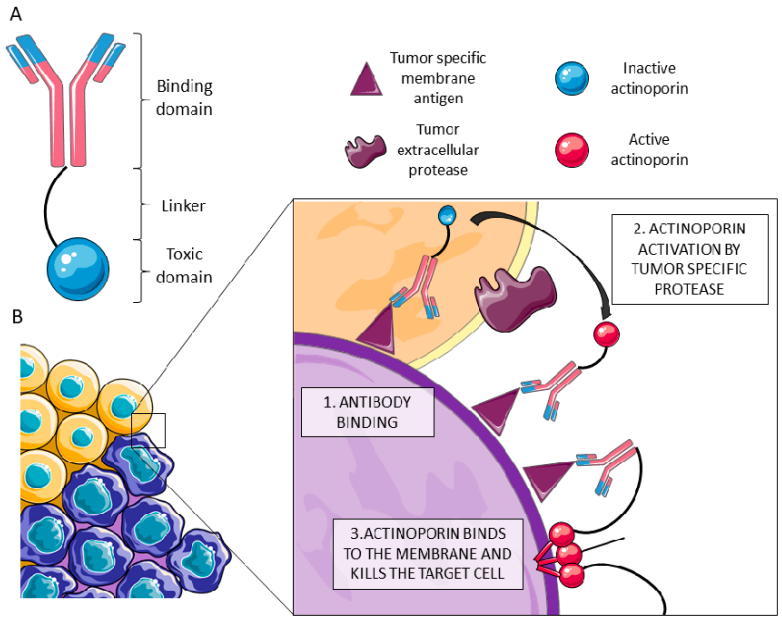

Figure 4. (**A**) Immunotoxins (IMTXs) are chimeric molecules composed of a monoclonal antibody that recognizes the malign cells and a toxin moiety that kills the targeted cells. (**B**) In order to improve the specificity of actinoporin IMTXs, protease-activated variants have been designed. Once the chimeric molecule binds specifically to malign cells (in purple) by recognition of a membrane motif missing in the healthy ones (in orange) (**1**), the toxic moiety is activated by a tumor specific protease (**2**). The activated actinoporin is then able to bind the membrane, oligomerize with other monomers, and form a pore, killing the targeted cell by an osmotic shock (**3**). This image was created using Servier Medical Art free images database (SERVIER, Paris, France).

3.2. The Biotechnological Potential of Arachnid PFPs as Bioinsecticides

Although the structural and the associated functional knowledge about LITs is restricted and further work has to be done to understand the activity of these toxins, the toxicity information detailed above and the structural characterization of α-LTX make LITs a suitable starting point to design bioinsecticides.

The world population has been increasing exponentially since 1900. By 2050, it is estimated to reach 9 billion, according to the United Nations. Obviously, this increase comes together with a greater need for sustenance. However, crop losses due to plagues are a major problem, worsened every day by climate change [109]. For decades, approximately since the 1940s, pest control relied on the use of dichlorodiphenyltrichloroethane (DDT). It was cheap, easy to produce and deliver, and effective, but its poor selectivity and high toxicity forced many countries to ban it. Within this context, bioinsecticides have emerged as a promising pest control tool [81], based on the use of natural toxins. Spiders, scorpions, and many other venomous animals have insects as preferred prey. Therefore, their toxic cocktails include compounds specifically directed to insects, which appear highly valuable to fight pests [110,111]. Thus, these biopesticide approaches would include two different strategies: the development of suitable tools for fumigation or the construction of transgenic variants which constitutively produce protective toxins to avoid damage caused by pests. Although there is still skepticism about the consumption of genetically modified organisms, no adverse effects have been observed so far [112], and proper legislation about their commercialization should be introduced in the near future to take advantage of their proven beneficial properties [113].

The ideal bioinsecticide should be stable in conditions of extreme humidity and temperature, active topically or orally, and should be rapidly lethal to pest insects, but innocuous to humans and other non-pest species like bees, fishes, or birds. In addition, it should not be bioaccumulated or produce harmful secondary or degradation products [111]. A priori, insecticidal toxins from spiders cover almost every one of these requirements, even regarding degradation, since proteins are completely biodegradable into innocuous amino acids.

The most successful example of bioinsecticide is *Bacillus thuringiensis* insecticidal three-domain Cry toxin (3d-Cry) [114], which is in fact a PFP. When a susceptible larva ingests the toxin, it gets activated in the gut, where it binds and leads to pore formation, provoking cell death and compromising larvae viability. The major issues encountered by this approximation is the UV sensitivity of the toxin that reduces its availability for spray dispersion and the emergence of insect resistance [115,116]. As introduced at the beginning of this article, venom effectivity/resistance is a constant race for survival and without insecticidal innovation pest would end up developing resistance.

The toxicity of LTXs, as well as many other components of the spider venom, is exerted at the level of neuromuscular junction. For spiders, reaching the target cells is easier through piercing chelicerae, but applying the toxins alone as biopesticides requires identification of an easier administration/delivery. There are two possible administration routes that imply different technological approaches: intoxication of the insect through ingestion or reaching the neuromuscular junctions through the spiracles connecting to the tracheas that transport the gases and connect with tissues for cellular respiration. Some spider toxins (like disulfide-rich knottin peptides, known as inhibitor-cystine knot (ICK)), have been already demonstrated to be potent, stable and orally active for insects [111,117–119]. If LITs were orally active, it would be possible to deliver them in aerosol, which would be the easiest way to commercialize them. However, big proteins are more prone to degradation, and the resistance to extreme humidity or temperature conditions is not guaranteed. Designing transgenic crops constitutively producing the compound is another option that has been successful for other toxins like the aforementioned *B. thuringiensis* toxins [120], which have been proven to be safe for human consumption. In addition, the toxins produced by the transgenic species only affect insects consuming the crop, avoiding the collateral damage to beneficial insects like bees and other critical species for the pollination maintenance. Since LTXs are PFPs and they increase the permeability of the target cells, their application in combination

with other bioinsecticide components whose activity is developed intracellularly [81,111] can increase the bioinsecticide activity synergistically.

The greatest inconvenience for insecticide application of LTX family raised by different authors is the high molecular mass of this class of toxins, and therefore, the difficulty of cloning and producing them in heterologous systems [111,121]. However, successful experience cloning and expressing the mature form of δ-LIT in bacteria has been already accomplished [69]. Moreover, according to the preliminary data obtained through the structural information for α-LTX pore, the whole protein is not necessary to promote pore formation. Given the high identity between α-LTX and LITs and assuming that the three-dimensional structure would be similar to that of α-LTX, it might be possible to eliminate the 'wing' domain, which is supposed to be implicated in receptor recognition. Although more studies need to be done on the selectivity of LITs, as well as the structural domain implicated in receptor recognition, restricting the cloned sequence to the minimum necessary to exert lytic activity would reduce the specificity of the attack, but it might increase the chances of success. Other approaches to increase the oral activity of toxins is conjugating them with carrier proteins recognized by insect midgut transporters like the mannose-specific lectin agglutinin from *Galanthus nivalis*. Upon ingestion by insects, it is recognized by a receptor located in the midgut cells. It is receptor-mediated endocytosed, followed by transportation and accumulation in the hemolymph [122].

Another interesting option is the use of baculoviruses as pest control agents. Natural baculoviruses have been already used for effective pest control. However, genetic engineering amplifies the possibilities of this tool, making them an even better alternative [123–126]. Natural baculoviruses kill pest by themselves within weeks, while recombinant baculoviruses including toxins would shorten the treatment time. In addition, this system has the advantage of being stable by itself, while also providing specificity for the host and the possibility of treatment maintenance due to the potential transmission of the virus both horizontally (among insects of the same species in the same development state) and vertically (from adult insects to their progeny) [125] (Figure 5). Interestingly, it has been very recently reported how a transgenic fungus expressing a potent insect-selective spider toxin can be effective against insecticidal resistant mosquitos [127].

4. *Omic* Techniques in the Discovery of New Potentially Useful PFPs

One of the most famous examples of toxin-inspired pharmacological drugs is captopril, a drug for hypertension treatment that inhibits angiotensin-converting enzyme (ACE). Its discovery was derived from studies with small toxic peptides from the snake *Bothrops jararaca* [128] and it was approved by the FDA in 1981. Research in this field is now booming as a consequence of the technological development of powerful techniques for identification of new bioactive compounds. Identification of new toxins is associated with a great variety of potential applications.

'Omic' techniques are instrumental and informatis-dependent tools that have reached new levels of performance within the past decade. As stated at the beginning of this article, venomous animals are usually small and venom yield production is low. These facts were major obstacles in venom research. The purification of bioactive compounds rendered small yields, such that only the more abundant compounds were detected and used in research, even if low-abundance molecules had a critical role in toxicity. Many of these new 'omic' approaches have reduced the amount of starting material needed for the analysis, making it affordable for venom studies [129–132]. In depth analysis of venoms from long-neglected organisms using these techniques not only increases the knowledge about venom composition, phylogeny, and evolution, but also allows the identification of underrepresented toxins which may exert unique biological properties and hold potential applications. These techniques are excellent for high throughput screening of new bioactive compounds. Venoms are a quite fascinating material from the evolutionary point of view, and genomic, transcriptomic, and proteomic analysis reveal quite interesting features about the evolution of venomous species [132,133].

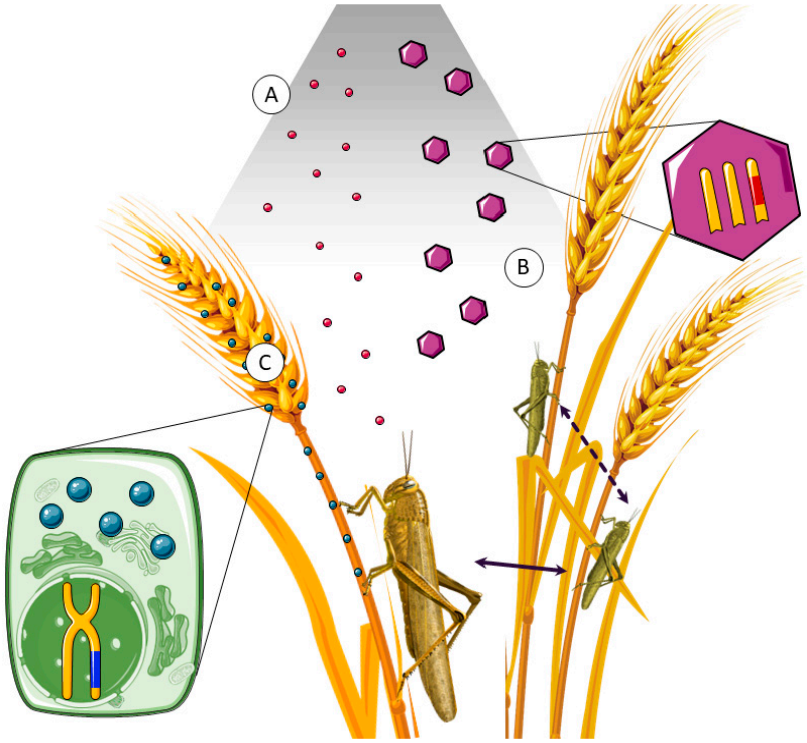

Figure 5. Bioinsecticides can be spread over crops as aerosols if they are orally active, or they can enter their target through insect spiracles. Bioinsecticides can be delivered directly as active toxic products (**A**) or as genetically modified baculovirus-based pesticides, containing toxin genes (**B**). After larvae ingest baculoviruses by feeding, they can develop a lethal disease, releasing new infective particles, suitable for horizontal (dashed arrow) or vertical (continuous arrow) infection. Genetically modified crops for biopesticide production eliminate the pest in both adult and larva state if they are orally active (C). This image was created using Servier Medical Art free images database (SERVIER, Paris, France).

Among all these massive analysis techniques, transcriptomics has arisen as the preferred analysis for this venom specific approximation, providing the most secure approach to assess general venom composition. The strength of genomics is its ability to work with a great amount of data, but de novo analysis is still slow. On the other hand, RNAseq analysis has proven to be a solid approximation for de novo assembly, thanks to algorithms like Trinity [134]. In addition, it provides information about transcript quantification, increasing the value of the obtained information when multi-tissue studies are developed. Dissecting the whole venom delivery system makes a good picture of the full toxin arsenal produced [132,135–137]. For a long time, transcriptomics has been the only way to analyze venom-related samples because it was not possible to obtain enough material to apply other high-throughput techniques, such as proteomics, which needs a greater starting material. Indeed, it is still the preferred pre-screening technique [6,135,138]. However, the sample requirements have been reduced by the progress of mass spectrometry (MS) instruments which now provide fragmentation techniques reducing the cost of massive peptide sequencing on tandem MS (MS/MS) [139]. Besides sequence and expression levels, proteomics reveals valuable information about multiple protein products translated from alternatively spliced transcripts and post-translational modifications (PTMs) such as phosphorylation, glycosylation, elimination of signal peptides, or cysteine scaffold patterns [136,139,140]. Indeed, glycomics is a proteomics subdivision which is gaining importance in translational venom research because the identification of glycosylated peptides and proteins can be very important in the identification of compounds suitable for therapeutic application, in particular identification of carbohydrate- and protein-based epitopes as allergic response promoters [136].

Most of the protein sequences annotated as toxins were predicted from RNA sequences with open reading frame-finding tools, they are not supported by any experimental data. Proteomics provides the necessary evidence to verify the transcripts obtained on transcriptomic analysis. Combination of proteomics and transcriptomics is critical in the identification of false-positive putative toxin transcripts [140–142].

'Omic' techniques come together with an intense bioinformatic progress. Assembly of the huge de novo transcriptomic and genomic jigsaws would not be possible without the appropriate programs [134,143] and the necessary computational power [6,135,143,144]. The availability of in silico applications that predict both the presence of a toxin with a completely new activity or the possible off-target effects that would limit the potential use of the toxin as a biotechnological tool opens up new opportunities for novel drug discovery [145]. In full agreement with this development, the term 'venomics' has been established to define the application of 'omic' techniques to venoms. Indeed, some authors have developed a standardized workflow for venomics [132,136,146].

Finally, the term 'pharmacomics' refers to the holistic focus on 'omic', merged with the functional characterization of newly discovered bioactive compounds, extending the classical venomic definition with the critical step of functional characterization [136]. The perspectives in the application of toxins as tools in pharmacology and bioinsecticides are promising, and the emerging techniques combined with bioinformatic advances will facilitate the discovery of new toxins suitable for its use in the biotechnology field.

5. Conclusions

Animal venoms have been recognized as a source for bioactive compounds such as peptides and proteins with potential use in different biotechnological fields. PFPs are a common family of proteins present in the vast majority of venoms. They share a widespread target, the plasma membrane, and promote cell death through osmotic shock and depolarization of the plasma membrane target cells. Their lytic properties can be resourceful if directed to specific targets, as well as in increasing their permeability, easing the access to other toxic components acting at the intracellular level. Actinoporins produced by sea anemones do not need a protein receptor, but SM, a lipidic receptor. This feature makes them wide-spectrum toxins. The biotechnological applications for this kind of PFPs include the design of probes for SM and SM-rich domains, and protein engineering for construction of immunotoxins against cancer cells or parasites. Regarding immunotoxins, although promising strategies have been applied to improve selectivity of the toxic moiety for the targeted cells, further work has to be done. On the other hand, spiders are professional insect hunters whose venomous arsenal is a potential source of insecticide compounds. Among their toxin arsenal, latrotoxins are a family of big PFPs that promote ion depolarization and massive neurotransmitter release at the neuromuscular junction of insects, provoking their paralysis and death within seconds. This kind of toxin is attractive for the development of new bioinsecticides that lack the already shown resistance of other biopesticides like the one based on the 3d-Crys toxins produced by *B. thuringiensis*. However, LITs suffer the lack of structural and functional characterization as well as the evidence of oral activity for their use as sprays or as part of transgenic crops, therefore extensive and detailed research has to be done to harvest beneficial applications.

The emergence and establishment of accessible high-throughput screening technology makes easier to find new bioactive compounds with unknown activities that can be used in new applications, always taking into account the native activity of the toxin. Transcriptomics is the most widely used technique for the search of new compounds, although the establishment of more complex workflows for venom identification and functional annotation is improving the accuracy and increasing the range of possibilities.

Author Contributions: All authors wrote, read, and revised the article and suggested changes and modifications which significantly improved the version submitted.

Funding: This work was supported by Santander-Universidad Complutense de Madrid project PR 75-18-21561 to Álvaro Martínez-del-Pozo.

Acknowledgments: We thank J. Peter Slotte from Åbo Akademi (Turku, Finland) for his encouragement and inestimable support. Jessica Garb (UMass Lowell, MA, USA) has provided us with the expertise and the starting materials needed to approach the engineering of PFPs from arachnids. This work was supported by a Banco Santander-UCM fellowship to Esperanza Rivera-de-Torre and a Real Colegio Complutense Postdoctoral Research Fellowship at Harvard University for Distinguished Junior Scholars to Sara García-Linares. Juan Palacios-Ortega has a funded doctoral position by ISB/ÅA. We thank Harvard Medical School PhD candidate Bradley M. Wierbowski for reading the manuscript and editing and correcting English language and style.

Conflicts of Interest: The authors declare no conflict of interest.

References

1. Casewell, N.R.; Wuster, W.; Vonk, F.J.; Harrison, R.A.; Fry, B.G. Complex cocktails: The evolutionary novelty of venoms. *Trends Ecol. Evol.* **2013**, *28*, 219–229. [CrossRef] [PubMed]
2. Calvete, J.J. Venomics: Integrative venom proteomics and beyond. *Biochem. J.* **2017**, *474*, 611–634. [CrossRef] [PubMed]
3. Arbuckle, K.; Rodriguez-de-la-Vega, R.C.; Casewell, N.R. Coevolution takes the sting out of it: Evolutionary biology and mechanisms of toxin resistance in animals. *Toxicon* **2017**, *140*, 118–131. [CrossRef] [PubMed]
4. Wang, Y.; Yap, L.L.; Chua, K.L.; Khoo, H.E. A multigene family of Heteractis magnificalysins (HMgs). *Toxicon* **2008**, *51*, 1374–1382. [CrossRef] [PubMed]
5. Valle, A.; Alvarado-Mesen, J.; Lanio, M.E.; Álvarez, C.; Barbosa, J.A.; Pazos, I.F. The multigene families of actinoporins (part I): Isoforms and genetic structure. *Toxicon* **2015**, *103*, 176–187. [CrossRef] [PubMed]
6. Rivera-de-Torre, E.; Martínez-del-Pozo, Á.; Garb, J.E. Stichodactyla helianthus' de novo transcriptome assembly: Discovery of a new actinoporin isoform. *Toxicon* **2018**, *150*, 105–114. [CrossRef] [PubMed]
7. Goñi, F.M. The basic structure and dynamics of cell membranes: An update of the Singer-Nicolson model. *Biochim. Biophys. Acta* **2014**, *1838*, 1467–1476. [CrossRef]
8. Tanaka, K.; Caaveiro, J.M.; Tsumoto, K. Bidirectional Transformation of a Metamorphic Protein between the Water-Soluble and Transmembrane Native States. *Biochemistry* **2015**, *54*, 6863–6866. [CrossRef]
9. Lella, M.; Mahalakshmi, R. Metamorphic Proteins: Emergence of Dual Protein Folds from One Primary Sequence. *Biochemistry* **2017**, *56*, 2971–2984. [CrossRef]
10. García-Linares, S.; Rivera-de-Torre, E.; Palacios-Ortega, J.; Gavilanes, J.G.; Martínez-del-Pozo, Á. The metamorphic transformation of a water-soluble monomeric protein into an oligomeric transmembrane pore. In *Advances in Biomembranes and Lipid Self-Assembly*; Iglic, A., García-Sáez, A., Rappolt, M., Eds.; Elsevier: Amsterdam, Netherlands, 2017; pp. 51–97.
11. Parker, M.W.; Feil, S.C. Pore-forming protein toxins: From structure to function. *Prog. Biophys. Mol. Biol.* **2005**, *88*, 91–142. [CrossRef]
12. García-Ortega, L.; Alegre-Cebollada, J.; García-Linares, S.; Bruix, M.; Martínez-del-Pozo, Á.; Gavilanes, J.G. The behavior of sea anemone actinoporins at the water-membrane interface. *Biochim. Biophys. Acta* **2011**, *1808*, 2275–2288. [CrossRef] [PubMed]
13. Rossjohn, J.; Feil, S.C.; McKinstry, W.J.; Tweten, R.K.; Parker, M.W. Structure of a cholesterol-binding, thiol-activated cytolysin and a model of its membrane form. *Cell* **1997**, *89*, 685–692. [CrossRef]
14. García-Linares, S.; Rivera-de-Torre, E.; Morante, K.; Tsumoto, K.; Caaveiro, J.M.; Gavilanes, J.G.; Slotte, J.P.; Martínez-del-Pozo, Á. Differential Effect of Membrane Composition on the Pore-Forming Ability of Four Different Sea Anemone Actinoporins. *Biochemistry* **2016**, *55*, 6630–6641. [CrossRef] [PubMed]
15. Anderluh, G.; Lakey, J.H. Disparate proteins use similar architectures to damage membranes. *Trends Biochem. Sci.* **2008**, *33*, 482–490. [CrossRef] [PubMed]
16. Bakrač, B.; Gutiérrez-Aguirre, I.; Podlesek, Z.; Sonnen, A.F.; Gilbert, R.J.; Macek, P.; Lakey, J.H.; Anderluh, G. Molecular determinants of sphingomyelin specificity of a eukaryotic pore-forming toxin. *J. Biol. Chem.* **2008**, *283*, 18665–18677. [CrossRef] [PubMed]

17. Schön, P.; García-Saez, A.J.; Malovrh, P.; Bacia, K.; Anderluh, G.; Schwille, P. Equinatoxin II permeabilizing activity depends on the presence of sphingomyelin and lipid phase coexistence. *Biophys. J.* **2008**, *95*, 691–698. [CrossRef] [PubMed]
18. Endapally, S.; Frias, D.; Grzemska, M.; Gay, A.; Tomchick, D.R.; Radhakrishnan, A. Molecular Discrimination between Two Conformations of Sphingomyelin in Plasma Membranes. *Cell* **2019**, *176*, 1040–1053. [CrossRef]
19. Orlova, E.V.; Rahman, M.A.; Gowen, B.; Volynski, K.E.; Ashton, A.C.; Manser, C.; van Heel, M.; Ushkaryov, Y.A. Structure of alpha-latrotoxin oligomers reveals that divalent cation-dependent tetramers form membrane pores. *Nat. Struct. Biol.* **2000**, *7*, 48–53.
20. Lau, M.T.; Manion, J.; Littleboy, J.B.; Oyston, L.; Khuong, T.M.; Wang, Q.P.; Nguyen, D.T.; Hesselson, D.; Seymour, J.E.; Neely, G.G. Molecular dissection of box jellyfish venom cytotoxicity highlights an effective venom antidote. *Nat. Commun.* **2019**, *10*, 1655. [CrossRef]
21. Maldonado, E.; Maillaud, C.; Barguil, Y.; Labadie, M. Rhabdomyolysis during envenomation by Physalia sp envenomation in New Caldonia. *Med. Sante Trop.* **2017**, *27*, 105–108.
22. Tezcan, O.D.; Gozer, O. Severe Toxic Skin Reaction Caused by a Common Anemone and Identification of the Culprit Organism. *J. Travel Med.* **2015**, *22*, 269–271. [CrossRef] [PubMed]
23. Rojko, N.; Dalla Serra, M.; Macek, P.; Anderluh, G. Pore formation by actinoporins, cytolysins from sea anemones. *Biochim. Biophys. Acta* **2016**, *1858*, 446–456. [CrossRef]
24. Macrander, J.; Broe, M.; Daly, M. Tissue-Specific Venom Composition and Differential Gene Expression in Sea Anemones. *Genome Biol. Evol.* **2016**, *8*, 2358–2375. [CrossRef] [PubMed]
25. Alegre-Cebollada, J.; Oñaderra, M.; Gavilanes, J.G.; Martínez-del-Pozo, Á. Sea anemone actinoporins: The transition from a folded soluble state to a functionally active membrane-bound oligomeric pore. *Curr. Protein Pept. Sci.* **2007**, *8*, 558–572. [CrossRef] [PubMed]
26. Bernheimer, A.W.; Avigad, L.S. Properties of a toxin from the sea anemone Stoichacis helianthus, including specific binding to sphingomyelin. *Proc. Natl. Acad. Sci. USA* **1976**, *73*, 467–471. [CrossRef] [PubMed]
27. Bjorkböm, A.; Rog, T.; Kaszuba, K.; Kurita, M.; Yamaguchi, S.; Lonnfors, M.; Nyholm, T.K.; Vattulainen, I.; Katsumura, S.; Slotte, J.P. Effect of sphingomyelin headgroup size on molecular properties and interactions with cholesterol. *Biophys. J.* **2010**, *99*, 3300–3308. [CrossRef]
28. Martínez, D.; Otero, A.; Álvarez, C.; Pazos, F.; Tejuca, M.; Lanio, M.E.; Gutiérrez-Aguirre, I.; Barlic, A.; Iloro, I.; Arrondo, J.L.; et al. Effect of sphingomyelin and cholesterol on the interaction of St II with lipidic interfaces. *Toxicon* **2007**, *49*, 68–81. [CrossRef]
29. Alm, I.; García-Linares, S.; Gavilanes, J.G.; Martínez-del-Pozo, Á.; Slotte, J.P. Cholesterol stimulates and ceramide inhibits Sticholysin II-induced pore formation in complex bilayer membranes. *Biochim. Biophys. Acta* **2015**, *1848*, 925–931. [CrossRef]
30. García-Linares, S.; Alm, I.; Maula, T.; Gavilanes, J.G.; Slotte, J.P.; Martínez-del-Pozo, Á. The effect of cholesterol on the long-range network of interactions established among sea anemone Sticholysin II residues at the water-membrane interface. *Mar. Drugs* **2015**, *13*, 1647–1665. [CrossRef]
31. Palacios-Ortega, J.; García-Linares, S.; Astrand, M.; Al Sazzad, M.A.; Gavilanes, J.G.; Martínez-del-Pozo, Á.; Slotte, J.P. Regulation of Sticholysin II-Induced Pore Formation by Lipid Bilayer Composition, Phase State, and Interfacial Properties. *Langmuir* **2016**, *32*, 3476–3484. [CrossRef]
32. Wacklin, H.P.; Bremec, B.B.; Moulin, M.; Rojko, N.; Haertlein, M.; Forsyth, T.; Anderluh, G.; Norton, R.S. Neutron reflection study of the interaction of the eukaryotic pore-forming actinoporin equinatoxin II with lipid membranes reveals intermediate states in pore formation. *Biochim. Biophys. Acta* **2016**, *1858*, 640–652. [CrossRef] [PubMed]
33. Palacios-Ortega, J.; García-Linares, S.; Rivera-de-Torre, E.; Gavilanes, J.G.; Martínez-del-Pozo, Á.; Slotte, J.P. Differential Effect of Bilayer Thickness on Sticholysin Activity. *Langmuir* **2017**, *33*, 11018–11027. [CrossRef] [PubMed]
34. Palacios-Ortega, J.; Garcia-Linares, S.; Rivera-de-Torre, E.; Gavilanes, J.G.; Martinez-Del-Pozo, A.; Slotte, J.P. Sticholysin, Sphingomyelin, and Cholesterol: A Closer Look at a Tripartite Interaction. *Biophys. J.* **2019**, *116*, 2253–2265. [CrossRef] [PubMed]
35. Martín-Benito, J.; Gavilanes, F.; de-Los-Rios, V.; Mancheño, J.M.; Fernández, J.J.; Gavilanes, J.G. Two-dimensional crystallization on lipid monolayers and three-dimensional structure of sticholysin II, a cytolysin from the sea anemone Stichodactyla helianthus. *Biophys. J.* **2000**, *78*, 3186–3194. [CrossRef]

36. Mancheño, J.M.; Martín-Benito, J.; Martínez-Ripoll, M.; Gavilanes, J.G.; Hermoso, J.A. Crystal and electron microscopy structures of sticholysin II actinoporin reveal insights into the mechanism of membrane pore formation. *Structure* **2003**, *11*, 1319–1328. [CrossRef] [PubMed]
37. Mechaly, A.E.; Bellomio, A.; Gil-Carton, D.; Morante, K.; Valle, M.; González-Manas, J.M.; Guerin, D.M. Structural insights into the oligomerization and architecture of eukaryotic membrane pore-forming toxins. *Structure* **2011**, *19*, 181–191. [CrossRef]
38. Rojko, N.; Kristan, K.C.; Viero, G.; Zerovnik, E.; Macek, P.; Dalla Serra, M.; Anderluh, G. Membrane damage by an alpha-helical pore-forming protein, Equinatoxin II, proceeds through a succession of ordered steps. *J. Biol. Chem.* **2013**, *288*, 23704–23715. [CrossRef]
39. Antonini, V.; Pérez-Barzaga, V.; Bampi, S.; Penton, D.; Martínez, D.; Dalla-Serra, M.; Tejuca, M. Functional characterization of sticholysin I and W111C mutant reveals the sequence of the actinoporin's pore assembly. *PLoS ONE* **2014**, *9*, e110824. [CrossRef]
40. Baker, M.A.; Rojko, N.; Cronin, B.; Anderluh, G.; Wallace, M.I. Photobleaching reveals heterogeneous stoichiometry for equinatoxin II oligomers. *Chembiochem* **2014**, *15*, 2139–2145. [CrossRef]
41. Subburaj, Y.; Ros, U.; Hermann, E.; Tong, R.; García-Saez, A.J. Toxicity of an alpha-pore-forming toxin depends on the assembly mechanism on the target membrane as revealed by single molecule imaging. *J. Biol. Chem.* **2015**, *290*, 4856–4865. [CrossRef]
42. Tanaka, K.; Caaveiro, J.M.; Morante, K.; González-Mañas, J.M.; Tsumoto, K. Structural basis for self-assembly of a cytolytic pore lined by protein and lipid. *Nat. Commun.* **2015**, *6*, 6337. [CrossRef] [PubMed]
43. Anderluh, G.; Krizaj, I.; Strukelj, B.; Gubensek, F.; Macek, P.; Pungercar, J. Equinatoxins, pore-forming proteins from the sea anemone Actinia equina, belong to a multigene family. *Toxicon* **1999**, *37*, 1391–1401. [CrossRef]
44. Uechi, G.; Toma, H.; Arakawa, T.; Sato, Y. Molecular characterization on the genome structure of hemolysin toxin isoforms isolated from sea anemone Actineria villosa and Phyllodiscus semoni. *Toxicon* **2010**, *56*, 1470–1476. [CrossRef] [PubMed]
45. De-los-Ríos, V.; Oñaderra, M.; Martínez-Ruiz, A.; Lacadena, J.; Mancheño, J.M.; Martinez-del-Pozo, A.; Gavilanes, J.G. Overproduction in Escherichia coli and purification of the hemolytic protein sticholysin II from the sea anemone Stichodactyla helianthus. *Protein Expr. Purif.* **2000**, *18*, 71–76. [CrossRef] [PubMed]
46. Rivera-de-Torre, E.; García-Linares, S.; Alegre-Cebollada, J.; Lacadena, J.; Gavilanes, J.G.; Martínez-del-Pozo, Á. Synergistic Action of Actinoporin Isoforms from the Same Sea Anemone Species Assembled into Functionally Active Heteropores. *J. Biol. Chem.* **2016**, *291*, 14109–14119. [CrossRef] [PubMed]
47. Athanasiadis, A.; Anderluh, G.; Macek, P.; Turk, D. Crystal structure of the soluble form of equinatoxin II, a pore-forming toxin from the sea anemone Actinia equina. *Structure* **2001**, *9*, 341–346. [CrossRef]
48. Hinds, M.G.; Zhang, W.; Anderluh, G.; Hansen, P.E.; Norton, R.S. Solution structure of the eukaryotic pore-forming cytolysin equinatoxin II: Implications for pore formation. *J. Mol. Biol.* **2002**, *315*, 1219–1229. [CrossRef] [PubMed]
49. García-Linares, S.; Castrillo, I.; Bruix, M.; Menendez, M.; Alegre-Cebollada, J.; Martínez-del-Pozo, Á.; Gavilanes, J.G. Three-dimensional structure of the actinoporin sticholysin I. Influence of long-distance effects on protein function. *Arch. Biochem. Biophys.* **2013**, *532*, 39–45. [CrossRef] [PubMed]
50. Malovrh, P.; Viero, G.; Serra, M.D.; Podlesek, Z.; Lakey, J.H.; Macek, P.; Menestrina, G.; Anderluh, G. A novel mechanism of pore formation: Membrane penetration by the N-terminal amphipathic region of equinatoxin. *J. Biol. Chem.* **2003**, *278*, 22678–22685. [CrossRef] [PubMed]
51. Cosentino, K.; Ros, U.; García-Saez, A.J. Assembling the puzzle: Oligomerization of alpha-pore forming proteins in membranes. *Biochim. Biophys. Acta* **2016**, *1858*, 457–466. [CrossRef] [PubMed]
52. Ros, U.; García-Saez, A.J. More Than a Pore: The Interplay of Pore-Forming Proteins and Lipid Membranes. *J. Membr. Biol.* **2015**, *248*, 545–561. [CrossRef] [PubMed]
53. Kristan, K.; Podlesek, Z.; Hojnik, V.; Gutiérrez-Aguirre, I.; Guncar, G.; Turk, D.; González-Mañas, J.M.; Lakey, J.H.; Macek, P.; Anderluh, G. Pore formation by equinatoxin, a eukaryotic pore-forming toxin, requires a flexible N-terminal region and a stable beta-sandwich. *J. Biol. Chem.* **2004**, *279*, 46509–46517. [CrossRef] [PubMed]
54. Kristan, K.; Viero, G.; Macek, P.; Dalla Serra, M.; Anderluh, G. The equinatoxin N-terminus is transferred across planar lipid membranes and helps to stabilize the transmembrane pore. *FEBS J.* **2007**, *274*, 539–550. [CrossRef] [PubMed]

55. Alegre-Cebollada, J.; Martínez-del-Pozo, Á.; Gavilanes, J.G.; Goormaghtigh, E. Infrared spectroscopy study on the conformational changes leading to pore formation of the toxin sticholysin II. *Biophys. J.* **2007**, *93*, 3191–3201. [CrossRef] [PubMed]
56. Anderluh, G.; Dalla Serra, M.; Viero, G.; Guella, G.; Macek, P.; Menestrina, G. Pore formation by equinatoxin II, a eukaryotic protein toxin, occurs by induction of nonlamellar lipid structures. *J. Biol. Chem.* **2003**, *278*, 45216–45223. [CrossRef] [PubMed]
57. Rojko, N.; Anderluh, G. How Lipid Membranes Affect Pore Forming Toxin Activity. *Acc. Chem. Res.* **2015**, *48*, 3073–3079. [CrossRef] [PubMed]
58. Morante, K.; Bellomio, A.; Gil-Carton, D.; Redondo-Morata, L.; Sot, J.; Scheuring, S.; Valle, M.; González-Mañas, J.M.; Tsumoto, K.; Caaveiro, J.M. Identification of a Membrane-Bound Prepore Species Clarifies the Lytic Mechanism of Actinoporins. *J. Biol. Chem.* **2016**, *291*, 19210–19219. [CrossRef]
59. Rojko, N.; Cronin, B.; Danial, J.S.; Baker, M.A.; Anderluh, G.; Wallace, M.I. Imaging the lipid-phase-dependent pore formation of equinatoxin II in droplet interface bilayers. *Biophys. J.* **2014**, *106*, 1630–1637. [CrossRef]
60. Camp, N.E. Black widow spider envenomation. *J. Emerg. Nurs.* **2014**, *40*, 193. [CrossRef]
61. Prentis, P.J.; Pavasovic, A.; Norton, R.S. Sea Anemones: Quiet Achievers in the Field of Peptide Toxins. *Toxins* **2018**, *10*, 36. [CrossRef]
62. Ikonomopoulou, M.P.; Fernandez-Rojo, M.A.; Pineda, S.S.; Cabezas-Sainz, P.; Winnen, B.; Morales, R.A.V.; Brust, A.; Sanchez, L.; Alewood, P.F.; Ramm, G.A.; et al. Gomesin inhibits melanoma growth by manipulating key signaling cascades that control cell death and proliferation. *Sci. Rep.* **2018**, *8*, 11519. [CrossRef] [PubMed]
63. Ushkaryov, Y.A.; Volynski, K.E.; Ashton, A.C. The multiple actions of black widow spider toxins and their selective use in neurosecretion studies. *Toxicon* **2004**, *43*, 527–542. [CrossRef] [PubMed]
64. Ushkaryov, Y.A.; Rohou, A.; Sugita, S. alpha-Latrotoxin and its receptors. *Handb. Exp. Pharmacol.* **2008**, *184*, 171–206. [CrossRef]
65. Yan, S.; Wang, X.C. Recent Advances in Research on Widow Spider Venoms and Toxins. *Toxins* **2015**, *7*, 5055–5067. [CrossRef] [PubMed]
66. Wang, X.; Tang, X.; Xu, D.; Yu, D. Molecular basis and mechanism underlying the insecticidal activity of venoms and toxins from Latrodectus spiders. *Pest Manag. Sci.* **2019**, *75*, 318–323. [CrossRef] [PubMed]
67. Rohou, A.; Nield, J.; Ushkaryov, Y.A. Insecticidal toxins from black widow spider venom. *Toxicon* **2007**, *49*, 531–549. [CrossRef] [PubMed]
68. Duan, Z.G.; Yan, X.J.; Cao, R.; Liu, Z.; Wang, X.C.; Liang, S.P. Proteomic Analysis of Latrodectus tredecimguttatus Venom for Uncovering Potential Latrodectism-Related Proteins. *J. Biochem. Mol. Toxicol.* **2008**, *22*, 328–336. [CrossRef]
69. Dulubova, I.E.; Krasnoperov, V.G.; Khvotchev, M.V.; Pluzhnikov, K.A.; Volkova, T.M.; Grishin, E.V.; Vais, H.; Bell, D.R.; Usherwood, P.N. Cloning and structure of delta-latroinsectotoxin, a novel insect-specific member of the latrotoxin family: Functional expression requires C-terminal truncation. *J. Biol. Chem.* **1996**, *271*, 7535–7543. [CrossRef]
70. McCowan, C.; Garb, J.E. Recruitment and diversification of an ecdysozoan family of neuropeptide hormones for black widow spider venom expression. *Gene* **2014**, *536*, 366–375. [CrossRef]
71. Krasnoperov, V.G.; Shamotienko, O.G.; Grishin, E.V. Isolation and properties of insect-specific neurotoxins from venoms of the spider Lactodectus mactans tredecimguttatus. *Bioorg. Khim.* **1990**, *16*, 1138–1140.
72. Grishin, E.V. Black widow spider toxins: The present and the future. *Toxicon* **1998**, *36*, 1693–1701. [CrossRef]
73. Kiyatkin, N.I.; Dulubova, I.E.; Chekhovskaya, I.A.; Grishin, E.V. Cloning and structure of cDNA encoding alpha-latrotoxin from black widow spider venom. *FEBS Lett.* **1990**, *270*, 127–131. [CrossRef]
74. Kiyatkin, N.; Dulubova, I.; Chekhovskaya, I.; Lipkin, A.; Grishin, E. Structure of the low molecular weight protein copurified with alpha-latrotoxin. *Toxicon* **1992**, *30*, 771–774. [CrossRef]
75. Volkova, T.M.; Pluzhnikov, K.A.; Woll, P.G.; Grishin, E.V. Low molecular weight components from black widow spider venom. *Toxicon* **1995**, *33*, 483–489. [CrossRef]
76. Grishin, E.V.; Himmelreich, N.H.; Pluzhnikov, K.A.; Pozdnyakova, N.G.; Storchak, L.G.; Volkova, T.M.; Woll, P.G. Modulation of functional activities of the neurotoxin from black widow spider venom. *FEBS Lett.* **1993**, *336*, 205–207. [CrossRef]
77. Kiyatkin, N.I.; Kulikovskaya, I.M.; Grishin, E.V.; Beadle, D.J.; King, L.A. Functional characterization of black widow spider neurotoxins synthesised in insect cells. *Eur. J. Biochem.* **1995**, *230*, 854–859. [CrossRef]

78. Pescatori, M.; Bradbury, A.; Bouet, F.; Gargano, N.; Mastrogiacomo, A.; Grasso, A. The cloning of a cDNA encoding a protein (latrodectin) which co-purifies with the alpha-latrotoxin from the black widow spider Latrodectus tredecimguttatus (Theridiidae). *Eur. J. Biochem.* **1995**, *230*, 322–328. [CrossRef]
79. Gasparini, S.; Kiyatkin, N.; Drevet, P.; Boulain, J.C.; Tacnet, F.; Ripoche, P.; Forest, E.; Grishin, E.; Menez, A. The low molecular weight protein which co-purifies with alpha-latrotoxin is structurally related to crustacean hyperglycemic hormones. *J. Biol. Chem.* **1994**, *269*, 19803–19809.
80. Chippaux, J.P. African Society of Toxinology: A new opportunity for integrating the control of envenomations in Africa. *J. Venom. Anim. Toxins Trop. Dis.* **2012**, *18*, 357–360. [CrossRef]
81. Olombrada, M.; Lázaro-Gorines, R.; López-Rodriguez, J.C.; Martínez-del-Pozo, Á.; Oñaderra, M.; Maestro-López, M.; Lacadena, J.; Gavilanes, J.G.; García-Ortega, L. Fungal Ribotoxins: A Review of Potential Biotechnological Applications. *Toxins* **2017**, *9*, 71. [CrossRef]
82. Jiménez, R.; Ikonomopoulou, M.P.; Lopez, J.A.; Miles, J.J. Immune drug discovery from venoms. *Toxicon* **2018**, *141*, 18–24. [CrossRef] [PubMed]
83. Bakrač, B.; Kladnik, A.; Macek, P.; McHaffie, G.; Werner, A.; Lakey, J.H.; Anderluh, G. A toxin-based probe reveals cytoplasmic exposure of Golgi sphingomyelin. *J. Biol. Chem.* **2010**, *285*, 22186–22195. [CrossRef] [PubMed]
84. Skočaj, M.; Resnik, N.; Grundner, M.; Ota, K.; Rojko, N.; Hodnik, V.; Anderluh, G.; Sobota, A.; Macek, P.; Veranic, P.; et al. Tracking cholesterol/sphingomyelin-rich membrane domains with the ostreolysin A-mCherry protein. *PLoS ONE* **2014**, *9*, e92783. [CrossRef] [PubMed]
85. Kreitman, R.J. Immunotoxins for targeted cancer therapy. *AAPS J.* **2006**, *8*, E532–E551. [CrossRef] [PubMed]
86. Kreitman, R.J.; Pastan, I. Immunotoxins in the treatment of refractory hairy cell leukemia. *Hematol. Oncol. Clin. N. Am.* **2006**, *20*, 1137–1151. [CrossRef]
87. Carreras-Sagrá, N.; Tomé-Amat, J.; García-Ortega, L.; Batt, C.A.; Oñaderra, M.; Martínez-del-Pozo, A.; Gavilanes, J.G.; Lacadena, J. Production and characterization of a colon cancer-specific immunotoxin based on the fungal ribotoxin alpha-sarcin. *Protein Eng. Des. Sel.* **2012**, *25*, 425–435. [CrossRef] [PubMed]
88. Tomé-Amat, J.; Menendez-Méndez, A.; García-Ortega, L.; Batt, C.A.; Oñaderra, M.; Martínez-del-Pozo, Á.; Gavilanes, J.G.; Lacadena, J. Production and characterization of scFvA33T1, an immunoRNase targeting colon cancer cells. *FEBS J.* **2012**, *279*, 3022–3032. [CrossRef]
89. Tomé-Amat, J.; Herrero-Galán, E.; Oñaderra, M.; Martínez-del-Pozo, Á.; Gavilanes, J.G.; Lacadena, J. Preparation of an engineered safer immunotoxin against colon carcinoma based on the ribotoxin hirsutellin A. *FEBS J.* **2015**, *282*, 2131–2141. [CrossRef]
90. Tomé-Amat, J.; Olombrada, M.; Ruiz-de-la-Herrán, J.; Pérez-Gómez, E.; Andradas, C.; Sánchez, C.; Martínez, L.; Martínez-del-Pozo, Á.; Gavilanes, J.G.; Lacadena, J. Efficient in vivo antitumor effect of an immunotoxin based on ribotoxin alpha-sarcin in nude mice bearing human colorectal cancer xenografts. *Springerplus* **2015**, *4*, 168. [CrossRef]
91. Tomé-Amat, J.; Ruiz-de-la-Herrán, J.; Martínez-del-Pozo, Á.; Gavilanes, J.G.; Lacadena, J. alpha-sarcin and RNase T1 based immunoconjugates: The role of intracellular trafficking in cytotoxic efficiency. *FEBS J.* **2015**, *282*, 673–684. [CrossRef]
92. Janus, A.; Robak, T. Moxetumomab pasudotox for the treatment of hairy cell leukemia. *Expert Opin. Biol. Ther.* **2019**, *19*, 501–508. [CrossRef] [PubMed]
93. Liu, C.C.; Hao, D.J.; Zhang, Q.; An, J.; Zhao, J.J.; Chen, B.; Zhang, L.L.; Yang, H. Application of bee venom and its main constituent melittin for cancer treatment. *Cancer Chemother. Pharmacol.* **2016**, *78*, 1113–1130. [CrossRef] [PubMed]
94. Zeng, L.; Wan, L.; Chen, L.; Li, S.; Lu, Y.; Huang, Q.; Wang, L.; Li, Y.; Cheng, J.; Lu, X. Selective depletion of activated T cells by recombinant immunotoxin containing anti-CTLA-4 single-chain fragment of variable antibody and N-terminal fragment of perforin. *Transplant. Proc.* **2006**, *38*, 2151–2153. [CrossRef] [PubMed]
95. Tejuca, M.; Anderluh, G.; Dalla-Serra, M. Sea anemone cytolysins as toxic components of immunotoxins. *Toxicon* **2009**, *54*, 1206–1214. [CrossRef] [PubMed]
96. Ávila, A.D.; Mateo-de-Acosta, C.; Lage, A. A new immunotoxin built by linking a hemolytic toxin to a monoclonal antibody specific for immature T lymphocytes. *Int. J. Cancer* **1988**, *42*, 568–571. [CrossRef] [PubMed]
97. Ávila, A.D.; Mateo-de-Acosta, C.; Lage, A. A carcinoembryonic antigen-directed immunotoxin built by linking a monoclonal antibody to a hemolytic toxin. *Int. J. Cancer* **1989**, *43*, 926–929. [CrossRef] [PubMed]

98. Tejuca, M.; Diaz, I.; Figueredo, R.; Roque, L.; Pazos, F.; Martínez, D.; Iznaga-Escobar, N.; Pérez, R.; Álvarez, C.; Lanio, M.E. Construction of an immunotoxin with the pore forming protein StI and ior C5, a monoclonal antibody against a colon cancer cell line. *Int. Immunopharmacol.* **2004**, *4*, 731–744. [CrossRef] [PubMed]
99. Maula, T.; Isaksson, Y.J.; García-Linares, S.; Niinivehmas, S.; Pentikainen, O.T.; Kurita, M.; Yamaguchi, S.; Yamamoto, T.; Katsumura, S.; Gavilanes, J.G.; et al. 2NH and 3OH are crucial structural requirements in sphingomyelin for sticholysin II binding and pore formation in bilayer membranes. *Biochim. Biophys. Acta* **2013**, *1828*, 1390–1395. [CrossRef]
100. García-Linares, S.; Richmond, R.; García-Mayoral, M.F.; Bustamante, N.; Bruix, M.; Gavilanes, J.G.; Martínez-del-Pozo, Á. The sea anemone actinoporin (Arg-Gly-Asp) conserved motif is involved in maintaining the competent oligomerization state of these pore-forming toxins. *FEBS J.* **2014**, *281*, 1465–1478. [CrossRef]
101. García-Linares, S.; Palacios-Ortega, J.; Yasuda, T.; Astrand, M.; Gavilanes, J.G.; Martínez-del-Pozo, Á.; Slotte, J.P. Toxin-induced pore formation is hindered by intermolecular hydrogen bonding in sphingomyelin bilayers. *Biochim. Biophys. Acta* **2016**, *1858*, 1189–1195. [CrossRef]
102. García-Linares, S.; Maula, T.; Rivera-de-Torre, E.; Gavilanes, J.G.; Slotte, J.P.; Martínez-del-Pozo, Á. Role of the Tryptophan Residues in the Specific Interaction of the Sea Anemone Stichodactyla helianthus's Actinoporin Sticholysin II with Biological Membranes. *Biochemistry* **2016**, *55*, 6406–6420. [CrossRef] [PubMed]
103. Bakrač, B.; Anderluh, G. Molecular mechanism of sphingomyelin-specific membrane binding and pore formation by actinoporins. *Adv. Exp. Med. Biol.* **2010**, *677*, 106–115. [PubMed]
104. Conlon, G.A.; Murray, G.I. Recent advances in understanding the roles of matrix metalloproteinases in tumour invasion and metastasis. *J. Pathol.* **2019**, *247*, 629–640. [CrossRef] [PubMed]
105. Kos, J.; Mitrovic, A.; Mirkovic, B. The current stage of cathepsin B inhibitors as potential anticancer agents. *Future Med. Chem.* **2014**, *6*, 1355–1371. [CrossRef] [PubMed]
106. Jaaks, P.; Bernasconi, M. The proprotein convertase furin in tumour progression. *Int. J. Cancer* **2017**, *141*, 654–663. [CrossRef] [PubMed]
107. Potrich, C.; Tomazzolli, R.; Dalla Serra, M.; Anderluh, G.; Malovrh, P.; Macek, P.; Menestrina, G.; Tejuca, M. Cytotoxic activity of a tumor protease-activated pore-forming toxin. *Bioconjug. Chem.* **2005**, *16*, 369–376. [CrossRef] [PubMed]
108. Rivera-de-Torre, E.; Palacios-Ortega, J.; García-Linares, S.; Gavilanes, J.G.; Martínez-del-Pozo, Á. One single salt bridge explains the different cytolytic activities shown by actinoporins sticholysin I and II from the venom of Stichodactyla helianthus. *Arch. Biochem. Biophys.* **2017**, *636*, 79–89. [CrossRef] [PubMed]
109. Deutsch, C.A.; Tewksbury, J.J.; Tigchelaar, M.; Battisti, D.S.; Merrill, S.C.; Huey, R.B.; Naylor, R.L. Increase in crop losses to insect pests in a warming climate. *Science* **2018**, *361*, 916–919. [CrossRef]
110. Ortiz, E.; Possani, L.D. The unfulfilled promises of scorpion insectotoxins. *J. Venom Anim. Toxins Trop. Dis.* **2015**, *21*, 16. [CrossRef]
111. King, G.F. Tying pest insects in knots: The deployment of spider-venom-derived knottins as bioinsecticides. *Pest Manag. Sci.* **2019**, *2019*. [CrossRef]
112. Delaney, B.; Goodman, R.E.; Ladics, G.S. Food and Feed Safety of Genetically Engineered Food Crops. *Toxicol. Sci.* **2018**, *162*, 361–371. [CrossRef] [PubMed]
113. Halford, N.G. Legislation governing genetically modified and genome-edited crops in Europe: The need for change. *J. Sci. Food Agric.* **2019**, *99*, 8–12. [CrossRef] [PubMed]
114. Pardo-López, L.; Soberón, M.; Bravo, A. Bacillus thuringiensis insecticidal three-domain Cry toxins: Mode of action, insect resistance and consequences for crop protection. *FEMS Microbiol. Rev.* **2013**, *37*, 3–22. [CrossRef] [PubMed]
115. Wei, J.; Zhang, Y.; An, S. The progress in insect cross-resistance among *Bacillus thuringiensis* toxins. *Arch. Insect. Biochem. Physiol.* **2019**, *2019*. [CrossRef] [PubMed]
116. Soberón, M.; Pardo, L.; Muñóz-Garay, C.; Sánchez, J.; Gomez, I.; Porta, H.; Bravo, A. Pore Formation by Cry Toxins. *Adv. Exp. Med. Biol.* **2010**, *677*, 127–142. [PubMed]
117. Herzig, V.; King, G.F. The Cystine Knot Is Responsible for the Exceptional Stability of the Insecticidal Spider Toxin omega-Hexatoxin-Hv1a. *Toxins* **2015**, *7*, 4366–4380. [CrossRef] [PubMed]
118. Kikuchi, K.; Sugiura, M.; Kimura, T. High Proteolytic Resistance of Spider-Derived Inhibitor Cystine Knots. *Int. J. Pept.* **2015**, *2015*, 537508. [CrossRef]

119. Hardy, M.C.; Daly, N.L.; Mobli, M.; Morales, R.A.V.; Keng, G.F. Isolation of an Orally Active Insecticidal Toxin from the Venom of an Australian Tarantula. *PLoS ONE* **2013**, *8*, e73136. [CrossRef]
120. Koch, M.S.; Ward, J.M.; Levine, S.L.; Baum, J.A.; Vicini, J.L.; Hammond, B.G. The food and environmental safety of Bt crops. *Front. Plant Sci.* **2015**, *6*, 283. [CrossRef]
121. King, G.F.; Hardy, M.C. Spider-venom peptides: Structure, pharmacology, and potential for control of insect pests. *Annu. Rev. Entomol.* **2013**, *58*, 475–496. [CrossRef]
122. Bonning, B.C.; Chougule, N.P. Delivery of intrahemocoelic peptides for insect pest management. *Trends Biotechnol.* **2014**, *32*, 91–98. [CrossRef] [PubMed]
123. Cory, J.S.; Hirst, M.L.; Williams, T.; Hails, R.S.; Goulson, D.; Green, B.M.; Carty, T.M.; Possee, R.D.; Cayley, P.J.; Bishop, D.H.L. Field Trial of a Genetically Improved Baculovirus Insecticide. *Nature* **1994**, *370*, 138–140. [CrossRef]
124. Inceoglu, A.B.; Kamita, S.G.; Hinton, A.C.; Huang, Q.H.; Severson, T.F.; Kang, K.D.; Hammock, B.D. Recombinant baculoviruses for insect control. *Pest Manag. Sci.* **2001**, *57*, 981–987. [CrossRef] [PubMed]
125. Williams, T.; Virto, C.; Murillo, R.; Caballero, P. Covert Infection of Insects by Baculoviruses. *Front. Microbiol.* **2017**, *8*, 1337. [CrossRef] [PubMed]
126. Szewczyk, B.; Hoyos-Carvajal, L.; Paluszek, M.; Skrzecz, W.; de Souza, M.L. Baculoviruses—re-emerging biopesticides. *Biotechnol. Adv.* **2006**, *24*, 143–160. [CrossRef] [PubMed]
127. Lovett, B.; Bilgo, E.; Millogo, S.A.; Ouattarra, A.K.; Sare, I.; Gnambani, E.J.; Dabire, R.K.; Diabate, A.; St Leger, R.J. Transgenic Metarhizium rapidly kills mosquitoes in a malaria-endemic region of Burkina Faso. *Science* **2019**, *364*, 894–897. [CrossRef] [PubMed]
128. Cushman, D.W.; Ondetti, M.A. History of the design of captopril and related inhibitors of angiotensin converting enzyme. *Hypertension* **1991**, *17*, 589–592. [CrossRef]
129. Clark, G.C.; Casewell, N.R.; Elliott, C.T.; Harvey, A.L.; Jamieson, A.G.; Strong, P.N.; Turner, A.D. Friends or Foes? Emerging Impacts of Biological Toxins. *Trends Biochem. Sci.* **2019**, *44*, 365–379. [CrossRef]
130. Schwager, E.E.; Sharma, P.P.; Clarke, T.; Leite, D.J.; Wierschin, T.; Pechmann, M.; Akiyama-Oda, Y.; Esposito, L.; Bechsgaard, J.; Bilde, T.; et al. The house spider genome reveals an ancient whole-genome duplication during arachnid evolution. *BMC Biol.* **2017**, *15*, 62. [CrossRef]
131. Garb, J.E. Extraction of venom and venom gland microdissections from spiders for proteomic and transcriptomic analyses. *J. Vis. Exp.* **2014**, *93*, e51618. [CrossRef]
132. Von Reumont, B.M. Studying Smaller and Neglected Organisms in Modern Evolutionary Venomics Implementing RNASeq (Transcriptomics)-A Critical Guide. *Toxins* **2018**, *10*, 292. [CrossRef] [PubMed]
133. Garb, J.E.; González, A.; Gillespie, R.G. The black widow spider genus Latrodectus (Araneae: Theridiidae): Phylogeny, biogeography, and invasion history. *Mol. Phylogenet. Evol.* **2004**, *31*, 1127–1142. [CrossRef] [PubMed]
134. Haas, B.J.; Papanicolaou, A.; Yassour, M.; Grabherr, M.; Blood, P.D.; Bowden, J.; Couger, M.B.; Eccles, D.; Li, B.; Lieber, M.; et al. De novo transcript sequence reconstruction from RNA-seq using the Trinity platform for reference generation and analysis. *Nat. Protoc.* **2013**, *8*, 1494–1512. [CrossRef] [PubMed]
135. Clarke, T.H.; Garb, J.E.; Hayashi, C.Y.; Haney, R.A.; Lancaster, A.K.; Corbett, S.; Ayoub, N.A. Multi-tissue transcriptomics of the black widow spider reveals expansions, co-options, and functional processes of the silk gland gene toolkit. *BMC Genom.* **2014**, *15*, 365. [CrossRef] [PubMed]
136. Wilson, D.; Daly, N.L. Venomics: A Mini-Review. *High Throughput* **2018**, *7*, 19. [CrossRef] [PubMed]
137. Haney, R.A.; Ayoub, N.A.; Clarke, T.H.; Hayashi, C.Y.; Garb, J.E. Dramatic expansion of the black widow toxin arsenal uncovered by multi-tissue transcriptomics and venom proteomics. *BMC Genom.* **2014**, *15*, 366. [CrossRef]
138. Macrander, J.; Brugler, M.R.; Daly, M. A RNA-seq approach to identify putative toxins from acrorhagi in aggressive and non-aggressive Anthopleura elegantissima polyps. *BMC Genom.* **2015**, *16*, 221. [CrossRef]
139. Xie, B.; Huang, Y.; Baumann, K.; Fry, B.G.; Shi, Q. From Marine Venoms to Drugs: Efficiently Supported by a Combination of Transcriptomics and Proteomics. *Mar. Drugs* **2017**, *15*, 103. [CrossRef]
140. Madio, B.; Undheim, E.A.B.; King, G.F. Revisiting venom of the sea anemone Stichodactyla haddoni: Omics techniques reveal the complete toxin arsenal of a well-studied sea anemone genus. *J. Proteom.* **2017**, *166*, 83–92. [CrossRef]
141. Zancolli, G.; Sanz, L.; Calvete, J.J.; Wuster, W. Venom On-a-Chip: A Fast and Efficient Method for Comparative Venomics. *Toxins* **2017**, *9*, 179. [CrossRef]

142. Brinkman, D.L.; Jia, X.; Potriquet, J.; Kumar, D.; Dash, D.; Kvaskoff, D.; Mulvenna, J. Transcriptome and venom proteome of the box jellyfish Chironex fleckeri. *BMC Genom.* **2015**, *16*, 407. [CrossRef] [PubMed]
143. Macrander, J.; Broe, M.; Daly, M. Multi-copy venom genes hidden in de novo transcriptome assemblies, a cautionary tale with the snakelocks sea anemone Anemonia sulcata (Pennant, 1977). *Toxicon* **2015**, *108*, 184–188. [CrossRef] [PubMed]
144. Tulin, S.; Aguiar, D.; Istrail, S.; Smith, J. A quantitative reference transcriptome for Nematostella vectensis early embryonic development: A pipeline for de novo assembly in emerging model systems. *Evodevo* **2013**, *4*, 16. [CrossRef] [PubMed]
145. Gao, B.; Peng, C.; Yang, J.; Yi, Y.; Zhang, J.; Shi, Q. Cone Snails: A Big Store of Conotoxins for Novel Drug Discovery. *Toxins* **2017**, *9*, 397. [CrossRef] [PubMed]
146. Macrander, J.; Panda, J.; Janies, D.; Daly, M.; Reitzel, A.M. Venomix: A simple bioinformatic pipeline for identifying and characterizing toxin gene candidates from transcriptomic data. *PeerJ* **2018**, *6*, e5361. [CrossRef] [PubMed]

DISCUSSION

NOTE: References to Figures appearing in the articles are indicated with Roman numerals referring to the article and the corresponding Arabic numerals which refer to the specific Figure within that article. Thus, for example, Figure I-1 refers to Figure 1 of article numbered as I.

Pore-forming toxins produced as part of animal venoms attack one of the most widespread and primordial structures of cells: the plasma membrane. Results obtained on the experiments developed on this PhD thesis contribute to understanding the molecular details and the functional implications derived from the structure-function relationship of pore forming toxins produced by sea anemones and black widow spiders.

Block I. Actinoporins: pore forming toxins produced by sea anemones

A single and fully exposed salt-bridge determines Stn activity

Toxins in general, and actinoporins in particular, appear as multigene families in sea anemone genomes, raising multiple isoforms of highly identical toxins in terms of sequences, but not necessarily in terms of toxic activity. The reason why a single specie should produce such a variety of similar toxins is still unknown, although some authors propose that the evolutive pressure underlying the predator-prey relationship could promote duplication and expansion of the toxic genes, increasing venom effectivity and expanding the range of susceptible prey (Arbuckle 2017, Calvete 2017, Clark 2019). In addition, the interaction between the similar but not identical venom components might also rise toxic activity regulation to a new dimension. Nevertheless, although many cytolysins sequences can be found in the sea anemone genomes, so far, only a small number of actinoporins has been detected in their milked venom and have been object of further characterization (García-Linares 2016b, Macrander 2015a, Macrander and Daly 2016, Madio 2017, Rojko 2016, Wang 2008). StnI and StnII represent an excellent system to study this complex relationship network since they are two actinoporin isoforms produced by the same sea anemone *S. helianthus* that share 93% of their sequence and display a great difference in their toxic activities (García-Linares 2016b). Such a small amount of amino acid sequence differences between StnI and StnII has nevertheless to account for the toxic activity variation. Most non-conserved changes between these two isoforms are located in the N-terminal region. In particular Glu-2 and Asp-9 residues in StnI are occupied by Ala in equivalent positions of StnII provoking a shift in the hydrophobic profile of the α-helical stretch responsible for wall pore-formation (Figure I-2). Previous work developed with peptides mimicking the first 30 amino acids of these proteins supported the conclusion that the different toxic activity exerted by the studied isoforms was due to the hydrophobicity of the stretched α-helices (Ros 2012). However, this particular hypothesis had not been tested with full-size proteins, leaving out the possible specific interactions between the N-terminal stretch and the β-sandwich core. Site-directed mutagenesis of StnI, substituting the aforementioned amino acid residues by the hydrophobic ones present in StnII, was used to design, clone, produce and purify three different variants to homogeneity. Their spectroscopic characterization was compatible with fully folded proteins conserving the wild-type three-dimensional structure (Figure I-3, 4). Substitution of Glu-2 by Ala in StnI had a negligible effect on thermostability, but replacement of Asp-9 had a profound effect on the protein stability (Table I-1). In the same direction, functional hemolytic (Figure I-5) and calcein release assays (Figure I-6) revealed that Asp-9 StnI mutants showed a similar behavior to StnII, while Glu-2 StnI mutants mostly resembled StnI wild-type activity, even though both mutations would particularly contribute in the same degree to the hydrophobicity profile of the amphipathic N-terminal α-helix (Figure I-2). Three-dimensional structure

inspection of the mutation location showed that Asp-9 in StnI could establish a solvent exposed salt bridge with Lys-68 located at the β-sandwich core (Figure I-8). This salt bridge would impair α-helical detachment, delaying the stretching process over the membrane that finally leads to crossing the hydrophobic core to build a pore. Then, the reverse equivalent StnII mutant was made. StnII Ala-8 was replaced by Asp. This variant was also produced and purified to homogeneity, with the aim of testing if the introduction of this residue would allow the formation of a new salt-bridge linking β-sheet core with its N-terminal stretch in StnII, therefore diminishing hemolytic activity. The spectroscopic characterization of this protein was also in good agreement with a globular folded protein resembling wild-type overall structure (Figure I-3, 4). Thermostability was higher than wild-type StnII (Table I-1), just the opposite that happened when the mutations introduced in StnI disabled the salt bridge. Functional characterization of this StnII mutant revealed a diminished efficiency, showing a behavior more similar to StnI. These results, in combination with membrane affinity binding assays, determined by ITC (Figure I-7, Table I-2), confirmed the formulated hypothesis about importance of the salt bridge in impairing α-helical detachment from the β-sandwich core and the subsequent steps leading to pore-formation. Indeed, these results were also compatible with the lytic activity registered for the other thoroughly studied actinoporins. When compared in identical conditions, EqtII and FraC were more similar to StnI than to StnII. Sequence inspection of EqtII and FraC revealed that, unlike StnII, they show equivalent amino acids to StnI at the positions studied (Figure 1). Therefore, EqtII-Asp10 and FraC-Asp10 would be also establishing salt bridges with their corresponding EqtII-Lys69 and FraC-Lys69 counterparts, explaining their reduced toxic activity in comparison with StnII (García-Linares 2016b).

Figure 1. Sequence alignment of the four-best studied actinoporins StnI and II from *S. helianthus*, EqtII from *Actinia equina*, and FraC from *Actinia fragacea*. The black background indicates the conserved residues, the gray background corresponds to conservative changes, and the white background to non-conserved amino acids. Read and blue arrowhead indicates the position of the amino acids mutated in this study (García-Linares 2016a). The Lys residue from StnI, EqtII, and FraC involved in the salt bridge with an acidic residue (blue arrowhead) is indicated with a green arrowhead.

In summary, hydrophobicity profile of the N-terminal domain is important for effectively crossing the membrane, but the main structural feature leading to a greater pore damaging efficiency is the easiness of this domain to detach from the β-sandwich core, which is much more easier in StnII because of the lack of this salt-bridge impairing the movement. Unlike disulfide bonds (Bastolla and Demetrius 2005), it is generally accepted that salt bridges do not play important roles in protein stability and functionality. However, their contribution should not be

necessary neglected since, as shown here, sometimes they can also play key roles in maintain both protein parameters.

StnI and StnII show synergistic activity

Multigene character is common in toxin protein families but not restricted to them. There are other proteins families that need such multiplicity to efficiently develop their biological function. Immunoglobulins, for example, have a wide variety of highly diverse genes intended to interact with a broad collection of antigens. Indeed, one of the proposed explanations for actinoporins multigene family character has been increasing the range of prey for a given species (Anderluh 1999, Gutiérrez 2000, Monastyrnaya 2010, Monastyrnaya 2002, Uechi 2010, Wang 2008). Another discussed possible reason is that different isoforms interact to each other in forming heteropores, thus taking toxic activity regulation to a new and more complex dimension. Indeed, it has been already suggested for mitochondrial apoptotic pore that Bax and Bak proteins involved in the process form heteropores. However, the biological implication of this interaction it still far to be understood (Dewson 2016).

However, as stated above, actinoporins tested so far are a small fraction from the wide variety that can be found in the sea anemones genomes. In addition, they have been always studied in isolation, although they are produced as part of ~~a~~ complex venom mixtures. Again, StnI and StnII represent an ideal model to study the possible interaction of different actinoporins isoforms since they are both produced by the same sea anemone species and appear together in the native venom (Bernheimer and Avigad 1976, Devlin 1974). They have been successfully produced in bacterial heterologous systems, avoiding the risk of cross contamination derived from purifying toxins from the crude extract.

Even though the stoichiometry of the actinoporin final pore and its detailed structure is still far from being definitively solved, there is a detailed crystalline octameric structure of FraC that serves as a model to study protein-protein interactions stablished in the oligomerization process (Tanaka 2015a). Structure inspection reveals that Val-60 and Trp-149 in FraC are the main residues implicated in such interaction and, in fact, chemically equivalent residues are found in the corresponding positions of StnI (Ile-59 and Trp-149) and StnII (Ile-58 and Trp-146). Thus, there was not an *a priori* impediment for the formation of heteropores.

To test the implications of a possible interaction between the studied isotoxins, mixtures of StnI and StnII in controlled proportions were functionally characterized. Hemolysis and calcein leakage assays suggested that both actinoporins were able to interact with each other (Figure II-1, II-3 and II-8) showing higher activity rates that expected if both actinoporins would act separately, existing therefore a synergistic effect. Such synergy is exerted by the formation of heteropores as demonstrated by cross-linking experiments (Figure II-4 and II-5). To determine in which step of the continuous and complex pore formation process does synergy take place, control experiments were developed using mutants that were able to bind to the membrane but not forming a pore (StnII A10P S28P) or were completely unable to bind the membrane (StnII Y111N) (Alegre-Cebollada 2004, Alegre-Cebollada 2007c). Hemolysis experiments with mixtures containing these mutants revealed that synergy took place at the membrane binding step rather than in the oligomerization or final pore formation steps (Figure II-2). Further analysis of protein-membrane interaction using StnI and StnII mixtures, analyzed through ITC measurements, confirmed such a hypothesis (Table II-1 and Figure II-7).

The mutants designed to study the activity differences between StnI and StnII, affecting the hydrophobicity of the N-terminal region and the formation of a salt-bridge between the α-helical domain and the β-sandwich core were assayed in mixtures. However, no synergistic effect was observed in any of the studied scenarios, reinforcing the hypothesis stating that synergistic interaction takes place in the membrane binding step, rather than in the pore formation phase.

The synergistic effect observed extends the complexity and regulatory capacity of toxin function, mimicking a rudimentary defense system (Wang 2008) and potentially increasing the range of prey that *S. helianthus* can attack or defend from.

S. helianthus transcriptome assembly allowed venom composition description

As it has been discussed previously, StnI and StnII have been the only actinoporins detected in *S. helianthus* so far (Lanio 2001, Valle 2015). In view of the results that reveal the synergistic effect developed by StnI and StnII, it was subsequently hypothesized that trace amounts of other actinoporins, not yet detected by the methods commonly used, could have a dramatic effect in venom toxicity (Rivera-de-Torre 2016).

Massive sequencing techniques are emerging tools to study nature from a new molecular biology dimension. Among the available options, next-generation RNA-sequencing offers a powerful choice to analyze samples in general and venom glands in particular. Assembling a transcriptome is faster than a analyzing a genome, which is a more complex structure including non-coding information such as introns. In addition, transcriptome analysis includes information about transcripts, and their corresponding encoded proteins, and allows relative quantification of expression (Macrander 2015b, Macrander and Daly 2016). Finally, this genetic information is useful to study the evolutionary relationships among toxins from different species, helping to elucidate venom evolution (Garb 2004, Haney 2016, Macrander and Daly 2016).

In order to study *S. helianthus*' venom composition and look for novel putatively active actinoporins, its transcriptome was assembled after Illumina RNA-sequencing method. BUSCO software report coupled with the transcriptomic assembly parameters revealed good coverage and completeness that confirmed the assembly was valid for annotation and further analysis (Table III-1 and 2). Sea anemone venom is a complex mixture of toxins which includes actinoporins, phospholipases and other enzymes that modify the membrane, and metalloproteases that digest the extracellular matrix. To annotate the venom composition in a comprehensive way, the toxic classes previously described by the transcriptomic and proteomic approaches for a sea anemone from the same genus (*S. haddoni*) were used (Madio 2019, Madio 2017). Although cytolysins were not the most numerous toxin group in terms of number of individual genes, they represented the major amount of the transcripts analyzed (Figure III-1). Considering the non-enzymatic nature of cytolysins it is easy to explain why they are highly expressed over catalytic protein components like phospholipases. Relative expression data revealed that the most highly expressed actinoporin was StnII (Table III-3), the most potent actinoporin produced by *S. helianthus* studied so far (García-Linares 2016b), potentially explaining the high cytolytic effect of its venom.

StnIII is a new actinoporin isoform discovered from *S. helianthus* transcriptome

To accomplish the main goal of the transcriptome analysis new sticholysin sequences were looked for within the built database. Even in the more restrictive analysis, it was possible to discover at least one new actinoporin sequence, with a possible allelic variant from the same locus. These two new isoforms were named StnIII and StnIV respectively (Figure III-2). The relative expression of this new variants was similar and lower than the relative values obtained for StnI and StnII (Table III-3), which could explain why it had not been detected before in the crude venom extract (Lanio 2001). The assembly method applied to the transcriptome was based on De Bruijn graphs connecting overlapping sequenced fragments (Haas 2013). As the presence of enough overlapping fragments, largely depends on the abundance of the original transcripts, it is easier and more accurate to sequence transcripts which are longer and more abundant in the complex mRNA mixture. This methodology implied a bias when seeking for highly similar and short sequences because fragments corresponding to different transcripts could be merged into a single one.

Full StnIII sequence was obtained upon amplification of a single PCR-product followed by Sanger sequencing. The cDNA used as departing material was obtained from one of the individuals used to generate the transcriptome libraries. C-terminal domain of StnIII overlapped with the sequence obtained for StnIV, with the only exception of three non-synonymous variations (Figure III-4).

The phylogenetic analysis suggested StnI and StnII are more closely related to each other than to StnIII. Therefore, StnIII gene could have appeared in a duplication event previous to StnI and StnII divergence (Figure III-5). In spite of their clear evolutive divergence, the signal peptide described for all the actinoporins produced by *S. helianthus* was highly conserved (Figure III-3). The signal peptide of around 30 amino acids and had two clearly differentiated regions: one constituted by hydrophilic and positively charged residues, followed by a pro-region comprising 15-16 more residues and containing mainly polar and charged amino acids. This pro-region was also highly conserved among actinoporins within the same species but seems to vary significantly in terms of length and net charge among different species (Figure III-3).

StnI and StnII sequences are 93% identical, while StnIII only shows 76% and 77% of identity to StnI and StnII respectively. A proof of their phylogenetic divergence. However, such degree of identity was still enough to predict StnIII three-dimensional structure by comparison with the already known structures of StnI and StnIII (Castrillo 2009, Mancheño 2003). StnIII model resembled the typical actinoporin fold characterized by a β-sandwich core flanked by two short α-helices (Figure III-6).

Amino acid sequence comparison raised some differences that could have relevance in terms of pore-forming activity. There is a Pro residue occupying the second position in the N-terminal stretch, which could impair that region to adopt a 100% α-helical structure. Position 9 in StnI is the Asp residue that, as discussed before, forms a salt bridge with Lys-68 located in the β-core sandwich. Lys 68 is conserved in StnIII (Lys-70) but Asp-9 is substituted by Gln-11 which although not a charged residue, displays enough negative charge density to stablish a strong dipolar interaction. StnIII N-terminal stretch is 2 and 3 amino acids longer in comparison with StnI and StnII, which could also implicate a different membrane thickness preference for optimal

pore formation in comparison with the membrane thickness required for StnI and StnII (Palacios-Ortega 2017). Another feasible option to explain a longer N-terminal stretch would be a different stoichiometry of the final pore assembly. Not much can be told in this regard, considering that this stoichiometry is precisely one of the most controversial subjects regarding actinoporins mechanism of action. The stoichiometry of the final pore is thus far from be definitively determined. Following with the N-terminal domain analysis, the hydrophobicity of the N-terminal region of StnIII is very similar to the value calculated for StnII, so their N-terminal α-helical domains share a common amphiphilicity and therefore have similar tendency to seek in the membrane interface. However, the hydrophobic moment of the same fragment in StnIII is lower than the values computed for StnI and StnII, expecting a lower tendency to cross the membrane and consequently a lower pore-forming activity (Figure IV-4).

The key residues part of the POC binding site, the cluster or aromatic residues and the array of basic amino acids are conserved or substituted by chemically equivalent residues (Figure IV-2). The only exception is Leu-113 in StnIII, which in StnI and StnII corresponds with W110 and W111 respectively, a residue part of the cluster of aromatic residues. However, the specific function of that specific Trp residue in protein functionality can be supplied by a big hydrophobic residue like Leu (Bakrač 2008).

StnIII is a functional actinoporin that resembles common actinoporin folding and functionality

To test the hypothesis raised about StnIII activity and its possible synergistic effect in mixtures with StnI or StnII, this new actinoporin was cloned and produced in an heterologous bacterial system that ensured overproduction and purification to homogeneity. StnIII was detected by a polyclonal antibody raised agains StnI, although the signal was of lower intensity than the obtained for StnI, in good agreement with their also lower sequence identity (76%) but confirming the presence of common epitopes (Figure IV-3). Its spectroscopic characterization was consistent StnIII resembling the common actinoporin fold with minor changes easily explained considering the chemical nature of the the individual amino acids which were different when compared to StnI and StnII. StnIII thermostability was, however, significantly lower (Figure IV-7 and Table IV-1). Such a lower thermal stability was translated in a lesser stability in solution too (Figure IV-8). Then, this lesser stability in combination with its also lower expression level, as revealed by the transcriptomic analysis (Table III-3), probably explains why this actinoporin isoform had not been discovered before in the crude extract venom of *S. helianthus*.

StnIII functional characterization by hemolysis and an calcein leakage experiments from DOPC:SM:Chol (1:1:1) vesicles (Figure IV-9 and IV-10) showed that it was fairly inactive until reaching a critical concentration of 20 nM, higher than the values found for the other two sticholysins. Once reached, StnIII exerted lysis rates well over StnI values. Binding affinity (Figure IV-10 and Table IV-2) to DOPC:SM:Chol (1:1:1) model vesicles was similar to StnI, although the the number of lipid moleculas affected by Stn monomer binding to the membrane was lower (Table IV-2). These results support the conclusion that StnIII uses a different mechanism of oligomerization at the surface membrane and probably assembles into a pore of different stoichiometry, as suggested above.

Finally, synergistic effect with StnII was confirmed. On the other hand, the existence of synergy between StnI and stnIII could not be proved. Nevertheless, these results confirmed, as *a priori* hypothesized, that StnIII is an interesting and unexpected piece in the puzzle of the versatile mechanisms of the poisonous activity of the Caribbean Sea *S. helianthus* anemone species.

Block II. The membrane pore-forming *latrotoxin macromolecular complex*: Latrodectins and latroinsectotoxins produced by black widow spiders

Black widow spiders (*Latrodectus spp*.) are professional insect hunters that produce high molecular weigth proteins called latrotoxins (LTXs) as part of their venomous cocktail. The toxic activity of these huge proteins relie in the formation of pores within presynaptic neurons, triggering the massive release of neurotransmitters that cause intense pain and paralysis to prey (Shatursky 1995, Ushkaryov 2002, Ushkaryov 2008). When purified from crude venom, LTXs co-purifiy with small cysteine-rich peptides called latrodectins (Ltds). Therefore, some authors speculate with the formation of a so called "*latrotoxin macromolecular complex*", composed by the assotiation of both LTXs and Ltds (Orlova 2000).

Five of these LTXs are isoforms that specifically affect insects. This explains why they are known as latroinsectotoxins (LITs) (Dulubova 1996, Kiyatkin 1995, Rohou 2007, Shatursky 1995). Again, and alike as with actinoporins, such a great variety of isotoxins suggests implications regarding different prey specificity. From a biotechnological point of view, and because of their selectivity for insects, they are a suitable starting point for the design of ecofriendly, and safe for humans, bioinsecticides. Therefore, and in order to explore these possibilities, we aimed to study the molecular mechanism of LITs and Ltds from the structural an functional points of view. With this purpose in mind, both components of the *latrotoxin molecular complex* were cloned, produced in a yeast hetelogous system, and purified to homogeneity without cross-contamination of other venom components that hindered previous studies developed with these proteins (Orlova 2000).

Latrodectins from *L. hesperus* are α-helical rich thermostable peptides

The two most highly expressed Ltds from *L. hesperus* were succesfully cloned and produced in the yeast *P. pastoris* (Figure V-4). They showed an anomalous electrophoretic migration behavior most probably due to their higly acidic isoelectric point, as it has been described for other proteins with similar physicochemical characteristics (García-Ortega 2005). Both proteins behaved as homodimers in size exclusion chromatography and showed and extremely high thermostability, the latter a quite common characteristic of toxic proteins (Abiko 2015, Alegre-Cebollada 2004, Honda 1992, Yang 2019). Mass spectrometry experiments confirmed the expected molecular weight for LtdII including its six Cys as forming three disulfide bonds (Figure V-5). The LtdII spectroscopic characterization (CD and NMR) (Figure V-7) was consistent with an structure with high α-helical content. Preliminar NMR data of ^{13}C-^{15}N-labelled LtdII allowed atomic asignation and modeling of amino acids occupying positions between

residues 1-30 and 42-69, revealing two well-defined α-helical (Figure V-9, Figure V-10 and Figure V-11). This NMR characterization has not been extended yet to LtdI.

LtdII does not show insecticide (Table V-2) or antifungal (Figure V-13, Figure V-14 and Figure V-15) activities. However, LtdII induced sporulation and changed the pigmentation of *Aspergillus parasiticus* cultures, suggesting stress induction in this microorganism (Figure V-13). Further studies are needed to elucidate Ltds function, but these results suggest that the original hypotesis of belonging to the larger latrotoxin macromolecular complex seems to be probably correct.

δ-LIT from *L. hesperus* has produced in *P pastoris*, purified to homogeneity and preliminary characterized

Toxins have extraordinary properties that makes them ideal candidates to formulate biotechnological products. As discussed above, toxins are highly thermostable products which are optimized through evolutive pressure to bind to their targets. Targeting this toxic activity to specific cells (Ruiz-de-la-Herrán 2019) or organisms that constitute plagues is a very interesting potential application of these proteins in the short-term future. After all, bioinsecticides are sustainable products intended to eliminate insect pests. They should be stable in extreme conditions, active topically or orally, rapidly lethal for specific insects and inocuous for humas and other non-pest species. Attending to this biotecnological potential as bioinsecticides, δ-LIT was selected as a candidate for cloning and production in an heterologous and safe system in order to to study its insecticidal properties and its membrane pore-forming features in the context of the so called *latrotoxin macromolecular complex*, in combinantion with Ltds.

δ-LIT has been succesfully cloned in an expression vector intended for production in the yeast *P. pastoris*. Sequencing allowed to obtain the actual mature cDNA sequence of δ-LIT of *L. hesperus,* which revealed some differences when compared with the assembled sequence obtained from the *L. hesperus* transcriptome (Figure IV-3). δ-LIT was also successfully produced in the *P. pastoris* KM71H strain and purified to homogeneity through several chromatographic steps, including ion-exchange and size exclussion chromatographies, attending to the physicochemical properties of the protein. Its spectroscopic characterization through far-UV circular dichroism was, however, compatible with an unstructured protein. In summary, we have preliminary promising results regarding the production and purification of this huge protein, but a great deal of protocols optimization is still due.

CONCLUSIONS

Actinoporins are pore-forming proteins produced by sea anemones which functional and structural detailed characterization would elucidate the biophysical challenge behind the metamorphosis from a water-soluble protein to a membrane-bound state.

It was known that StnII was more active than StnI when assayed against sheep red blood cells or model membranes. Site directed mutagenesis within the N-terminal α-helical stretch of StnI and StnII revealed the existence of a key salt bridge linking N-terminal domain of StnI to its β-sandwich core, absent in StnII. The mechanism described might be of general application for other actinoporins and reinforces the importance of salt bridges as key factor of protein design with impact in folding and stability.

Although StnI, StnII and StnIII display very different lytic efficiencies, they can act in synergy. Such synergistic effect takes place at the membrane binding step rather than during the pore-formation stage. Such synergy could represent a new mechanism for venom activity modulation, translated into a more versatile defense and/or attach responses in their natural environment. That observation raises the question, with biological functionality consequences, of whether this mechanism could represent a general strategy employed by other pore-forming proteins.

In order to study in depth *S. helianthus*' venom, and look for new actinoporin isoforms, the first *de novo* transcriptome of this species was successfully assembled. Transcriptome analysis revealed its venom composition distribution, highlighting the wide phospholipases A2-like enzymes diversity and the high expression levels of cytolysins, in good agreement with the non-enzymatic nature of these protein family. The new actinoporin StnIII isoform was discovered from the analysis of these transcriptomic data. StnIII expression levels were well below the ones described for StnI and StnII.

StnIII was successfully cloned, produced in *E. coli* and purified to homogeneity. Its spectroscopic characterization by far-UV circular dichroism was compatible with the actinoporin's common fold, characterized by β-sheet rich content. StnIII is much less thermostable than StnI and StnII. Near-UV circular dichroism and fluorescence emission spectra differences with StnI and StnII were also compatible with their different content of aromatic residues. Hemolysis, calcein release and ITC experiments showed that the membrane binding affinity and relative lytic activities were more similar to StnI than to StnII. Kinetic behavior however suggested that the mechanism of protein oligomerization on the membrane, as well as the final stoichiometry of the pore, might be significantly different between StnIII and the other two previously known sticholysins. Synergistic activity between StnII and StnIII was also proved reinforcing the importance and complexity of protein-protein interactions among different isotoxins in modulating the venom specificity, versatility and toxicity.

Actinoporins are rather simple water-soluble proteins with the ability to incorporate into a membrane, being driven by the presence of sphingomyelin. They represent an optimal model to study this type of transitions just because of their simplicity. Pore-forming-proteins are however ubiquitous and, in many cases, are part of extremely complex mixtures in which different components could have a profound effect in pore forming proteins toxicity. Within this context, the *latrotoxin macromolecular complex* represents the other edge of the spectrum. It is a huge, very intricate macromolecular complex constituted by, maybe, more than one type of protein, assembled to produce a lethal pore. It is alike to actinoporins in its function, the

formation of a cation-specific pore, but it is completely different, not only regarding their much higher complexity, but also its specificity, in terms of membrane requirements and prey, but also in terms of its potential biotechnological applications. Therefore, and with the actinoporins scientific and expertise background at hand, we decided to approach the elucidation of this interesting and almost unknown membrane macromolecular structure.

The most highly expressed Ltds from *L. hesperus* were cloned, produced in the yeast *P. pastoris,* and purified to homogeneity. The producing system was optimized enough as to be able to approach the isolation of milligram amounts of ^{15}N,^{13}C-labeled LtdII, fit for NMR three-dimensional structure determination. Their spectroscopic and structural characterization revealed that they are α-helical rich peptides, highly thermostable, and containing three-disulfide bridges. Unfortunately, the determination of their three-dimensional structure with atomic resolution has not been completed yet. LtdII functional characterization did not disclose any antifungal nor insecticide activity.

The task was also undertaken to produce and purify one of the other proteins that can be assembled into what has been called the *latrotoxin macromolecular complex*: δ-LIT. It is a huge protein composed of almost 1000 amino acids and with presumably specific insecticidal properties. This protein was successfully produced in the *P. pastoris* system and purified to electrophoretic homogeneity. In this case, its circular dichroism spectroscopic spectrum suggested a rather non-structured polypeptide. These are, anyway, highly preliminary results that should only be considered yet as *proof of concept* that it is possible to produce and isolate this enormous spider δ-LIT using a yeast heterologous protein production system. Yeast culture conditions and protein purification protocols must however be optimized. This is a difficult but very interesting high risk-high rewarding project, not only because its development will teach us basic information about protein-membrane interactions, but also because LITs are insect-specific toxins with high biotechnological potential to become new safe and ecofriendly bioinsecticides in the middle term future.

BIBLIOGRAPHY

Abiko, K., Iwayama, A., and Shiomi, K. (2015) "Detection and Some Properties of a High Molecular Weight Toxin in the Hypobranchial Gland of Strawberry Conch Strombus Luhuanus." *Toxicon* 1051-3.

Alegre-Cebollada, J., Clementi, G., Cunietti, M., Porres, C., Oñaderra, M., Gavilanes, J.G., and Martínez-del-Pozo, A. (2007a) "Silent Mutations at the 5'-End of the Cdna of Actinoporins from the Sea Anemone *Stichodactyla Helianthus* Allow Their Heterologous Overproduction in *Escherichia Coli*." *J Biotechnol* 127, 2: 211-221.

Alegre-Cebollada, J., Cunietti, M., Herrero-Galán, E., Gavilanes, J.G., and Martínez-del-Pozo, A. (2008) "Calorimetric Scrutiny of Lipid Binding by Sticholysin Ii Toxin Mutants." *J Mol Biol* 382, 4: 920-930.

Alegre-Cebollada, J., Lacadena, V., Oñaderra, M., Mancheño, J.M., Gavilanes, J.G., and Martínez-del-Pozo, A. (2004) "Phenotypic Selection and Characterization of Randomly Produced Non-Haemolytic Mutants of the Toxic Sea Anemone Protein Sticholysin Ii." *FEBS Lett* 575, 1-3: 14-18.

Alegre-Cebollada, J., Martínez-del-Pozo, A., Gavilanes, J.G., and Goormaghtigh, E. (2007b) "Infrared Spectroscopy Study on the Conformational Changes Leading to Pore Formation of the Toxin Sticholysin Ii." *Biophys J* 93, 9: 3191-3201.

Alegre-Cebollada, J., Oñaderra, M., Gavilanes, J.G., and Martínez-del-Pozo, A. (2007c) "Sea Anemone Actinoporins: The Transition from a Folded Soluble State to a Functionally Active Membrane-Bound Oligomeric Pore." *Curr Protein Pept Sci* 8, 6: 558-572.

Alm, I., García-Linares, S., Gavilanes, J.G., Martínez-del-Pozo, A., and Slotte, J.P. (2015) "Cholesterol Stimulates and Ceramide Inhibits Sticholysin Ii-Induced Pore Formation in Complex Bilayer Membranes." *Biochim Biophys Acta - Biomembranes* 1848925-931.

Álvarez, C., Mancheño, J.M., Martínez, D., Tejuca, M., Pazos, F., and Lanio, M.E. (2009) "Sticholysins, Two Pore-Forming Toxins Produced by the Caribbean Sea Anemone *Stichodactyla Helianthus*: Their Interaction with Membranes." *Toxicon* 54, 8: 1135-1147.

Anderluh, G., Krizaj, I., Strukelj, B., Gubensek, F., Maček, P., and Pungercar, J. (1999) "Equinatoxins, Pore-Forming Proteins from the Sea Anemone *Actinia Equina*, Belong to a Multigene Family." *Toxicon* 37, 10: 1391-1401.

Anderluh, G., and Lakey, J.H. (2008) "Disparate Proteins Use Similar Architectures to Damage Membranes." *Trends Biochem Sci* 33, 10: 482-490.

Andreosso, A., Bansal, P.S., Smout, M.J., Wilson, D., Seymour, J.E., and Daly, N.L. (2018) "Structural Characterisation of Predicted Helical Regions in the Chironex Fleckeri Cftx-1 Toxin." *Mar Drugs* 16, 6.

Arbuckle, K., Rodriguez de la Vega, R.C., and Casewell, N.R. (2017) "Coevolution Takes the Sting out of It: Evolutionary Biology and Mechanisms of Toxin Resistance in Animals." *Toxicon* 140118-131.

Athanasiadis, A., Anderluh, G., Maček, P., and Turk, D. (2001) "Crystal Structure of the Soluble Form of Equinatoxin Ii, a Pore-Forming Toxin from the Sea Anemone *Actinia Equina*." *Structure* 9, 4: 341-346.

Bakrač, B., and Anderluh, G. (2009) "Molecular Mechanism of Sphingomyelin-Specific Membrane Binding and Pore Formation by Actinoporins." *Adv Exp Med Biol* 677106-115.

Bakrač, B., Gutierrez-Aguirre, I., Podlesek, Z., Sonnen, A.F., Gilbert, R.J., Maček, P., Lakey, J.H., and Anderluh, G. (2008) "Molecular Determinants of Sphingomyelin Specificity of a Eukaryotic Pore-Forming Toxin." *J Biol Chem* 283, 27: 18665-18677.

Bartlett, G.R. (1959) "Phosphorus Assay in Column Chromatography." *J Biol Chem* 234, 3: 466-468.

Bastolla, U., and Demetrius, L. (2005) "Stability Constraints and Protein Evolution: The Role of Chain Length, Composition and Disulfide Bonds." *Protein Eng Des Sel* 18, 9: 405-415.

Beadnell, C.E., Rider, T.A., Williamson, J.A., and Fenner, P.J. (1992) "Management of a Major Box Jellyfish (Chironex Fleckeri) Sting. Lessons from the First Minutes and Hours." *Med J Aust* 156, 9: 655-658.

Bernheimer, A.W., and Avigad, L.S. (1976) "Properties of a Toxin from the Sea Anemone Stoichacis Helianthus, Including Specific Binding to Sphingomyelin." *Proc Natl Acad Sci U S A* 73, 2: 467-471.

Bjorkbom, A., Rog, T., Kaszuba, K., Kurita, M., Yamaguchi, S., Lonnfors, M., Nyholm, T.K., Vattulainen, I., Katsumura, S., and Slotte, J.P. (2010) "Effect of Sphingomyelin Headgroup Size on Molecular Properties and Interactions with Cholesterol." *Biophys J* 99, 10: 3300-3308.

Brinkman, D., and Burnell, J. (2007) "Identification, Cloning and Sequencing of Two Major Venom Proteins from the Box Jellyfish, Chironex Fleckeri." *Toxicon* 50, 6: 850-860.

Brinkman, D.L., Konstantakopoulos, N., McInerney, B.V., Mulvenna, J., Seymour, J.E., Isbister, G.K., and Hodgson, W.C. (2014) "*Chironex Fleckeri* (Box Jellyfish) Venom Proteins: Expansion of a Cnidarian Toxin Family That Elicits Variable Cytolytic and Cardiovascular Effects." *J Biol Chem* 289, 8: 4798-4812.

Bryant, D.M., Johnson, K., DiTommaso, T., Tickle, T., Couger, M.B., Payzin-Dogru, D., Lee, T.J., Leigh, N.D., Kuo, T.H., Davis, F.G., Bateman, J., Bryant, S., Guzikowski, A.R., Tsai, S.L., Coyne, S., Ye, W.W., Freeman, R.M., Jr., Peshkin, L., Tabin, C.J., Regev, A., Haas, B.J., and Whited, J.L. (2017) "A Tissue-Mapped Axolotl De Novo Transcriptome Enables Identification of Limb Regeneration Factors." *Cell Rep* 18, 3: 762-776.

Calvete, J.J. (2017) "Venomics: Integrative Venom Proteomics and Beyond." *Biochem J* 474, 5: 611-634.

Camp, N.E. (2014) "Black Widow Spider Envenomation." *J Emerg Nurs* 40, 2: 193-194.

Casallanovo, F., de Oliveira, F.J., de Souza, F.C., Ros, U., Martínez, Y., Penton, D., Tejuca, M., Martínez, D., Pazos, F., Pertinhez, T.A., Spisni, A., Cilli, E.M., Lanio, M.E., Álvarez, C., and Schreier, S. (2006) "Model Peptides Mimic the Structure and Function of the N-Terminus of the Pore-Forming Toxin Sticholysin Ii." *Biopolymers* 84, 2: 169-180.

Casewell, N.R., Wuster, W., Vonk, F.J., Harrison, R.A., and Fry, B.G. (2013) "Complex Cocktails: The Evolutionary Novelty of Venoms." *Trends Ecol Evol* 28, 4: 219-229.

Castrillo, I., Alegre-Cebollada, J., Martínez-del-Pozo, A., Gavilanes, J.G., and Bruix, M. (2009) "^{1}h, ^{13}c, and ^{15}n Nmr Assignments of Stnii-R29q, a Defective Lipid Binding Mutant of the Sea Anemone Actinoporin Sticholysin Ii." *Biomol NMR Assign* 3, 2: 239-241.

Chomczynski, P. (1993) "A Reagent for the Single-Step Simultaneous Isolation of Rna, DNA and Proteins from Cell and Tissue Samples." *Biotechniques* 15, 3: 532-534, 536-537.

Clark, G.C., Casewell, N.R., Elliott, C.T., Harvey, A.L., Jamieson, A.G., Strong, P.N., and Turner, A.D. (2019) "Friends or Foes? Emerging Impacts of Biological Toxins." *Trends Biochem Sci* 44, 4: 365-379.

Cosentino, K., Ros, U., and García-Sáez, A.J. (2016) "Assembling the Puzzle: Oligomerization of α-Pore Forming Proteins in Membranes." *Biochim Biophys Acta* 1858, 3: 457-466.

Delaglio, F., Grzesiek, S., Vuister, G.W., Zhu, G., Pfeifer, J., and Bax, A. (1995) "Nmrpipe: A Multidimensional Spectral Processing System Based on Unix Pipes." *J Biomol NMR* 6, 3: 277-293.

Devlin, J.P. (1974) "Isolation and Partial Purification of Hemolytic Toxin from Sea Anemone, Stoichactis Helianthus." *J Pharm Sci* 63, 9: 1478-1480.

Dewson, G. (2016) "Doughnuts, Daisy Chains and Crescent Moons: The Quest for the Elusive Apoptotic Pore." *EMBO J* 35, 4: 371-373.

Dorca-Arevalo, J., Blanch, M., Pradas, M., and Blasi, J. (2018) "Epsilon Toxin from Clostridium Perfringens Induces Cytotoxicity in Frt Thyroid Epithelial Cells." *Anaerobe* 5343-49.

Duan, Z.G., Yan, X.J., Cao, R., Liu, Z., Wang, X.C., and Liang, S.P. (2008) "Proteomic Analysis of Latrodectus Tredecimguttatus Venom for Uncovering Potential Latrodectism-Related Proteins." *Journal of Biochemical and Molecular Toxicology* 22, 5: 328-336.

Dulubova, I.E., Krasnoperov, V.G., Khvotchev, M.V., Pluzhnikov, K.A., Volkova, T.M., Grishin, E.V., Vais, H., Bell, D.R., and Usherwood, P.N. (1996) "Cloning and Structure of Delta-Latroinsectotoxin, a Novel Insect-Specific Member of the Latrotoxin Family: Functional Expression Requires C-Terminal Truncation." *J Biol Chem* 271, 13: 7535-7543.

Endapally, S., Frias, D., Grzemska, M., Gay, A., Tomchick, D.R., and Radhakrishnan, A. (2019) "Molecular Discrimination between Two Conformations of Sphingomyelin in Plasma Membranes." *Cell* 176, 5: 1040-1053 e1017.

Garb, J.E., Gonzalez, A., and Gillespie, R.G. (2004) "The Black Widow Spider Genus Latrodectus (Araneae: Theridiidae): Phylogeny, Biogeography, and Invasion History." *Mol Phylogenet Evol* 31, 3: 1127-1142.

Garb, J.E., and Hayashi, C.Y. (2013) "Molecular Evolution of α-Latrotoxin, the Exceptionally Potent Vertebrate Neurotoxin in Black Widow Spider Venom." *Mol Biol Evol* 30, 5: 999-1014.

Garcia-Diaz, M., Gil-Serna, J., Vazquez, C., Botia, M.N., and Patino, B. (2020) "A Comprehensive Study on the Occurrence of Mycotoxins and Their Producing Fungi During the Maize Production Cycle in Spain." *Microorganisms* 8, 1.

García-Linares, S., Alm, I., Maula, T., Gavilanes, J.G., Slotte, J.P., and Martínez-del-Pozo, A. (2015) "The Effect of Cholesterol on the Long-Range Network of Interactions Established among Sea Anemone Sticholysin Ii Residues at the Water-Membrane Interface." *Mar Drugs* 13, 4: 1647-1665.

García-Linares, S., Castrillo, I., Bruix, M., Menéndez, M., Alegre-Cebollada, J., Martínez-del-Pozo, A., and Gavilanes, J.G. (2013) "Three-Dimensional Structure of the Actinoporin Sticholysin I. Influence of Long-Distance Effects on Protein Function." *Arch Biochem Biophys* 532, 1: 39-45.

García-Linares, S., Maula, T., Rivera-de-Torre, E., Gavilanes, J.G., Slotte, J.P., and Martínez-del-Pozo, A. (2016a) "Role of the Tryptophan Residues in the Specific Interaction of the Sea Anemone *Stichodactyla Helianthus*'s Actinoporin Sticholysin Ii with Biological Membranes." *Biochemistry* 55, 46: 6406-6420.

García-Linares, S., Richmond, R., García-Mayoral, M.F., Bustamante, N., Bruix, M., Gavilanes, J.G., and Martínez-del-Pozo, A. (2014) "The Sea Anemone Actinoporin (Arg-Gly-Asp) Conserved Motif Is Involved in Maintaining the Competent Oligomerization State of These Pore-Forming Toxins." *FEBS J* 281, 5: 1465-1478.

García-Linares, S., Rivera-de-Torre, E., Morante, K., Tsumoto, K., Caaveiro, J.M., Gavilanes, J.G., Slotte, J.P., and Martínez-del-Pozo, Á. (2016b) "Differential Effect of Membrane Composition on the Pore-Forming Ability of Four Different Sea Anemone Actinoporins." *Biochemistry* 55, 48: 6630-6641.

García-Linares, S., Rivera-de-Torre, E., Palacios-Ortega, J., Gavilanes, J.G., and Martínez-del-Pozo, A. "The Metamorphic Transformation of a Water-Soluble Monomeric Protein into an Oligomeric Transmembrane Pore." In *Advances in Biomembranes and Lipid Self-Assembly*, edited by A. Iglič, M. Rappolt and A. J. García-Sáez, 51-97, 2017.

García-Ortega, L., Alegre-Cebollada, J., García-Linares, S., Bruix, M., Martínez-del-Pozo, A., and Gavilanes, J.G. (2011) "The Behavior of Sea Anemone Actinoporins at the Water-Membrane Interface." *Biochim Biophys Acta* 1808, 9: 2275-2288.

García-Ortega, L., de los Ríos, V., Martínez-Ruiz, A., Oñaderra, M., Lacadena, J., Martínez-del-Pozo, A., and Gavilanes, J.G. (2005) "Anomalous Electrophoretic Behavior of a Very Acidic Protein: Ribonuclease U2." *Electrophoresis* 26, 18: 3407-3413.

Gasparini, S., Kiyatkin, N., Drevet, P., Boulain, J.C., Tacnet, F., Ripoche, P., Forest, E., Grishin, E., and Menez, A. (1994) "The Low Molecular Weight Protein Which Co-Purifies with Alpha-Latrotoxin Is Structurally Related to Crustacean Hyperglycemic Hormones." *J Biol Chem* 269, 31: 19803-19809.

Gendreau, K.L., Haney, R.A., Schwager, E.E., Wierschin, T., Stanke, M., Richards, S., and Garb, J.E. (2017) "House Spider Genome Uncovers Evolutionary Shifts in the Diversity and Expression of Black Widow Venom Proteins Associated with Extreme Toxicity." *BMC Genomics* 18, 1: 178.

Goddard, T.D., and Kneller, D.G. (2005) "Sparky 3, University of California, San Francisco."

Gonzalez-Bullon, D., Uribe, K.B., Largo, E., Guembelzu, G., Garcia-Arribas, A.B., Martin, C., and Ostolaza, H. (2019) "Membrane Permeabilization by Bordetella Adenylate Cyclase Toxin Involves Pores of Tunable Size." *Biomolecules* 9, 5.

Goñi, F.M. (2014) "The Basic Structure and Dynamics of Cell Membranes: An Update of the Singer-Nicolson Model." *Biochim Biophys Acta* 1838, 6: 1467-1476.

Grabherr, M.G., Haas, B.J., Yassour, M., Levin, J.Z., Thompson, D.A., Amit, I., Adiconis, X., Fan, L., Raychowdhury, R., Zeng, Q., Chen, Z., Mauceli, E., Hacohen, N., Gnirke, A., Rhind, N., di Palma, F., Birren, B.W., Nusbaum, C., Lindblad-Toh, K., Friedman, N., and Regev, A. (2011) "Full-Length Transcriptome Assembly from Rna-Seq Data without a Reference Genome." *Nat Biotechnol* 29, 7: 644-652.

Grishin, E.V., Himmelreich, N.H., Pluzhnikov, K.A., Pozdnyakova, N.G., Storchak, L.G., Volkova, T.M., and Woll, P.G. (1993) "Modulation of Functional Activities of the Neurotoxin from Black Widow Spider Venom." *FEBS Lett* 336, 2: 205-207.

Gutiérrez, S., Casqueiro, J., and Martín, J.F. (2000) "Los Hongos Como Factorías Celulares: Biodiversidad De Metabolitos Secundarios." *Rev. Iberoamericana Micol.* 17, Revisión: S-54/S-60.

Haas, B.J., Papanicolaou, A., Yassour, M., Grabherr, M., Blood, P.D., Bowden, J., Couger, M.B., Eccles, D., Li, B., Lieber, M., MacManes, M.D., Ott, M., Orvis, J., Pochet, N., Strozzi, F., Weeks, N., Westerman, R., William, T., Dewey, C.N., Henschel, R., LeDuc, R.D., Friedman, N., and Regev, A.

(2013) "De Novo Transcript Sequence Reconstruction from Rna-Seq Using the Trinity Platform for Reference Generation and Analysis." *Nat Protoc* 8, 8: 1494-1512.

Haney, R.A., Clarke, T.H., Gadgil, R., Fitzpatrick, R., Hayashi, C.Y., Ayoub, N.A., and Garb, J.E. (2016) "Effects of Gene Duplication, Positive Selection, and Shifts in Gene Expression on the Evolution of the Venom Gland Transcriptome in Widow Spiders." *Genome Biol Evol* 8, 1: 228-242.

Hinds, M.G., Zhang, W., Anderluh, G., Hansen, P.E., and Norton, R.S. (2002) "Solution Structure of the Eukaryotic Pore-Forming Cytolysin Equinatoxin Ii: Implications for Pore Formation." *J Mol Biol* 315, 5: 1219-1229.

Ho, S.F., Hunt, H.D., Horton, R.M., Pullen, J.K. and Pease, L.R. (1989) "Site-Directed Mutagenesis by Overlap Extension Using the Polymerase Chain Reaction." *Gene 77, 51-59*.

Honda, T., Ni, Y.X., Miwatani, T., Adachi, T., and Kim, J. (1992) "The Thermostable Direct Hemolysin of Vibrio Parahaemolyticus Is a Pore-Forming Toxin." *Canadian Journal of Microbiology* 381175-1180.

Hong, Q., Gutiérrez-Aguirre, I., Barlič, A., Malovrh, P., Kristan, K., Podlesek, Z., Maček, P., Turk, D., González-Mañas, J.M., Lakey, J.H., and Anderluh, G. (2002) "Two-Step Membrane Binding by Equinatoxin Ii, a Pore-Forming Toxin from the Sea Anemone, Involves an Exposed Aromatic Cluster and a Flexible Helix." *J Biol Chem* 277, 44: 41916-41924.

Hyberts, S.G., Frueh, D.P., Arthanari, H., and Wagner, G. (2009) "Fm Reconstruction of Non-Uniformly Sampled Protein Nmr Data at Higher Dimensions and Optimization by Distillation." *J Biomol NMR* 45, 3: 283-294.

Ikonomopoulou, M.P., Fernandez-Rojo, M.A., Pineda, S.S., Cabezas-Sainz, P., Winnen, B., Morales, R.A.V., Brust, A., Sanchez, L., Alewood, P.F., Ramm, G.A., Miles, J.J., and King, G.F. (2018) "Gomesin Inhibits Melanoma Growth by Manipulating Key Signaling Cascades That Control Cell Death and Proliferation." *Sci Rep* 8, 1: 11519.

Kayal, E., Bentlage, B., Pankey, M.S., Ohdera, A.H., Medina, M., Plachetzki, D.C., Collins, A.G., and Ryan, J.F. (2018) "Phylogenomics Provides a Robust Topology of the Major Cnidarian Lineages and Insights on the Origins of Key Organismal Traits." *Bmc Evolutionary Biology* 18.

King, G.F. (2011) "Venoms as a Platform for Human Drugs: Translating Toxins into Therapeutics." *Expert Opinion on Biological Therapy* 11, 11: 1469-1484.

Kiyatkin, N., Dulubova, I., Chekhovskaya, I., Lipkin, A., and Grishin, E. (1992) "Structure of the Low Molecular Weight Protein Copurified with α-Latrotoxin." *Toxicon* 30, 7: 771-774.

Kiyatkin, N.I., Dulubova, I.E., Chekhovskaya, I.A., and Grishin, E.V. (1990) "Cloning and Structure of Cdna Encoding Alpha-Latrotoxin from Black Widow Spider Venom." *FEBS Lett* 270, 1-2: 127-131.

Kiyatkin, N.I., Kulikovskaya, I.M., Grishin, E.V., Beadle, D.J., and King, L.A. (1995) "Functional Characterization of Black Widow Spider Neurotoxins Synthesised in Insect Cells." *Eur J Biochem* 230, 3: 854-859.

Koch, T.L., and Grimmelikhuijzen, C.J.P. (2019) "Global Neuropeptide Annotations from the Genomes and Transcriptomes of Cubozoa, Scyphozoa, Staurozoa (Cnidaria: Medusozoa), and Octocorallia (Cnidaria: Anthozoa)." *Front Endocrinol (Lausanne)* 10831.

Kondos, S.C., Hatfaludi, T., Voskoboinik, I., Trapani, J.A., Law, R.H., Whisstock, J.C., and Dunstone, M.A. (2010) "The Structure and Function of Mammalian Membrane-Attack Complex/Perforin-Like Proteins." *Tissue Antigens* 76, 5: 341-351.

Krasnoperov, V.G., Shamotienko, O.G., and Grishin, E.V. (1990) "Isolation and Properties of Insect-Specific Neurotoxins from Venoms of the Spider *Lactodectus Mactans Tredecimguttatus*." *Bioorg Khim* 16, 8: 1138-1140.

Kristan, K., Viero, G., Maček, P., Dalla Serra, M., and Anderluh, G. (2007) "The Equinatoxin N-Terminus Is Transferred across Planar Lipid Membranes and Helps to Stabilize the Transmembrane Pore." *Febs J* 274, 2: 539-550.

Krueger, F. "Trim Galore! Version 0.4.3." http://www.bioinformatics.babraham.ac.uk/projects/trim_galore/ (

Lanio, M.E., Morera, V., Álvarez, C., Tejuca, M., Gómez, T., Pazos, F., Besada, V., Martínez, D., Huerta, V., Padrón, G., and Chavez, M.A. (2001) "Purification and Characterization of Two Hemolysins from *Stichodactyla Helianthus*." *Toxicon* 39, 2-3: 187-194.

Lau, M.T., Manion, J., Littleboy, J.B., Oyston, L., Khuong, T.M., Wang, Q.P., Nguyen, D.T., Hesselson, D., Seymour, J.E., and Neely, G.G. (2019) "Molecular Dissection of Box Jellyfish Venom Cytotoxicity Highlights an Effective Venom Antidote." *Nature Communications* 10.

Law, R.H., Lukoyanova, N., Voskoboinik, I., Caradoc-Davies, T.T., Baran, K., Dunstone, M.A., D'Angelo, M.E., Orlova, E.V., Coulibaly, F., Verschoor, S., Browne, K.A., Ciccone, A., Kuiper, M.J., Bird, P.I., Trapani, J.A., Saibil, H.R., and Whisstock, J.C. (2010) "The Structural Basis for Membrane Binding and Pore Formation by Lymphocyte Perforin." *Nature* 468, 7322: 447-451.

Lella, M., and Mahalakshmi, R. (2017) "Metamorphic Proteins: Emergence of Dual Protein Folds from One Primary Sequence." *Biochemistry* 56, 24: 2971-2984.

Li, B., and Dewey, C.N. (2011) "Rsem: Accurate Transcript Quantification from Rna-Seq Data with or without a Reference Genome." *BMC Bioinformatics* 12323.

Machkour-M'Rabet, S., Henaut, Y., Winterton, P., and Rojo, R. (2011) "A Case of Zootherapy with the Tarantula Brachypelma Vagans Ausserer, 1875 in Traditional Medicine of the Chol Mayan Ethnic Group in Mexico." *J Ethnobiol Ethnomed* 712.

Macrander, J., Broe, M., and Daly, M. (2015a) "Multi-Copy Venom Genes Hidden in De Novo Transcriptome Assemblies, a Cautionary Tale with the Snakelocks Sea Anemone Anemonia Sulcata (Pennant, 1977)." *Toxicon* 108184-188.

Macrander, J., Brugler, M.R., and Daly, M. (2015b) "A Rna-Seq Approach to Identify Putative Toxins from Acrorhagi in Aggressive and Non-Aggressive *Anthopleura Elegantissima* Polyps." *BMC Genomics* 16221.

Macrander, J., and Daly, M. (2016) "Evolution of the Cytolytic Pore-Forming Proteins (Actinoporins) in Sea Anemones." *Toxins (Basel)* 8, 12.

Madio, B., King, G.F., and Undheim, E.A.B. (2019) "Sea Anemone Toxins: A Structural Overview." *Mar Drugs* 17, 6.

Madio, B., Undheim, E.A.B., and King, G.F. (2017) "Revisiting Venom of the Sea Anemone Stichodactyla Haddoni: Omics Techniques Reveal the Complete Toxin Arsenal of a Well-Studied Sea Anemone Genus." *Journal of Proteomics* 16683-92.

Mancheño, J.M., Martín-Benito, J., Martínez-Ripoll, M., Gavilanes, J.G., and Hermoso, J.A. (2003) "Crystal and Electron Microscopy Structures of Sticholysin Ii Actinoporin Reveal Insights into the Mechanism of Membrane Pore Formation." *Structure* 11, 11: 1319-1328.

Martín-Benito, J., Gavilanes, F., de Los Ríos, V., Mancheño, J.M., Fernández, J.J., and Gavilanes, J.G. (2000) "Two-Dimensional Crystallization on Lipid Monolayers and Three-Dimensional Structure of Sticholysin Ii, a Cytolysin from the Sea Anemone *Stichodactyla Helianthus*." *Biophys J* 78, 6: 3186-3194.

Martínez, D., Morera, V., Álvarez, C., Tejuca, M., Pazos, F., García, Y., Raida, M., Padrón, G., and Eliana Lanio, M. (2002) "Identity between Cytolysins Purified from Two Morphos of the Caribbean Sea Anemone *Stichodactyla Helianthus*." *Toxicon* 40, 8: 1219.

McCowan, C., and Garb, J.E. (2014) "Recruitment and Diversification of an Ecdysozoan Family of Neuropeptide Hormones for Black Widow Spider Venom Expression." *Gene* 536, 2: 366-375.

Mechaly, A.E., Bellomio, A., Gil-Carton, D., Morante, K., Valle, M., González-Mañas, J.M., and Guerin, D.M. (2011) "Structural Insights into the Oligomerization and Architecture of Eukaryotic Membrane Pore-Forming Toxins." *Structure* 19, 2: 181-191.

Monastyrnaya, M., Leychenko, E., Isaeva, M., Likhatskaya, G., Zelepuga, E., Kostina, E., Trifonov, E., Nurminski, E., and Kozlovskaya, E. (2010) "Actinoporins from the Sea Anemones, Tropical *Radianthus Macrodactylus* and Northern *Oulactis Orientalis*: Comparative Analysis of Structure-Function Relationships." *Toxicon* 56, 8: 1299-1314.

Monastyrnaya, M.M., Zykova, T.A., Apalikova, O.V., Shwets, T.V., and Kozlovskaya, E.P. (2002) "Biologically Active Polypeptides from the Tropical Sea Anemone *Radianthus Macrodactylus*." *Toxicon* 40, 8: 1197-1217.

Morante, K., Bellomio, A., Gil-Cartón, D., Redondo-Morata, L., Sot, J., Scheuring, S., Valle, M., González-Mañas, J.M., Tsumoto, K., and Caaveiro, J.M.M. (2016) "Identification of a Membrane-Bound Prepore Species Clarifies the Lytic Mechanism of Actinoporins."

Nylander, J.A., Ronquist, F., Huelsenbeck, J.P., and Nieves-Aldrey, J.L. (2004) "Bayesian Phylogenetic Analysis of Combined Data." *Syst Biol* 53, 1: 47-67.

Orlova, E.V., Rahman, M.A., Gowen, B., Volynski, K.E., Ashton, A.C., Manser, C., van Heel, M., and Ushkaryov, Y.A. (2000) "Structure of Alpha-Latrotoxin Oligomers Reveals That Divalent Cation-Dependent Tetramers Form Membrane Pores." *Nat Struct Biol* 7, 1: 48-53.

Palacios-Ortega, J., García-Linares, S., Astrand, M., Al Sazzad, M.A., Gavilanes, J.G., Martínez-del-Pozo, A., and Slotte, J.P. (2016) "Regulation of Sticholysin Ii-Induced Pore Formation by Lipid Bilayer Composition, Phase State, and Interfacial Properties." *Langmuir* 32, 14: 3476-3484.

Palacios-Ortega, J., Garcia-Linares, S., Rivera-de-Torre, E., Gavilanes, J.G., Martinez-Del-Pozo, A., and Slotte, J.P. (2019) "Sticholysin, Sphingomyelin, and Cholesterol: A Closer Look at a Tripartite Interaction." *Biophys J* 116, 12: 2253-2265.

Palacios-Ortega, J., García-Linares, S., Rivera-de-Torre, E., Gavilanes, J.G., Martínez-del-Pozo, A., and Slotte, J.P. (2017) "Differential Effect of Bilayer Thickness on Sticholysin Activity." *Langmuir* 33, 41: 11018-11027.

Parker, M.W., and Feil, S.C. (2005) "Pore-Forming Protein Toxins: From Structure to Function." *Prog Biophys Mol Biol* 88, 1: 91-142.

Patiño, B., Vázquez, C., Manning, J.M., Roncero, M.I.G., Córdoba-Canero, D., Di Pietro, A., and Martínez-del-Pozo, A. (2018) "Characterization of a Novel Cysteine-Rich Antifungal Protein from *Fusarium Graminearum* with Activity against Maize Fungal Pathogens." *Int J Food Microbiol* 28345-51.

Pena-Blanco, A., and Garcia-Saez, A.J. (2018) "Bax, Bak and Beyond - Mitochondrial Performance in Apoptosis." *FEBS J* 285, 3: 416-431.

Pescatori, M., Bradbury, A., Bouet, F., Gargano, N., Mastrogiacomo, A., and Grasso, A. (1995) "The Cloning of a Cdna Encoding a Protein (Latrodectin) Which Co-Purifies with the Alpha-Latrotoxin from the Black Widow Spider Latrodectus Tredecimguttatus (Theridiidae)." *Eur J Biochem* 230, 1: 322-328.

Petrenko, A.G., Lazaryeva, V.D., Geppert, M., Tarasyuk, T.A., Moomaw, C., Khokhlatchev, A.V., Ushkaryov, Y.A., Slaughter, C., Nasimov, I.V., and Sudhof, T.C. (1993) "Polypeptide Composition of the α-Latrotoxin Receptor. High Affinity Binding Protein Consists of a Family of Related High Molecular Weight Polypeptides Complexed to a Low Molecular Weight Protein." *J Biol Chem* 268, 3: 1860-1867.

Rivera-de-Torre, E., García-Linares, S., Alegre-Cebollada, J., Lacadena, J., Gavilanes, J.G., and Martínez-del-Pozo, A. (2016) "Synergistic Action of Actinoporin Isoforms from the Same Sea Anemone Species Assembled into Functionally Active Heteropores." *J Biol Chem* 291, 27: 14109-14119.

Rivera-de-Torre, E., Martínez-del-Pozo, A., and Garb, J.E. (2018) "*Stichodactyla Helianthus*' De Novo Transcriptome Assembly: Discovery of a New Actinoporin Isoform." *Toxicon* 150105-114.

Rivera-de-Torre, E., Palacios-Ortega, J., Gavilanes, J.G., Martínez-del-Pozo, A., and García-Linares, S. (2019) "Pore-Forming Proteins from Cnidarians and Arachnids as Potential Biotechnological Tools." *Toxins (Basel)* 11, 6.

Rohou, A., Nield, J., and Ushkaryov, Y.A. (2007) "Insecticidal Toxins from Black Widow Spider Venom." *Toxicon* 49, 4: 531-549.

Rojko, N., Cronin, B., Danial, J.S., Baker, M.A., Anderluh, G., and Wallace, M.I. (2014) "Imaging the Lipid-Phase-Dependent Pore Formation of Equinatoxin Ii in Droplet Interface Bilayers." *Biophys J* 106, 8: 1630-1637.

Rojko, N., Dalla Serra, M., Maček, P., and Anderluh, G. (2016) "Pore Formation by Actinoporins, Cytolysins from Sea Anemones." *Biochim Biophys Acta* 1858, 3: 446-456.

Rojko, N., Kristan, K.C., Viero, G., Zerovnik, E., Maček, P., Dalla Serra, M., and Anderluh, G. (2013) "Membrane Damage by an α-Helical Pore-Forming Protein, Equinatoxin Ii, Proceeds through a Succession of Ordered Steps." *J Biol Chem* 288, 33: 23704-23715.

Ronquist, F., Teslenko, M., van der Mark, P., Ayres, D.L., Darling, A., Hohna, S., Larget, B., Liu, L., Suchard, M.A., and Huelsenbeck, J.P. (2012) "Mrbayes 3.2: Efficient Bayesian Phylogenetic Inference and Model Choice across a Large Model Space." *Syst Biol* 61, 3: 539-542.

Ros, U., Pedrera, L., Diaz, D., Karam, J.C., Sudbrack, T.P., Valiente, P.A., MartInez, D., Cilli, E.M., Pazos, F., Itri, R., Lanio, M.E., Schreier, S., and Avarez, C. (2012) "The Membranotropic Activity of N-Terminal Peptides from the Pore-Forming Proteins Sticholysin I and Ii Is Modulated by Hydrophobic and Electrostatic Interactions as Well as Lipid Composition." *J Biosci* 36, 5: 781-791.

Rossjohn, J., Feil, S.C., Mckinstry, W.J., Tweten, R.K., and Parker, M.W. (1997) "Structure of a Cholesterol-Binding, Thiol-Activated Cytolysin and a Model of Its Membrane Form." *Cell* 89685-692.

Rossjohn, J., Polekhina, G., Feil, S.C., Morton, C.J., Tweten, R.K., and Parker, M.W. (2007) "Structures of Perfringolysin O Suggest a Pathway for Activation of Cholesterol-Dependent Cytolysins." *J Mol Biol* 367, 5: 1227-1236.

Ruiz-de-la-Herrán, J., Tomé-Amat, J., Lázaro-Gorines, R., Gavilanes, J.G., and Lacadena, J. (2019) "Inclusion of a Furin Cleavage Site Enhances Antitumor Efficacy against Colorectal Cancer Cells of Ribotoxin α-Sarcin- or Rnase T1-Based Immunotoxins." *Toxins (Basel)* 11, 10.

Schendel, V., Rash, L.D., Jenner, R.A., and Undheim, E.A.B. (2019) "The Diversity of Venom: The Importance of Behavior and Venom System Morphology in Understanding Its Ecology and Evolution." *Toxins (Basel)* 11, 11.

Shatursky, O.Y., Pashkov, V.N., Bulgacov, O.V., and Grishin, E.V. (1995) "Interaction of α-Latroinsectotoxin from *Latrodectus Mactans* Venom with Bilayer Lipid Membranes." *Biochimica et Biophysica Acta - Biomembranes* 123314-20.

Simao, F.A., Waterhouse, R.M., Ioannidis, P., Kriventseva, E.V., and Zdobnov, E.M. (2015) "Busco: Assessing Genome Assembly and Annotation Completeness with Single-Copy Orthologs." *Bioinformatics* 31, 19: 3210-3212.

Subburaj, Y., Ros, U., Hermann, E., Tong, R., and García-Sáez, A.J. (2015) "Toxicity of an α-Pore-Forming Toxin Depends on the Assembly Mechanism on the Target Membrane as Revealed by Single-Molecule Imaging." *J Biol Chem* 2904856-4865.

Sudhof, T.C. (2001) "Alpha-Latrotoxin and Its Receptors: Neurexins and Cirl/Latrophilins." *Annu Rev Neurosci* 24933-962.

Tanaka, K., Caaveiro, J.M., Morante, K., González-Mañas, J.M., and Tsumoto, K. (2015a) "Structural Basis for Self-Assembly of a Cytolytic Pore Lined by Protein and Lipid." *Nat Commun* 66337.

Tanaka, K., Caaveiro, J.M., and Tsumoto, K. (2015b) "Bidirectional Transformation of a Metamorphic Protein between the Water-Soluble and Transmembrane Native States." *Biochemistry* 54, 46: 6863-6866.

Technau, U., and Steele, R.E. (2011) "Evolutionary Crossroads in Developmental Biology: Cnidaria." *Development* 138, 8: 1447-1458.

Tezcan, O.D., and Gozer, O. (2015) "Severe Toxic Skin Reaction Caused by a Common Anemone and Identification of the Culprit Organism." *J Travel Med* 22, 4: 269-271.

Trento, M.V.C., Sales, T.A., de Abreu, T.S., Braga, M.A., Cesar, P.H.S., Marques, T.R., and Marcussi, S. (2019) "Exploring the Structural and Functional Aspects of the Phospholipase A2 from Naja Spp." *Int J Biol Macromol* 14049-58.

Uechi, G.I., Toma, H., Arakawa, T., and Sato, Y. (2010) "Molecular Characterization on the Genome Structure of Hemolysin Toxin Isoforms Isolated from Sea Anemone *Actineria Villosa* and *Phyllodiscus Semoni*." *Toxicon* 56, 8: 1470-1476.

Ushkaryov, Y. (2002) "Α-Latrotoxin: From Structure to Some Functions." *Toxicon* 40, 1: 1-5.

Ushkaryov, Y.A., Rohou, A., and Sugita, S. (2008) "Α-Latrotoxin and Its Receptors." *Handb Exp Pharmacol*, 184: 171-206.

Ushkaryov, Y.A., Volynski, K.E., and Ashton, A.C. (2004) "The Multiple Actions of Black Widow Spider Toxins and Their Selective Use in Neurosecretion Studies." *Toxicon* 43, 5: 527-542.

Valcarcel, C.A., Dalla Serra, M., Potrich, C., Bernhart, I., Tejuca, M., Martínez, D., Pazos, F., Lanio, M.E., and Menestrina, G. (2001) "Effects of Lipid Composition on Membrane Permeabilization by Sticholysin I and Ii, Two Cytolysins of the Sea Anemone *Stichodactyla Helianthus*." *Biophys J* 80, 6: 2761-2774.

Valle, A., Alvarado-Mesen, J., Lanio, M.E., Alvarez, C., Barbosa, J.A., and Pazos, I.F. (2015) "The Multigene Families of Actinoporins (Part I): Isoforms and Genetic Structure." *Toxicon* 103176-187.

Vetter, R.S., and Isbister, G.K. (2008) "Medical Aspects of Spider Bites." *Annu Rev Entomol* 53409-429.

Volkova, T.M., Pluzhnikov, K.A., Woll, P.G., and Grishin, E.V. (1995) "Low Molecular Weight Components from Black Widow Spider Venom." *Toxicon* 33, 4: 483-489.

Wang, X., Tang, X., Xu, D., and Yu, D. (2018) "Molecular Basis and Mechanism Underlying the Insecticidal Activity of Venoms and Toxins from *Latrodectus* Spiders." *Pest Manag Sci*.

Wang, Y., Yap, L.L., Chua, K.L., and Khoo, H.E. (2008) "A Multigene Family of *Heteractis* Magnificalysins (Hmgs)." *Toxicon* 51, 8: 1374-1382.

"World Spider Catalog: Species List for Latrodectus." National History Museum Bern, https://wsc.nmbe.ch/specieslist/3502 (accessed 2019-12-28).

Yan, S., and Wang, X.C. (2015) "Recent Advances in Research on Widow Spider Venoms and Toxins." *Toxins* 7, 12: 5055-5067.

Yang, F., Wang, D., Tong, Y., Qin, C., Yang, L., Yu, F., Huang, X., Liu, S., Cao, Z., Guo, L., Li, W., Wu, Y., and Zhao, X. (2019) "Thermostable Potassium Channel-Inhibiting Neurotoxins in Processed Scorpion Medicinal Material Revealed by Proteomic Analysis: Implications of Its Pharmaceutical Basis in Traditional Chinese Medicine." *J Proteomics* 206103435.

ANNEX

Other articles obtained as a direct consequence of the work carried out along this Doctoral Thesis:

- García-Linares, S., **Rivera-de-Torre, E.**, Morante, K., Tsumoto, K., Caaveiro, J.M., Gavilanes, J.G., Slotte, J.P., and Martínez-del-Pozo, Á. (2016) "Differential Effect of Membrane Composition on the Pore-Forming Ability of Four Different Sea Anemone Actinoporins." Biochemistry 55, 48: 6630-6641.
- García-Linares, S., Maula, T., **Rivera-de-Torre, E.**, Gavilanes, J.G., Slotte, J.P., and Martínez-del-Pozo, A. (2016) "Role of the Tryptophan Residues in the Specific Interaction of the Sea Anemone Stichodactyla Helianthus's Actinoporin Sticholysin Ii with Biological Membranes." Biochemistry 55, 46: 6406-6420.
- Palacios-Ortega, J., García-Linares, S., **Rivera-de-Torre, E**., Gavilanes, J.G., Martínez-del-Pozo, A., and Slotte, J.P. (2017) "Differential Effect of Bilayer Thickness on Sticholysin Activity." Langmuir 33, 41: 11018-11027.
- Palacios-Ortega, J., Garcia-Linares, S., **Rivera-de-Torre, E.**, Gavilanes, J.G., Martinez-Del-Pozo, A., and Slotte, J.P. (2019) "Sticholysin, Sphingomyelin, and Cholesterol: A Closer Look at a Tripartite Interaction." Biophys J 116, 12: 2253-2265.
- Palacios-Ortega, J., **Rivera-de-Torre, E.**, Gavilanes, J.G., Slotte, J.P., Martinez-Del-Pozo, A. (2020) "Evaluation of different approaches used to study membrane permeabilization by actinoporins on model lipid vesicles." BBA-Biomembranes, 1862, 9.

Book chapter:

- García-Linares, S., **Rivera-de-Torre, E**., Palacios-Ortega, J., Gavilanes, J.G., and Martínez-del-Pozo, A. "The Metamorphic Transformation of a Water-Soluble Monomeric Protein into an Oligomeric Transmembrane Pore." In Advances in Biomembranes and Lipid Self-Assembly, edited by A. Iglič, M. Rappolt and A. J. García-Sáez, 51-97, 2017.

BIOCHEMISTRY
including biophysical chemistry & molecular biology

Article

pubs.acs.org/biochemistry

Differential Effect of Membrane Composition on the Pore-Forming Ability of Four Different Sea Anemone Actinoporins

Sara García-Linares,[†,‡] Esperanza Rivera-de-Torre,[†] Koldo Morante,[§] Kouhei Tsumoto,[§] Jose M. M. Caaveiro,[§] José G. Gavilanes,[†] J. Peter Slotte,[‡] and Álvaro Martínez-del-Pozo*[,†]

[†]Departamento de Bioquímica y Biología Molecular I, Universidad Complutense, Madrid, Spain

[‡]Biochemistry, Faculty of Science and Engineering, Åbo Akademi University, Turku, Finland

[§]Department of Bioengineering, Graduate School of Engineering, The University of Tokyo, 7-3-1 Hongo, Bunkyo-ku, Tokyo 113-8656, Japan

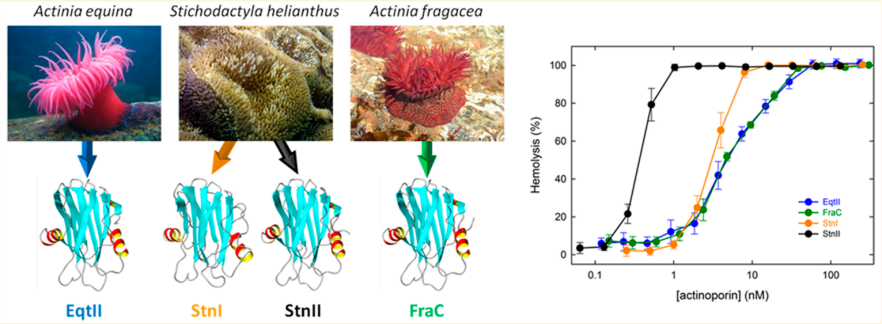

ABSTRACT: Sea anemone actinoporins constitute a protein family of multigene pore-forming toxins (PFT). Equinatoxin II (EqtII), fragaceatoxin C (FraC), and sticholysins I and II (StnI and StnII, respectively), produced by three different sea anemone species, are the only actinoporins whose molecular structures have been studied in depth. These four proteins show high sequence identities and practically coincident three-dimensional structures. However, their pore-forming activity can be quite different depending on the model lipid system employed, a feature that has not been systematically studied before. Therefore, the aim of this work was to evaluate and compare the influence of several distinct membrane conditions on their particular pore-forming behavior. Using a complex model membrane system, such as sheep erythrocytes, StnII showed hemolytic activity much higher than those of the other three actinoporins studied. In lipid model systems, pore-forming ability when assayed against 4:1 1,2-dioleoyl-*sn*-glycero-3-phosphocholine (DOPC)/sphingomyelin (SM) vesicles, with the membrane binding being the rate-limiting step, decreased in the following order: StnI > StnII > EqtII > FraC. When using 1:1:1 DOPC/SM/cholesterol LUVs, the presence of Chol not only enhanced membrane binding affinities by ~2 orders of magnitude but also revealed how StnII was much faster than the other three actinoporins in producing calcein release. This ability agrees with the proposal that explains this behavior in terms of their high sequence variability along their first 30 N-terminal residues. The influence of interfacial hydrogen bonding in SM- or dihydro-SM-containing bilayers was also shown to be a generalized feature of the four actinoporins studied. It is finally hypothesized that this observed variable ability could be explained as a consequence of their distinct specificities and/or membrane binding affinities. Eventually, this behavior can be modulated by the nature of their natural target membranes or the interaction with not yet characterized isotoxin forms from the same sea anemone species.

Pore-forming toxins (PFT) constitute a fascinating family of proteins because of their dual behavior at the water−membrane interface. In water, they are mostly monomeric and remain stably folded as soluble globular proteins. However, upon interaction with lipid membranes of a specific composition, they become oligomeric integral membrane structures, resulting in lytic pores that are lethal for their target cells. Given their small size and rather simple three-dimensional structure, sea anemone actinoporins[1−6] represent a particularly optimal PFT system for studying this transition from a soluble monomeric folded conformation to an oligomeric transmembrane protein.

The incorporation of actinoporins into a membrane largely depends on their lipid bilayer composition and physicochemical state.[6−13] Both factors influence the molecular mechanism involved in the transition from the water-based medium to the inserted state of the protein.[14,15] It has been overtly demonstrated that high-affinity recognition of sphingomyelin (SM) is crucial for the specific attachment of actinoporins to the membrane. However, the subsequent effects observed in

Received: October 3, 2016
Revised: November 10, 2016
Published: November 10, 2016

DOI: 10.1021/acs.biochem.6b01007
Biochemistry 2016, 55, 6630−6641

BIOCHEMISTRY
including biophysical chemistry & molecular biology

Article

pubs.acs.org/biochemistry

Role of the Tryptophan Residues in the Specific Interaction of the Sea Anemone *Stichodactyla helianthus*'s Actinoporin Sticholysin II with Biological Membranes

Sara García-Linares,[†,‡] Terhi Maula,[‡] Esperanza Rivera-de-Torre,[†] José G. Gavilanes,[†] J. Peter Slotte,[‡] and Álvaro Martínez-del-Pozo*[,†]

[†]Departamento de Bioquímica y Biología Molecular I, Universidad Complutense, Madrid, Spain
[‡]Biochemistry, Faculty of Science and Engineering, Åbo Akademi University, Turku, Finland

Supporting Information

ABSTRACT: Actinoporins are pore-forming toxins from sea anemones. Upon interaction with sphingomyelin-containing bilayers, they become integral oligomeric membrane structures that form a pore. Sticholysin II from *Stichodactyla helianthus* contains five tryptophans located at strategic positions; its role has now been studied using different mutants. Results show that W43 and W115 play a determinant role in maintaining the high thermostability of the protein, while W146 provides specific interactions for protomer−protomer assembly. W110 and W114 sustain the hydrophobic effect, which is one of the major driving forces for membrane binding in the presence of Chol. However, in its absence, additional interactions with sphingomyelin are required. These conclusions were confirmed with two sphingomyelin analogues, one of which had impaired hydrogen bonding properties. The results obtained support actinoporins' Trp residues playing a major role in membrane recognition and binding, but their residues have an only minor influence on the diffusion and oligomerization steps needed to assemble a functional pore.

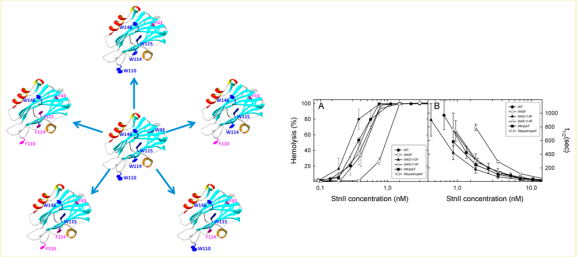

Actinoporins make up a group of small, basic α-pore-forming toxins secreted by sea anemones.[1] They are believed to participate in functions such as predation, defense, and digestion and have been shown to be lethal to small crustaceans, mollusks, fish, and protozoans.[2,3] Cell death takes place after a colloid-osmotic shock induced by cation-selective pores formed on cell membranes.[4−6] All proteins of this family show a high degree of sequence identity and appear as multigene families.[7−9] Four of them have been characterized in great detail: sticholysins I and II (StnI and StnII, respectively) from *Stichodactyla helianthus*,[10,11] equinatoxin II (EqtII) from *Actinia equina*,[7,12] and fragaceatoxin C (FraC) from *Actinia fragacea*.[13]

Actinoporins are globular proteins that remain stably folded in aqueous solution, but upon interaction with lipid bilayers, they become integral membrane structures that oligomerize to form a pore.[10−12,14] Their incorporation into a membrane depends largely on lipid bilayer composition and membrane physicochemical state.[4,6,12,14−20] Thus, membranes must contain sphingomyelin (SM),[16,21−23] but some other conditions, such as the presence of sterols, the coexistence of various phases or domains, compactness, fluidity, and the strength of the interfacial hydrogen bonding network, seem to have a strong influence on their membrane pore-forming ability, as well.[14,16,18−20,24−30]

Monomeric and water-soluble actinoporins appear as a β-sandwich motif composed of 10−12 β-strands flanked by two α-helices that interact with both sides of the β-sandwich (Figure 1A).[31−36] One of these helices (α1) is located near the N-terminal end (Figure 1A) and has been shown to be extremely important for the final function of the pore. This helix seems to extend to the first 30 residues of the protein and become inserted into the membrane to form its walls.[20,31,37−39] This feature, together with the amphipathic character of this stretch, seems to be extremely important for the final functionality of the pore.[37−39]

The formation of a functional pore is, however, still the subject of intense debate. One of the most accepted models explaining the mechanism of actinoporins' pore formation[20,38−42] assumes a toroidal protein−lipid structure without a well-defined fixed stoichiometry.[39−42] Alternative models for FraC have been also proposed on the basis of octameric or nonameric nontoroidal crystalline structures.[34,36] Within this context, the order of events leading to the insertion of the N-terminus into the membrane is also controversial.[36,38,43] Nevertheless, there is general consensus that independent of the mechanism, in addition to the N-terminal α-helix, three

Received: September 12, 2016
Revised: November 2, 2016
Published: November 2, 2016

DOI: 10.1021/acs.biochem.6b00935
Biochemistry 2016, 55, 6406−6420

LANGMUIR Article
Cite This: Langmuir 2017, 33, 11018-11027 pubs.acs.org/Langmuir

Differential Effect of Bilayer Thickness on Sticholysin Activity

Juan Palacios-Ortega,[†,‡] Sara García-Linares,[†,‡] Esperanza Rivera-de-Torre,[†] José G. Gavilanes,[†] Álvaro Martínez-del-Pozo,[*,†] and J. Peter Slotte[*,‡]

[†]Departamento de Bioquímica y Biología Molecular I, Universidad Complutense, Madrid 28040, Spain
[‡]Biochemistry, Faculty of Science and Engineering, Åbo Akademi University, 20500 Turku, Finland

Supporting Information

ABSTRACT: In this study, we examined the influence of bilayer thickness on the activity of the actinoporin toxins sticholysin I and II (StnI and StnII) at 25 °C. Bilayer thickness was varied using dimonounsaturated phosphatidylcholine (PC) analogues (with 14:1, 16:1, 18:1, 20:1, and 22:1 acyl chains). In addition, *N*-14:0-sphingomyelin (SM) was always included because StnI and StnII are SM specific. Cholesterol was also incorporated as indicated. In cholesterol-free large unilamellar vesicles (LUVs) the PC:SM molar ratio was 4:1, and when cholesterol was included, the complete molar ratio was 4:1:0.5 (PC:SM:cholesterol, respectively). Stn toxins promote bilayer leakage through pores formed by oligomerized toxin monomers. Initial calcein leakage was moderately dependent on bilayer PC acyl chain length (and thus bilayer thickness), with higher rates observed with di-16:1 and di-18:1 PC bilayers. In the presence of cholesterol, the maximum rates of calcein leakage were observed in di-14:1 and di-16:1 PC bilayers. Using isothermal titration calorimetry to study the Stn−LUV interaction, we observed that the bilayer affinity constant (K_a) peaked with LUVs containing di-18:1 PC, and was lower in shorter and longer PC acyl chain bilayers. The presence of cholesterol increased the binding affinity approximately 30-fold at the optimal bilayer thickness (di-18:1-PC). We conclude that bilayer thickness affects both functional and conformational aspects of Stn membrane binding and pore formation. Moreover, the length of the actinoporins' N-terminal α-helix, which penetrates the membrane to form a functional pore, appears to be optimal for the membrane thickness represented by di-18:1 PC.

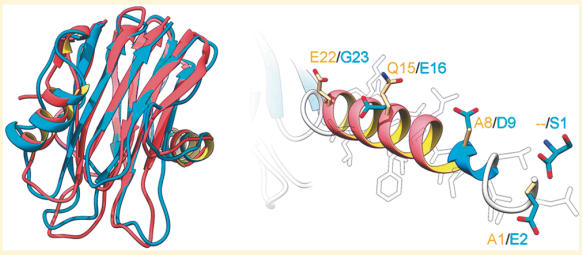

Lipid bilayers are one of the few structures found in all known living organisms. They provide the compartmentalization required for regulated molecular interactions. They also form the boundary that constitutes the first line of cellular defense against extracellular compounds. Because of this extracellular exposure, all membrane components are subject to a very strong selective pressure.[1] If enough generations of a species experience a similar environment, all their constituents are optimized for specific tasks under those given conditions.

Bilayer thickness has been recognized as a key membrane property regulating the activity of intrinsic membrane proteins.[2,3] A mismatch in length between the hydrophobic part of a protein and hydrophobic thickness of the bilayer can cause conformational alterations in either or both of them: transmembrane protein segments may tilt or kink, and membrane lipids might stretch or fold in order to completely avoid either protein or lipid hydrophobic exposure. Rhodopsin, for example, is known to increase its helical content in the presence of thicker bilayers, but in doing so, its activity changes.[4−6] Another example is MscL, a mechanosensitive channel found in *Escherichia coli*. Conformational changes favor its opening in thin bilayers and its closure in thicker bilayers.[7,8] Protein sensitivity to bilayer thickness can be such that some proteins, such as DesK in *Bacillus subtilis*, detect thickness changes caused by temperature-dependent phase states of lipids.[9,10] Thus, the activities of many intrinsic proteins are dependent on bilayer thickness.

Because of their universality and exposure to extracellular compounds, lipid membranes are also an exceptional target for toxins. In fact, pore forming toxins (PFTs) are widely found in nature. One well-known example is the human membrane attack complex, a part of the complement system, which participates in the nonadaptive immune response.[11,12] Some other extensively studied examples are cytolysin A in *E. coli*, α-hemolysin in *Staphylococcus aureus*, lysenin in *Eisenia fetida*, or actinoporins in sea anemones. Actinoporins constitute a widely studied family of α-PFTs that comprise approximately 175 amino acids, and bind to lipid membranes via sphingomyelin (SM) recognition.[13−18] Their well-known three-dimensional water-soluble structure consists of a β-sandwich flanked by two α-helices, one of which is at the N-terminal end of the structure (Figure 1).[20−26] This helix is a key component because it extends and penetrates the membrane to form the functional pore. In fact, it displays longitudinal amphipathicity in order to

Received: May 26, 2017
Revised: September 20, 2017
Published: September 21, 2017

DOI: 10.1021/acs.langmuir.7b01765
Langmuir 2017, 33, 11018−11027

Biophysical Journal
Article

Biophysical Society

Sticholysin, Sphingomyelin, and Cholesterol: A Closer Look at a Tripartite Interaction

Juan Palacios-Ortega,[1,2] Sara García-Linares,[1] Esperanza Rivera-de-Torre,[1] José G. Gavilanes,[1] Álvaro Martínez-del-Pozo,[1,*] and J. Peter Slotte[2,*]
[1]Departamento de Bioquímica y Biología Molecular, Universidad Complutense, Madrid, Spain and [2]Biochemistry, Faculty of Science and Engineering, Åbo Akademi University, Turku, Finland

ABSTRACT Actinoporins are a group of soluble toxic proteins that bind to membranes containing sphingomyelin (SM) and oligomerize to form pores. Sticholysin II (StnII) is a member of the actinoporin family produced by *Stichodactyla helianthus*. Cholesterol (Chol) is known to enhance the activity of StnII. However, the molecular mechanisms behind this activation have remained obscure, although the activation is not Chol specific but rather sterol specific. To further explore how bilayer lipids affect or are affected by StnII, we have used a multiprobe approach (fluorescent analogs of both Chol and SM) in combination with a series of StnII tryptophan (Trp) mutants to study StnII/bilayer interactions. First, we compared StnII bilayer permeabilization in the presence of Chol or oleoyl-ceramide (OCer). The comparison was done because both Chol and OCer have a 1-hydroxyl, which helps to orient the molecule in the bilayer (although OCer has additional polar functional groups). Both Chol and OCer also have increased affinity for SM, which StnII may recognize. However, our results show that only Chol was able to activate StnII-induced bilayer permeabilization; OCer failed to activate it. To further examine possible Chol/StnII interactions, we measured Förster resonance energy transfer between Trp in StnII and cholestatrienol, a fluorescent analog of Chol. We could show higher Förster resonance energy transfer efficiency between cholestatrienol and Trps in position 100 and 114 of StnII when compared to three other Trp positions further away from the bilayer binding region of StnII. Taken together, our results suggest that StnII was able to attract Chol to its vicinity, maybe by showing affinity for Chol. SM interactions are known to be important for StnII binding to bilayers, and Chol is known to facilitate subsequent permeabilization of the bilayers by StnII. Our results help to better understand the role of these important membrane lipids for the bilayer properties of StnII.

SIGNIFICANCE Sticholysin II (StnII) is a pore-forming toxin that interacts with sphingomyelin in target membranes. Cholesterol (Chol) is known to modulate pore formation. In our study, we examine in detail the molecular interactions between StnII and both pyrene-sphingomyelin and cholestatrienol, a fluorescent Chol analog. We show that both lipids interact with StnII in the bilayer. Using tryptophan mutants of StnII, we also obtained information about which tryptophan residues Chol preferentially interacted with. Our findings provide new, to our knowledge, details on the process of StnII pore formation as influenced by sphingomyelin and Chol.

INTRODUCTION

Pore-forming toxins (PFTs) constitute an important family of membrane-binding proteins. In solution, PFTs are monomeric and behave like globular proteins, with a defined stable conformation. When PFTs encounter membranes with certain lipid compositions, these proteins are capable of forming pores that cause an osmotic shock in the targeted cells (1,2). The proteins undergo a molecular metamorphosis that allows the PFTs not only to bind but also to oligomerize and transform into integral membrane proteins. Therefore, these proteins are also called metamorphic or amphitropic proteins because of this dual behavior (3–6). PFTs can assemble into structures inserted across the bilayer to form pores. This process occurs without covalent modification of the polypeptides involved but also without coupling to any other chemical reaction, although the overall process must be thermodynamically favorable. Taken together, these facts suggest that this family of proteins constitutes a very good model for studying the molecular

Submitted March 15, 2019, and accepted for publication May 10, 2019.
*Correspondence: alvaromp@ucm.es or jpslotte@abo.fi
Sara García-Linares's present address is Cell Biology Department, Harvard Medical School, Boston, Massachusetts.
Editor: Tommy Nylander.
https://doi.org/10.1016/j.bpj.2019.05.010

BBA - Biomembranes 1862 (2020) 183311

Contents lists available at ScienceDirect

BBA - Biomembranes

journal homepage: www.elsevier.com/locate/bbamem

Evaluation of different approaches used to study membrane permeabilization by actinoporins on model lipid vesicles

Juan Palacios-Ortega[a,b], Esperanza Rivera-de-Torre[a,b], José G. Gavilanes[a], J. Peter Slotte[b,*], Álvaro Martínez-del-Pozo[a,**]

[a] Departamento de Bioquímica y Biología Molecular, Universidad Complutense, Madrid, Spain
[b] Biochemistry, Faculty of Science and Engineering, Åbo Akademi University, Turku, Finland

ARTICLE INFO

Keywords:
Pore-forming-proteins
Leakage
Calcein
Rhodamine
Terbium
NBD-dithionite

ABSTRACT

Release of aqueous contents from model lipid vesicles has been a standard procedure to evaluate pore formation efficiency by actinoporins, such as sticholysin II (StnII), for the last few decades. However, regardless of the probe of choice, the results reported that StnII action was never able to empty the vesicles completely. This was hard to explain if StnII pores were to be stable and always leaky for the probes used. To address this question, we have used a variety of probes, including rhodamine 6G or Tb^{3+}, to test the permeability of StnII's pores. Our results indicate that calcein was in fact too large to fit through StnII's pores, and that the standard method in the field is actually reporting StnII-induced transient permeation of the membrane rather than the passage of solutes through the stable assembled pores. In order to evaluate the permeability of these structures, we used a dithionite-based assay, which showed that the final pores were in fact open. Thus, our results indicate that the stable actinoporins' pores are open in spite of plateaued classic release curves. Besides the proper pore, the first stages of pore formation would inflict serious damage to living cells as well.

1. Introduction

Sea anemone actinoporins represent an optimal system to study the transition from a water-soluble monomeric protein conformation to an oligomeric transmembrane pore [1–3]. These pore-forming toxins constitute multigenic families that have been detected in many sea anemone species [3–7]. However, only four of them have been characterized in detail: Sticholysins I and II (StnI and StnII, respectively) from *Stichodactyla helianthus* [1–3], equinatoxin II from *Actinia equina* [4,8], and fragaceatoxin C from *Actinia fragacea* [9]. All show almost identical monomeric water-soluble three-dimensional structure composed of a β-sandwich motif flanked by two α-helices [10–15]. One of these helices, located at the N-terminal end, is responsible for the actual formation of the pore penetrating the membrane [16–22]. The incorporation of these proteins to the bilayer depends largely on the lipid composition and the physicochemical properties of the membrane [8,20,23–31]. Sphingomyelin (SM) is required [26,32–34], but other factors, such as the presence of sterols, the coexistence of various phases or domains, lateral packing, fluidity, membrane thickness, and the strength of the SM interfacial hydrogen bonding network, have a strong influence on the pore-forming ability of these proteins [20,26,28–31,34–47].

Almost forty years have passed since it was demonstrated, using different K^+ or Ca^{2+} containing solutions, that these proteins form cation-selective pores at neutral pH [23,35,48–52]. Altogether, those studies evidenced that actinoporins increase cell membrane permeability for monovalent and divalent cations. Only a few years later, these pores were also characterized using different electrophysiological approaches, including the use of lipid planar membranes. These studies confirmed their specificity for cations and revealed a pore size in the order of 1–2 nm of radius [16,49–52]. In fact, the only two available crystalline structures of actinoporin pores fit rather well within this size range (Fig. 1) [13,15]. Interestingly, despite the specificity of the pore for cations, most researchers in the field, including us, have been using negatively charged fluorophores, such as calcein or carboxyfluorescein, as the main probes to explore the molecular features of these pores. In this work, we challenge this approach and suggest a more sensitive procedure to study the pore-forming mechanism of these intriguing metamorphic proteins.

Abbreviations: $C_{12}E_8$, octaethylene glycol monododecyl ether; Chol, cholesterol; DOPC, 1,2-dioleoyl-sn-glycero-3-phosphocholine; eSM, egg sphingomyelin; LUV, large unilamelar vesicle; POPE-NBD, 1,2-dioleoyl-sn-glycero-3-phosphoethanolamine-N-(7-nitro-2-1,3-benzoxadiazol-4-yl); SM, sphingomyelin; Stn, sticholysin

* Correspondence to: J.P. Slotte, Biochemistry, Faculty of Science and Engineering, Åbo Akademi University, 20520 Turku, Finland.
** Correspondence to: Á. Martínez-del-Pozo, Departamento de Bioquímica y Biología Molecular, Universidad Complutense, 28040 Madrid, Spain.
E-mail addresses: jpslotte@abo.fi (J.P. Slotte), alvaromp@quim.ucm.es (Á. Martínez-del-Pozo).

https://doi.org/10.1016/j.bbamem.2020.183311
Received 26 December 2019; Received in revised form 12 March 2020; Accepted 13 April 2020
Available online 27 April 2020
0005-2736/

CHAPTER TWO

The Metamorphic Transformation of a Water-Soluble Monomeric Protein Into an Oligomeric Transmembrane Pore

Sara García-Linares, Esperanza Rivera-de-Torre, Juan Palacios-Ortega, José G. Gavilanes, Álvaro Martínez-del-Pozo[1]

Universidad Complutense, Madrid, Spain
[1]Corresponding author: e-mail address: alvaromp@quim.ucm.es

Contents

1. Three-Dimensional Structure of Actinoporins 54
2. Interaction of Actinoporins With Lipid Membranes: The Role of Membrane Composition and Biophysical Properties 59
   - 2.1 Lipid Domains and Boundaries: Effects of Sterols on Actinoporins' Functionality 62
   - 2.2 Implication of the Interfacial Hydrogen-Bonding Network of SM Molecules 67
   - 2.3 Anionic and Nonlamellar Lipids 68
3. Pore Formation by Actinoporins 69
4. The Role of Particular Residues of Actinoporins 77
   - 4.1 30 First Residues Stretch 77
   - 4.2 POC-Binding Site 80
   - 4.3 Cluster of Aromatic Residues 81
   - 4.4 Trp Residues 83
   - 4.5 Competent Oligomerization for Pore Formation 85
5. From Particular to General: Actinoporins as a Family 86
6. Perspectives and Final Remarks 88

References 89

Abstract

Sea anemones produce venoms containing different toxic molecules. Among them, actinoporins are some of the best characterized ones. They constitute a family of toxic polypeptides that belong to the much larger group of pore-forming toxins. Actinoporins remain mostly monomeric and stably folded in aqueous solution but, upon interaction with lipid membranes of specific composition, they become

Advances in Biomembranes and Lipid Self-Assembly, Volume 26
ISSN 2451-9634
http://dx.doi.org/10.1016/bs.abl.2017.06.004

oligomeric integral membrane structures to build a pore. They insert an α-helix stretch within biological membranes, forming cation-selective pores with a diameter of 1–2 nm, which result in a colloid osmotic shock that leads to cell death. They are believed to participate in functions like predation, defense, and digestion and have been shown to be lethal for small crustaceans, mollusks, and fish. The best-known actinoporins are equinatoxin II (from *Actinia equina*), fragaceatoxin C (from *Actinia fragacea*), and sticholysins I and II (from *Stichodactyla helianthus*). In order to fully understand the pore formation mechanism of these proteins, several approaches have been used: (i) characterization of natural and artificial variants of actinoporins to determine the role of specific residues, (ii) study of their water-soluble and transmembrane structures, and (iii) employment of different lipids to evaluate the influence of membrane properties and composition. Further research is still needed, however, in order to fully understand the complex mechanism underlying actinoporins' functionality.

Cnidaria is the oldest animal venomous lineage. It shows great diversity in the uses of venom, which is critical to prey capture, digestion, and intraspecific aggression [1,2]. Among cnidarians, venom is best characterized in sea anemones. Toxic polypeptides that have been well characterized within these animals fall into three major classes: phospholipases A2s, cytolysins, and neurotoxins [2,3]. There are four types of sea anemone cytolysins, but all of them form pores in the cellular membrane, creating an ionic imbalance that results in cytolysis [4–8]. Actinoporins (type II cytolysins) constitute a family of toxins that has been classically thought to be stored in the nematocysts of sea anemones [9], although cnidarians lack a centralized venom gland and toxins secretion can be detected through almost every tissue [3]. Actinoporins are single polypeptide chains of around 175 amino acids, which usually display basic p*I* and are cysteinless [6,10,11]. They belong to the much larger group of pore-forming toxins (PFTs) and their toxic activity relies, as stated earlier, in their capacity to form pores into biological membranes. All PFTs show a very similar dual behavior by which they remain mostly monomeric and stably folded in aqueous solution but, upon interaction with lipid membranes of specific composition, they become oligomeric integral membrane structures. Sphingomyelin (SM) is the key membrane component recognized by actinoporins [12–20], so specifically that it has been even proposed to act as a lipidic membrane receptor [18]. However, the physicochemical nature of the bilayer and the presence of cholesterol (Chol) [21] and other "membrane disturbing" lipids [14,22,23] seem to exert an important influence on actinoporins'